UNIVERSITAT DE BARCELONA

Mesozoic extension and Cenozoic contraction in the Eastern Iberian Chain (Maestrat Basin)

Tectònica extensiva mesozoica i contractiva cenozoica a la Cadena Ibèrica oriental

Marina Nebot Miralles

Mesozoic extension and Cenozoic contraction in the Eastern Iberian Chain (Maestrat Basin)

Tectònica extensiva mesozoica i contractiva cenozoica a la Cadena Ibèrica oriental

Marina Nebot Miralles

Ph. D. Thesis. October 2016

Supervisor: Joan Guimerà

Institut de Recerca Geomodels

Dept. de Dinàmica de la Terra i de l'Oceà. Universitat de Barcelona

Institut de Recerca Geomodels
Departament de Dinàmica de la Terra i de l'Oceà
Universitat de Barcelona

Mesozoic extension and Cenozoic contraction in the Eastern Iberian Chain (Maestrat Basin)

Tectònica extensiva mesozoica i contractiva cenozoica a la Cadena Ibèrica oriental

Memòria presentada per **Marina Nebot Miralles** per optar al grau de Doctora en Geologia. Aquesta memòria s'ha realitzat dins del Programa de Doctorat de Ciències de la Terra, sota la dirección del **Dr. Joan Guimerà Roso**.

Marina Nebot Miralles
Barcelona, Octubre de 2016

Dr. Joan Guimerà Roso

This work has been carried out in the *Departament de Dinàmica de la Terra i de l'Oceà,* formerly *Departament de Geodinàmica i Geofísica,* and the Geomodels Research Institute (Universitat de Barcelona). Finantial support was provided by a predoctoral grant, Ajuts al Personal Investigador en Formació (APIF), from the University of Barcelona, and by the projects INTECTOSAL (CGL2010-21968-C02-01/BTE) from the *Ministerio de Ciencia e Innovación* and CGL2008-04916/BTE from the *Ministerio de Economía y Competitividad*.

Als meus pares,

Penyagolosa, gegant de pedra,
la teua testa plena de neu,
Penyagolosa, Penyagolosa,
a la tempesta, al sol i al vent:
fita senyera del poble meu.

Agraïments

En primer lloc voldrie agrair al meu tutor Joan Guimerà, per haver-me donat l'oportunitat de treballar en una zona tan maca com és el Maestrat, una zona a la que li tinc molta estima. Agrair-li que m'hagi donat sempre llibertat per anar fent, però sempre atenent a que no em despistés. Ja són uns quants anys rodant pel Maestrat sota la seva supervisió, des de que vaig veure el cartell que proposava un treball de final de carrera al Desert de les Palmes, fins ara que estic finalitzant aquesta tesi. Moltes gràcies.

Moltes gràcies també al Ramón Salas, que sempre que li he demanat, m'ha aclarit els dubtes i m'ha donat la informació necessària. I també al Juan Diego Martín, amb qui vaig anar al camp per primera vegada al Desert de les Palmes i em va ajudar en els primers contactes amb l'Aptià de la Conca del Maestrat, mentre feia el treball de final de carrera, deixant-me que li consultés sempre que vaig tenir dubtes. Moltes gràcies.

Gràcies al Josep Antón Moreno Bedmar, al Miquel Company, el José Sandoval i el Luis Moliner, que des de la distància em va ajudar a datar els ammonits que vaig trobar al camp. Gràcies al Ken McClay per permetre'm fer l'estada al Fault Dynamics Research Group. A l'Eduard Roca, per permetre'm viure l'experiència d'una AGU a San Francisco, i a la Bet Beamud i l'Eloi Carola, per ser uns companys de viatge fantàstics, gràcies Casstores! Moltes gràcies al Pablo Granado pels seus bons consells i a la Núria Carrera per les xerrades de política o del que sigui, a Mireia Butillé per ajudar-me amb la georeferenciació de la sísmica i amb el pas a profunditat. A l'Oriol Ferrer per ajudar-me tant amb l'estada a la Royal Holloway. Al Daniel Bello, que sempre està disposat a donar un cop de mà, al Pau Arbués pel seu ajut amb el Microstation i altres programes, a l'Òscar Gratacós, al Frede Escosa, Marco DeMatteis, Marco Snidero, l'Ester Izquierdo, la Maria Roma, l'Oriol Pla i a la resta de companys de la 226 i del departament. Gràcies també a l'Adrià Ramos, que fins i tot em va acompanyar a la primera campanya de camp de la tesi una mica accidentada. I per què no, m'agradaria agrair als amos de les pensions de Mirambell, Cantavieja, Castellote, Molinos, Cuevas de Cañart, Olocau del Rei... que em van tractar molt bé i em van alimentar encara millor.

Als companys de dinars, cafès, geosortides, Eduard Albert, Luis Valero, Rubén Calvo, Cristina Biete, el Telm Bover-Arnal, la gent de marina, a la Berta López i el Jorge Belenguer, que van marxar quan jo començava la tesi. Moltes gràcies a la Patricia Cabello i la Montse Puig pels riures i pels ànims. Vull agrair també als companys de la carrera, amb qui seguim quedant de tant en tant i que van ser com una segona família, especialment al Marc Tudela, la Luz Gomis, Diana Rodríguez i Mónica Torres.

Moltes gràcies a Mónica Viu i Elisa Revah, perquè van ser unes companyes de pis estupendes, amb qui vaig compartir uns anys molt especials, en que ens ho vam passar molt bé i que també van haver de patir un poc la meva ofuscació mentre acabava el treball de màster. Moltes gràcies també a l'Ester Pujadas, genial companya de pis. Amb qui vam compartir el seu final de tesi i quasi bé el meu, gràcies per les xarrades motivadores que teníem i pels ànims.

Moltes gràcies als amics de Castelló i molt especialment a Sirio Canós, Mariona Herrera i Jordi Trilles. A Sirio que em va acompanyar per Londres mentre estava d'estada i sempre m'ha ajudat amb els dubtes d'anglès, i tot i que ens veiem poc, quan ens trobem és com si només fes una estona que ens havíem separat. A Mariona i Jordi, perquè sempre han estat amb mi, des de que teníem 4 anys? Fins i tot em van acompanyar uns dies al camp i els vaig fer posar per uns barrancs on no em feia massa ganes de posar-m'hi sola. Moltes gràcies també a Jordi, per fer-me una classe magistral i fugaç de maquetació i pel seu ajut amb la informàtica per maquetar la tesi.

Segur que al final m'he deixat algú, disculpeu-me! Gràcies a tothom que ha esta amb mi durant els darrers mesos de redacció de la tesi, per la paciència que han hagut de tindre.

Moltes gràcies a Floripes, pels seus *tuppers* de macarrons, i per les vistes de la mar i la muntanya mentre escrivia la tesi alguns dies d'estiu des de la villa.

Gràcies als meus pares i als meus avis per deixar-me una casa tan fantàstica a la meua tornada a Castelló, on m'he passat taaaaantes hores tancada durant els últims mesos d'elaboració de la tesi.

Gràcies al meu germà Daniel, i als meus pares Teresa i Vicent, perquè sempre m'han ajudat i m'han donat el seu suport en tot el que han pogut i més. Des del dia que vaig dir que volie anar a Barcelona a fer geologia, amb tot lo que aquella decisió ha comportat, fins 10 anys més tard, que estic a punt d'acabar la tesi doctoral.

Moltes gràcies a Sergi, per la paciència, pels ànims, per cuidar-me i per estimar-me tant.

Contents

1. ABSTRACT

1.1 ABSTRACT

The Maestrat basin was one of the most subsident basins of the Mesozoic Iberian Rift system, which experienced two main rifting events: Late Permian-Late Triassic and Late Jurassic-Early Cretaceous. The Maestrat Basin developed during the second rifting event, by a listric normal fault system which divided it into sub-basins. It was inverted during the Cenozoic Alpine orogeny generating the Linking Zone between the NW-SE-trending Iberian Chain, and the NE-SW-trending Catalan Coastal Chain. During the inversion, the E-W-trending, N-verging Portalrubio–Vandellòs fold-and-thrust belt developed along its northern margin, detached in the Triassic evaporites, while southwards it also involved the Variscan Basement. The study area is located in the northern margin of the Maestrat Basin, in the central part of the Portalrubio-Vandellòs fold-and-thrust belt, including the transition from thin (N) to thick-skinned (S) areas. The main objectives of the present thesis are to characterize the structures developed during the Mesozoic extension and during the Cenozoic contraction, and the influence of the former on the latter, as well as to characterize the transition from thin to thick- skinned style of deformation areas. Finally it aims to propose a kinematic evolutionary model for the northern margin of the basin and a reconstruction of the Maestrat Basement Thrust geometry. This study is based on the interpretation of subsurface data–2D seismic and exploration wells–and new field data.

Regarding the Mesozoic structure, during the first stage of extensional activity (Late Permian-Late Triassic) a high angle normal fault system developed, which fragmented the Variscan Basement into a system of horsts, grabens and half-grabens. Those faults were active during the deposition of the Buntsandstein facies and lasted until the lower part of the Middle Muschelkalk facies was deposited, filling the system of horsts and grabens and generating depositional thickness variations of this evaporitic unit. The fault system was overstepped by the upper part of the Middle Muschelkalk, indicating a decrease in the extensional activity, which lasted until the carbonates of the Upper Muschelkalk facies was deposited, as it has a nearly constant thickness in all the basin. During the Keuper facies deposition, the extensional activity of some normal faults in the acoustic or sub-salt basement resumed, triggering the Middle Muschelkalk salt flow, which developed salt anticlines and welds, increasing the thickness variations of this facies. The age of the salt flow is deduced from the Keuper facies reflectors lapping on the folded Upper Muschelkalk above the salt accumulations. Growth-strata above some Upper Muschelkalk forced folds are also recognized, developed above some reactivated normal faults in the acoustic basement. The different load exerted by the Keuper facies could have also enhanced the salt flow.

During the second stage of extensional activity (Late Jurassic-Early Cretaceous) a segmented system of listric normal faults, connected by relay ramps developed bounding the different sub-basins, as suggested by the distribution of the Lower Cretaceous rocks and the extensional structures in the study area, which display varying orientations. The Maestrat basin filling, broadly becomes thinner towards the north, towards the northern boundary of the basin. However, the geometry of the Lower Cretaceous syn-rift filling of the Salzedella sub-basin –the most extensive sub-basin within the Maestrat basin– resembles a wide wedge that thickens progressively towards the North, from 350m to 1100m, to the hanging wall of the S-dipping main normal faults. Major extension occurred during the Barremian, as units of this age

display bigger thickness variations, while the Aptian units show more constant thicknesses.

During the Cenozoic Alpine orogeny, the Maestrat basin was inverted, and the broadly E-W-trending, N-verging Maestrat Basement Thrust developed, traversing the entire basin, as a result of the inversion of the Mesozoic normal fault system in its segment across the acoustic basement. A wide uplifted area –about 40km-wide in the N-S direction- can be observed in the hinterland of the Linking Zone, which contains subhorizontal and slightly deformed Upper Cretaceous and locally Cenozoic rocks, with topographic elevations from 1400 to 2000m. In the study area, this uplifted area is limited to the North by the E–W-trending, N-verging Calders monocline, whose limb is about 13km wide in its central part, dips about 5ºN, and generates a vertical tectonic step of 800-1200m. This monocline is interpreted as a fault-bend fold; therefore, a flat-ramp-flat geometry is assumed in depth for the Maestrat Basement Thrust. The northern synformal hinge of the Calders monocline broadly coincides with the transition from a thick-skinned style of deformation to the S, to a thin-skinned style to the N.

The low-dip of the Calders monocline tilted limb, together with the vast extension of the uplifted area suggest a very low-dip for the basement ramp, rooted in the upper crust. It contains a low-dip ramp (~9°) extended southwards more than 40km, attaining a depth of 7.5km below the sea level. As this thrust reached the Mesozoic cover to the foreland, it propagated across the Middle Muschelkalk evaporitic detachment, generating a nearly horizontal short-cut thrust which transported the supra-salt cover, and the normal fault segments within it, for c. 12km towards the NNE. The displacement of the basement in the hanging-wall of the low-dip basement ramp generated the 40km-wide uplifted area, while the superficial shortening was accumulated in the northern margin of the basin –which contains the thinnest Mesozoic cover– developing the Portalrubio–Vandellòs fold-and-thrust belt.

The structure in the Portalrubio–Vandellòs fold-and-thrust belt displays, in the study area, a salient geometry, convex to the foreland, to the NNE sense of transport, whose formation is attributed to different factors: a thick Middle Muschelkalk evaporitic detachment that terminates laterally to the W, a basement high (Montalbán anticline) that interacted with the propagation of the E-W-trending thrust front west of the study area, and the inheritance of the orientation of preexisting Mesozoic normal faults.

1.2 RESUM

La Conca del Maestrat va ser una de les més subsidents del Sistema de Rift Ibèric Mesozoic, el qual va experimentar dos episodis de rift principals: el primer durant el Permià superior-Triàsic i el segon durant el Juràssic superior-Cretaci inferior. La conca del Maestrat es va formar durant el segon episodi de rift, per un sistema de falles normals lístriques que la van dividir en sub-conques. Es va invertir durant l'Orogènia Alpina Cenozoica, formant la Zona d'Enllaç entre la Serralada Ibèrica, d'orientació NW-SE, i la Cadena Costanera Catalana, d'orientació NE-SW. Durant la inversió es va formar, en el marge nord de la conca, el cinturó de plecs i encavalcaments de Portalrubio-Vandellòs, d'orientació predominant E-W i vergència cap al N, desenganxat a les evaporites Triàsiques, però que cap al S passa a involucrar el sòcol Varisc.

La zona d'estudi es situa al marge nord de la Conca del Maestrat, a la part central del cinturó de plecs i encavalcaments de Portalrubio-Vandellòs, i inclou la zona de trànsit d'un estil de deformació de pell fina (N) a un de pell gruixuda (S). Els principals objectius d'aquesta tesi són caracteritzar les estructures formades durant l'extensió Mesozoica i durant la contracció Cenozoica, i la influència de les primeres en la formació de les darreres, així com caracteritzar com es produeix el trànsit d'una zona amb deformació de pell fina a una de pell gruixuda. Finalment, pretén proposar un model d'evolució cinemàtica del marge nord de la conca i una reconstrucció de la geometria de l'Encavalcament de Sòcol del Maestrat. Aquest estudi està basat en la interpretació de dades de subsòl (sísmica 2D i sondeigs d'exploració) i dades noves de camp.

Pel que fa a l'estructura Mesozoica, durant la primera etapa de rift (Permià superior-Triàsic superior) es va formar un sistema de falles normals d'alt angle que va fragmentar el sòcol Varisc en un sistema de *horsts, grabens* i *semi-grabens*. Aquestes falles foren actives durant el depòsit de la fàcies Buntsandstein, fins que es va dipositar la part inferior de la fàcies Muschelkalk mitjà, reomplint el sistema de *horst* i *grabens* i donant lloc a diferències de gruix deposicionals en aquesta unitat evaporítica. La part alta del Muschelkalk mitjà va sobrepassar i cobrir el sistema de falles, indicant una disminució de l'activitat extensiva, que va durar fins que es van dipositar els carbonats de la fàcies Muschelkalk superior, que presenta un gruix quasi constant a tota la conca. Mentre es dipositava la fàcies Keuper es va reactivar l'activitat extensiva d'algunes falles normals del sòcol acústic o infra-salí, desencadenant el flux de la sal del Muschelkalk mitjà, que va formar anticlinals de sal i *welds*, incrementant les diferències de gruix d'aquesta fàcies. L'edat del flux de sal es dedueix a partir dels reflectors sísmics del Keuper, que es disposen en *onlap* a sobre del Muschelkalk superior plegat sobre les acumulacions de sal. Alguns ventalls de capes també es poden reconèixer sobre plecs forçats del Muschelkalk superior a sobre d'algunes falles normals reactivades en el sòcol acústic. La càrrega diferencial exercida pel Keuper hauria incrementat o afavorit el flux de sal.

Durant el segon episodi de rift (Juràssic superior- Cretaci inferior) es va formar un sistema de falles normals lístriques segmentades i connectades per rampes de relleu, que separaven les diferents sub-conques, tal i com suggereix la distribució de les roques del Cretaci inferior i de les estructures extensives

en la zona d'estudi, que presenten diverses orientacions. El rebliment de la conca del Maestrat a grans trets s'aprima cap al Nord, cap al marge de la conca. Tot i això, el Cretaci inferior de la sub-conca de la Selzedella – la més extensa de la conca del Maestrat – presenta una geometria de tascó que s'engruixeix progressivament cap al Nord, de 350m a 1100m, cap al bloc superior del sistema de falles normals inclinades cap al S. Durant el Barremià, l'activitat extensiva va ser major que durant l'Aptià, ja que les unitats barremianes presenten variacions de gruix més acusades, mentre que les aptianes presenten gruixos més constants.

Durant l'orogènia alpina cenozoica, la conca del Maestrat es va invertir. La inversió del sistema de falles normals Mesozoiques, en el seu segment a través del sòcol acústic, va generar l'Encavalcament de Sòcol del Maestrat, d'orientació aproximadament E-W i vergència cap al N, que travessa tota la conca. Al rerepaís de la Zona d'Enllaç es pot observar una extensa zona elevada, d'uns 40km d'amplada en direcció N-S, que conté roques del Cretaci superior i del Cenozoic poc deformades i sub-horitzontals, que es situen a cotes entre 1400 i 2000m. A la zona d'estudi, aquesta zona elevada està limitada al nord pel Monoclinal de Calders, d'orientació E-W i vergència cap al N, que té un flanc basculat cap al N uns 5º amb una amplada màxima d'uns 13km a la part central, i que genera un esglaó tectònic vertical de 800-1200m. Aquest monoclinal s'interpreta com un plec d'adaptació, a partir del qual se'n dedueix una geometria de replà-rampa-replà per a l'Encavalcament de Sòcol del Maestrat. La xarnera sinforme septentrional del Monoclinal de Calders coincideix a grans trets amb el pas d'un estil de deformació de pell gruixuda al Sud, a un estil de deformació de pell fina al Nord.

El baix angle del flanc inclinat del Monoclinal de Calders, i la gran extensió de la zona aixecada suggereixen un baix angle per a l'encavalcament basal en el sòcol, que estaria arrelat a l'escorça superior. Aquest encavalcament tindria una rampa de baix angle (~9º), que es propagaria més de 40km cap al S, arribant a una profunditat d'uns 7.5km sota el nivell del mar. Quan aquest encavalcament va arribar a la cobertora Mesozoica cap a l'avant-país, es va propagar a través del nivell de desenganxament del Muschelkalk mitjà salí, generant un *short-cut* quasi horitzontal que va transportar la cobertora supra-salina i els segments de les falles normals a través d'aquesta uns 12km cap al NNE. El desplaçament del sòcol en el bloc superior de la rampa de baix-angle va generar l'extensa zona aixecada, d'uns 40km d'amplada, mentre que l'escurçament en superfície es va acumular a la zona externa de la conca, situada al N, que conté la cobertora Mesozoica més prima, formant el cinturó de plecs i encavalcament de Portalrubio-Vandellòs.

L'estructura del cinturó de plecs i encavalcament de Portalrubio-Vandellòs presenta, a la zona d'estudi, una geometria arquejada, convexa cap a l'avantpaís, cap al NNE, en el sentit del transport. La formació d'aquesta geometría es pot atribuir a diversos factors: a la presència d'un nivell de desenganxament salí (Muschelkalk mitjà) que acaba lateralment, cap a l'Oest; a un alt de basament (Anticlinal de Montalbán) que hauria interactuat amb la propagació cap al Nord del front d'encavalcaments d'orientació E-O, a l'oest de la zona estudiada, i per últim a l'herència de l'orientació de les falles normals Mesozoiques.

1.3 RESUMEN

La Cuenca del Maestrat fue una de las más subsidentes del Sistema de Rift Ibérico mesozoico, el cual experimentó dos episodios de rift principales: el primero durante el Pérmico superior-Triásico y el segundo durante el Jurásico superior-Cretácico inferior. La Cuenca del Maestrat se formó durante el segundo episodio de rift, por un sistema de fallas normales lístricas que la dividieron en sub-cuencas. Se invirtió durante la Orogenia Alpina cenozoica, formando la Zona de Enlace entre la Cadena Ibérica, de orientación NW-SE, y la Cadena Costera Catalana, de orientación NE-SW. Durante la inversión, se formó en el margen norte de la cuenca el cinturón de pliegues y cabalgamientos de Portalrubio-Vandellòs, de orientación predominante E-W y vergencia hacia el N, despegado en las evaporitas triásicas, que hacia el S pasa a involucrar el zócalo varisco.

La zona de estudio se sitúa en el margen norte de la cuenca del Maestrat, en la parte central del cinturón de pliegues y cabalgamientos de Portalrubio-Vandellòs, e incluye la zona de tránsito de un estilo de deformación de piel fina (N) a piel gruesa (S). Los principales objetivos de esta tesis son caracterizar las estructuras formadas durante la extensión mesozoica y durante la contracción cenozoica, y la influencia de las primeras en la formación de las segundas, así como caracterizar cómo se produce el tránsito de una zona con deformación de piel fina a una de piel gruesa. Finalmente, se pretende proponer un modelo de evolución cinemática del margen norte de la cuenca y una reconstrucción de la geometría del Cabalgamiento de Zócalo del Maestrat. Este estudio está basado en la interpretación de datos de subsuelo (sísmica 2D y sondeos de exploración) y de nuevos datos de campo.

En cuanto a la estructura Mesozoica, durante la primera etapa de rift (Pérmico superior-Triásico superior) se formó un sistema de fallas normales de alto ángulo que fragmentaron el zócalo varisco en un sistema de *horsts*, *grabens* y *semi-grabens*. Estas fallas fueron activas durante el depósito de la facies Buntsandstein, hasta que se depositó la parte inferior de la facies Muschelkalk medio, rellenando el sistema de *horsts* y *grabens*, y dando lugar a diferencias de espesor deposicionales en esta unidad evaporítica. La parte superior de la facies Muschelkalk medio sobrepasó y cubrió el sistema de fallas, indicando una disminución de la actividad extensiva, que duró hasta que se depositaron los carbonatos de la facies Muschelkalk superior, que presentan una potencia casi constante en toda la cuenca. Mientras se depositaba la facies Keuper, se reactivó la actividad extensiva de algunas fallas normales en el zócalo acústico o infra-salino, desencadenando el flujo de la sal del Muschelkalk medio, que formó anticlinales de sal y *welds*, incrementando las diferencias de espesor de esta facies. La edad del flujo de sal se deduce a partir de los reflectores sísmicos del Keuper, que se disponen en *onlap* sobre el Muschelkalk superior plegado sobre las acumulaciones de sal. Algunos abanicos de capas también pueden reconocerse sobre pliegues forzados del Muschelkalk superior sobre algunas fallas normales reactivadas en el zócalo acústico. La carga diferencial ejercida por el Keuper habría incrementado o favorecido el flujo de sal.

Durante el segundo episodio de rift (Jurásico superior-Cretácico inferior) se formó un sistema de fallas normales lístricas segmentadas y conectadas por rampas de relevo, que separaban las diferentes sub-cuencas, tal y como sugiere la distribución de las rocas del Cretácico inferior y de las estructuras

extensivas en la zona de estudio, que presentan diversas orientaciones. El relleno de la cuenca del Maestrat, a grandes rasgos se adelgaza hacia el norte, hacia el margen de la cuenca. Aun así, el Cretácico inferior de la sub-cuenca de la Salzedella – la más extensa de la cuenca del Maestrat – presenta una geometría de cuña que se engrosa progresivamente hacia el norte, de 350m a 1100m, hacia el bloque superior del sistema de fallas normales inclinadas hacia el S. Durante el Barremiense la actividad extensiva fue mayor que durante el Aptiense, ya que las unidades barremienses presentan variaciones de espesor más acentuadas, mientras que las aptienses presentan espesores más constantes.

Durante la Orogenia Alpina cenozoica la cuenca del Maestrat se invirtió. La inversión del sistema de fallas normales mesozoicas, en su segmento a través del zócalo acústico, generó el Cabalgamiento de Zócalo del Maestrat, de orientación aproximadamente E-W y vergencia hacia el N, que atraviesa toda la cuenca. En el postpaís de la Zona de Enlace se puede observar una extensa zona elevada, de unos 40km de anchura en dirección N-S, que contiene rocas del Cretácico superior y del Cenozoico podo deformadas y sub-horizontales, que se sitúan en cotas entre 1400 y 2000m. En la zona de estudio, esta zona elevada está limitada al norte por el Monoclinal de Calders, de orientación E-W y vergencia hacia el N, que tiene un flanco inclinado hacia el N unos 5º, con una anchura máxima de unos 13km en su parte central, y que genera un escalón tectónico vertical de 800-1200m. Este monoclinal se interpreta como un pliegue de adaptación, a partir del que se deduce una geometría de rellano-rampa-rellano del Cabalgamiento de Zócalo del Maestrat. La charnela sinforme septentrional del Monoclinal de Calders coincide, a grandes rasgos, con el paso de un estilo de deformación de piel gruesa al Sur, a un estilo de deformación de piel fina al Norte.

El bajo ángulo del flanco inclinado del Monoclinal de Calders, y la gran extensión de la zona levantada sugieren un bajo ángulo para el cabalgamiento basal en el zócalo, que estaría enraizado en la corteza superior. Este cabalgamiento tendría una rampa de bajo ángulo (~9º), que se propagaría más de 40km hacia el S, alcanzando una profundidad de unos 7,5km bajo el nivel del mar. Cuando este cabalgamiento llegó a la cobertera mesozoica hacia el antepaís, se propagó a través del nivel de despegue del Muschelkalk medio salino, generando un *short-cut* casi horizontal, que transportó la cobertera supra-salina y los segmentos de las fallas normales a través de ésta unos 12km hacia el NNE. El desplazamiento del zócalo en el bloque superior de la rampa de bajo ángulo generó la extensa zona elevada, de unos 40km de ancho, mientras que el acortamiento en superficie se acumuló en la zona externa de la cuenca, situada al N, que contiene la cobertera mesozoica más delgada, formando el cinturón de pliegues y cabalgamientos de Portalrubio-Vandellòs.

La estructura del cinturón de pliegues y cabalgamientos de Portalrubio-Vandellòs presenta, en la zona de estudio, una geometría arqueada, convexa hacia el antepaís, hacia el NNE, en el sentido del transporte. La formación de esta geometría se puede atribuir a varios factores: a la presencia de un nivel de despegue salino (Muschelkalk medio) que termina lateralmente, hacia el Oeste; a un alto de basamento (Anticlinal de Montalbán) que habría interactuado con la propagación hacia el norte del frente de cabalgamientos E-W, al oeste de la zona estudiada, y por último a la herencia de la orientación de las fallas normales mesozoicas.

2. INTRODUCTION

2.1 MOTIVATIONS AND MAIN OBJECTIVES OF THE THESIS

This thesis studies the eastern part of the Iberian Chain, which is an intraplate thrust-belt owing to the Cenozoic contractional inversion of the Mesozoic Iberian Rift System (ÁLVARO et al., 1979; SALAS et al., 2001). More specifically it focuses on the northern central part of the Linking Zone between the Iberian Chain and the Catalan Coastal Chain. The Linking Zone is the result of the inversion of the northern margin of the Maestrat Basin, one of the most subsident basins of the Iberian Rift System.

The main structural features of this area are:

(1) A N-verging fold-and-thrust belt developed in the northern part of the Linking Zone, detached in the Middle Muschelkalk. Its trend is roughly E-W, although it also contains structures with other orientations. Towards the south, a tectonic vertical step is observed, which is interpreted as the superficial expression of a basement thrust, thus the thrust-sheet involved the Variscan Basement. This transition area is known as the Turmell Fault Zone (SALAS and GUIMERÀ, 1996), which extends throughout the Maestrat Basin, from E to W.

(2) A wide tectonically elevated area developed to the hinterland, in the Variscan Basement involved area. It is of about 35km in the N-S direction per 50km in the E-W direction, with topographic elevations from 1400 to 2000m. This elevated area contains subhorizontal and slightly deformed Upper Cretaceous and locally Cenozoic rocks, the youngest pre-contractional rocks (GUIMERÀ et al., 2010). It is a tectonically and topographically elevated area that has been only slightly eroded, coinciding with a thickened crust revealed by a large and negative Bouguer anomaly (SALAS and CASAS, 1993; GUIMERÀ et al., 2016).

(3) A regional detachment in the Middle Muschelkalk has been recognized, which differentiated two structural packages, the sub-salt basement and the supra-salt cover (GUIMERÀ and ÁLVARO, 1990). This evaporitic unit also experienced some salt tectonics (BARTRINA and HERNÁNDEZ, 1990).

This thesis aims to propose a kinematic evolutionary model for the frontal fold-and-thrust belt, and to reconstruct the geometry of the sole thrust which generated the tectonic vertical step observed, and is able to maintain the tectonically elevated area for about 40km southwards. It also aims to understand how the transition from thin-skinned to thick-skinned styles of deformation occurs. To achieve these objectives, a reconstruction of the extensional structures developed during the Mesozoic rift, and the contractional structures developed during the Cenozoic is needed, in order to understand the influence of the former structures on the latter ones.

2.2 THESIS ORGANIZATION

The present thesis has been elaborated as a compendium of articles, which are shown in the **Appendix I**. The complete references of these articles are the following:

-NEBOT, M. and GUIMERÀ, J. 2016a. Structure of an inverted basin from subsurface and field data: the Late Jurassic-Early Cretaceous Maestrat basin (Iberian Chain). *Geologica Acta*, 14 (2), 155-177, doi: 10.1344/GeologicaActa2016.14.2.5

-NEBOT, M. and GUIMERÀ, J. 2016b. Kinematic evolution of a fold-and-thrust belt developed during basin inversion: the Mesozoic Maestrat basin, E Iberian Chain. *Geological Magazine*, published online: October 2016, doi:10.1017/S001675681600090X

The first article (NEBOT and GUIMERÀ, 2016a), focuses on the southern part of the study area, and it is based on field data and the subsurface data obtained in the Maestrat basin during the 1970s and 1980s. It presents a reconstruction of the Mesozoic extensional and Cenozoic contractional structure of the area, and reconstructs the transition from thin to thick–skinned areas. A new macrostructure is described in this paper: the Calders monocline, which produces a tectonic vertical step which can be recognized throughout the Maestrat basin. This structure reveals that the Turmell Fault Zone concept (SALAS and GUIMERÀ, 1996) is more complex than it has been described previously, so it reviews it.

The interpretation of the seismic profiles network also permitted to reconstruct the stratigraphy and structure of the Triassic rifting event in the substratum of the Maestrat basin, which is not possible to perform from field data, as these units do not crop out in the studied area. Some salt tectonic structures were observed in the evaporites of the Middle Muschelkalk facies, which could be studied from the subsurface data. The relationship between the extensional structure in the sub-salt basement and in the supra-salt cover, with the differently oriented structures developed during the Cenozoic contraction is also analyzed in this paper.

The second article (NEBOT and GUIMERÀ, 2016b) focuses on the northern part of the study area, the northern fold-and-thrust belt, where no subsurface data is available. It describes the structure of the fold-and-thrust belt and tries to figure out the Mesozoic extensional structure, whose Cenozoic inversion developed the present contractional structures. It also gives a horizontal shortening value for the fold-and-thrust belt. Finally, this paper presents a kinematic evolution model for the northern margin of the Maestrat basin, combining the interpretation of the basement involved hinterland done in the first article, with the interpretation of the structure, the transport direction, and the shortening value obtained in the second paper for the northern fold-and-thrust belt.

To sum up, as a whole these papers present a reconstruction of the Triassic extensional structure in the substratum of the Maestrat basin in the area with subsurface data available, and an interpretation of the salt tectonic structures observed in the Middle Muschelkalk evaporites. It also presents a reconstruction of the main extensional structures of the Maestrat basin, developed during the Late

Jurassic-Early Cretaceous rifting event, and a reconstruction of the main sub-basins in which it has been divided, which differ slightly of those previously defined. These papers also present a reconstruction of the contractional structures developed during the Cenozoic inversion of the Maestrat basin, and try to figure out their relationship with the previous extensional structures. Finally, it proposes a kinematic evolutionary model for the northern margin of the Maestrat basin, based on the structures recognized, the cross-sections and the shortening values obtained.

This memory presents a global summary of the results, the discussion and the conclusions presented in these articles, as well as additional unpublished results and discussion. In the introductory chapter, the geological setting, the stratigraphy and the main structural background of the studied area have been expanded in comparison with the articles.

Additionally, two extended abstracts presented to the *IX Congreso Geológico de España (2016)* are shown in the **Appendix II**.

2.3 GEOGRAPHICAL SETTING OF THE STUDIED AREA

The studied area is located in the eastern part of the Iberian Peninsula, more specifically it is located in the eastern part of the Teruel province, including the northwestern part of the Castelló province (Fig. 2.1). It approximately covers the area comprised between the villages of Calanda (North) to Mosqueruela (South), and from Morella (East) to Villarluengo (West). Most of the Iberian Chain topography exceeds 1000m while several places reach more than 2000m (GUIMERÀ et al., 2010). The highest location in the studied area, and in the Linking Zone, is the Mount Peñarroya with 2028m above the sea level (m asl).

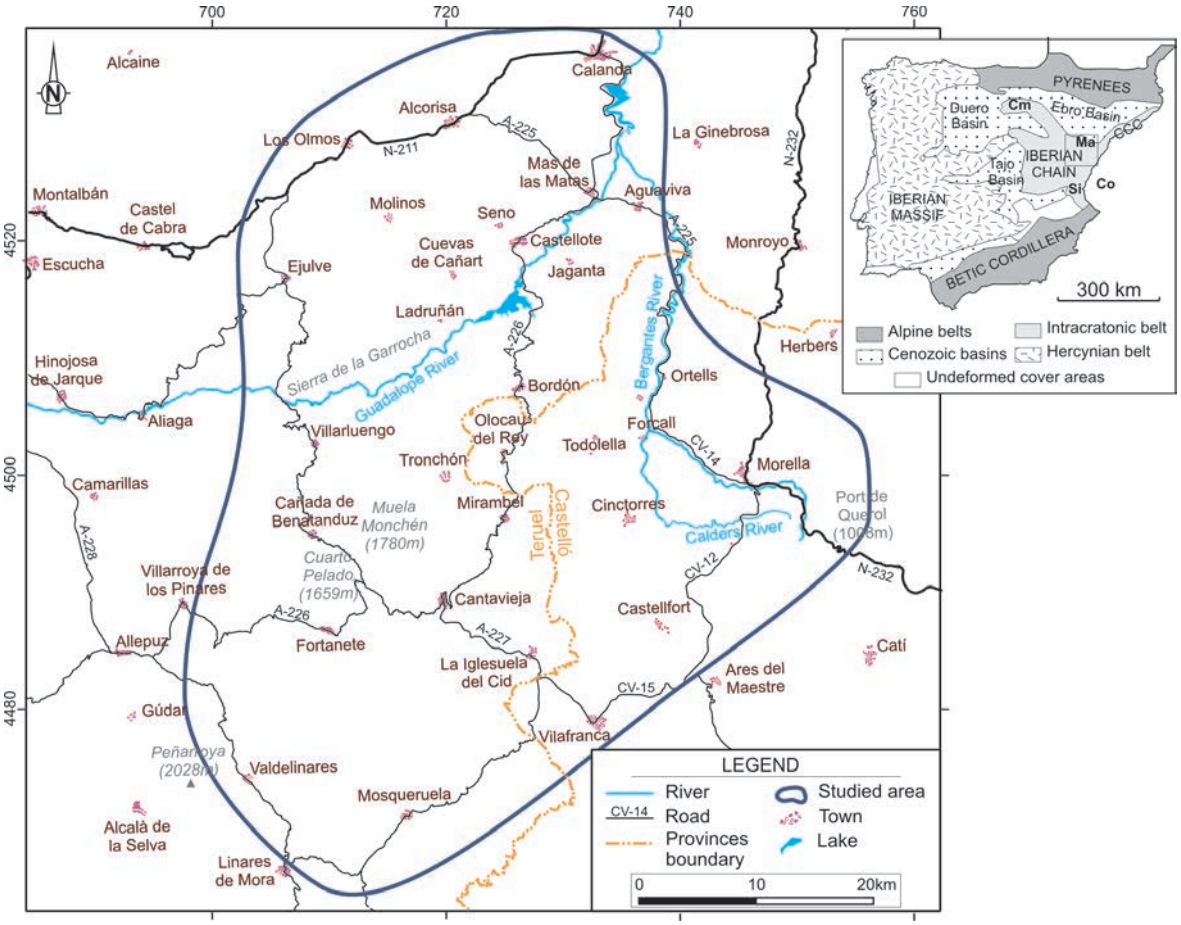

Figure 2.1. (a) Detailed map showing the location of the study area. (b) Location of the study area in the Iberian Peninsula. The main structural units are differentiated (CCC-Catalan Coastal Chain). The Iberian Chain is shown, and also the location of its Late Jurassic-Early Cretaceous extensional basins: Ma-Maestrat basin, Cm-Cameros basin, Co-Columbretes basin, Si-South Iberian basin (Modified from SALAS et al., 2001).

2.4 GEOLOGICAL SETTING OF THE STUDIED AREA

The study area is located in the E-W-trending, N-verging Linking Zone between the NW-SE-trending Iberian Chain and the NE-SW-trending Catalan Coastal Chain (Fig. 2.1b), which is the result of the Cenozoic inversion of the Late Jurassic-Early Cretaceous Maestrat Basin, which was one of the most subsident basins of the Mesozoic Iberian Rift System (GUIMERÀ, 1988; SALAS et al., 2001).

2.4.1 The Iberian Rift System

The Iberian Rift System developed during the Mesozoic and experienced two major rifting events, during the Late Permian-Late Triassic and the Late Oxfordian-Late Albian. Both of them were followed by episodes of lower extensional activity, during the Early-Middle Jurassic and the Late Albian-Maastrichtian) (Fig. 2.2, ÁLVARO, 1987; SALAS and CASAS, 1993; SALAS et al., 2001, 2010).

First rifting event: Late Permian-Late Triassic.- An intraplate rift system developed within the central and eastern Iberian plate during this period, the NE-SW-trending Catalonia-Valencia and Prebetic basins, the E-W-trending Pyrenean-Cantabrian basins and the NW-SE-trending Iberian rift system (ÁLVARO et al., 1979; SALAS and CASAS, 1993, SALAS et al., 2010), producing the collapse of the Variscan orogeny (VISSERS, 1992; VISSERS and MEIJER, 2012a). This rifting event was related to the westward propagation of the Tethys rift system and the southward propagation of the Arctic-North Atlantic rift system (ZIEGLER, 1988; SALAS and CASAS, 1993; SALAS et al., 2001).

The Iberian Rift System was bounded by high-angle normal faults, and sediments ranging from continental siliciclastics (Buntsandstein) to marine carbonates (Muschelkalk) where deposited (SALAS et al., 2001) unconformably overlying the Variscan Basement (discontinuity D1). In the study area, a more complex extensional history can be deduced for this extensional period, from the interpretation of the seismic profiles available. As it will be explained later, a period of low extensional activity occurred while the upper part of the Middle Muschelkalk facies and the Upper Muschelkalk facies were being deposited.

First post-rift event: Early Jurassic-base of the Late Jurassic.- During this period the evolution of the basin was controlled by a period of relative tectonic quiescence and thermal subsidence, during which shallow marine carbonate platforms developed, overlaying the previous extensional structures (SALAS et al., 2001, 2010). However, some extension is needed during this event (AURELL et al., 1992), as in some areas, an angular unconformity (D2) developed between the Jurassic and the tilted Triassic rocks (GUIMERÀ, 1988; AURELL et al., 1992; ROCA and GUIMERÀ, 1992; SAN ROMÁN and AURELL, 1992; ROCA et al., 1994; CAMPOS et al., 1996). In some places the Jurassic directly overlies the Buntsandstein rocks, as in the Desert de les Palmes area, located north of Castelló (Fig. 2.3a) (GUIMERÀ, 1988; ROCA et al., 1994). Some thickness variations in the Lower Lias are also observed, as it will be explained later.

Second rifting event: Late Jurassic- Early Cretaceous.- During this extensional period, the carbonate platform was fragmented and the Iberian basin was divided into several basins (Fig. 2.1b, Cameros,

Maestrat, Columbretes and South Iberian basins), separated by thresholds. In the Maestrat basin, one of the most subsident basins of the rift system (SALAS and GUIMERÀ 1996; SALAS et al. 2001), the extension started at the Late Oxfordian and lasted until the Middle Albian (SALAS et al., 2005). This rifting event coincides with the gradual opening of the North Atlantic basin and the opening of the Bay of Biscay rift system, which, during the Aptian, separated Iberia from the Eurasian plate (SALAS et al., 2001). Within the Maestrat basin, a system of listric normal faults developed, which divided it into several sub-basins (Fig. 2.3), having their detachment located in the basement and in the Triassic evaporites. This rifting cycle was interrupted by a short period of decelerated subsidence and erosion occurred during the Late Berriasian-Hauterivian (SALAS et al. 2001), which is reflected in the sedimentary filling of the basin as a regional unconformity (D3, Fig. 2.4) Therefore, this extensional event can also be divided into two rifting events, the Late Jurassic and the Early Cretaceous ones, separated by the Late Berriasian-Hauterivian post-rift event (SALAS et al., submitted).

Second post-rift event: Late Cretaceous (Late Albian-Maastrichtian).- During this period Iberia was separated from the Eurasian plate and the evolution of the basin was mainly controlled by thermal subsidence and the most important sea level rise occurred during the Mesozoic (HAQ et al., 1988; HARDENBOL et al., 1998; SALAS et al., 2001). Fluvial sediments were deposited (Utrillas Fms., Late Albian) unconformably overlaying the previous sin-rift units, above the intra-Albian regional unconformity developed at the end of the preceding rifting event (D4, Fig. 2.4). A sea level transgression occurred at the Cenomanian-Turonian, and a large carbonate platform developed connecting the Tethys with the Atlantic (Fig. 2.2; SALAS et al., 2001, 2005).

2.4.2 The Maestrat Basin

The Maestrat Basin was bounded by normal fault systems of listric geometry. The one that bounded the basin towards the north was roughly E-W-trending and S-dipping, while its southwestern boundary was composed of NW-SE-trending normal faults, dipping both towards the NE and the SW (Fig. 2.3a). The rollover fold in the hanging wall of both normal fault systems generated two sub-basins, the Salzedella sub-basin to the North and the Penyagolosa sub-basin to the south, separated by the Vistabella threshold (Fig. 2.3b). The Maestrat basin, with a Mesozoic sequence up to 5800 m thick (SALAS et al., 2001) was an asymmetric basin, as its depocenter was located in its northern side –in the hanging wall of the Xert normal fault, located in the Salzedella sub-basin– as a result of the larger displacement of the northern fault system, in comparison with the southern one (SALAS et al. 2005).

The Turmell Fault zone was defined by SALAS and GUIMERÀ (1996) as one of the most important extensional faults within the Maestrat basin, which controlled the sedimentation during the Late Jurassic-Early Cretaceous rifting event. This ESE-WNW-trending, S-dipping normal fault zone, involving the Variscan Basement, produced the northward tilting of its hanging wall, separating the Salzedella and the Galve sub-basins, located in its subsident hanging wall, from the Morella and the Aliaga sub-basins, in its footwall. The last ones were separated from the former ones by the threshold generated by the uplifted footwall of the fault zone.

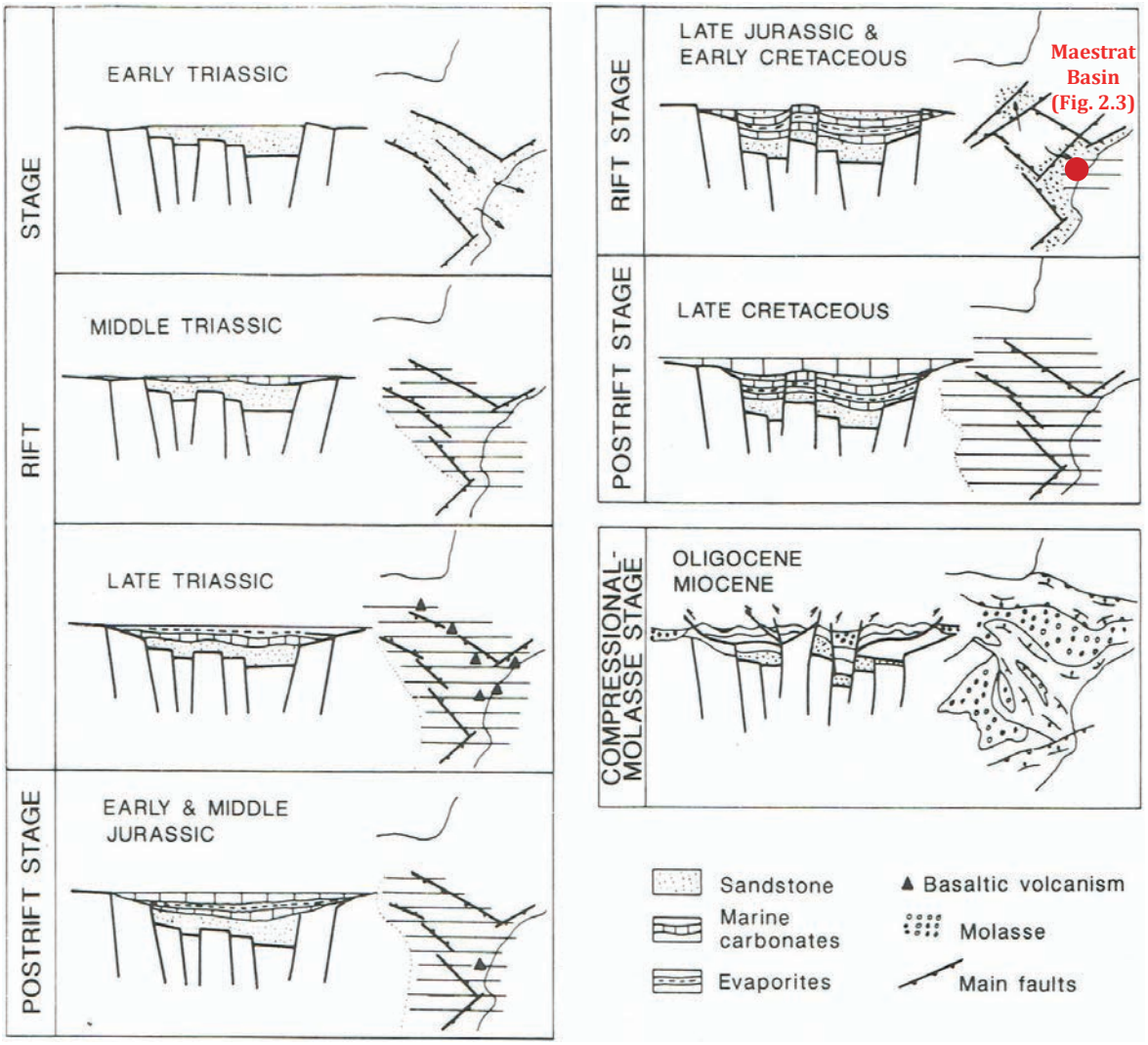

Figure 2.2. Schematic evolution of the Iberian Rift System. From SALAS et al. (2001), after ÁLVARO et al. (1979).

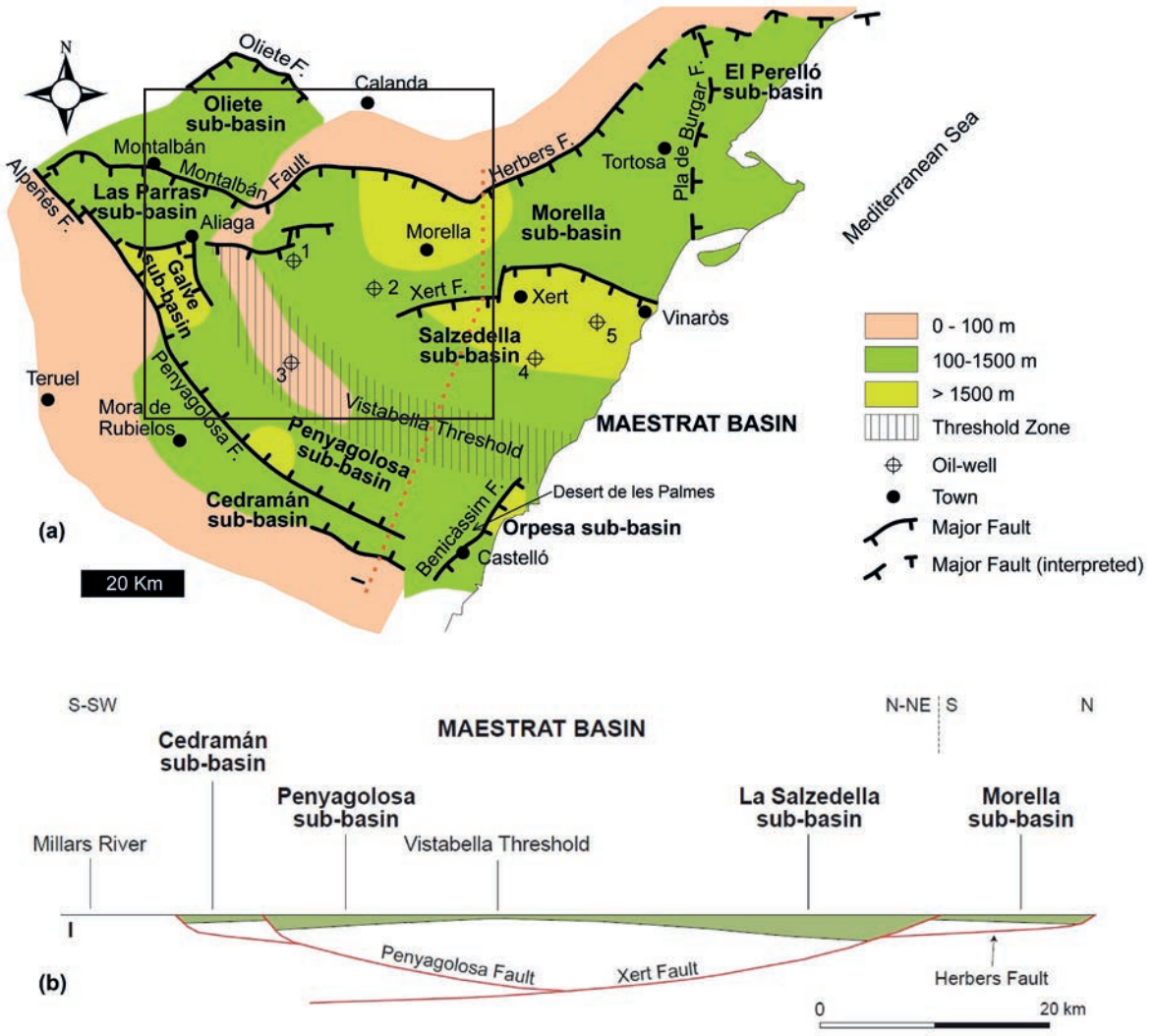

Figure 2.3. (a) Schematic structural map of the Maestrat basin, developed during the Late Jurassic-Early Cretaceous rifting event. It was divided into several sub-basins: Ol= Oliete sub-basin, Al=Aliaga sub-basin, Mo= Morella sub-basin, Pe= Perelló sub-basin, Ga= Galve sub-basin, Sa=Salzedella sub-basin and Pg= Penyagolosa sub-basin. Wells: 1= Mirambell-1, 2= Bovalar-1 and Bovalar-2, 3= Maestrazgo-2, 4= Salzedella-1, 5= Maestrazgo-1. The location of maps in Fig. 2.1 and 2.17 is shown. (b) Schematic section of the Maestrat basin. Modified from SALAS et al. (submitted).

2.4.3 Stratigraphy

The materials found in the study area, both the rocks filling the Late Jurassic-Early Cretaceous Maestrat basin and in its substratum, are divided in four supersequences which are bounded by regional unconformities (Fig. 2.4, D1-D5): the Upper Permian-Triassic, the Jurassic, the Lower Cretaceous and the Upper Cretaceous, deposited during the different rift and post-rift events occurred in the Iberian Rift System (SALAS and CASAS, 1993).

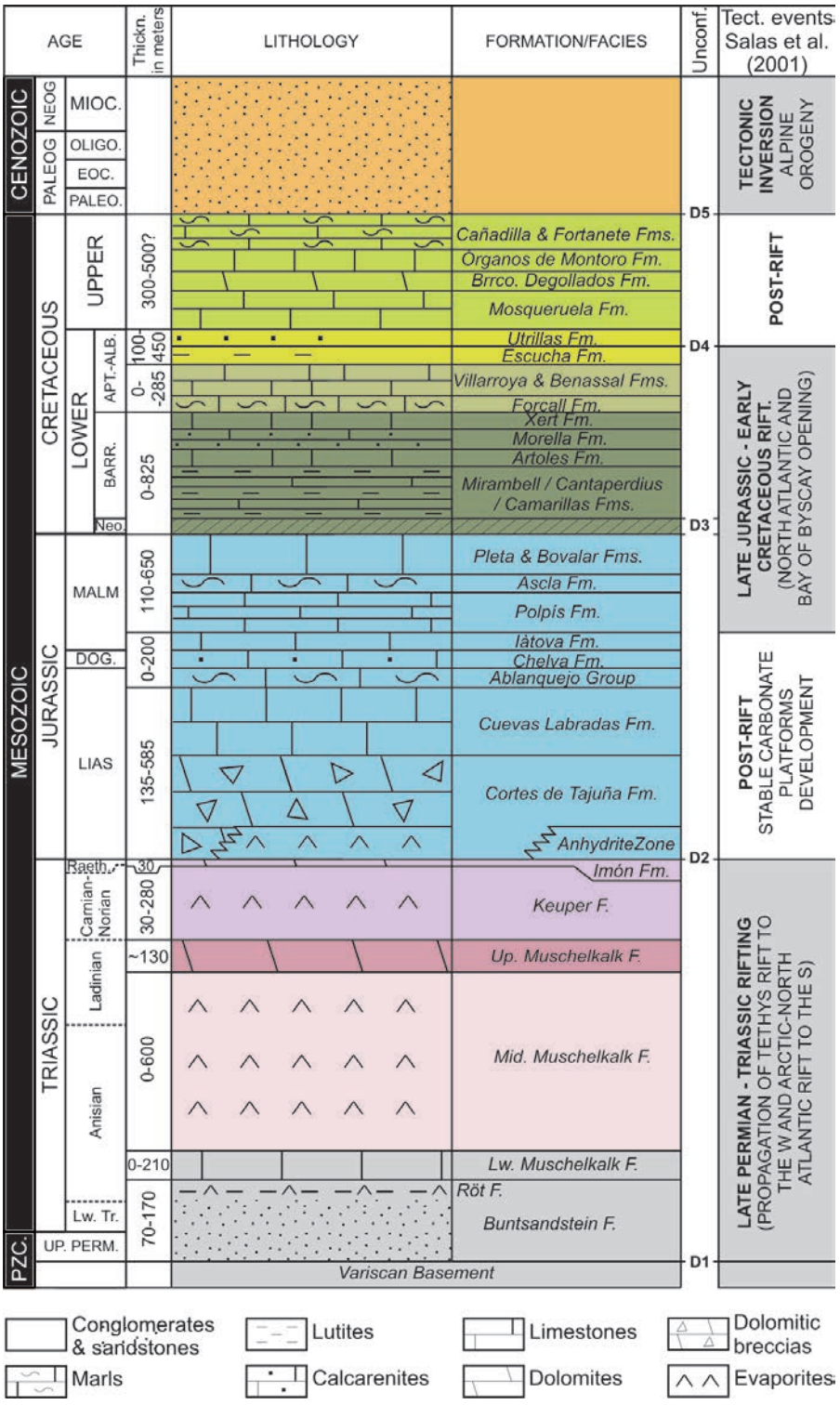

Figure 2.4. Generalized stratigraphic sequence of the Eastern Salzedella sub-basin. Modified from NEBOT and GUIMERÀ (2016a,b), after SALAS (1987), SALAS et al. (2001), AURELL et al. (1992) for the Lias, and BOVER-ARNAL et al. (2015) for the Barremian–Aptian boundary. Thickness values are based on the exploration wells (Fig. 2.5, MARTÍNEZ-ABAD, 1991) and from the stratigraphic sections in Fig. 3.5.

Upper Permian-Triassic (First rifting event)

The Triassic deposited in the substratum of the Late Jurassic-Early Cretaceous Maestrat Basin is represented in Germanic facies. The lowermost units (Buntsandstein and Lower Muschelkalk) are only known by the exploration wells (LANAJA, 1987; MARTÍNEZ-ABAD, 1991), as they only crop out in some punctual locations of the Maestrat basin.

Buntsandstein facies (RAMOS, 1979; LÓPEZ-GÓMEZ and ARCHE, 1992) *Late Permian-Anisian*. This facies only crops out in the study area in the Montalbán anticline. It is constituted by red to ochre clays and sandstones, deposited in a continental fluvial environment. The thickness of the Buntsandstein facies varies from 70 and 170m in the exploration wells (Fig. 2.5) available in the study area (LANAJA, 1987; MARTÍNEZ-ABAD, 1991). An hiatus is found in the Permian-Triassic boundary, which represents nearly 10M.y. of non-deposition or erosion (BOURQUIN et al., 2007).

Lower Muschelkalk facies (LÓPEZ-GÓMEZ and ARCHE, 1992) *Anisian*. It is composed by an alternation of limestones and dolostones, although the latter are predominant. It includes some intercalations of clays. It represents the first transgression of the Tethys, when marine sediments prograded towards the west and covered the basin for the first time, as it consists of intertidal an d shallow shelf deposits (LÓPEZ-GÓMEZ et al., 1993, 1998). The Lower Muschelkalk in the Maestrat basin attains thicknesses of between 0 and 210m (Fig. 2.5, MARTÍNEZ-ABAD, 1991).

Middle Muschelkalk facies (LÓPEZ-GÓMEZ and ARCHE, 1992) *Anisian-Ladinian*. It is formed by an alternation of halite, anhydrite and clay, with some intercalations of grey marls at its base. It has a distal alluvial–sabkha origin (LÓPEZ-GÓMEZ et al., 1993, 1998). The exploration wells (Fig. 2.5, MARTÍNEZ-ABAD, 1991) and the seismic profiles show that its thickness can vary between nearly 0m to more than 1000m in the salt accumulations.

Upper Muschelkalk facies (LÓPEZ-GÓMEZ and ARCHE, 1992) *Ladinian*. This facies is composed of an alternation of limestones and dolostones with some intercalations of clays deposited in intertidal and shallow platforms (LÓPEZ-GÓMEZ et al., 1993, 1998). It presents a nearly constant thickness of about 130m in all the study area and in the Maestrat basin (MARTÍNEZ-ABAD, 1991).

Keuper facies (ORTÍ, 1974, VARGAS et al., 2009) *Carnian-Norian*. It is formed by marls and red clays that contain gypsum of shallow marine origin, and sandstones of fluvial to coastal origin (Fig.2.6a). It can also contain intercalations of limestones and dolostones. Its thickness varies from 30 to 280m in the study area (MARTÍNEZ-ABAD, 1991).

Imón Fm. – (GOY et al., 1976; GOY and YÉBENES, 1977) *Norian-Rhaetian*. This formation is composed of tabular dolostones (Fig. 2.6b) that represent shallowing sequences. It is a transgressive unit that was deposited in intertidal and shallow platforms. It has a nearly constant thickness of about 30m.

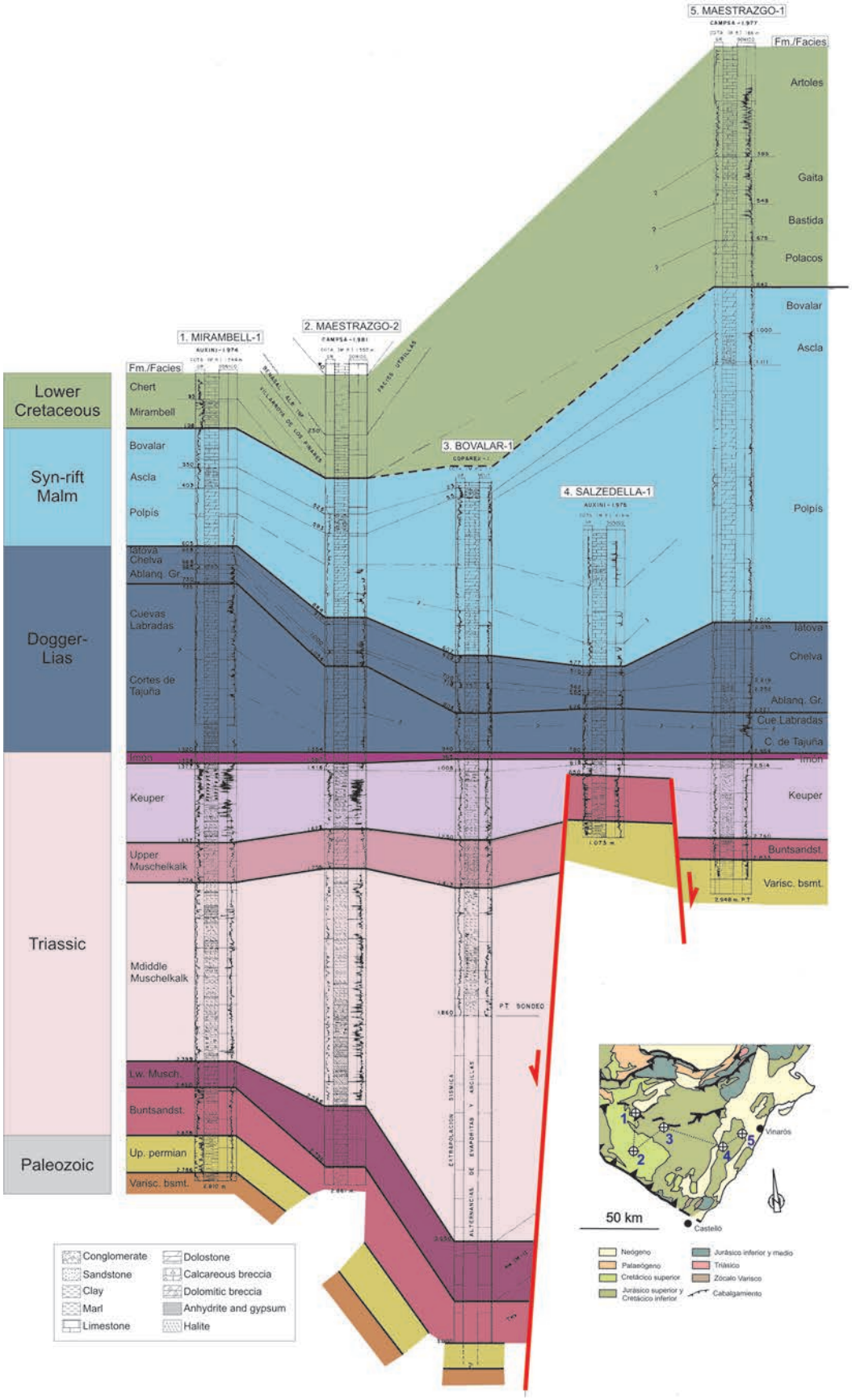

Figure 2.5. Exploration-wells interpretation and correlation. Modified from SALAS (unpublished), after MARTÍNEZ-ABAD (1991).

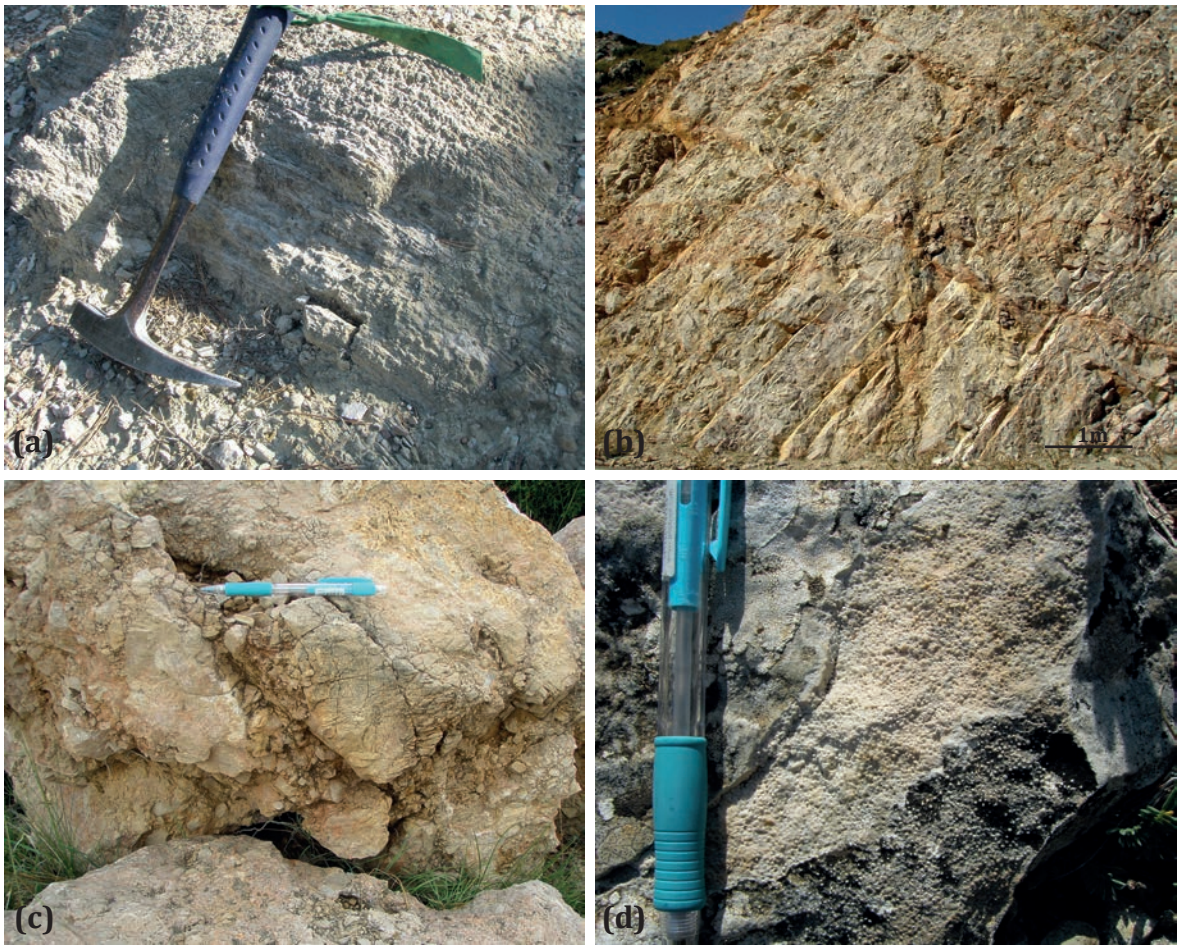

Figure 2.6. (a) Keuper facies gypsum, (b) Imón Fm. Dolomites (c) Cortes de Tajuña carbonatic breccias (d) Cuevas Labradas oolithic grainstone.

Early-Middle Jurassic (First post-rift event)

The Jurassic rocks of the Iberian Chain are mostly composed of marine limestones and marls, with only some lacustrine intercalations at the end of the Jurassic sequence (Pürbeck facies).

Lécera Fm. or "Anhydrite zone" (CASTILLO HERRADOR, 1974; GÓMEZ and GOY, 1998) *Rhaetian-Hettangian*. It is an aggradational unit composed of evaporites (massive and laminated gypsum) with limestone and dolostone intercalations. It is equivalent in age to the breccias of the Cortes de Tajuña Fm. This unit does not crop out in the study area, where the Cortes de Tajuña Fm directly overlies the Imón Fm. but it appears in the exploration wells (Fig. 2.5).

Cortes de Tajuña Fm. (GOY et al., 1976) *Hettangian*. This Formation is composed of crystalline dolostones and angular dolomitic breccias (Fig. 3.6c). Occasionally it contains limestones and carneols. The boundary between both facies, the crystalline and the breccia, is usually irregular. These are massive or poorly layered and unconformably overlie the previous units. It would have been deposited in a tidal flat, in a hypersaline environment or sabkha.

Cuevas Labradas Fm. (GOY et al., 1976) *Late Sinemurian- Pliensbachian*. It is contituted by shallowing sequences composed by a lower marly subtidal unit, followed by oolithic grainstone (Fig. 3.6d) with cross bedding, and by an upper unit of limestones and dolostones. It was deposited in a carbonate platform in shallow peritidal to subtidal environment (GÓMEZ and GOY, 2004).

Ablanquejo Group (GOY et al., 1976) *Late Pliensbachian-Toarcian*. It is composed of three formations, which are, from base to top: Cerro del Pez Fm., Barahona Fm. and Turmiel Fm (Fig. 2.7). The three formations are mostly marly, with some intercalations of calcarenites that indicate marine transgressions.

Summing up, the Lias can be divided into a calcareous lower one (Cortes de Tajuña and Cuevas Labradas fms.) with thicknesses between 135 and 585m, and a marly upper one (Ablanquejo Group), whose thickness varies less, from 54m to 105m (Fig. 2.5; MARTÍNEZ-ABAD, 1991).

Chelva Fm. (GÓMEZ and GOY, 1979) *Toarcian-Oxfordian*. This formation is composed of a calcarenite with brachiopods and belemnites. At its base it has a ferruginous or phosphate oolith (Fig. 2.7a). It was deposited in a carbonatic platform ramp environment. Its thickness varies from 40 to 90m in the studied area, although it reaches 184 m more to the west, in the Maestrazgo-1 well (Fig. 2.5; MARTÍNEZ-ABAD, 1991).

Figure 2.7. (a) contact between Chelva Fm (left) and Turmiel Fm. (right). (b) Contact between Turmiel Fm. (left) and Barahona Fm. (right). (c) Contact between Barahona Fm (left) and Cerro del Pez Fm. (right). Outcrops in la Ginebrosa thrust sheet (See Fig. 2.17 for location).

Iàtova Fm. (GÓMEZ, 1979; GINER, 1980; CANÉROT, et al., 1984) *Middle Oxfordian*. It is composed of micritic and bioclastic limestones with abundant sponge fragments. It also contains ammonites, belemnites and abundant foraminifera. A ferruginous oolith developed at its base, which corresponds to a condensed level representing the Callovian to Oxfordian transition. It was deposited in a shallow carbonate platform rich in sponges.

The Iàtova Fm. is the last post-rift unit of the Early to Middle Jurassic post-rift event, having a nearly constant thickness of about 25m (Fig. 2.5; MARTÍNEZ-ABAD, 1991). The Late Jurassic-Early Cretaceous rifting event started with the deposition of the Polpís Fm. carbonates.

Figure 2.8. (a) Tabular limestones of the Polpís Formation, (b) Lower Kimmeridgian Ataxioceratin Ardescia ammonites (Polpís Fm.), (c) Algal lamination of the Pleta Formation, (d) Collecting strike-and-dip data in the Bovalar formation.

Late Oxfordian-Middle Albian (Second rifting event)

Polpís Fm. (SALAS, 1987) *Early Kimmeridgian*. It is formed by tabular limestones (mudstone), with decimetric stratification, thickening upwards (Fig. 2.8a). Only some bioclast accumulations, brachiopodes, echinoderms, ammonites (Fig. 2.8b) and locally sponge spicules can be recognized. It presents a very homogeneous facies and extends regionally. Its thickness varies from 50m in the Ginebrosa anticline, in the northern external part of the basin (SALAS, 1989), to 200 m in the Mirambell-1 well and to nearly 900m in the Maestrazgo-1 well, located in the depocenter of the basin (Fig. 2.5; MARTÍNEZ-ABAD, 1991). This formation was deposited in a wide low dip carbonate platform ramp.

Mas d'Ascla Fm. (SALAS, 1987) *Late Kimmeridgian-Early Tithonian*. This formation is composed of clayey and silty mudstones, well laminated and with intercalations of marls rich in organic matter. It has scarce fossil content. Its thickness varies from 32 to 110m in the exploration wells (Fig. 2.5; MARTÍNEZ-ABAD, 1991), and up to 300m in the basin depocenter (SALAS, 1989). It was deposited in the distal part of a carbonate platform.

Bovalar Fm. (SALAS, 1987) *Late Kimmeridgian-Berriassian*. It is composed of an alternance of wackestones-grainstones with decimetric to metric stratification, which display shallowing-upwards sequences. Its upper part is more micritic and marly. It is oolitic, and can contain corals and Nerineids. It can reach thicknesses of 925m (SALAS, 1989). The calcarenitic layers correspond to high energy marginal bars while the micritic ones correspond to lagoon facies.

Pleta Fm. (SALAS, 1987) *Late Kimmeridgian-Berriassian*. Grey mudstone and dolomicrites with decametric to centimetric stratification, thinning upwards, and cryptoalgal lamination (Fig. 2.8c). It was deposited in a carbonate tidal flat.

The Bovalar and the Pleta formations appear intercalated and pass laterally and vertically one to each other (Fig. 2.8d) (SALAS, 1989).

The Barremian (Lower Cretaceous) units appear directly overlying the Jurassic. The Berriassian to Hauterivian units were not deposited or were eroded in the study area, as a hiatus of this age exist. These units are only present in the Maestrat basin depocenter, located in the Salzedella sub-basin (SALAS, 1987), east of the studied area.

The Barremian and Aptian formations can be divided into two units, the continental (Weald facies) and the marine (Urgon facies). The continental ones (Weald facies) include the Camarillas, Cantaperdius and Mirambell formations (Early Barremian). These units pass laterally one to each other, and all of them pass vertically and laterally to the Artoles Formation, which constitutes the transition to the marine units. The marine units (Urgon facies) are composed of the Artoles, Morella and Xert fms. (Upper Barremian) and the Forcall, Villarroya de los Pinares and Benassal fms. (Aptian) (BOVER-ARNAL et al., 2016). Continental sediments were also deposited at the end of the Lower Cretaceous, represented by the Escucha and the Utrillas formations.

Camarillas Fm. (CANÉROT, 1974; SALAS, 1987) *Early Barremian*. Its base contains red to brown sandstones with clay and limestone intercalations which in the middle of the series contain charophytes. The lower part is composed of red lutites with intercalations of sandstone bodies, usually channeled with cross bedding. In was deposited in a fluvial environment with tidal influence in its upper part.

Cantaperdius Fm. (SALAS, 1987) *Early Barremian*. It is composed of an alternation of mudstone and wackestone limestones with charophytes, vertical bioturbation, nodulose marls and lutites, displaying flooding sequences (Fig. 2.9a). This formation was deposited in a lacustrine environment with events of subaereal exposure.

Mirambell Fm. (CANÉROT et al., 1982) *Early Barremian*. It is composed of two sequences which contain, from bottom to top, a first level of quartzitic sandstones and conglomerates with cross bedding, a level of green marls more or less sandy with intercalartions of marly limestones or sandstones (Fig. 2.9b), and a last level of beige sandy to coquina limestones with benthonic or dasycladaceans foraminifera. It reaches 60m thick in the surroundings of Mirambell and Forcall and about 100m in the surroundings of Ladruñán. It was deposited in a lacustrine environment.

Figure 2.9. (a) Nodulose carbonate with bioturbation perpendicular to bedding from the Cantaperdius Fm. (b) Marls of the Mirambell Fm. (c) Rich in ostrids marls from the Artoles Fm. (d) Cross-bedding in the Xert Fm.

Artoles Fm. (SALAS, 1987) *Barremian*. It is composed of an alternation of marls and limestones, with sandy limestones and some limestones levels containing a huge ammount of ostreids (Fig. 2.9c). It reaches about 750m thick in the basin depocenter (BOVER-ARNAL et al., 2016). This formation developed in a shallow carbonate platform, containing facies from lagoon to marginal bars and more distal facies.

Morella Fm. (CANÉROT et al., 1982) *Late Barremian*. This formation if constituted by red lutites and clays with intercalations of channeled sandstone bodies that can contain cross bedding (SALAS, 1987). It includes some intercalations of bioclastic limestones and vertebrate remains. It reaches a maximum thickness of 80m. This formation was deposited in a deltaic environment controlled by tides.

Xert Fm. (CANÉROT et al., 1982; SALAS, 1987) *Late Barremian*. Alternation of limestones, beige to brown marls and marine sandstones with cross-bedding (Fig. 2.9d). Limestones are distributed in decimetric to centimetric bars that display a thickening-upward sequence. The limestone bars are sandy at the bottom and bioclastic at the top of the formation. It is characterized by the presence of Palorbitolina lenticularis, the abundance of echinoderms, benthonic foraminifera and calcareous algae. Its thickness varies approximately between 60 and nearly 180m. It was deposited in an internal carbonate platform with orbitolinid-rich sandy bars.

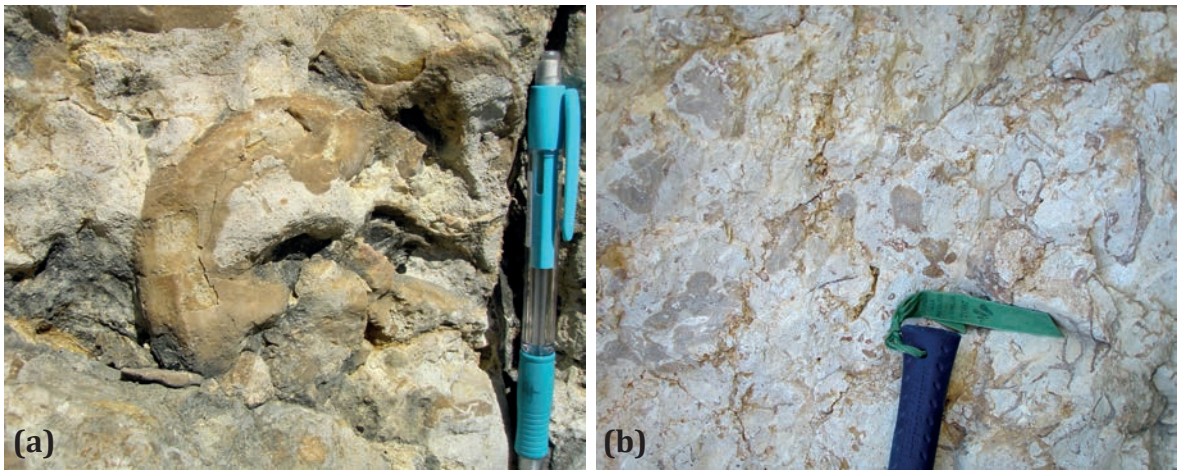

Figure 2.10. (a) Toucasia in the Viallarroya Fm. (b) Rudists and corals in the Benassal Fm.

Forcall Fm. (CANÉROT et al., 1982; SALAS, 1987) *Late Barremian-Early Aptian*. Three members can be differentiated in Forcall, two are composed of marls, and are separated by the third member composed of metric bars of beige bioclastic limestones. The lowest marly member contains abundant fossil fauna (Plicatula, Palorbitolina lenticularis, molluscs, ammonites, corals, brachiopods...). The upper marly member is more argillaceous and homogeneous. The limestone bar of the intermediate member disappears eastwards. It reaches its maximum thickness, more than 100m in the surroundings of Morella, decreasing laterally in all directions. This formation was deposited in an open carbonate platform.

Villarroya de los Pinares Fm. (CANÉROT et al., 1982; SALAS, 1987) *Early Aptian*. This formation is composed of grey to beige bioclastic, oolitic and micritic limestones, with intercalations of marls and marly limestones. Some layers are nodulose. It is characterized by the presence of Toucasia (Fig. 2.10a). It also contains Orbitolina lenticularis, corals, bivalves, echinoderms... A hardground is found in its top. Its thickness varies widely, from 50m in its type section, in the surroundings of Villarroya de los Pinares, to 300 (CANÉROT, 1974) or 500m (SALAS, 1987) in the Orpesa sub-basin (Fig. 2.3) It was deposited in a carbonate platform with bars.

Benassal Fm. (CANÉROT et al., 1982; SALAS, 1987) *Late Aptian-Early Albian*. It is constituted by up to three T-R sequences formed at their base by marls with ammonites and brachiopods, and a level of grey limestones with decimetric to metric stratification with some micritic and calcarenitic intercalations. It contains rudists, corals, echinoderms, bivalves, Orbitolina Texana and Parva...(Fig. 2.10b) Its thickness also varies widely, from 80-200m to nearly 1500m in the Orpesa sub-basin (BOVER-ARNAL et al., 2009; MARTÍN-MARTÍN et al., 2013). It was deposited in an internal carbonate platform.

Escucha Fm. (AGUILAR et al., 1971; CERVERA et al., 1976; QUEROL et al., 1992; SALAS, 1987) *Early-middle Albian*. It has been divided into three members: i) the Barriada Mb. which is composed of an alternation of lutitic and marly layers with intercalations of lignite and some sandstone and sandy bioclastic limestone bodies, ii) the Regachuelo Mb. composed of carbonatic and silty clays and thin intercalations of sandstones that can contain a huge concentration of lignite at the base (Fig. 2.11a), and

iii) De la Orden Mb. composed of channeled bodies of sandstone. Its thickness can vary between 100 and 260m (PARDO, 1974). This formation was deposited in a deltaic plane environment, controlled by the fluvial action.

Late Albian-Maastrichtian (Second post-rift event)

The deposition of the Utrillas Fm. represents the beginning of the post-rift event during the end of the Early Cretaceous, which extended during the Late Cretaceous. Its expansive nature makes it to unconformably overlie the previous syn-rift units.

Utrillas Fm. (AGUILAR et al., 1971; SALAS, 1987) *Late Albian*. It is composed of white to purple poorly cemented and compacted micaceous to quartzitic sand. It displays cross-bedding (Fig. 2.11b) and can contain intercalations of lutites and kaolinite. Some intercalations of carbonatic lutites, carbonatic sandstone and brown calcarenite with bioturbations appear towards the top of this formation. Its global thickness varies between 15-185m (PARDO, 1974). It was deposited in a fluvial environment.

Mosqueruela Fm. (CANÉROT et al., 1982) *Late Albian-Cenomanian*. It is composed of three members, each one formed by a positive lithosequence, containing marls and sandstones at the base and limestones at the top (Fig. 2.12a). Its global thickness varies between 180-200m. The limestones have metric to centimetric stratification. This formation was deposited in a shallow marine environment.

Barranco de los Degollados Fm. (CANÉROT et al., 1982; GIL et al., 2004) *Late Cenomanian-Middle Turonian*. It is composed of white dolostones (Fig. 2.12b), finely crystallized and in small banks, followed by grey to beige more massive dolostones. Its thickness is about 40m. It was deposited in a shallow marine environment.

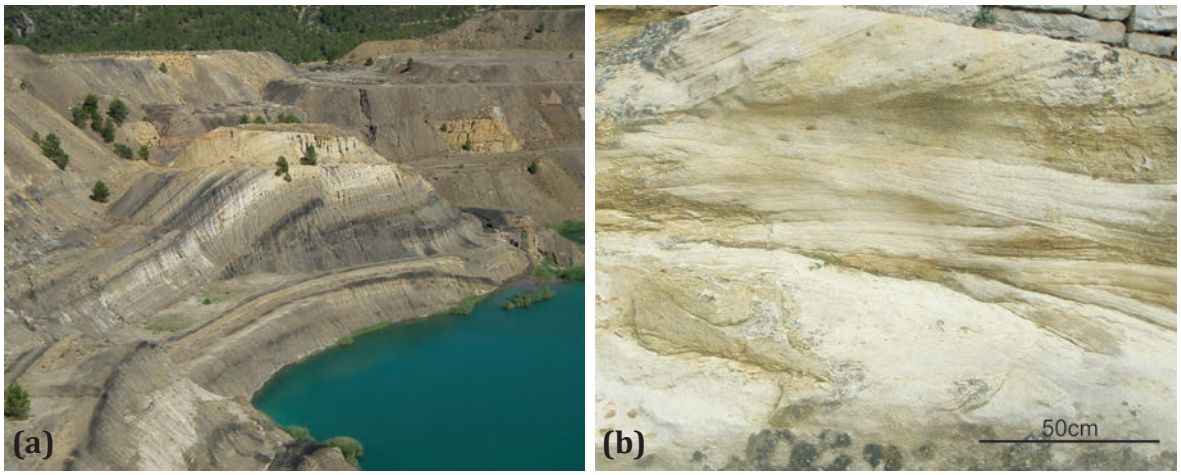

Figure 2.11. (a) Escucha Fm. quarry, which was exploited to obtain coal, concentrated in the black layers. (b) Cross-beding in the Utrillas sandstones.

Órganos de Montoro Fm. (CANÉROT et al., 1982) *Coniacian*. It is formed of white and grey limestones in thin layers alternating with marls. It contains miliolids, lacasina, rudists, rhodoliths, bioturbation and some vegetal rests. Its thickness was estimated in 80m in the type section, although it can vary from 0 to 200m. This formation was also deposited in a shallow marine environment.

Cañadilla and Fortanete fms. (CANÉROT et al., 1982) *Santonian-Campanian-Maastrichtian*. Both formations are composed of an alternation of marls and limestones with black intraclasts (Fig. 2.12c) and nodulose levels that indicate that they were deposited in a shallow marine to coastal (Cañadilla Fm.) to lacustrine and palustrine (Fortanete Fm.) environments. The Cañadilla Fm. is a bit more massive and grey than the Fortanete Fm., which is more marly and white. Their thickness of the Cañadilla Fm. is of about 50m in the outcrops in the area of Villarluengo-Fortanete-Mosqueruela, while the Fortenete Fm is about 30m thick.

The thickness of the Upper Cretaceous package is difficult to stablish in all its outcrops, as its top hardly ever crops out, as it was eroded, or thrusted, or it is covered by Cenozoic rocks.

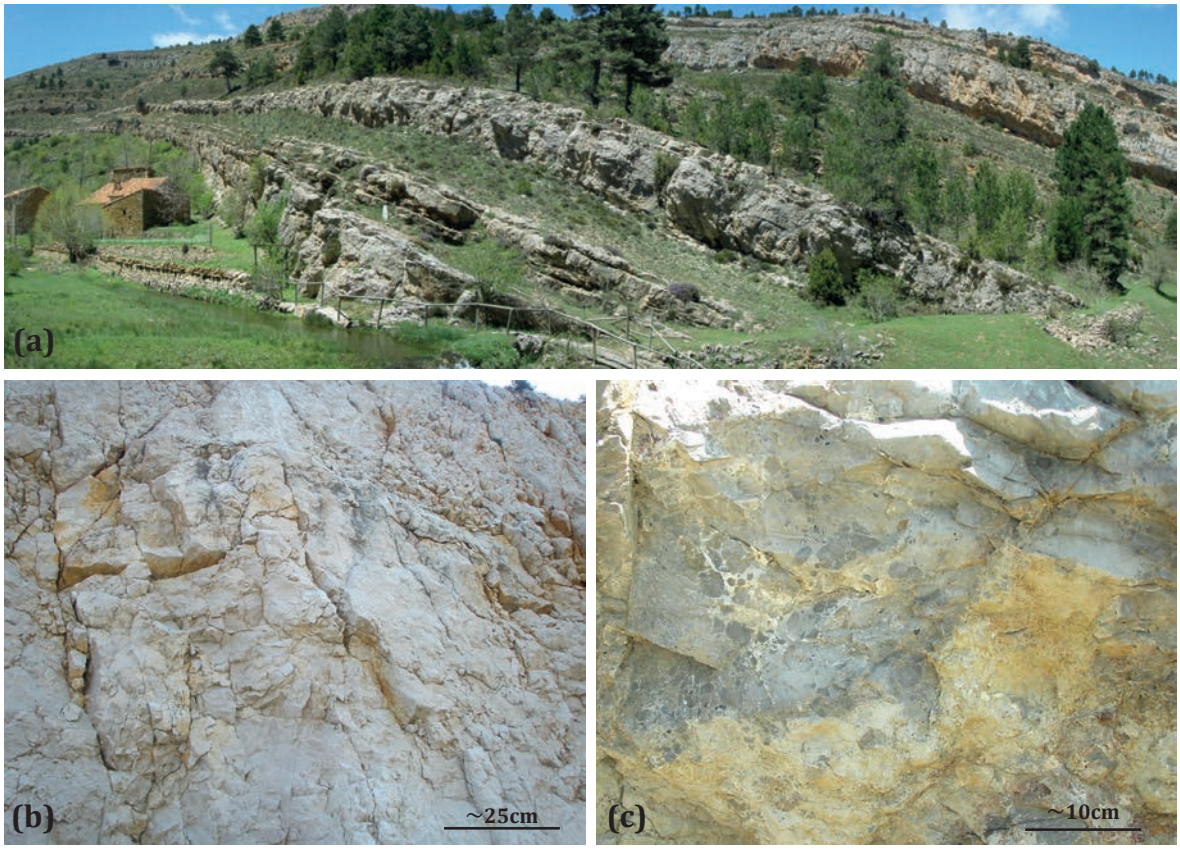

Figure 2.12. (a) Mosqueruela Fm. above the Utrillas and the Escucha fms (in the left part of the image, below the house). (b) White dolostones of the Barranco de los Degollados Fm. (c) Intraclasts in the Cañadilla-Fortanete formations.

Cenozoic

The Cenozoic rocks are composed mostly of conglomerates, sandstones and lutites, with some intercalations of continental limestones and gypsum. These detrital sediments were deposited in a continental environment, in alluvial fans attached to the emergent reliefs that registered the Cenozoic contraction. The carbonates were deposited in lacustrine environments, generated in the more distal parts.

2.4.4 Cenozoic Contraction: basin inversion

Since the Santonian (83Ma) and during the Cenozoic, Iberia and Europe converged (Fig. 2.2), (ZIEGLER, 1988; ROEST & SRIVASTAVA, 1991; OLIVET, 1996; ROSENBAUM et al., 2002). During this period the Mesozoic basins were inverted and the Mesozoic extensional structures were reactivated as contractional structures (ÁLVARO et al., 1979; SALAS et al., 2001). The timing and the amount of inversion was different depending on their location in the Pyrenees, the Iberian Chain or the Betics. In the Iberian Chain, contraction began in the Late Eocene (SALAS et al., 2001), although in the Late Cretaceous some activity is deduced, as a transition from marine limestones (Órganos de Montoro Fm.) to lacustrine continental rocks (Cañadilla and Fortanete Fms.) occurs, related to an eustatic fall in the Campanian (HAQ et al., 1988). The Cenozoic contraction lasted until the Late Oligocene-Early Miocene in the eastern part of the Iberian Chain (GONZÁLEZ et al., 1998).

The Iberian Chain: The Iberian Chain is an intraplate, double vergent thrust-belt, resulting from the Cenozoic contractional inversion of the Mesozoic Iberian Rift System. The Iberian Chain, the Linking Zone and the Catalan Coastal Chain should be considered as a whole, as they experienced a very similar extensional and contractional evolution (Fig. 2.2, 2.13; GUIMERÀ, 2004). The elevated topography of the Iberian Chain –over 1000m asl in most of their extension–, and a large and negative Bouguer anomaly below it (reaching -110mGal, SALAS and CASAS, 1993; GUIMERÀ et al., 2016), indicate a crustal thickening of at least 6km, which is the result of the Cenozoic contraction (GUIMERÀ et al., 2010). The velocity-depth model obtained from a NE-SW refraction/wide-angle reflection seismic transect is consistent with the Bouguer gravity anomaly (SEILLÉ et al., 2015, MANCILLA and DIAZ, 2015; GUIMERÀ et al., 2016). This velocity-depth model indicates that the crustal thickness reaches values of 40km (GUIMERÀ et al., 2010) or between 32 to 44km (GUIMERÀ et al., 2016), and becomes thinner towards the NE (30km thick below the Iberian Chain-Ebro basin boundary) and towards the SW (Tajo Basin). This data combined with magnetotelluric and gravity data showed that this crustal thickening is concentrated in the upper crust (SEILLÉ et al., 2015), which is in agreement with GUIMERÀ and ÁLVARO (1990), who interpreted that the contractional faults only involved the upper crust and suggested a detachment level at a depth of 7-11km. The uplifting of the Iberian Chain, which generated the present day elevated topography is the result of the crustal thickening resulting from the Cenozoic contraction event.

The estimated shortening in the western part of the Iberian Chain is 41km (18.9%) (GUIMERÀ, 2013), in which the Cameros basin fault accumulates most of the horizontal displacement (20-30km after CASAS-SAINZ, 1993; and 25-30km after GUIMERÀ, 2013) of the total shortening. In the eastern

part of the Iberian Chain shortening is of about 37km (13.9%) (GUIMERÀ, 2013), in which about 15km correspond to the Portalrubio-Vandellòs fold-and-thrust belt (GUIMERÀ, 2004).

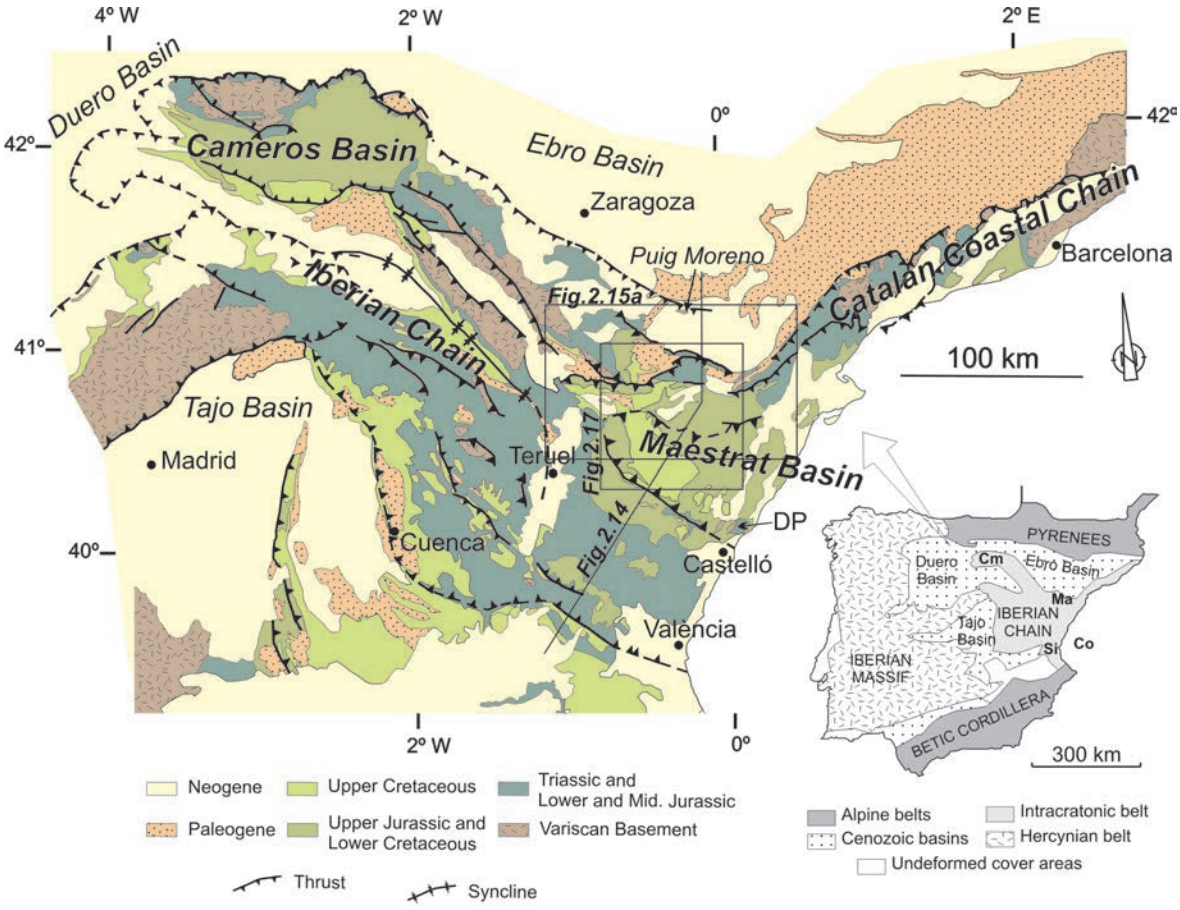

Figure 2.13. Simplified geological map of the NW-SE-trending Iberian Chain, the NE-SW-trending Catalan Coastal Chain and the E-W-trending Linking Zone located between them. DP-Desert de les Palmes. Its location in the Iberian Peninsula and is shown. Modified from GUIMERÀ et al. (2004, 2013)

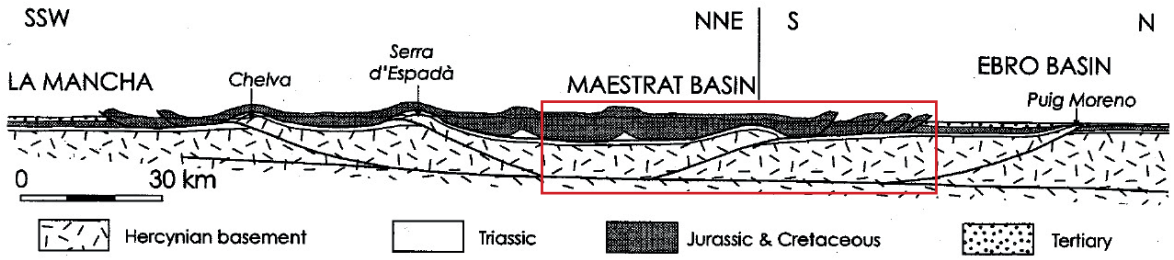

Figure 2.14. Schematic structural cross-section of the southeastern part of the Iberian Chain. See location in Fig. 2.13. The location of the studied area is highlighted with a box. Obtained from SALAS et al. (2001).

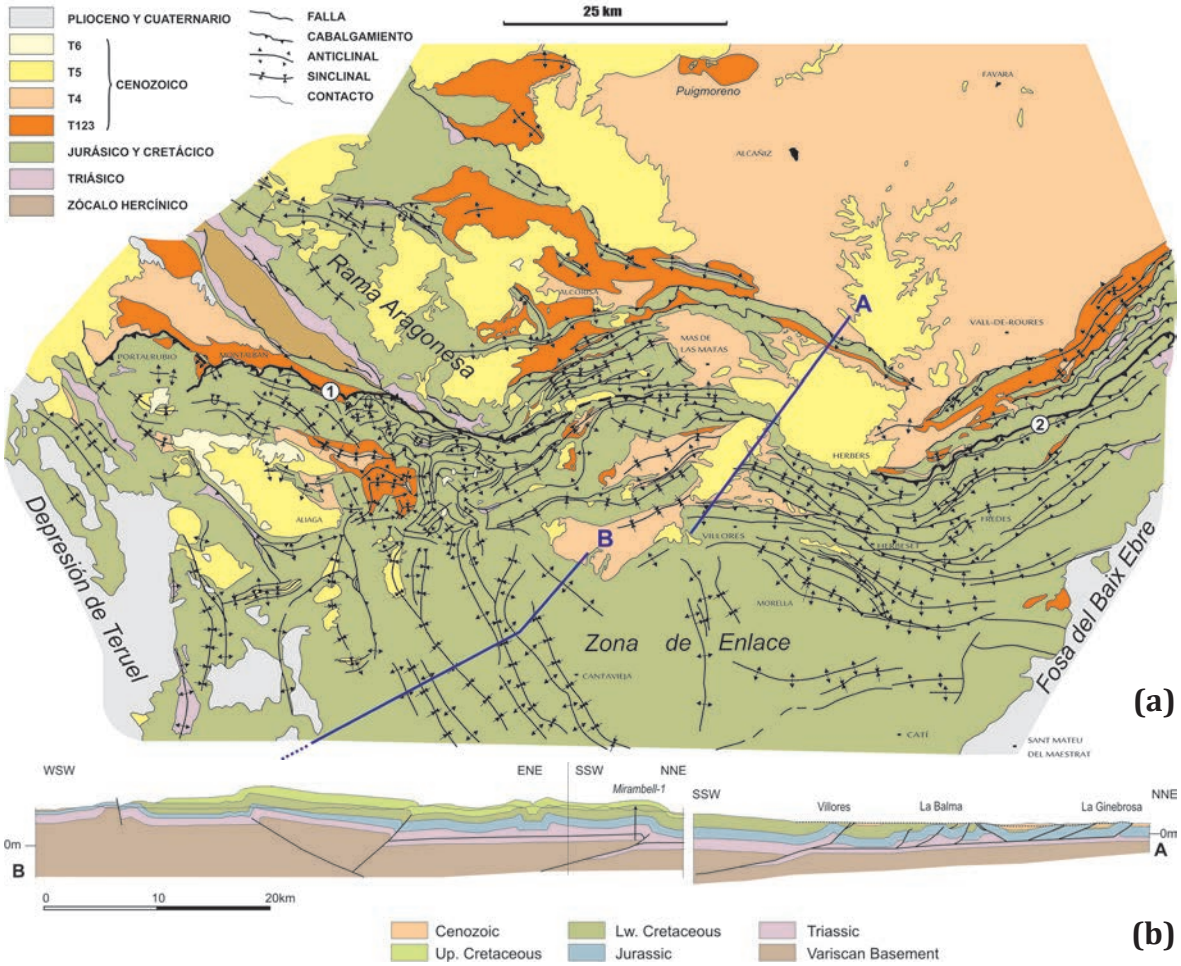

Figure 2.15. (a) Geological map of the Portalrubio-Vandellòs fold-and-thrust belt. 1- Utrillas or Muela de Montalbán thrust. 2- Herbers thrust. Modified from GUIMERÀ (2004). (b)Regional cross-section across the northern part of the Iberian Chain. Modified from GUIMERÀ (2013).

The Linking Zone: The Linking Zone is the result of the contractional inversion of the Late Jurassic-Early Cretaceous Maestrat basin. In the northern margin of the Linking Zone, the E-W-trending, N-verging Portalrubio-Vandellòs fold-and-thrust belt developed (GUIMERÀ, 1988), previously referenced by CANÉROT (1974) as the Portalrubio-Beceite fold-and-thrust belt, (Fig. 2.14, 2.15) detached in the Triassic evaporites (Middle Muschelkalk and locally the Keuper facies). The main orientation in this fold-and-thrust belt is roughly E-W, which is the predominant orientation of structures in the Linking Zone, although structures experience two virgations in which structures take a NE-SW trend (Fig. 2.15a), interpreted as the result of NE-SW left-lateral wrench faults in the Variscan Basement (SIMÓN, 1981; GUIMERÀ, 1988).

Southwards, towards the hinterland, the sole thrust of this fold-and-thrust system, involved the Variscan Basement (Fig. 2.14). The transition from thin to thick-skinned areas occurs in the Turmell Fault Zone (SALAS and GUIMERÀ, 1996), whose Cenozoic inversion would had generated the tectonic vertical step observed by GONZÁLEZ et al. (1994) and GUIMERÀ and SALAS (1996) between the uplifted

hanging-wall and the downthrown footwall of the fault zone, indicating that it was rooted in the Variscan Basement. The amount of inversion of this fault zone varies laterally. In the western sector, which separates the Galve and the Aliaga sub-basins, the normal fault is inverted, although in the easternmost segment, the extensional structure is conserved (SALAS and GUIMERÀ, 1996). South of the Turmell fault zone, the amount of internal deformation of the Mesozoic cover decreases and an almost flat-lying area is observed (CANÉROT, 1974; SIMÓN, 1982; GUIMERÀ, 1988), which corresponds to the topographically and tectonically elevated area above the basement involved area.

Inside the northern fold-and-thrust belt some synclinal cores represent relative geographic depressions that were filed with Cenozoic sediments (GONZÁLEZ, 1989). The syn-tectonic nature of these sediments permitted the dating of the Cenozoic contraction in the Linking Zone, which started during the Late Eocene and lasted until the Late Oligocene-Early Miocene (SALAS et al., 2001).

GUIMERÀ and ÁLVARO (1990) proposed a kinematic evolutionary model for the Iberian Chain in the eastern Iberian Peninsula, and a NNE- transport for the Linking Zone (Fig. 2.16). In this model, the cover structures are parallel to basement convergent wrench-faults, which are left-lateral, NE-SW-trending faults in the Catalan Coastal Chain and right-lateral, NW-SE-trending faults in the Iberian Chain. The deduced synchronism between structures of the different orientations, including the E-W-trending predominant structural trend in the Linking Zone, led them to interpret a roughly N-S shortening orientation.

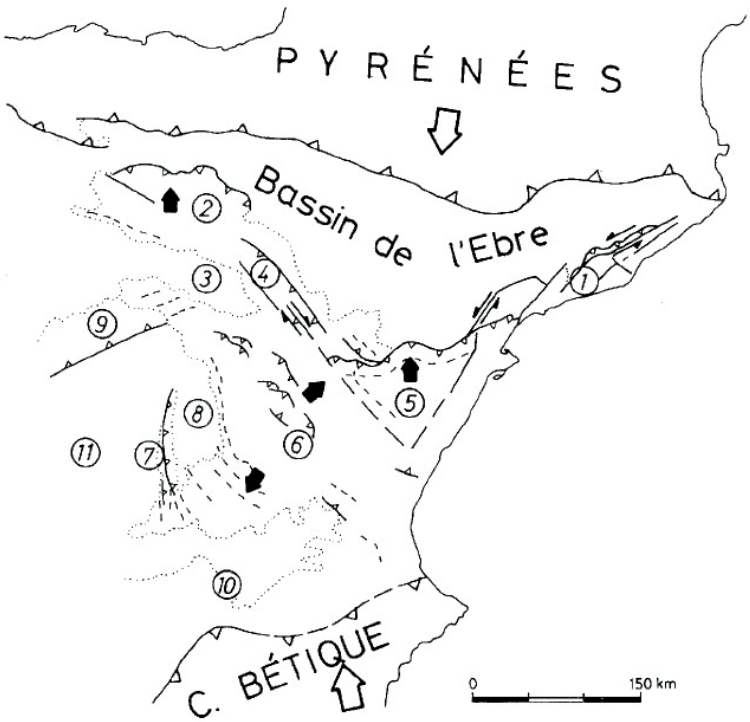

Figure 2.16. Kinematic model proposed by GUIMERÀ and ÁLVARO (1990) for the Iberian Chain. Black arrows indicate the sense of displacement of the Mesozoic cover, while white arrows indicate the sense of displacement of thrusts of the Pyrenees (Paleogene) and the Betic Chain (Early-Middle Miocene). Modified from GUIMERÀ and ÁLVARO (1990)

2.4.5 Neogene extension

Finally , during the Neogene, another extensional event occurred in the eastern side of Iberia, related with the rifting event that that originated the Valencia trough and coastal rifts (ÁLVARO et al., 1979; SIMÓN, 1982), during the Late Oligocene-Early Miocene. Extensional faults developed, trending NE-SW to NNE-SSW, and were superimposed to the contractional structures in the eastern part of the Pyrenees, the Catalan Coastal Chain and the easternmost part of the Iberain Chain (VEGAS et al., 1979).

2.5 DETAILED OBJECTIVES OF THE THESIS

As previously explained, this thesis studies the northern margin of the Maestrat basin in order to reconstruct its Mesozoic extensional structure, its influence on the subsequent Cenozoic contractional structure and its kinematic evolution. More specifically the objectives of this thesis are the following:

1.- Characterization of the Mesozoic extensional structure:

- Characterization of the Triassic structure and stratigraphy in the substratum of the Maestrat basin, taking advantage of the seismic profiles network and the exploration wells available in the southern part of the study area.

- Differentiation of the main sedimentary domains of the Late Jurassic-Early Cretaceous Maestrat basin and identification of the structures bounding them.

2.- Characterization of the Cenozoic contractional structure:

- Characterization of the structure of the transition between the thin-skinned and the thick-skinned areas, which coincides at the surface with a roughly E-W-trending vertical tectonic step.

- To establish the influence of the extensional structures on the contractional ones developed during the Cenozoic.

3.- Identification of the role of the Triassic evaporitic layers during the extension and the contraction, and characterization of the salt structures observed in the evaporites of the Middle Muschelkalk facies.

4.- To propose a kinematic evolution model for the northern margin of the Maestrat basin and the Portalrubio-Vandellòs fold-and-thrust belt, developed during its Cenozoic inversion.

- Estimation of the transport direction and the amount of shortening of the inverted northern margin of the Maestrat Basin, which includes the Portalrubio-Vandellòs fold-and-thrust belt.

- Reconstruction of the geometry of the basement fault, whose inversion generated the tectonic vertical step and the maintained tectonic relief observed, and subsequently, revision of the Turmell Fault Zone concept (SALAS and GUIMERÀ, 1996; GONZÁLEZ and GUIMERÀ, 1997).

2.6 METHODOLOGY

2.6.1 Data

Subsurface data: The seismic data comprises 29 2D seismic reflection profiles obtained in 1973 by Auxini, in 1979 by Campsa and in 1987-88 by Shell in the Maestrat Basin (Fig. 2.17). Four oil exploration wells were used to constrain the seismic interpretation and the construction of the cross-sections: Mirambell-1, drilled by Auxini in 1974; Maestrazgo-2, by Campsa in 1981; and Bovalar-1 and Bovalar-2, drilled in 1963 by Coparex. Some of the subsurface data were collected from the Instituto Geológico y Minero de España (SIGECO) and from the Archivo Técnico de Hidrocarburos web databases. The other seismic profiles were scanned from printed copies. Exploration wells interpretations from LANAJA (1987) and MARTÍNEZ-ABAD (1991) (Fig. 2.5) were considered.

Field data: More than 1900 strike-and-dip data were collected in the field; while another 1200 strike-and-dip data were obtained after drawing the geological contacts on the ortho-images and the 3D topographic contour lines in a georeferenced environment (Microstation), using in-house macros developed by FERNÁNDEZ (2004). The 3D visualization, using Global Mapper, of the ortho-images draped on the Digital Terrain Model and their comparison with data collected in the field allowed us to monitor the quality of the in-room dip data.

Previous geological maps: Previous geological maps were considered for elaborating the geological map (Fig. 2.17) (ALMELA et al., 1975; ALMERA et al., 1982; CANÉROT & LEYVA, 1972; CANÉROT & PIGNATELLI, 1972, 1977; CANÉROT et al., 1977; ESNAOLA & CANÉROT, 1972; GARCÍA DE DOMINGO & LÓPEZ OLMEDO, 1982; GAUTIER, 1978, 1979; GAUTIER and BARNOLAS, 1979; GONZÁLEZ, 1989; MARÍN & DUVAL, 1976; MARÍN et al., 1974; MARTÍN et al., 1972; NAVARRO-VÁZQUEZ et al., 1972; TRELL et al., 1979).

2.6.2 Methods

Seismic interpretation: Seismic profile images were converted to seg-y files using the IMAGE2SEGY Matlab® application (FARRAN, 2008) and interpreted using the KINGDOM SUITE® software in a georeferenced environment. The seismic interpretation was constrained with the Mirambell-1 well tops, previously converted to two-way-time (TWT) with the velocities obtained from its sonic-log (Δt), which was digitalized from a scanned copy. The seismic interpretation was later converted to depth in meters using the same velocities obtained from the Mirambell-1 sonic-log. The techniques used for depth to time conversion and vice versa, follow the methodology described by MENCOS (2010). A correction factor was applied to the sonic-log (Δt + 10%) in order to improve the fitting between the sonic log and the seismic profiles (MENCOS, 2010). The velocities obtained for the different packages defined were 1) Replacement velocity: 3250m/s, 2) Cretaceous: 4985m/s, 3) Jurassic and Imón Fm.: 5043m/s, 4) Keuper and Upper Muschelkalk: 3491m/s, 5) Middle Muschelkalk: 5441m/s.

Cross-sections construction: Nine cross-sections were constructed, normal to the different orientations of faults and axial fold planes observed in the study area, in order to better characterize the geometry of the differently oriented structures. Two of them contain the roughly NNE-SSW deduced displacement direction of the linking zone (GUIMERÀ and ÁLVARO, 1990), so after their restoration a shortening value was obtained. The other sections do not contain the transport direction, and so are not restorable, but they were unfolded using the flexural slip unfolding algorithm and the Upper Cretaceous base as a datum, in order to approximately display the geometry of the syn-rift units. Cross-sections are based on field data, and in the southern part of the study area they are also based in wells, and seismic interpretation converted to depth. Cross-section construction –using the Kink method– as well as unfolding –using the flexural-slip unfolding algorithm– were done both with Move software and manually with Microstation software. Area conservation was assumed for the evaporitic units.

An idealized cross-section of the entire northern margin of the basin was also elaborated by combining different cross-section segments, which allowed us to reconstruct, with the Move software, the geometry of the basement fault that better fits the generation of the elevated area during the Cenozoic inversion.

Geologic surfaces construction: Two geological surfaces, the depth to the base of the Jurassic and the depth to the top of the acoustic basement, and an isopach map showing the vertical thickness of the Middle Muschelkalk evaporitic facies were constructed with Gocad, based on the seismic interpretation converted to depth, the cross-sections and the well-tops of the exploration wells. The contours were later manually modified to better fit the structural trends and geometries, using the Microstation software.

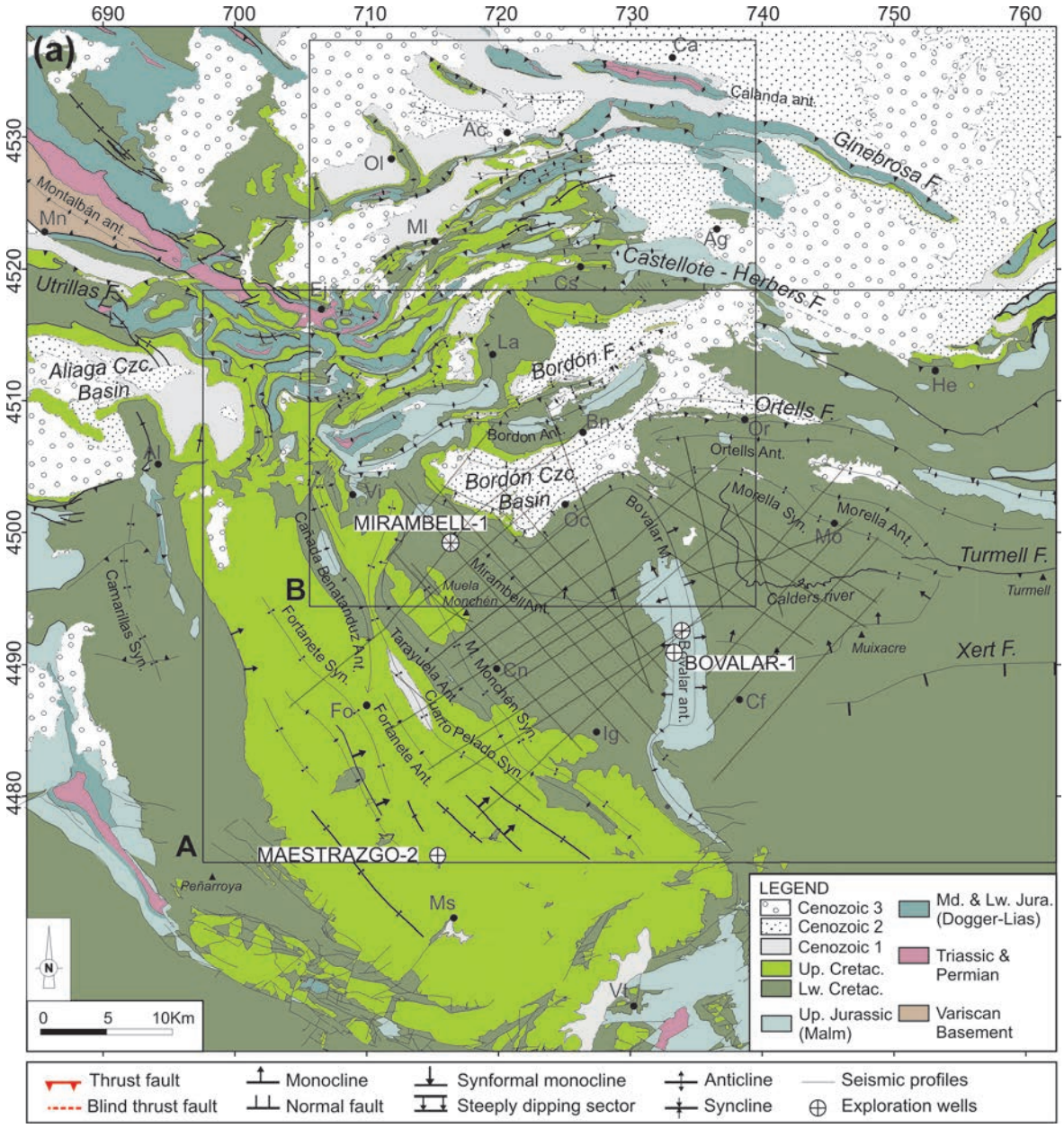

Figure 2.17. Geological map of the studied area. A. Area covered in the first paper (NEBOT and GUIMERÀ, 2016a). B. Area covered in the second paper (NEBOT and GUIMERÀ, 2016b). The location of the seismic profiles network and the location of the exploration wells is shown.

3. RESULTS

The structure resulting from the rifting and post-rifting events in the Late Jurassic-Early Cretaceous Maestrat basin, and in its substratum, was characterized using field data and the subsurface data available in the southern part of the study area (Fig. 3.1), as well as the structure resulting from the Cenozoic contractional inversion of the northern margin of the Maestrat basin.

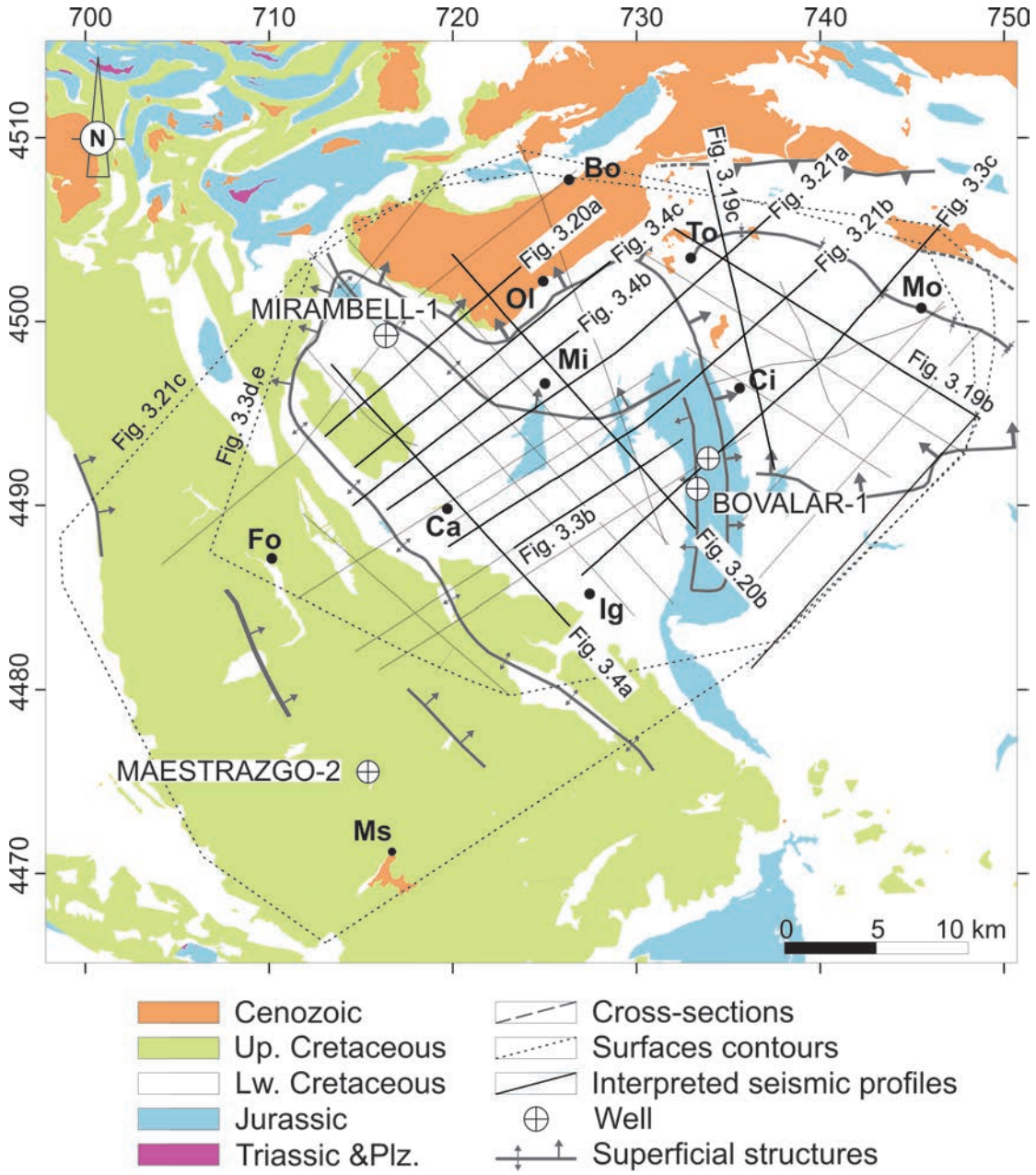

Figure 3.1. Location of the interpreted seismic profiles network and of the exploration-wells. The location of the sub-surface data available is also shown in Fig. 2.17.

3.1 DESCRIPTION OF THE SEISMIC FACIES OBSERVED IN THE SEISMIC PROFILES

Four seismic facies were differentiated in the Triassic rocks (Fig. 3.2): (1) the Acoustic Basement (Bs) includes the Lower Muschelkalk, the Buntsandstein and the Variscan Basement, although these units cannot be differentiated in the seismic profiles, as the entire package displays a chaotic seismic facies. The top of the Acoustic Basement is characterized by a couple of seismic reflectors of almost constant thickness. (2) The Middle Muschelkalk (TrM2) is characterized by nearly transparent seismic facies. Above it, (3) the Upper Muschelkalk (TrM3) is composed of three parallel seismic reflectors of near-constant thickness. Finally, (4) the Keuper (TrK) is also a nearly transparent unit although it locally contains some parallel reflectors.

The top of the Keuper facies, and base of the Jurassic package, is reflected in the seismic as a couple of continuous and parallel reflectors of constant thickness (Fig. 3.2). The uppermost Triassic Imón Fm. should be located below the Jurassic but it is too thin (about 30 m) to be recognized in the seismic profiles. The Jurassic (J) package presents at its base a nearly transparent facies, with some discontinuous reflectors, which is probably the seismic response to the massive dolomitic breccia of the Cortes de Tajuña Fm, and locally, to its equivalent in age Lécera Fm. or "Anhidrite Zone" (Fig. 2.4), as some anhydrite is observed at the base of the Jurassic in some exploration wells (Fig. 2.5, Mirambell-1 and Maestrazgo-1).

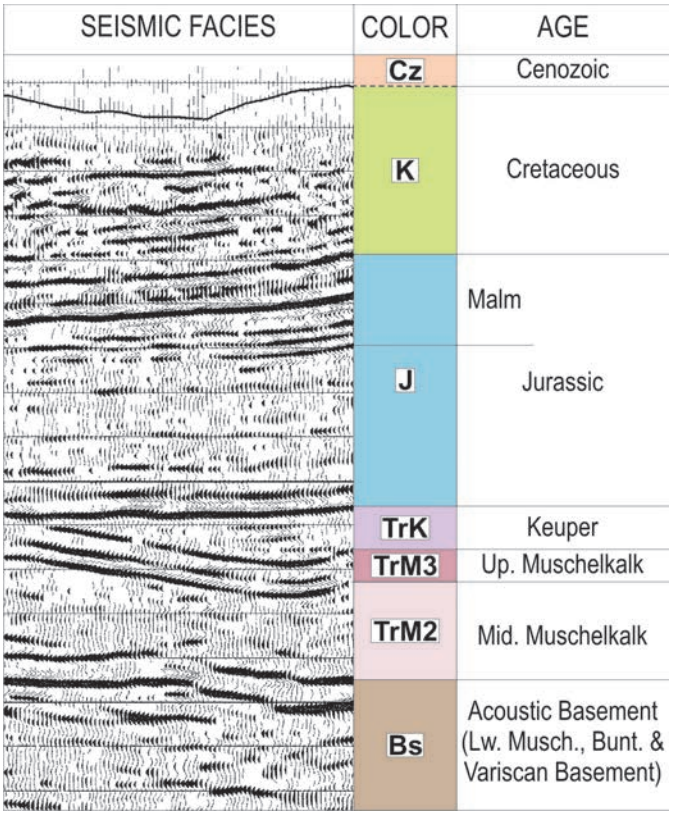

Figure 3.2. Seismic facies and horizons interpreted in the seismic profiles, and their correlation to the stratigraphy of the studied area. The seismic-line shown is a segment of the northern part of the seismic profile CT88-15 (Fig. 3.21a).

The Upper Lias and Dogger units have almost transparent facies with some quite continuous reflectors, while the Malm unit is characterized locally by continuous parallel seismic reflectors. The Jurassic units were not differentiated in the seismic profiles interpretation as their limits are not continuous in all profiles, and their seismic facies vary laterally. The Cretaceous (K) is characterized by continuous parallel seismic reflectors, but with higher wavelength than those observed in the Malm (Fig. 3.2).

3.2 TRIASSIC STRUCTURE IN THE SUBSTRATUM OF THE MAESTRAT BASIN

The Triassic rocks only crop out in the study area in some specific places: in the Calanda anticline core, which is formed by the Keuper facies and two outcrops of Upper Muschelkalk limestones (ANADÓN and ALBERT, 1973); in the Ejulve area, and in other anticline cores located in the northwestern part of the study area. This scarcity of outcrops makes it difficult to study the Triassic rifting event in the substratum of the Maestrat basin based on field-work. However, the seismic profiles network and the exploration wells available in the southern part of the study area allowed the study of the stratigraphy and structure of the Triassic rocks.

3.2.1 Description of the Triassic structure

The acoustic basement is fragmented by a system of high-angle normal faults, mainly oriented NW-SE to WNW-ESE, and some N-S. These faults have lengths between 2 and 7km, with dip-slips up to 500m, and define a system of horsts, grabens and half-grabens (Fig. 3.3). Two NW-SE-trending basement highs were recognized. The Monchén basement high is the western one, located below the Muela de Monchén. It is a horst bounded by NW-SE-trending normal faults. More to the east, the Iglesuela basement high is found, bounded to the south by NW-SE-trending, SW-dipping normal faults, while its northern boundary progressively deepens towards the north (Fig. 3.3d).

Immediately above the acoustic basement, the Middle Muschelkalk facies display very variable thicknesses, as it is shown in the isopach map for this unit (Fig. 3.3e). Analyzing the isopach map together with the depth to the acoustic basement top contour map (Fig. 3.3d), it can be observed that the Middle Muschelkalk minor thicknesses coincide with acoustic basement elevated areas, while the major Middle Muschelkalk thicknesses coincide with depressed areas of the acoustic basement. Although the evaporites of the Middle Muschelkalk facies are able to flow, their distribution, which adapts to the acoustic basement structure, indicates that at least the lower part of the Middle Muschelkalk facies was deposited during the extension, as previously suggested by BARTRINA and HERNÁNDEZ (1990). Furthermore, some fan-shaped reflectors are interpreted in the hanging wall of a normal fault, which is part of the NW-SE-trending, SW-dipping system of half-grabens developed in the northeastern part of the seismic survey, in the surroundings of Morella (Fig. 3.3c), which indicates that at least the lower part of the Middle Muschelkalk is syn-extension.

Conversely, the upper part of the Middle Muschelkalk surpasses and covers this structure. The non-deformed Upper Muschelkalk (of nearly constant thickness), the Keuper and the Jurassic lie nearly flat above it in some parts of the area covered by the seismic network (Fig. 3.3b), indicating that the thick-

ness variations of the lower part of the Middle Muschelkalk facies are depositional, and that they did not vary after their deposition, except for the salt tectonic event registered later.

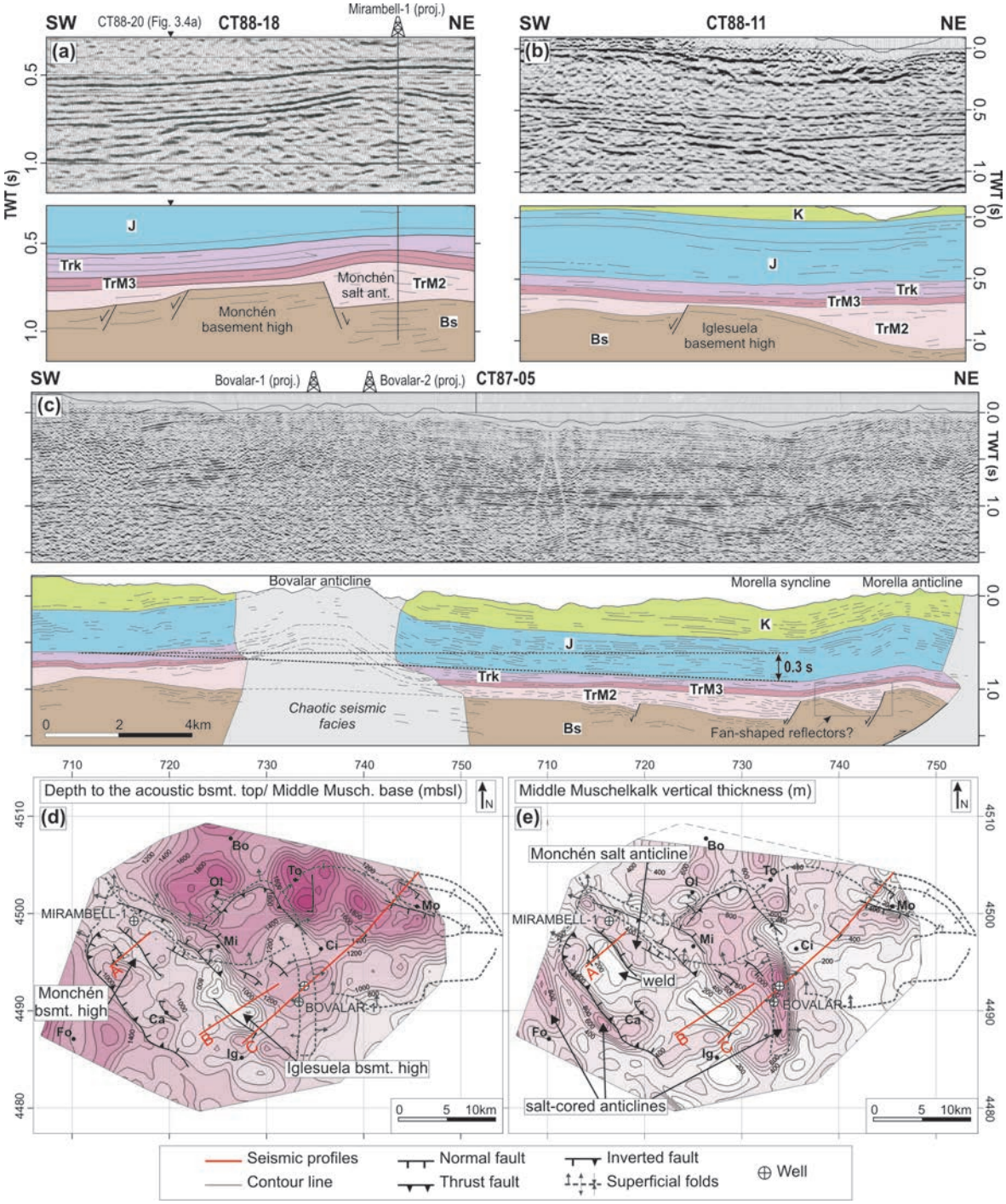

Figure 3.3. (a, b) Details of seismic profiles CT88-18 and CT88-11 and their interpretation, showing transversal sections of the Monchén and Iglesuela basement highs, respectively. (c) Seismic profile CT87-05 and its interpretation. See Figure 3.2 for legend. (d) Contour map of the depth to the top of the acoustic basement, i.e. base of the Middle Muschelkalk evaporitic unit (in m below the sea level). (e) Contour map of the Middle Muschelkalk vertical thickness (in m). See Figure 3.1 for location. The location of A, B and C is shown in D and E. UTM projection (zone 30, coordinates in km), ED50 datum. Modified from NEBOT and GUIMERÀ (2016a).

3.2.2 Salt-related structures

The seismic profiles revealed some salt anticlines and welds in the Middle Muschelkalk evaporitic facies, which indicate that some salt flow occurred. The most significant structure is the NW-SE-trending Monchén salt anticline, located north of the Monchén basement high, in the hanging wall of the N-dipping normal fault that bounds it to the north (Figs. 3.3a, d-e; 3.4b,c). The Upper Muschelkalk is folded above these salt structures in the Middle Muschelkalk evaporites, and the Keuper facies reflectors are found to lap on the folded Upper Muschelkalk carbonates, on both limbs of the Monchén salt anticline. Towards the SE, a forced fold appears in the northern limb of the Monchén salt anticline, coinciding with a normal fault in the acoustic basement (Fig. 3.4c). It involves the folded Upper Muschelkalk above the salt accumulation, while the Keuper reflectors display growth-strata above the downthrown limb of the forced fold (Fig. 3.4c). Above the Muela de Monchén basement high, a salt weld is also observed in the seismic profiles (Fig. 3.4.a), which could be the result of the salt flow towards the Monchén salt anticline, located north of it (Fig. 3.3e). This salt structure is observed in the seismic profiles (Fig. 3.3a) and is also confirmed by the Mirambell-1 well (Figs. 2.5, 3.3a), which crossed more than 625m of Middle Muschelkalk facies, while the average thickness of the Middle Muschelkalk in the area covered by the seismic network is of about 400 m (Fig. 3.3e).

3.2.3 Interpretation of the salt structures

The onlap and growth-strata geometries observed in the Keuper reflectors above the Upper Muschelkalk folded by the salt accumulations, indicate that the Middle Muschelkalk salt flow occurred during the deposition of the Keuper facies (Late Triassic). The forced folds in the Upper Muschelkalk above some normal faults in the acoustic basement indicate that some extension occurred after the Upper Muschelkalk deposition, and during the Keuper deposition, as deduced form the growth strata described. The extension during the Late Triassic could have triggered the Middle Muschelkalk salt to flow, while the differential load exerted by the Keuper facies, which was deposited adapting to the folded Upper Muschelkalk, could have enhanced it.

Other elongated salt accumulations developed in some anticline cores (Fig. 3.3e), as the Bovalar anticline, the Tarayuela or the Cañada de Benatanduz anticlines. These salt-cored anticlines formed during the Cenozoic contraction, when the supra-salt cover was folded detached in the Middle Muschelkalk evaporites.

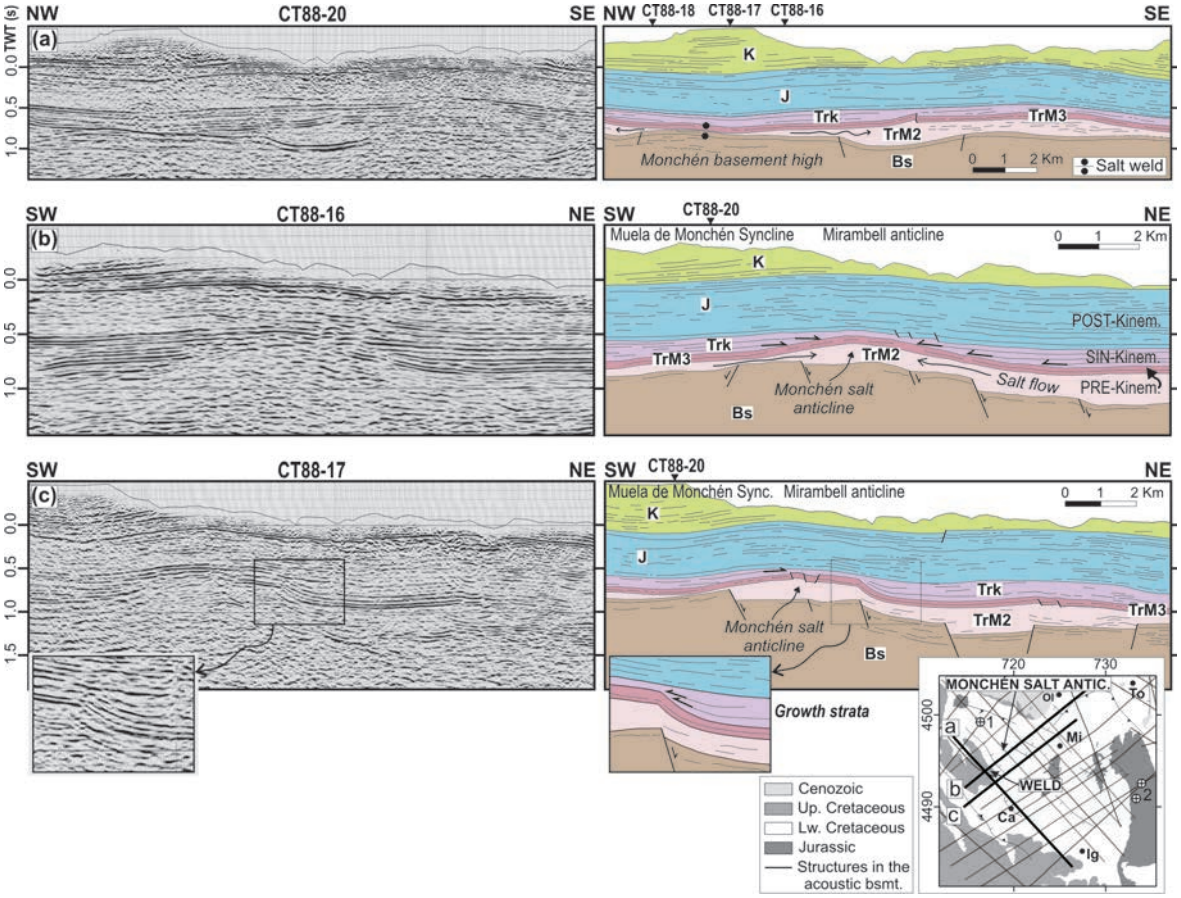

Figure 3.4. Seismic profiles (a) CT88-20, (b) CT88-16 and (c) CT88-17 and their interpretation. (a) A salt weld is observed over the Monchén basement high. The Middle Muschelkalk thickness variations are thus displayed. (b) The Monchén salt anticline developed N of the Monchén basement high is shown, being the Keuper reflectors onlapping the folded Upper Muschelkalk. (c) A drape fold of the Upper Muschelkalk forced by the resumed extensional activity of high-angle normal faults in the acoustic basement during the Late Triassic is shown. Some growth-strata in the Keuper reflectors are deduced, indicating that it was deposited during the extension. See location in Figure 3.1, and Figure 3.2 for legend. Modified from NEBOT and GUIMERÀ (2016a).

3.3 JURASSIC EXTENSIONAL STRUCTURE

The Jurassic thicknesses are difficult to stablish, as its base only crops out in the northwestern part of the area, in the surroundings of Ejulve, and in few other places, as in the frontal thrust-sheets of Calanda (Fig. 2.17). However, the exploration wells and the field data available, show some thickness variations and unconformities within the Jurassic.

The thickness variations affect both the syn-rift Malm and the Lias-Dogger package, commonly attributed to the Triassic post-rift. The entire Jurassic broadly thickens towards the south, basinwards, from about 400 m in the northern external zone of the basin (Fig. 3.5. Ejulve, Bnco. Degollados or Bnco. Redondo series) to 1122 m in the Mirambell-1 well (Figs 2.5, 3.5).

In the field, some thickness variations in the Malm units and the Dogger-Lias package can be observed. As an example, in the Cabezo Gordo section (Fig. 3.5) the Malm units have a minimum thickness of 240m, being the Dogger-Lias units of about 370m. This 610m of Jurassic thickness contrasts with the 1122m of Jurassic found in the Mirambell-1 well, containing Malm units 430m-thick and Dogger-Lias units of 692m (Fig. 3.5a). After analyzing the exploration-wells located in the southern half of the study area, MARTÍNEZ-ABAD (1991) stablished that the greatest thickness variations occur in the Lower Lias units (Cortes de Tajuña and Cuevas Labradas Fms.), from about 135m in the Bovalar-1 and Bovalar-2 wells, to 585m in the Mirambell-1 well towards the NW, having the Anhydrite zone at its base (Fig. 2.5). The other Lias units (Ablanquejo Group) and the Chelva Formation (Dogger) show gentle thickness variations, of only about 50m in the area covered by the exploration wells (Fig. 2.5). The Iàtova Fm. (Lower Malm), which is considered as the last post-rift unit (SALAS, 1987), has a nearly constant thickness of about 25m (Fig. 2.5).

An unconformity is observed within the Jurassic units. In some Jurassic outcrops located in the northernmost part of the fold-and-thrust belt, in the northern external zone of the basin, the Ablanquejo Group, the Chelva and the Iàtova formations are not present, and the Polpís Fm. (Kimmeridgian) directly overlies the Cuevas Labradas Fm. (Pliensbachian). Therefore, the Upper Lias, the Dogger and the Lower Malm units are missing, and where these units are present in the study area, they are thinner than in the surrounding areas, as in the Maestrazgo-1 well (Fig. 2.5). Consequently, those units were eroded or were not deposited in the northern external zone of the basin, probably related to a decrease of the extensional activity during the Lower and Middle Jurassic post-rift.

Regarding the Malm units – except for the Iàtova Fm.– they broadly become thinner towards the W, from about 650m in the Bovalar-1 well to 407m in the Mirambell-1 well (Figs. 2.5, 3.5), and mainly to the N, to about 150m in the Barranco del Redondo thrust sheet (Fig. 3.5). Also to be considered is the thickness variatio n between the area covered by the seismic profiles and the exploration wells, with values between 650 and 400 m thick, and the adjacent area of Albarracín, where the same Malm units are about 250-270 m thick (HERNÁNDEZ, 1985).

3.4 LOWER CRETACEOUS EXTENSIONAL STRUCTURE

Figure 3.5 shows the distribution of thicknesses of the Lower Cretaceous. It can be observed that thickness variations occur mainly in the Barremian units, while the Aptian units have more constant thicknesses. Attending to the thickness distribution of the Lower Cretaceous units, some of the faults observed at surface should have been extensional faults during the Mesozoic. Some of them were partially inverted during the Cenozoic contraction, while others remain as normal faults. From the internal zone to the northern external zone of the basin, the main normal faults are:

Xert fault: This E-W-trending, S-dipping, listric normal fault (Figs. 2.3, 2.17) was not inverted during the Cenozoic contraction, at least its segment within the Mesozoic cover. Its hanging wall contains more than 2.5km of Lower Cretaceous rocks, displaying rollover geometry (SALAS et al., 1995), which correspond to the depocenter of the Maestrat basin. In its foot wall the Lower Cretaceous units are about 1000m thick (SALAS, 1987).

Villarluengo fault: It is an E-W-trending, S-dipping normal fault, not inverted during the Cenozoic contraction. This fault puts in contact the Lower Cretaceous rocks, in its hanging wall, with the Jurassic rocks in its footwall. The Escucha Fm. (Albian) overlies this structure indicating that the extensional activity of the fault terminated before its deposition (Fig. 3.7a).

Bordón fault: The Bordón fault is a NE-SW-trending, SE-dipping normal fault which separates a series of Barremian and Aptian units up to 1040m thick (more than 800m of Barremian and more than 200 m of Aptian rocks) in its hanging wall (Fig. 3.5, Bordón anticline series), from a series of about 525m of the same units in its footwall (Fig. 3.5, Ladruñán series). A series of 150-200m of Barremian rocks are found in a Cenozoic-cored syncline in the footwall of the Bordón fault, attached to the fault. These thicknesses distribution makes clear that the Bordón fault was active during the Lower Cretaceous extensional event. The Bordón fault ends up towards the east as the series of Jaganta, to the N, and Bordón anticline East, to the S, are very similar, both of them of about 800-900 m thick (Fig. 3.5).

Ortells fault: This ESE-WNW-trending, S-dipping fault (Fig. 3.5) separates series of Lower Cretaceous rocks of about 1100m in its hanging wall from others of about 800m in its footwall, of which about 750m in its hanging wall and about 570m in its footwall correspond to the Barremian units. This normal fault was partially inverted in its westernmost and easternmost segments, but in its central part it was only deformed by folding (Guimerà, pers. Comm .).

Garrocha fault: It is an ENE-WSW-trending, S-dipping fault which separates series of Barremian and Aptian units of about 160-170 m thick (Higueral and Raspador series, Fig. 3.5) in its hanging wall, from a series of about 30 m of the same units in its footwall (Carrascal series, Fig. 3.5).

Castellote-Herbers fault: This is the most external and the longest normal fault recognized in the study area, included in the Montalbán-Herbers-Llaberia fault zone described by SALAS and GUIMERÀ (1996). This fault varies its trend along-strike. In the surroundings of Castellote and Jaganta, the Castellote-Her-

bers takes an ESE-WNW trend, and separates a series of Barremian and Aptian units up to 800 m thick in its hanging wall, south of the fault, from a series of 0 to 300 m in its footwall, north of the fault (Fig. 3.5). Towards the west this normal fault takes a NE-SW-trend and ends up south of Cuevas de Cañart. Conversely, towards the east it takes a NW-SE-trend and it is supposed to continue below the Cenozoic basin of Aiguaviva, up to linking with the Herbers fault, northeast of Herbers (Fig. 2.17).

Normal faults system north of the Castellote fault: Some minor normal faults can be deduced in the footwall of the Castellote and the Garrocha normal faults (Fig. 3.5). These are mostly ENE-WSW to NE-SW-trending, S-dipping normal faults with throws of tens to few hundreds of meters. Most of them are located in the Lower Cretaceous outcrop in the surroundings of Seno, North of Castellote. They controlled the sedimentation of the small Lower Cretaceous outcrops located in the external part of the Maestrat basin.

Some blind normal faults have also been deduced below the (non-deformed) Upper Cretaceous and Cenozoic post-rift rocks, which are located in the relay zones between some of the described normal faults, and are oriented N-S, perpendicular to the other normal faults:

Carrascosa fault: This NNE-SSW-trending, E-dipping normal fault has been deduced below the Upper Cretaceous and Cenozoic outcrop of Muela Carrascosa, as more than 1000 m of Barremian and Aptian units can be measured below the eastern boundary of this outcrop (Fig. 3.5, Bordón anticline series), while in its western side only 165m of the Lower Cretaceous units are found (Fig. 3.5, Muela Carrascosa series). A normal fault was interpreted to explain this sharp thickness variation in a distance of about 2km below non-deformed post-rift rocks. This normal fault is located in the relay zone between the Bordón and the Villarluengo normal faults, so it can be considered a breached relay ramp.

Ladruñán fault: In the relay zone between the Castellote-Herbers and the Garrocha normal faults, another NNE-SSW-trending, E-dipping normal fault can be interpreted below the Upper Cretaceous and the Cenozoic outcrop located west of Ladruñán. A series of more than 500m of Barremian and Aptian units is found in the surroundings of Ladruñán (Fig. 3.5, Ladruñán series) in the hanging wall of the fault, while to the west, only about 30m of Aptian rocks are found in its footwall (Fig. 3.5, Carrascal series). The eastern boundary of the Upper Cretaceous outcrop dips towards the West (Fig. 3.8) suggesting a partial inversion of a nearly N-S-trending, E-dipping blind normal fault.

Tarayuela fault: The Tarayuela normal fault has been interpreted in the southwestern boundary of the Salzedella sub-basin, coinciding with the southern limb of the Tarayuela anticline, parallel to the fold trend (Fig. 3.5a). It would be a NW-SE-trending, N-dipping normal fault that towards the west, takes a NNE-SSW-trend as the Tarayuela anticline changes its trend along-strike. It separates series of 380m and 350m of Barremian and Aptian rocks in its hanging wall (Fig. 3.5,Tarayuela anticline and Mirambell anticline W series), from 150 and 180m in its footwall (Figs. 3.5, Cañada de Benatanduz-Villarluengo road series, 2.5,Maestrazgo-2 well).

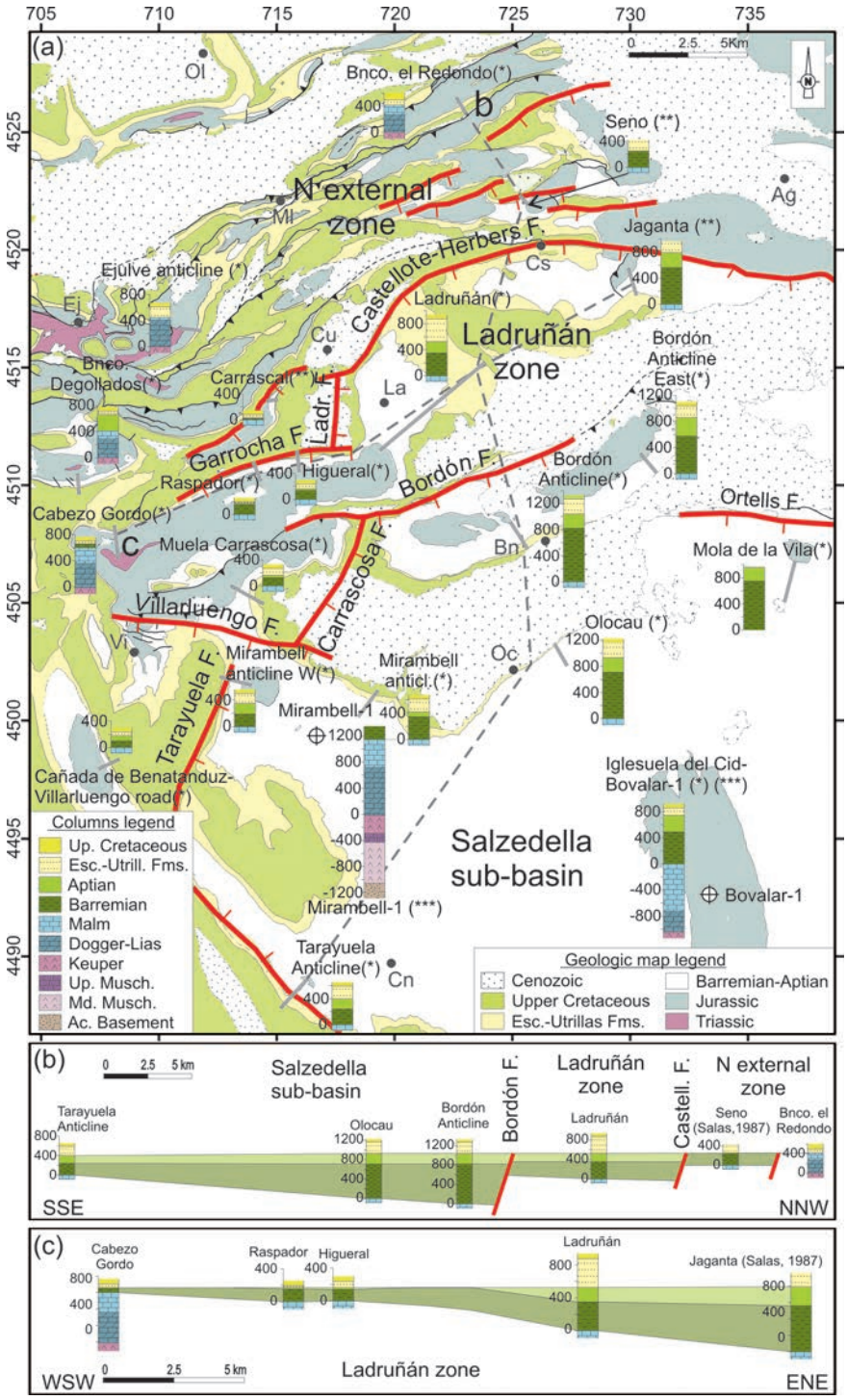

Figure 3.5. (a) Map showing the main tectonostratigraphic domains recognized and the structures bounding them, and also the stratigraphic sections of the studied area. The normal faults interpreted for the Barremian and Aptian period are shown. The stratigraphic sections were obtained from new field data (∗) and were combined with sections obtained by SALAS (1987) (∗∗), and with sub-surface data (∗∗∗) (exploration wells (MARTÍNEZ-ABAD, 1991), and seismic data converted to depth by (NEBOT and GUIMERÀ, 2016)). (b, c) Simplified correlation of the Barremian and Aptian units in some stratigraphic sections in directions roughly perpendicular (b) and parallel (c) to the geological structures. The datum is the base of the Escucha Fm. (top of the Aptian), as this formation developed small sub-basins different from the Barremian–Aptian ones. For towns' legend see Fig. 2.17.

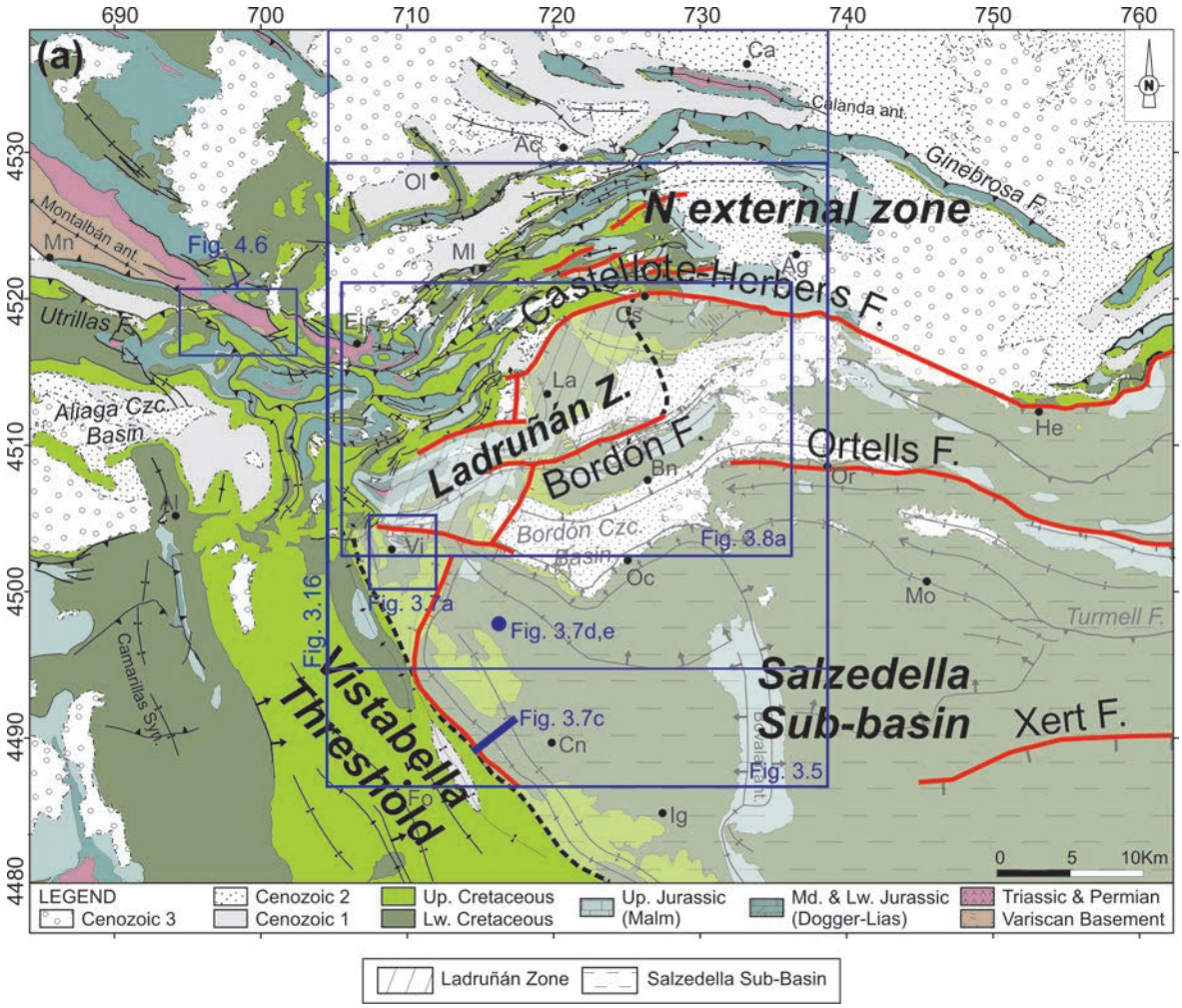

Figure. 3.6. Main tectonostratographic domains differentiated in the study area for the Lower Cretaceous syn-rift period. The location of the geological map in Fig. 3.5 is shown, as well as that of photographs in Fig. 3.7.

3.4.1 Main tectonostratigraphic domains defined by the Lower Cretaceous units

The thicknesses distribution of the Lower Cretaceous rocks and the normal faults described, define three tectonostratigraphic domains in the studied sector of the Maestrat basin, from South to North: the Vistabella threshold, the Salzedella sub-basin –which contains the Ladruñán zone with intermediate characteristics– and the northern external zone (Fig. 3.6).

Vistabella threshold: The Vistabella threshold (Figs. 2.3, 3.6), first recorded by CANÉROT (1974), is an elongated area with poor deposition and erosion of the Lower Cretaceous and the Jurassic, as it contains only local remains of Lias and Dogger rocks, incomplete Upper Jurassic –locally overlying the Triassic rocks– and reduced Lower Cretaceous series. In the Maestrazgo-2 well, located in the Vistabella threshold, only 150 m of Aptian units were deposited, which overlay directly the Upper Jurassic Bovalar Fm. (Fig. 2.5, MARTÍNEZ-ABAD, 1991). More to the east, the Aptian series becomes thinner, being 100m thick in the surroundings of Vistabella (Fig. 2.17), overlying the Polpís Fm. (Lower Kimmeridgian), and in turn, the Polpís Fm. overlies the Triassic rocks (CANÉROT, 1974). It was an elevated area during the Mesozoic rifting, produced by the rollover fold developed in the hanging wall of the Mesozoic normal fault system (SALAS et al., 2005). It constitutes the southern and western boundaries of the Salzedella sub-basin, and the northern boundary of the Penyagolosa sub-basin located south of it (Fig. 2.3, SALAS and GUIMERÀ, 1996).

Salzedella sub-basin: The Salzedella sub-basin was defined by SALAS and GUIMERÀ (1996) as the widest sub-basin of the Maestrat basin, located in its eastern central part, bounded to the north by the Turmell Fault Zone, and containing the depocenter of the Maestrat basin, located in the hanging-wall of the Xert fault, containing more than 2.5km of Lower Cretaceous rocks (SALAS, 1987). The present work proposes to modify its northern boundary in the studied sector, displacing it northwards, to the Castellote-Herbers normal fault and, in its northwestern part, to the Bordón, the Carrascosa and the Villarluengo normal faults (Fig. 3.6), as all the northeastern part of the studied sector south of the Castellote fault contains Lower Cretaceous series of about 1000m thick (Fig. 3.5, Jaganta, Bordón, Mola de la Vila, Olocau series), which become thinner towards the S and towards the W. Consequently, the Ortells and the Xert faults are located within the Salzedella sub-basin.

The Barremian and Aptian filling of the Salzedella sub-basin broadly displays a wedge geometry, thickening towards the N, from 350 m in the Tarayuela anticline to about 1000 m in the northeastern part of the basin, controlled by the S-dipping normal faults with throws of hundreds of meters (Castellote, Bordón, Ortells faults, etc), and a system of normal faults of metric throws found throughout the basin (LIESA et al., 2006; NEBOT and GUIMERÀ, 2016a) (Fig. 3.7).

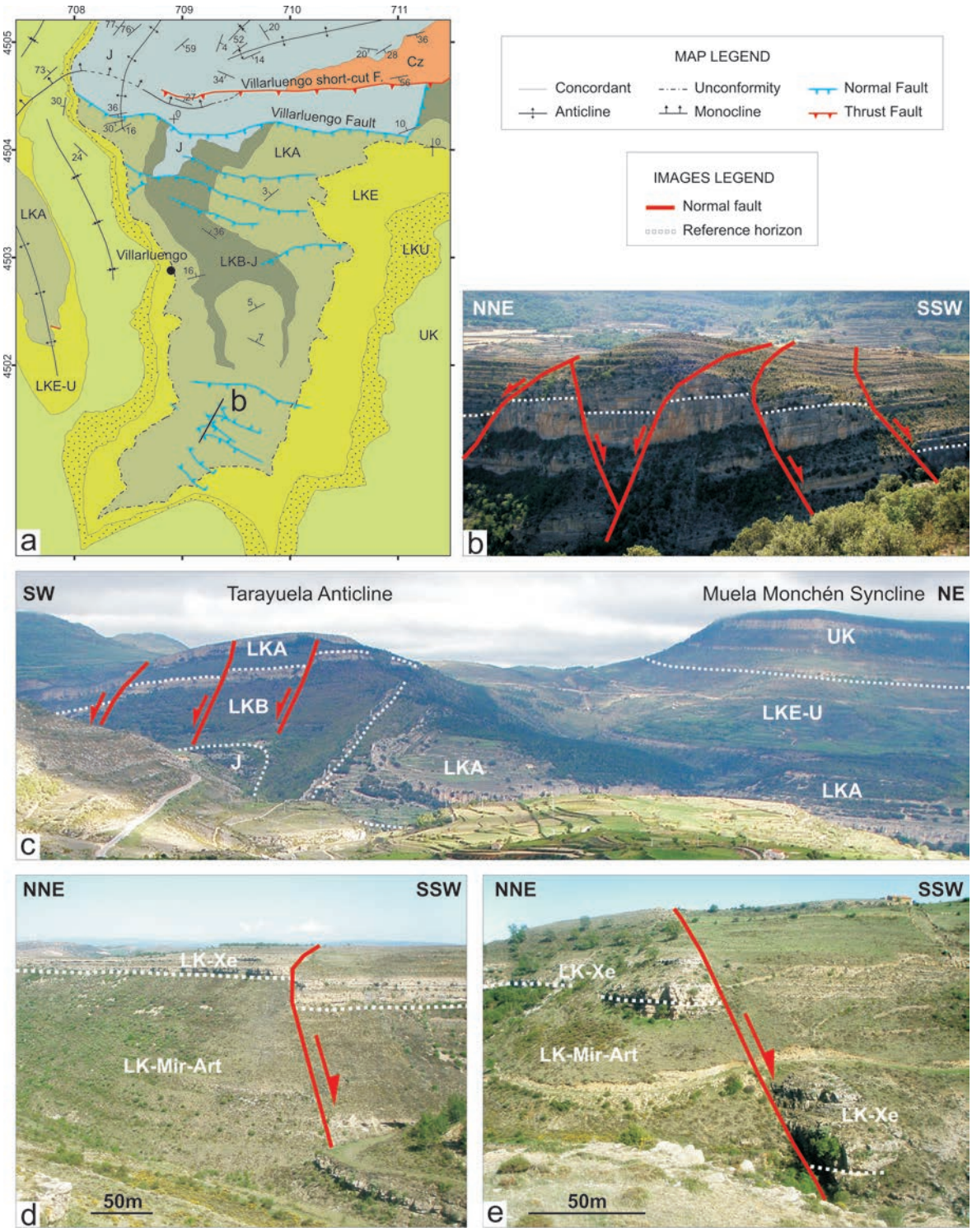

Figure 3.7. Mesozoic normal faults of metric throws found throughout the Salzedella sub-basin (a) Geologic map of the Villarluengo normal fault. Minor synthetic and antithetic normal faults have been recognized in its hanging wall. See location in Fig. 3.6. (b) Panoramic view of some normal faults mapped in (a), affecting the Villarroya de los Pinares and the Benassal fms. (c) Antithetic normal faults in the hanging wall of the Tarayuela normal fault, affecting the Aptian and the Barremian units. (d,e) Normal faults affecting the Barremian units. See Fig. 3.6 for location, and Fig. 3.8 for units abbreviations.

Ladruñán zone: The Ladruñán zone (Fig. 3.8a) has been described here in, to refer to the area located to the northwestern end of the Salzedella sub-basin, which is separated from the Salzedella sub-basin by the Bordón, the Carrascosa and the Villarluengo normal faults, and is characterized by containing thinner Lower Cretaceous series than the overall Salzedella sub-basins (Fig. 3.6). The Barremian and Aptian rocks in the Ladruñán zone broadly thicken towards the NE, from the 60m measured in the Cabezo Gordo series to the nearly 800m measured in the Jaganta series (SALAS, 1987) (Fig. 3.5c). Towards the E the Bordón normal fault ends up, as the Barremian and Aptian units have similar thicknesses at both sides of the fault (Fig. 3.5a). In this sector, the Ladruñán zone merges with the Salzedella sub-basin (Fig. 3.6), as it is observed in the cross-sections (Figs. 3.9, 3.10B-B', C-C', E-E').

An angular unconformity is observed at both sides of the Ladruñán zone, as the post-rift units (Upper Cretaceous and the Utrillas Fm , although the last may be missing locally.) unconformably overly different terms of the syn-rift Lower Cretaceous units (Fig. 3.8). The tilted Lower Cretaceous syn-rift units describe a N-S-trending anticline located parallel to the Ladruñán normal fault, in its hanging wall, developed before the post-rift units were deposited, probably as a transverse fold in the relay zone between the Castellote and the Garrocha normal faults (Fig. 3.8a).

Northern external zone: This zone comprises the area located in the footwall of the Castellote-Herbers, the Ladruñán and the Garrocha normal faults, where the Lower Cretaceous and the Jurassic sedimentation was poor or absent, or where erosion occurred. In most of the external zone, no Barremian nor Aptian units are found, so the Escucha Fm. directly overlies the Jurassic or older units, except specific Lower Cretaceous outcrops as the one located in the surroundings of Seno, north of Castellote (Fig. 3.5), which is the largest one, and where up to 300m of these units can be measured. The Lower Cretaceous units appear again more to the east. North of Aiguaviva, the Barremian and Aptian units reach locally 600m of thickness (Fig. 3.5).

In the external zone, the Escucha Fm. is characterized by an erosive base and by significant thickness variations. It unconformably overlies the older units, from the Aptian to the Keuper (Upper Triassic) in short distances. This indicates that the Escucha Fm. was deposited during extension (QUEROL, 1992), but the structures and the sub-basins developed during this period are different to those that controlled the sedimentation of the Barremian and the Aptian units, as it can be observed in the Villarluengo normal fault, which is overlaid by the Escucha Fm. (Fig. 3.7a), or as shown in the restored cross-sections (Figs. 3.10, 3.12).

3.5 LATE ALBIAN – UPPER CRETACEOUS POST-RIFT STRUCTURE

During this period the Utrillas Fm. was deposited covering the intra-Albian unconformity above the Lower Cretaceous, Jurassic, Triassic and even the Paleozoic rocks, throughout the Maestrat basin. The fluvial siliciclastic rocks of the Utrillas formation were followed by the upper Cretaceous carbonate platforms. Gentle extensional activity along the major basin-bounding normal faults have been described, with syndepositional displacements of up to 500m (SALAS et al., 2001).

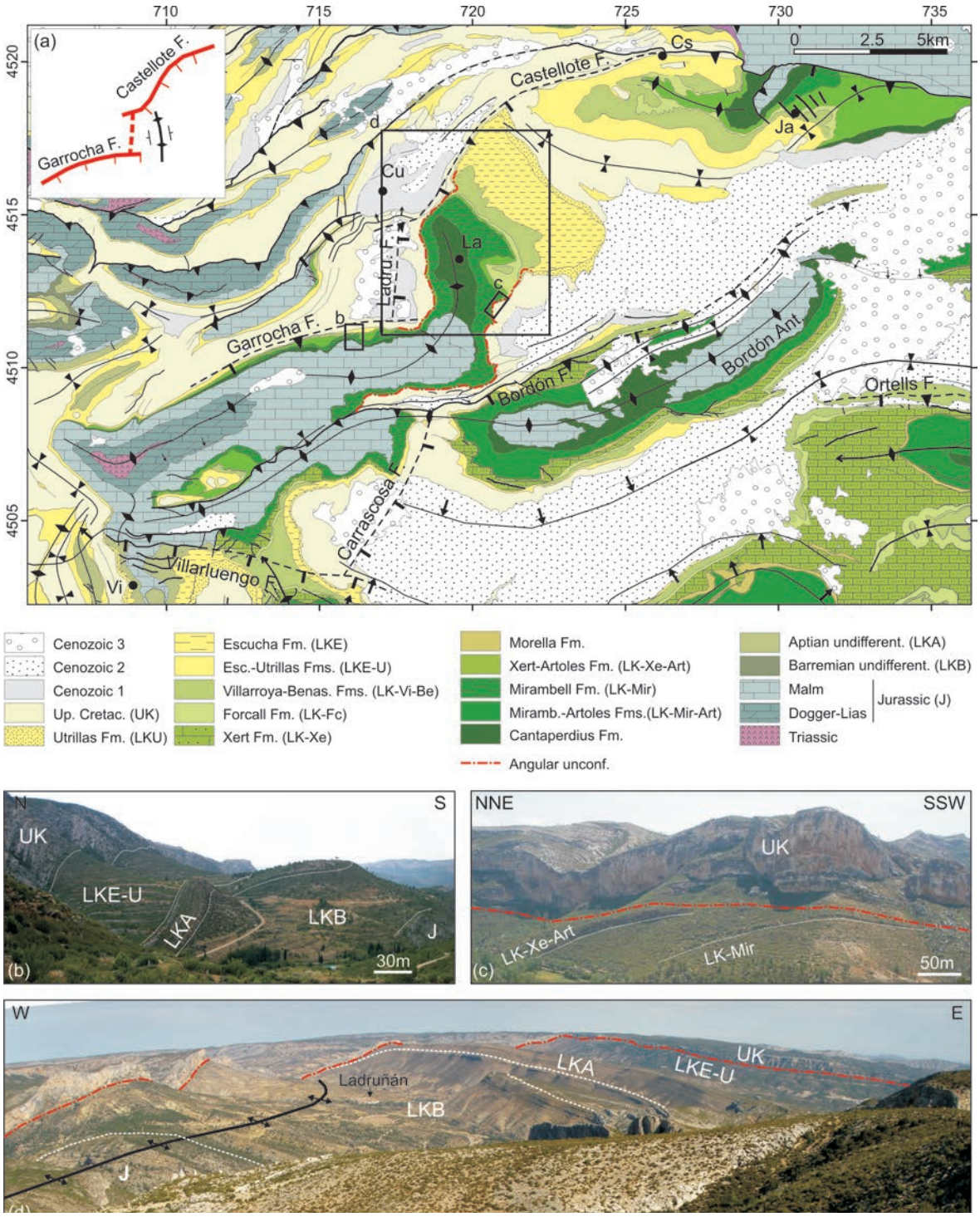

Figure 3.8. (a) Detailed geological map of the Ladruñán zone, and sketch showing the simplified structure of the Ladruñán zone. It is bounded to the north by normal faults which relay laterally (Castellote and Garrocha faults). In the relay zone a breached relay ramp was interpreted (the Ladruñán fault). A N-S-trending transversal anticline also developed in the relay zone (Ladruñán anticline). See location in Fig. 3.6. (b) Field panoramic photograph of the el Higueral series in Fig. 3.5, with about 160m of Barremian and Aptian units. (c) Field panoramic photograph of the angular unconformity developed in the Ladruñán zone, as the post-rift rocks were deposited above the N-S-trending Ladruñán anticline. (d) Field panoramic photograph of the Ladruñán series in Fig. 3.5, containing more than 500m of Barremian and Aptian units, unconformably overlaid by the post-rift rocks. A thick Escucha formation can be observed (LKE-U).

3.6 CENOZOIC CONTRACTIONAL STRUCTURE

In order to study the Cenozoic contractional structure in the study area, nine cross-sections were constructed. Five of these cross-sections are located across the northern fold-and-thrust belt structure, two of them containing the deduced NNE-SSW transport orientation (Fig. 3.9D-D', E-E'). The other four sections are located in the southern slightly deformed area in the hinterland (Fig. 3.9F-F', G-G', H-H', I-I').

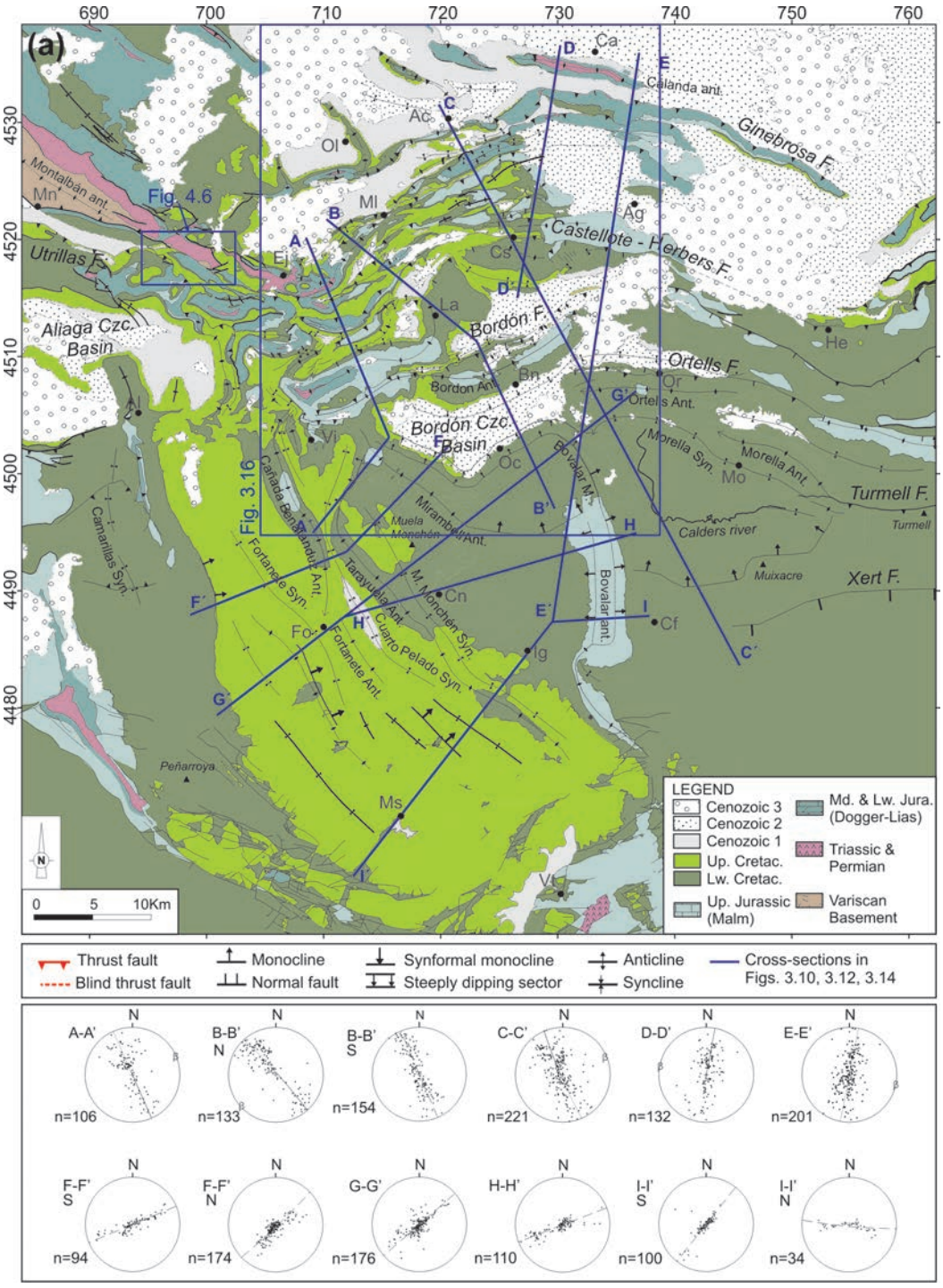

Figure 3.9. Geologic map of the study area showing the traces of the cross-sections constructed. (UTM projection (zone 30, coordinates in km), ED50 datum)

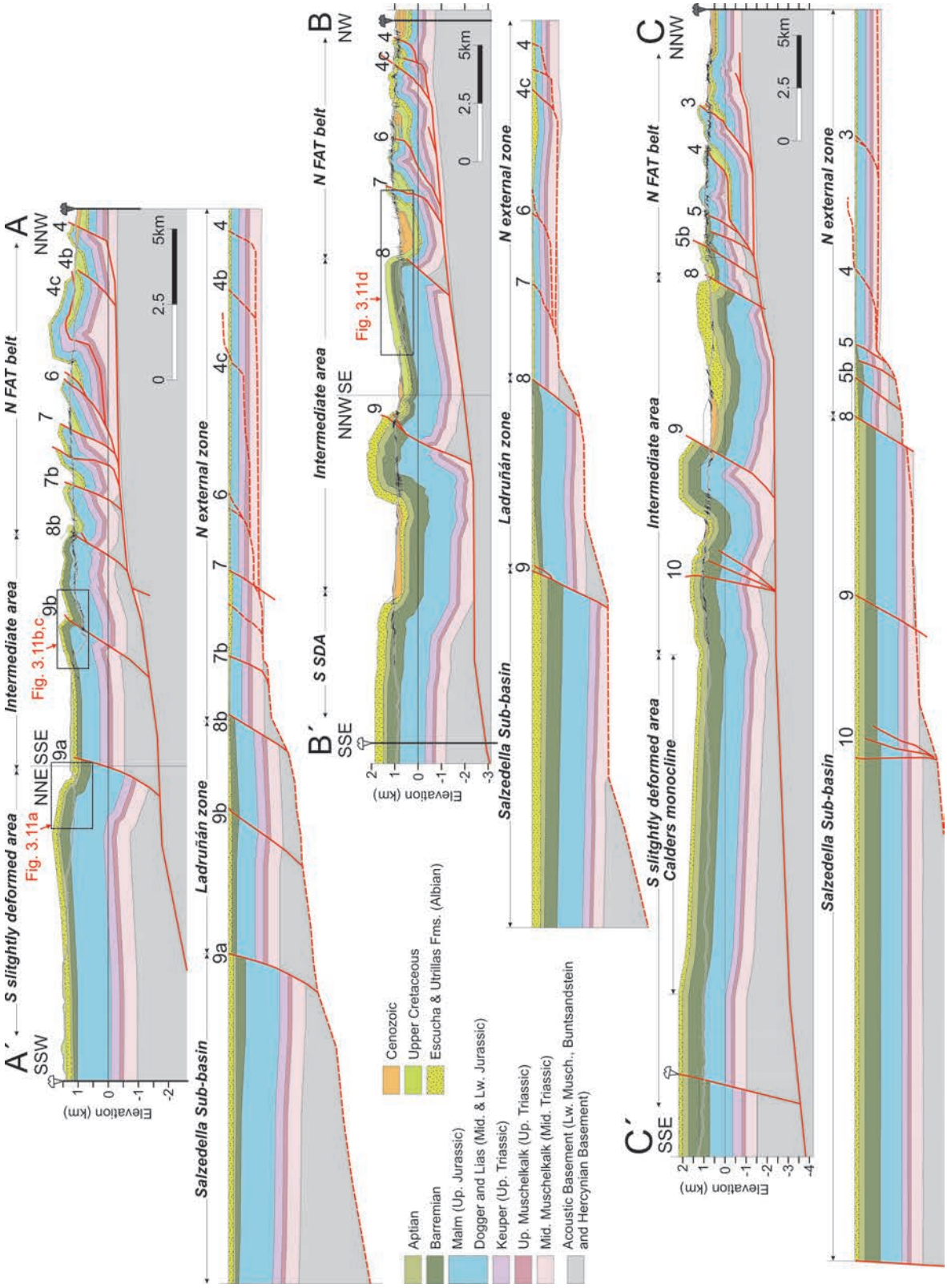

Figure 3.10. Cross-sections A-A', B-B' and C-C'. See location in Figure 3.9. These cross-sections do not contain the transport direction and they are not restorable. However, they were unfolded using the flexural slip unfolding algorithm in order to display an approximation to the Mesozoic extensional structure.

Figure 3.11. (a) Panoramic view from the road between Tronchón and Villarluengo towns, at the foot of the Muela Carrascosa. (b,c) Panoramic view of fault 9b from the west (b) and from the E (c). (d) Panoramic view of the Ladruñán zone, the Castellote fault (folding the Upper Cretaceous post-rift rocks) and the Cuevas de Cañart syncline, filled with Cenozoic rocks (Obtained from Google Earth®). See location in Fig. 3.10.

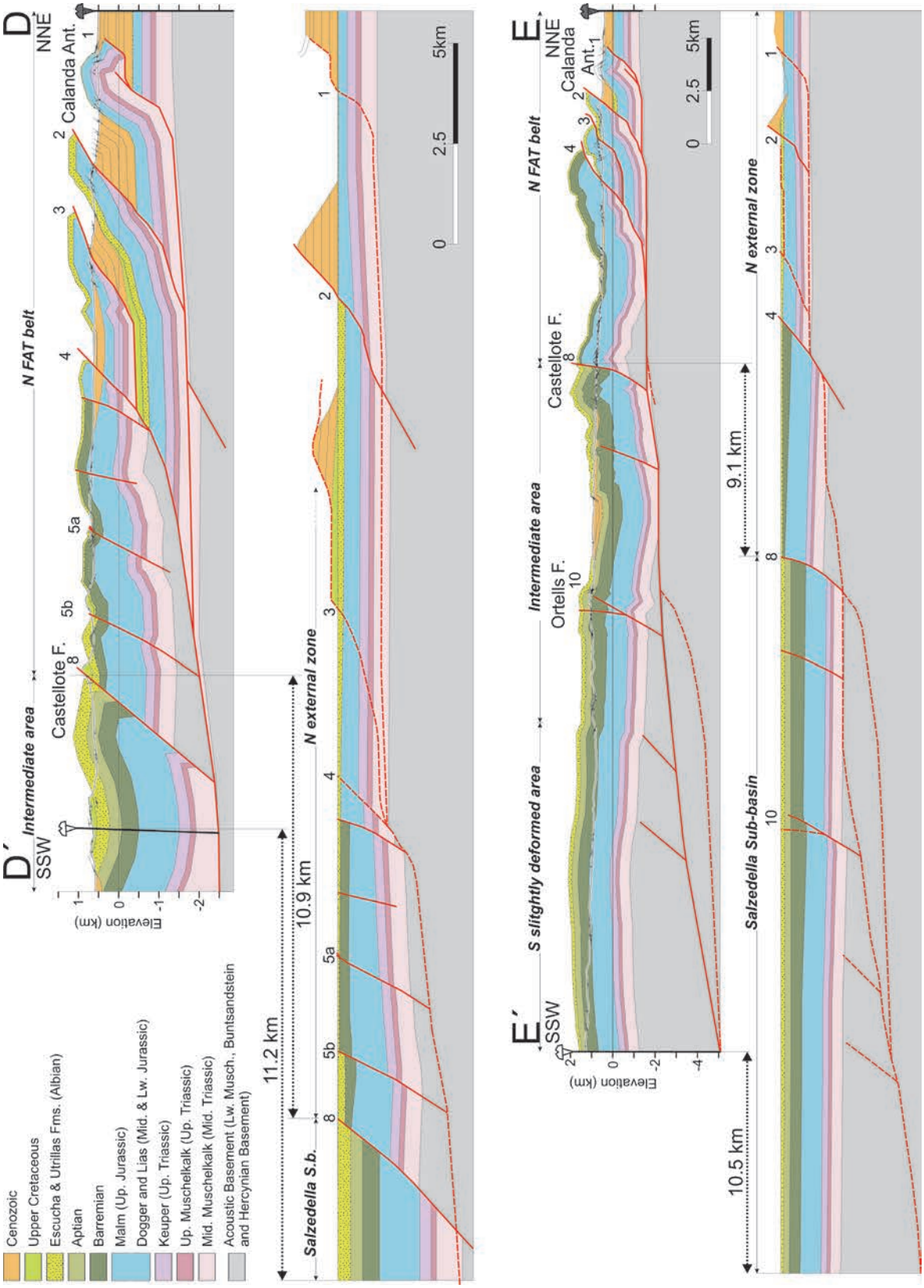

Figure 3.12. Cross-sections D–D' and E–E' containing the NNE–SSW transport direction. See location in Figure 3.9.

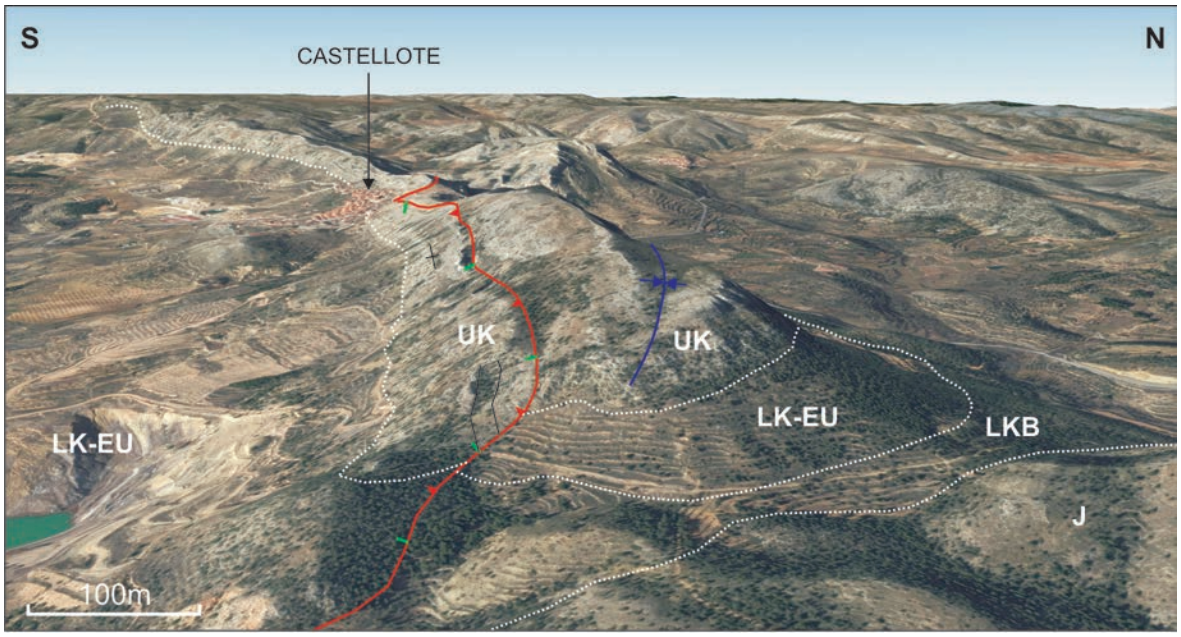

Figure 3.13. Panoramic view of the Castellote Fault Abbreviations: J= Jurassic, LKB= Barremian, LK-EU= Escucha and Utrillas Formations, UK= Upper Cretaceous. The Castellote fault experienced extension during the Lower Cretaceous (green) and contractional inversion during the Cenozoic (red). The Upper Cretaceous rocks in the hanging wall of the fault (S) are vertical or even inverted. Image obtained from Google Earth®.

3.6.1 Inversion structures

Some of the extensional faults developed during the Mesozoic rifting event were reactivated as contractional faults during the Cenozoic, inverting the Mesozoic sub-basins. However, as it is recognized in the field, and shown in the cross-sections, the normal faults were only partially inverted, being their extensional displacements not totally recovered. In some cases the post-rift was cut by the resulting thrust, with dip-slips of few meters, as the Castellote fault in its ESE-WNW-trending segment (Fig. 3.13 and fault 8 in Fig. 3.12D-D', E-E') or the Bordón fault (fault 9 in Fig. 3.10B-B'). In other cases the partial inversion of the normal fault only folded the Upper Cretaceous post-rift rocks, as the Garrocha fault (fault 8b in Fig. 3.10A-A'), the Castellote fault in its NE-SW-trending segment (Fig. 3.11d, fault 8 in Fig. 3.10B-B'), the Ortells fault in its eastern part (fault 10 in Fig. 3.10C-C', 3.12E-E') or the Tarayuela fault (Fig. 3.14F-F', G-G', H-H').

New thrusts also formed, as the E-W-trending, N-verging Turmell thrust (Fig. 3.9) or the Villarluengo thrust (Fig. 3.7a), as no thickness variations can be observed between both sides of them. However, these thrusts developed in the footwall of two non-inverted Mesozoic normal faults, the Xert fault and the Villarluengo fault, respectively. Therefore, these new thrusts could have developed as short-cut thrusts resulting from the inversion of the lower segments of the normal faults, containing in their hanging walls the upper, non-inverted segments of the Mesozoic normal faults. . In all these cases, the contractional structures, generated as a result of the Cenozoic inversion, inherited the geometry and orientation of the previous Mesozoic normal faults.

In the hanging walls of these partially inverted normal faults, the different sub-basins experienced some internal deformation. The Ladruñán zone was uplifted in response to the contractional displacement in the hanging wall of its northern boundary faults, which are blind thrusts (Figs. 3.8a, 3.11d. A strongly asymmetric, N-verging anticline developed in the hanging wall of the Castellote fault, parallel to it, with a southern limb gentle dipping towards the S and a northern frontal limb nearly vertical or even inverted (Figs. 3.8a, 3.10B-B', 3.11d). To the southwestern part of the Ladruñán zone, a N-verging anticline developed, which inherited the trend of the Ladruñán and the Garrocha normal faults (Fig. 3.8a). The N-S-trending transverse anticline developed during the Lower Cretaceous extension in the hanging wall of the Ladruñán fault, was probably reactivated during the Cenozoic contraction, propagating towards the SW as a NE-SW-trending anticline.

The Salzedella sub-basin also experienced internal deformation. Its sedimentary filling was folded, mainly in detachment folds and monoclines associated to basement thrusts. Also folds involving the Acoustic Basement are observed in the seismic profiles, as it is the Mirambell anticline (Fig. 3.4b). Some inverted faults are found within the Salzedella sub-basin. Its southern part was uplifted, generating a wide, slightly deformed, elevated area which contains wide outcrops of Upper Cretaceous and local remains of basal Cenozoic rocks, the youngest pre-contractional ones.

In the northern external zone some of thrusts seem to be the result of the inversion of Mesozoic extensional faults which controlled the deposition of the Escucha Fm., as the fault 4c in cross section B-B' (Fig. 3.10) or even the Jurassic, as the fault 2 in cross-section D-D' (Fig. 3.12). In these faults, the extensional displacements were totally recovered. Besides the inversion structures, most thrusts in this zone seem to be new thrusts developed during the Cenozoic contraction.

3.6.2 Structural domains

After the interpretation of the cross-sections and the geological map, the studied area can be divided into three structural units: the frontal fold-and-thrust belt, an intermediate area and the southern slightly deformed area (Fig. 3.15).

3.6.2.1 The northern fold-and-thrust belt

This area is characterized by structures with wavelengths of hundreds of meters to few kilometers (Fig. 3.15) which are detached in the evaporites of the Middle Muschelkalk facies, and locally in the Keuper facies. In the Calanda anticline, which is the most frontal structure of this fold-and-thrust belt, two Upper Muschelkalk outcrops are found in its core (ANADÓN and ALBERT, 1973), indicating that it is detached in the Middle Muschelkalk evaporites (Fig. 3.12D-D'). Locally, the thrust sheets also incorporate some fragments of the Acoustic Basement (Figs. 3.10, 3.12).

This fold-and-thrust belt coincides with the northern external zone of the Maestrat basin, located in the footwall of the Castellote-Herbers and the Garrocha normal faults, which is the area containing the thinnest supra-salt cover. The structural trends of this belt display a salient geometry (in the sense of MARSHAK, 2004), as they describe an arched geometry convex towards the N, to the sense of

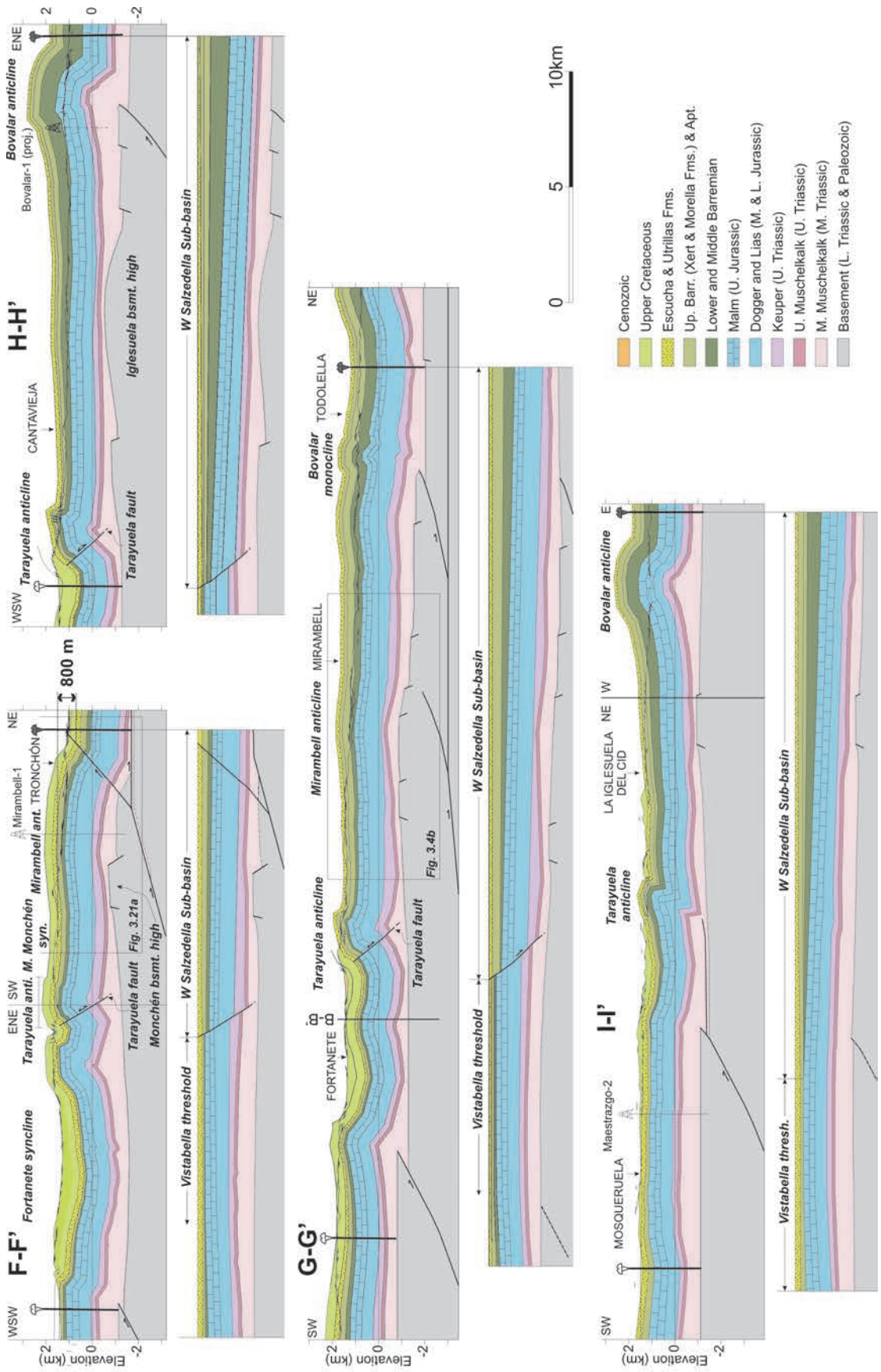

Figure 3.14. Cross-sections of the southern part of the study area. See location in Figure 3.9.

displacement (Fig. 3.9). The eastern part of this salient is mostly covered by Cenozoic rocks, so this study focused on the western and central parts of it (Fig. 3.16). Attending to this interpretation, the adjacent areas of Ejulve-Aliaga, to the W, and Herbers, to the E (Fig. 3.9), could be associated with recesses, in which superposition of structures with different orientations occurred (SIMÓN, 1980, 2004; GUIMERÀ, 1988).

3.6.2.2 The intermediate area

The northern boundary of this area is formed by the Castellote-Herbers and the Garrocha normal faults. To the south it is bounded by the Morella syncline and the southern boundary of the Bordón Cenozoic basin (Fig. 3.9), which, as it will be explained later, constitute the northern synformal hinge of the Calders monocline (Fig. 3.15). This intermediate area is the southern part of the Portalrubio-Vandellòs fold-and-thrust belt. It contains folds of kilometric wavelengths, which are wider than folds in the frontal fold-and-thrust belt. These folds are detached in the Middle Muschelkalk evaporites, although some fragments of the Acoustic Basement were incorporated locally in the thrusts sheets (Figs. 3.10, 3.12). This area comprises the northern part of the Salzedella sub-basin, including the Ladruñán zone.

Along-strike structural variations

It is noted that structures in the studied sector of the Portalrubio-Vandellòs fold-and-thrust belt –in which the frontal fold-and-thrust belt and the intermediate areas have been differentiated– change their trend along-strike (Castellote-Herbers fault, Figs. 3.9, 3.16), relay laterally (Castellote and Garrocha faults or Bordón and Villarluengo faults, Figs. 3.5, 3.16), and also terminate laterally (Ortells fault towards the W, thrust 3 towards the W, or the Bordón Fault towards the E, Fig. 3.16). In the relay zones of some faults some oblique and transversal folds can be observed, as the N-S-trending folds observed west of Cuevas de Cañart, linking the NE-SW-trending faults 7 with 7b, and 7b with 8 (Fig. 3.16), or the NE-SW-trending anticline located N of Castellote, linking the E-W-trending faults 5a and 5b (Fig. 3.16).

The major thrust-sheet displacement also varies laterally, as it is transferred from W to E towards the foreland, to more external structures (Fig. 3.16). In cross-sections A-A' and B-B' (Fig. 3.10) the Molinos thrust sheet (fault 4) is the structure that accumulates a major displacement, in section C-C' (Fig. 3.10) thrust 3 has the major displacement, while in sections D-D' and E-E' (Fig. 3.12) structures that concentrate most displacement are the Ginebrosa and Calanda thrust sheets (faults 2 and 1). As previously described, the amount of inversion of structures also varies along-strike, as well as their trend. The best example is the Castellote fault, as the resulting thrust cut the post rift rocks in its ESE-WNW-trending segment while it only folded the post-rift in its NE-SW-trending segment.

In the western part of the described salient, the NW-SE-trending structures of the Iberian Chain converge with the NE-SW to ENE-WSW-trending structures of the frontal fold-and-thrust belt (Figs. 3.9, 3.16), and fold interferences occur . The best example in the study area is the Los Olmos fold, described by SIMÓN (1980, 2004). It is a NW-SE-fold that has an ENE-WSW-trending anticline attached to its southern termination, which deforms it. This anticline developed in the hanging-wall of an ENE-WSW-trending, SE-verging back-thrust, which continues throughout the interference area (Fault 0, Fig. 3.16).

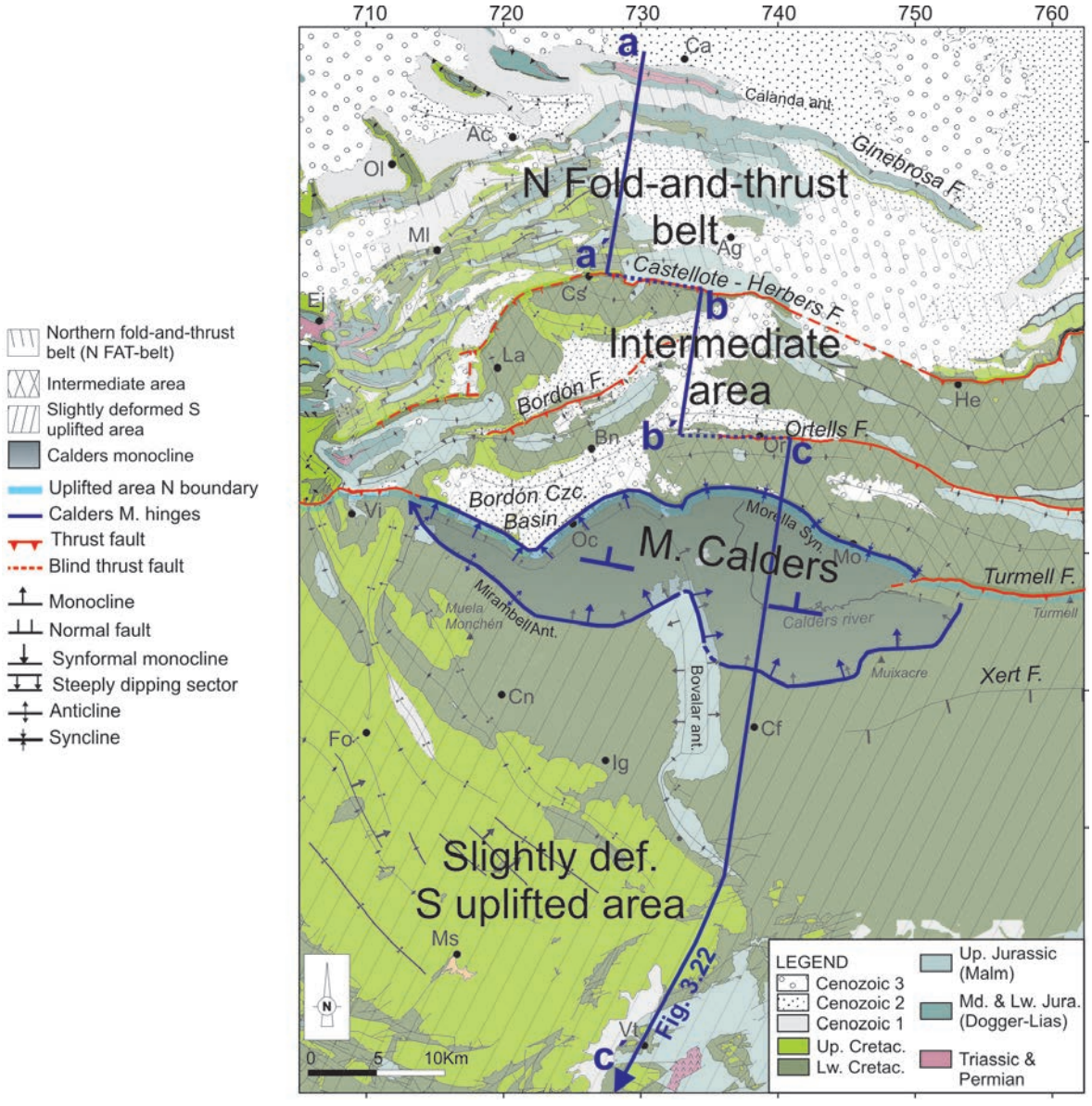

Figure 3.15. Structural domains differentiated in the study area. UTM projection (zone 30, coordinates in km), ED50 datum

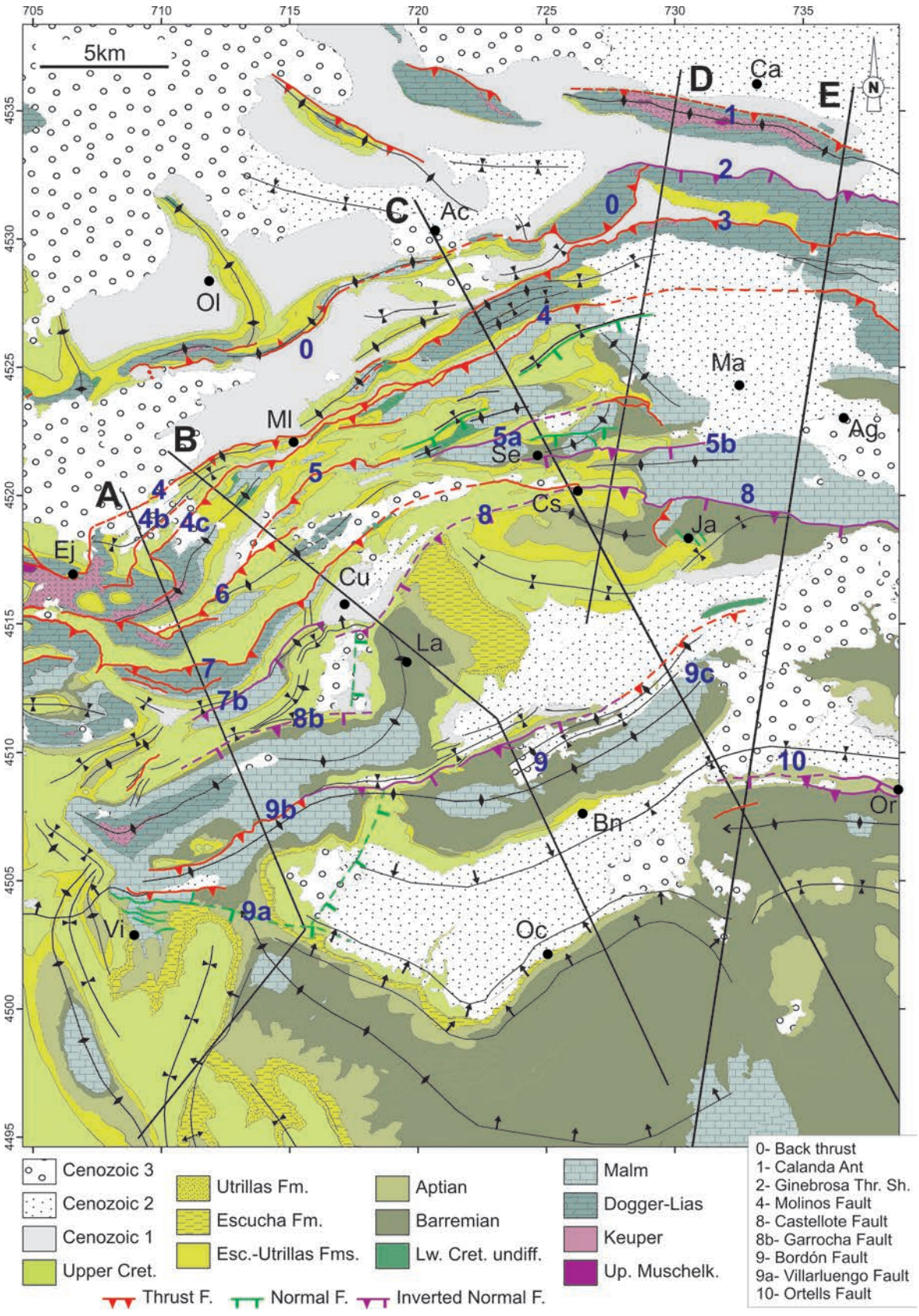

Figure 3.16. Structural and geological map of the frontal fold-and-thrust belt in the study area. The location of cross-sections is shown. Main structures are numbered as in the cross-sections of Figs. 3.10, 3.12. See location in Figure 3.9.

3.6.2.3 The slightly deformed southern uplifted area

The southern part of the study area experienced low internal deformation. At surface it is characterized, in its western part, in the surroundings of Fortanete-Mosqueruela, by a system of NW-SE-trending large folds –some of them are longer than 10km– with wavelengths of about 5km (Fig. 3.9). These folds are detached in the Middle Muschelkalk evaporitic facies, although some of them also involve the Acoustic Basement, as the Mirambell anticline (Figs. 3.4b, 3.14F-F'). At their northwestern end, some folds progressively change their orientation and become NNE-SSW-trending folds (Cuarto Pelado syncline and Tarayuela anticline, Fig. 3.9). The Tarayuela anticline also becomes a W-verging monocline in its N-S-trending segment, and generates a tectonic vertical step of about 450m, related to the inversion of the Tarayuela fault. In the supra-salt cover, other NW-SE-trending, N-verging monoclines of different scales are also observed, which can be attributed to thrusts in the Acoustic Basement, and some of them could be associated to inverted Triassic normal faults (Figs. 3.9, 3.14).

This area contains the wide uplifted area that remains elevated for about 40km in the N-S-direction, and contains a wide extension of Upper Cretaceous rocks (the Maestrat basin post-rift rocks) and some remains of Cenozoic rocks, the last pre-contractional rocks, located above 1000m asl and wide extensions even above 1500m asl, reaching locally 2000 m asl (GUIMERÀ et al., 2010). The uplifted area coincides mostly with the Salzedella sub-basin and with the Vistabella threshold. In the study area, the uplifted area is bounded to the north by the ESE-WNW-trending, N-verging Calders monocline (Fig. 3.15). A tectonic step of 800 to 1200m can be deduced between units in the southern uplifted area and the downthrown area located north of it. This step was interpreted as the area where the sole thrust of the northern fold-and-thrust belt starts to involve the basement (GONZÁLEZ et al., 1998; GUIMERÀ and SALAS, 1996).

Cut off of the sub-salt/Acoustic Basement

As it has been explained previously, the sole thrust of the northern fold-and-thrust belt and the intermediate area is detached in the Middle Muschelkalk evaporites. Southwards, to the hinterland, this sole thrust also involves the Acoustic Basement, including the Variscan basement, below the slightly deformed uplifted area and the Calders monocline (Fig. 3.9, 3.10, 3.11, 3.14), as it developed as the contractional inversion of the Mesozoic normal fault system rooted in the basement (Fig. 2.3b). However, in the northern thin-skinned sector, some fragments of the Acoustic Basement were incorporated to some thrust sheets and transported to the north in the thrust system, mainly in the footwall of the main normal faults (Fig. 3.17), as in the footwall of the Castellote, Ladruñán and Garrocha normal faults. This sub-salt basement fragment is bounded to the north by the normal fault 7b in the western part, and by the fault 4 in the eastern part of the study area (Figs. 3.10, 3.12, 3.17). A fragment of the Acoustic Basement is also found in the footwall of the western part of the Bordón fault (Fig. 3.17). As it is observed in the cross-section A-A' (Fig. 3.10), the entire western part of the Ladruñán zone was accompanied by a fragment of the Acoustic Basement, in the footwall of the Carrascosa and the Villarluengo faults (Fig. 3.17). Another fragment of Acoustic Basement was incorporated in the hanging wall and footwall of the Ortells normal fault.

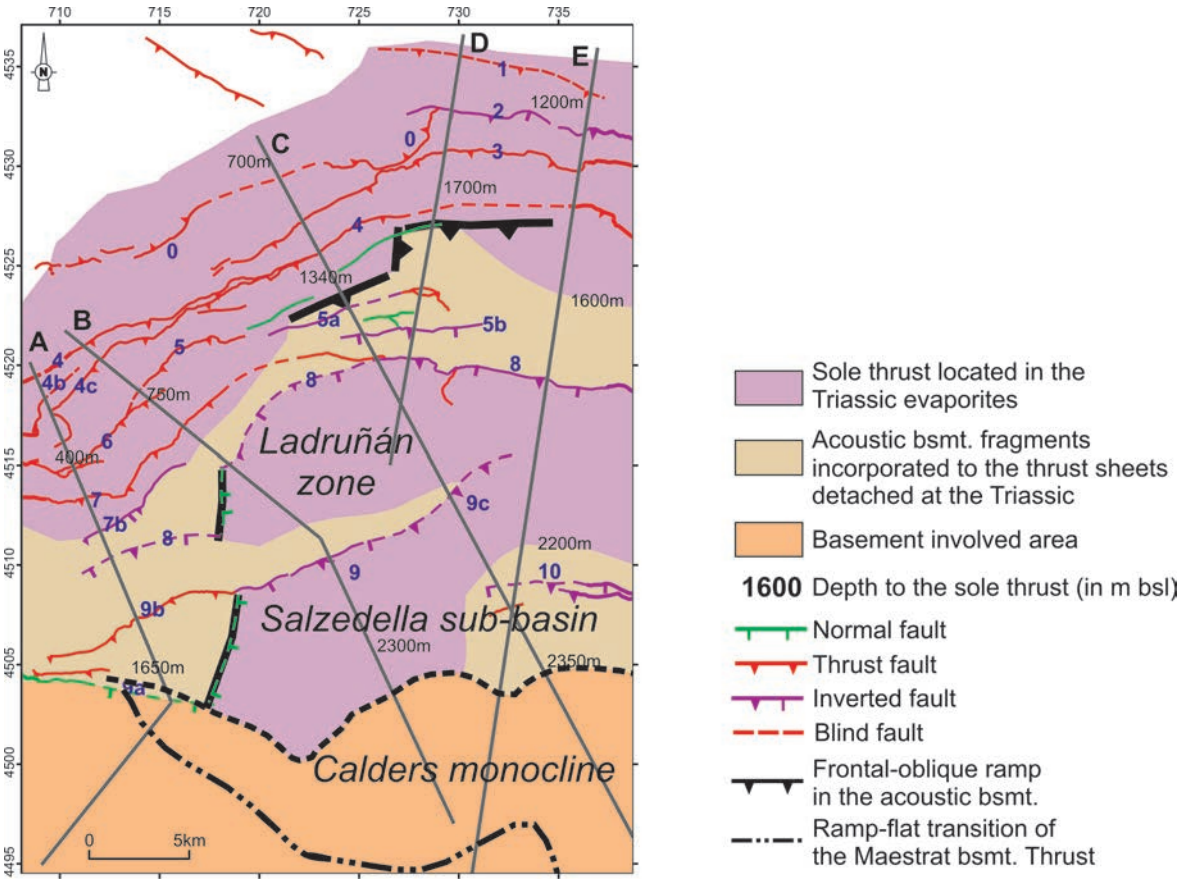

Figure 3.17. Simplified structural map displaying both the areas detached in the sub-salt or Acoustic Basement (Lower Muschelkalk, Buntsandstein and Variscan Basement) and those detached in the Triassic evaporitic units.

3.6.3 The Calders Monocline

The approximately E-W-trending, N-verging Calders monocline frontal tilted limb dips about 5ºN and is about 13km wide in its central widest part. Laterally, it becomes narrower (Fig. 3.18). It is the superficial structure of the tectonic step of 800-1200m, which in the study area can be measured between the base of the post-rift units in its southern uplifted horizontal limb and the northern termination of its tilted limb (Fig. 3.3c, 3.14F-F', 3.19-21, NEBOT and GUIMERÀ, 2016). It is modified in its central part by the N-S-trending box-fold Bovalar anticline, differentiating its eastern and western sectors (Fig. 3.18).

Structure of the eastern part of the Calders monocline

The eastern sector contains the widest part of the Calders monocline (Fig. 3.19), containing a tectonic vertical step of about 0.3s (about 800m) (Fig. 3.3c). In this sector, the northern synformal hinge of the Calders monocline is constituted by the Morella syncline (Fig. 3.18). The southern antiformal hinge of the monocline is located north of the Muixacre hill (Fig. 3.18), and changes its trend along-strike. It displays two broadly E-W-trending segments, joined by broadly N-S-trending segments (Fig. 3.18). Towards the E, its tilted limb narrows, as the Morella syncline and the antiformal southern hinge converge in the E-W-trending, N-verging Turmell fault, which cuts across the Calders monocline tilted limb (Fig. 3.18). The

Turmell fault terminates laterally, towards the W, and an E-W-trending, N-verging monocline is found at surface above its westward termination, modifying the structure of the Calders monocline limb (Fig. 3.18).

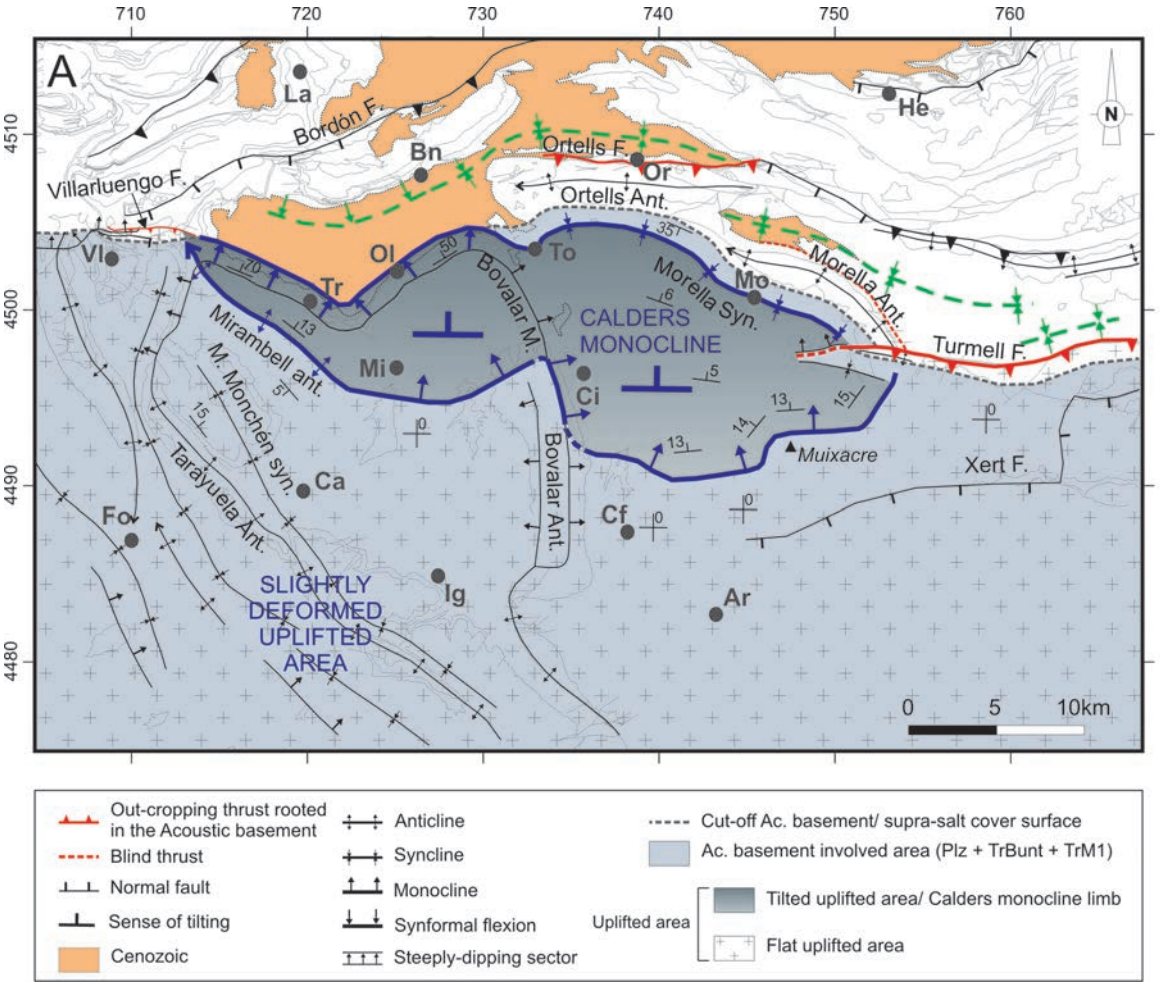

Figure 3.18. Structural map showing the major structures of the area studied and the location of schematic cross-sections (UTM projection (zone 30, coordinates in km), ED50 datum).

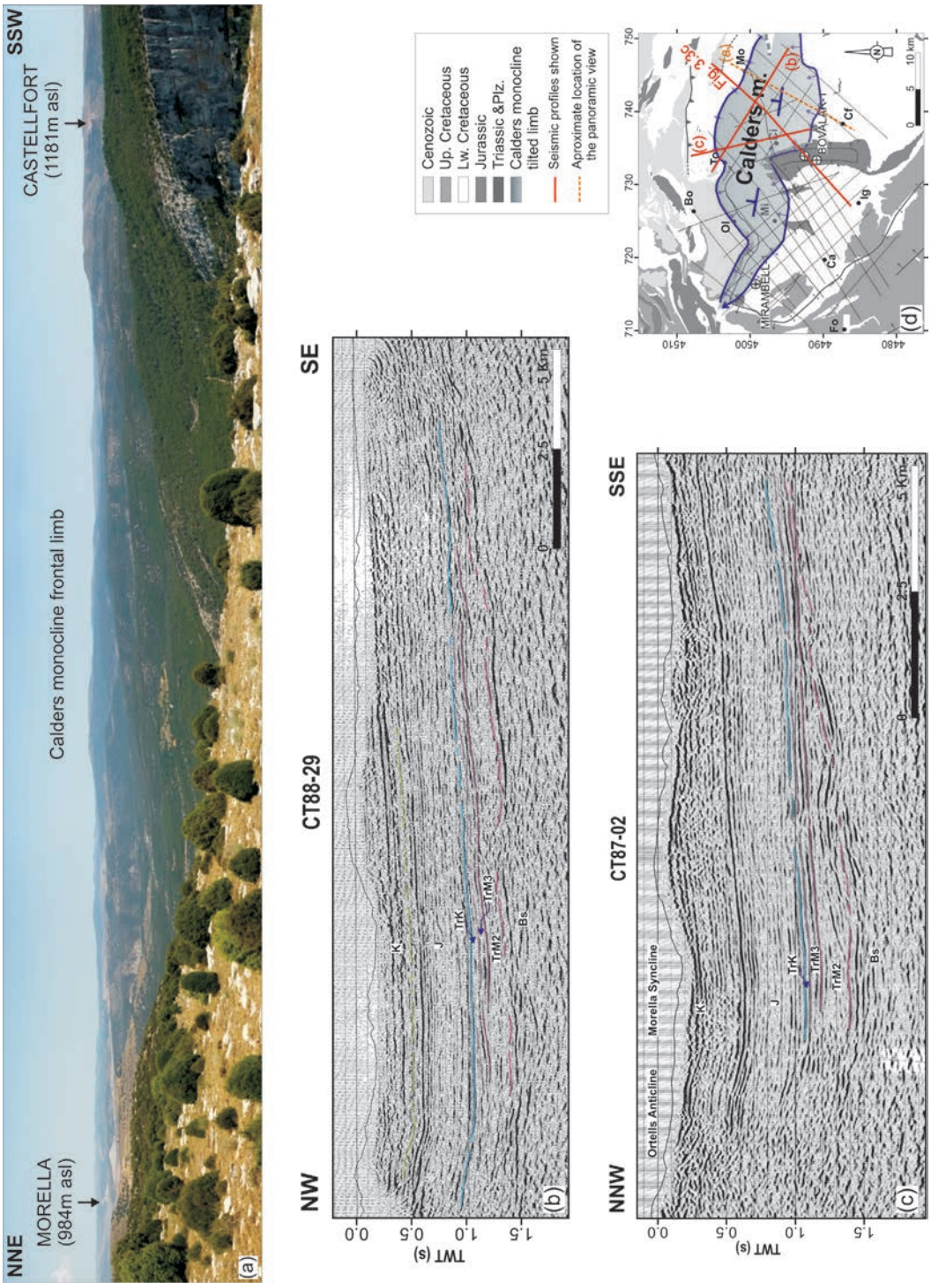

Figure 3.19. The eastern part of the Calders monocline observed in the seismic profiles and in the field. (a) Panoramic view of the Calders monocline from the Bovalar anticline. Castellfort, placed in the Artoles Fm. (Barremian) and Morella, placed in the Forcall and Villarroya de los Pinares fms. (Aptian) are identified, as well as their heights (in meters above the sea level). The tilting of the Lower Cretaceous rocks towards the north in of the Calders monocline limb, from Castellfort to Morella, can be observed. (b, c) Seismic profiles CT88-29 and CT87-02, across the eastern part of the Calders monocline limb. They traverse the monocline with different orientations (d), which are oblique to the Calders monocline dip direction. (d) Simplified geologic map for location of the seismic profiles shown, in the eastern part of the Calders monocline. See also Figure 3.3c. See location in Figs. 2.17, 3.1.

Structure of the western part of the Calders monocline

The asymmetrical NW-SE-trending, N-verging Mirambell anticline is the western continuation of the Calders monocline. Its southern limb gentle dips towards the south, while its frontal northern limb is divided into two dips domains: the southern, wider one dips about 3-15ºN, and the steeply dipping northern one dips between 25 and 70ºN (Figs. 3.11a, 3.14F-F', 3.18, 3.20a). Eastwards, the frontal limb of the Mirambell anticline becomes wider and changes its trend to NE-SW, maintaining the two dip domains (Figs. 3.18, 3.20b). A tectonic vertical step is recognized between the base of the Upper Cretaceous below the Cenozoic rocks of the Bordón Cenozoic basin, in the downthrown limb of this structure, and in the southern uplifted limb. This step is of about 800m, or 0.3s in the seismic profiles (Figs. 3.20a, 3.14F-F'), in the NW-SE-trending part, and of about 1000m (0.4s) in the NE-SW-trending side (Fig. 3.20b).

The steeply dipping northern limb of the Mirambell anticline ends in a synformal flexion parallel to the Mirambell anticline frontal limb (Fig. 3.18), being beds nearly flat to the north, below the Bordón Cenozoic basin (Fig. 3.20). This synformal flexion is the western continuation of the Morella syncline, while the southern antiformal hinge of the monocline is located in the Mirambell anticline hinge (Fig. 3.18). Westwards, the Calders monocline narrows and finally disappears in the hanging wall of the E-W-trending, S-dipping Villarluengo short-cut thrust (Fig. 3.19).

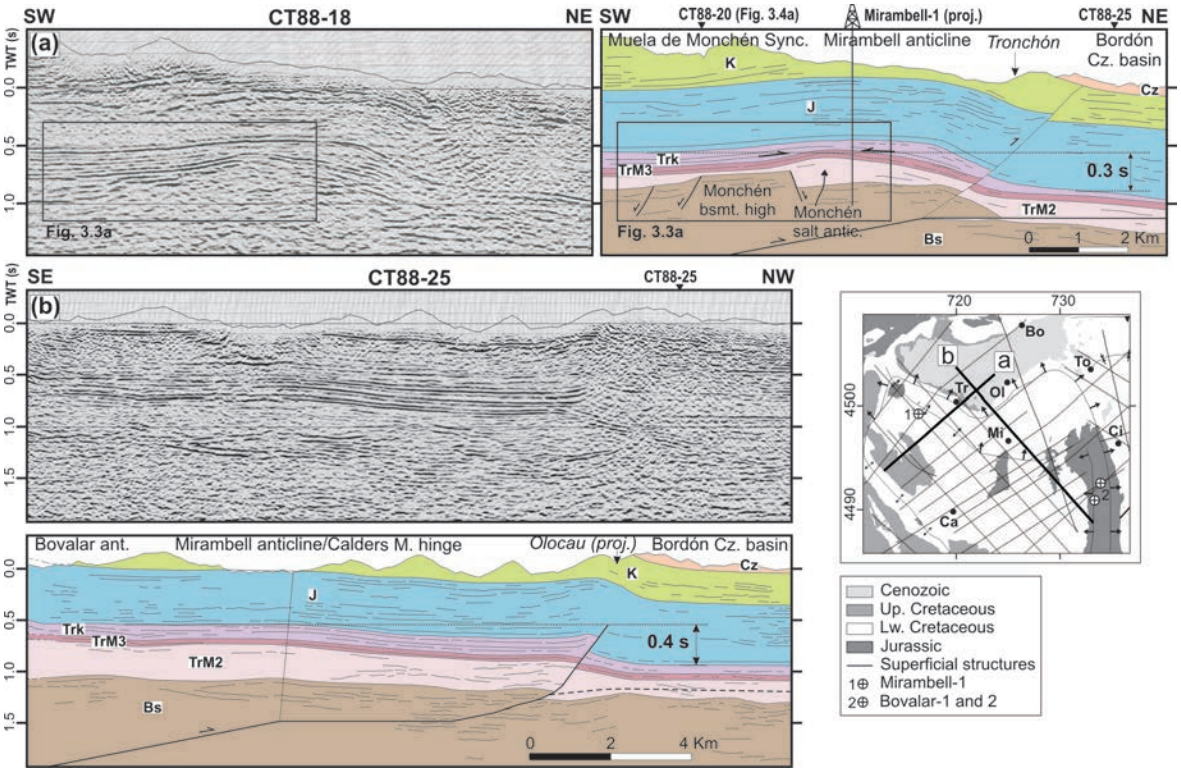

Figure 3.20. (a) Seismic profile CT88-18 and its interpretation. A vertical tectonic step of 0.3s (about 800m) is deduced between the base of the Jurassic in the Muela Monchén syncline and below the Cenozoic Bordón Basin. See Fig. 3.3a for a detail of the Keuper reflectors onlapping the folded Upper Muschelkalk. (b) Seismic profile CT88-25 and its interpretation. The Calders monocline limb and its southern hinge are shown. A vertical tectonic step of 0.4s (about 1000m) is measured comparing the base of the Jurassic. See Figure 3.2 for legend.

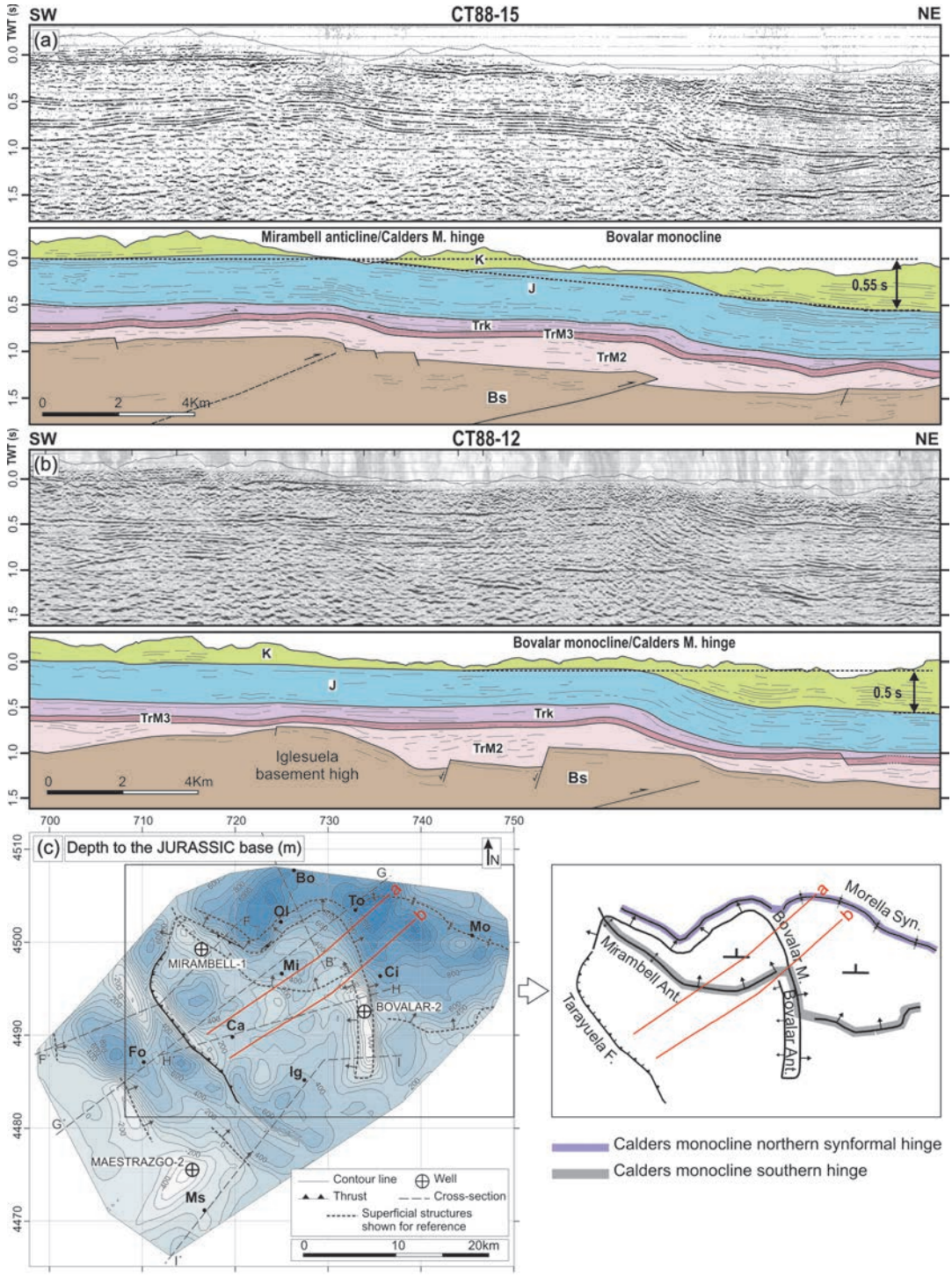

Figure 3.21. (a) Seismic profile CT88-15 and its interpretation. The tilted limb of the Calders monocline and its southern hinge –which is the transition from the tilted limb to the flat uplifted area south of it– are displayed. Within the Calders monocline limb, the Bovalar monocline is superimposed. (b) Seismic profile CT88-12 and its interpretation. The southern hinge of the Calders monocline is also observed, coinciding with the Bovalar monocline. A vertical tectonic step of at least 0.5s (about 1200m) can be measured between the flat uplifted area and the deepest parts of the tilted limb. (c) Contour map of the depth to the base of the Jurassic (in m below the sea level). Some superficial folds are shown for reference, and the trend of the Calders monocline hinges has been traced in a sketch. See Figure 3.2 for legend and figures 3.1 and 3.19 for location. UTM projection (zone 30, coordinates in km), ED50 datum.

Structure within the Calders monocline tilted limb: the Bovalar anticline

In the central part of the Calders monocline, the N-S-trending Bovalar anticline modifies its structure (Fig. 3.18). Two segments can be differentiated in this anticline: a northern NNW-SSE-trending, ENE-verging monoclinal segment –between La Todolella and Cinctorres– and a southern NNW-SSE to N-S-trending box-fold anticline (Figs. 3.18). The northern part of the monoclinal segment is located within the frontal tilted limb of the Calders monocline (Fig. 3.21a), while the southern part of the monoclinal segment coincides with the Calders monocline southern antiformal hinge (Fig. 3.21b). In this sector the highest tectonic vertical step of the Calders monocline can be measured, which is of about 0.5 s (about 1200 m) (Fig. 3.21). Towards the S, the Bovalar monocline becomes a box-fold anticline, near Cinctorres, having its western limb more elevated than the eastern one (Fig. 3.14H-H', 3.3c). More to the south, in the N-S-trending segment of the Bovalar anticline, the tectonic vertical step disappears, as both limbs of the anticline are at the same elevation (Fig. 3.14I-I'), being located in the southern slightly deformed uplifted area (fig. 3.18).

Structure north of the Calders monocline

North of the Calders monocline, a synformal area is find partially filled with Cenozoic terrigenous rocks (green dashed structure in Fig. 3.18). In the western part of the monocline, this synformal area is constituted by the Bordón Cenozoic basin, a flat-lying Cenozoic basin, bounded to the south by the Calders monocline northern synformal hinge. This Cenozoic basin terminates to the east, thrusted by the Ortells fault. In the eastern part of the monocline, two anticlines modify the structure of the northern synformal hinge of the Calders monocline, which become the Morella syncline. These structures are the E-W-trending Ortells anticline, located in the hanging wall of the Ortells fault, and the NW-SE-trending Morella anticline, also located in the hanging wall of a blind thrust. These thrusts relay laterally, as their associated anticlines (Ortells and Morella anticlines) have in common the NE limb of the Morella syncline (Fig. 3.18). The synformal structure located north of the Calders monocline (green dashed structure, Fig. 3.18) is interrupted in this sector, north of the Ortells anticline, and continues in a more internal position, north of the Morella anticline –containing a local remain of Cenozoic rocks– propagating to the east in the footwall of the Turmell fault. Therefore it is a complex synformal area, composed of different synclines that relay laterally.

The northern synformal hinge of the Calders monocline, constituted by the Morella syncline and the synformal flexion in the southern boundary of the Bordón Cenozoic basin, represents the northern boundary of the uplifted zone in the studied area.

Lateral continuation of the tectonic vertical step east and west of the Calders monocline

Towards the west, the Calders monocline terminates in the hanging wall of the Villarluengo thrust. This E-W-trending thrust continues to the W as a bling thrust, appearing at surface as a N-verging monocline for some kilometers more (Fig. 3.7a). More to the W, a tectonic vertical step of about 1.5km is measured in the southern and western margins of the Aliaga Cenozoic Basin, between the base of the Upper Cretaceous below the Cenozoic rocks of the Aliaga Cenozoic basin and south of it (Fig. 3.9,

GONZÁLEZ and GUIMERÀ, 1993; GUIMERÀ and SALAS, 1996), which could be the lateral equivalent of the tectonic vertical step observed in the studied area. The tectonic step of Aliaga has been interpreted as a result of a basement thrust (GUIMERÀ and SALAS, 1996), which could be considered as the lateral continuation of the Maestrat Basement Thrust (Fig. 3.15). Towards the east, the tectonic vertical step also continues beyond the Calders monocline termination, as the hanging wall of the Turmell thrust (Fig. 3.15) is uplifted, resulting in a fault throw of about 800m (GUIMERÀ, 1988).

Summing up, in the study area the Calders monocline constitutes the northern boundary of the wide, slightly deformed, uplifted area found in the hinterland of the Linking Zone. It is associated to a vertical tectonic step of about 1200m – 0.5s in its central part. The Calders monocline narrows laterally and the associated vertical step also decreases laterally, being to the E and W of about 800m – 0.3s. The Calders monocline terminates laterally, but the tectonic vertical step is maintained to the E in the Turmell thrust and to the W in the N-verging monocline found in the hanging wall of the Villarluengo thrust, and more to the west in the southern margin of the Aliaga Cenozoic basin. The uplifted area also extends beyond the study area, from the Turmell fault to the southern boundary of the Cenozoic Aliaga basin, containing, to the south, the Peñarroya mountain (2028m asl).

3.6.4 Transport direction and estimated shortening

The transport direction was interpreted to be NNE-SSW, which is the vector normal to the main trend of structures in the studied area, which is ESE-WNW, coinciding with the trend of the Calders monocline, the Ortells fault, the Calanda anticline and the two thrusts south of it, the Castellote fault in its northernmost segment (Fig. 3.9). West of the area studied it also coincides with the overall strike of the Utrillas thrust. The sense of transport is towards the NNE. This transport direction is coincident with the one proposed by GUIMERÀ and ÁLVARO (1990) for the Iberian Chain. It also coincides with the total transport vector estimated by Simón and Liesa (2011) for the Utrillas thrust, oriented to the N032E, with a displacement of 5.9km.

The shortening value was estimated after restoring the cross-sections D-D' and E-E' (Fig. 3.12), which contain the deduced transport direction. The shortening value obtained from restoring the cross-section E-E' is 10.5km, which is mostly concentrated in the northern fold-and-thrust belt. It has to be considered that this is a minimum shortening value, as the cross-section was constructed in a conservative manner, and the structures interpreted below the Cenozoic outcrops could accumulate additional shortening. Furthermore, the deformation associated to mesostructures was not considered. The shortening value obtained after restoring the cross-section D-D' is 11.2km. This cross-section only traverses the northern fold-and-thrust belt (Fig. 3.9). If the shortening in the N FAT belt is calculated, placing the pin line in the Cenozoic rocks in the footwall of the Calanda thrust sheet, and the loose line in the Castellote fault, a shortening value of 10.9km (40%) is obtained for the cross-section D–D' and a value of 9.1km (35%) for the cross-section E–E' (Fig. 3.12). Assuming that shortening does not vary laterally in this ESE– WNW-trending part of the N FAT belt, shortening obtained in both cross-sections for the N FAT belt should be similar. However a difference of 1.8km of shortening is obtained, which was not recorded in cross-section B–B' probably due to the Cenozoic rocks covering some of the Mesozoic outcrops. Consequently,

cross-section B-B' could accumulate 1.8km of additional shortening in the N FAT belt, reaching a total shortening of 12.3km.

Considering the NNE-SSW transport direction and some segments of the cross-sections, an idealized cross-section of the entire northern margin of the Maestrat basin was constructed, from the Vistabella threshold to the Ebro foreland basin, and including the Penyagolosa sub-basin towards the S (Fig. 3.22). This idealized cross-section was also unfolded in order to obtain an overall vision of the extensional structure of the norther margin of the Maestrat basin. Based on this idealized-cross section, a reconstruction of the geometry of the basement thrust that generated the slightly deformed uplifted area in the hinterland was obtained (Fig. 3.23).

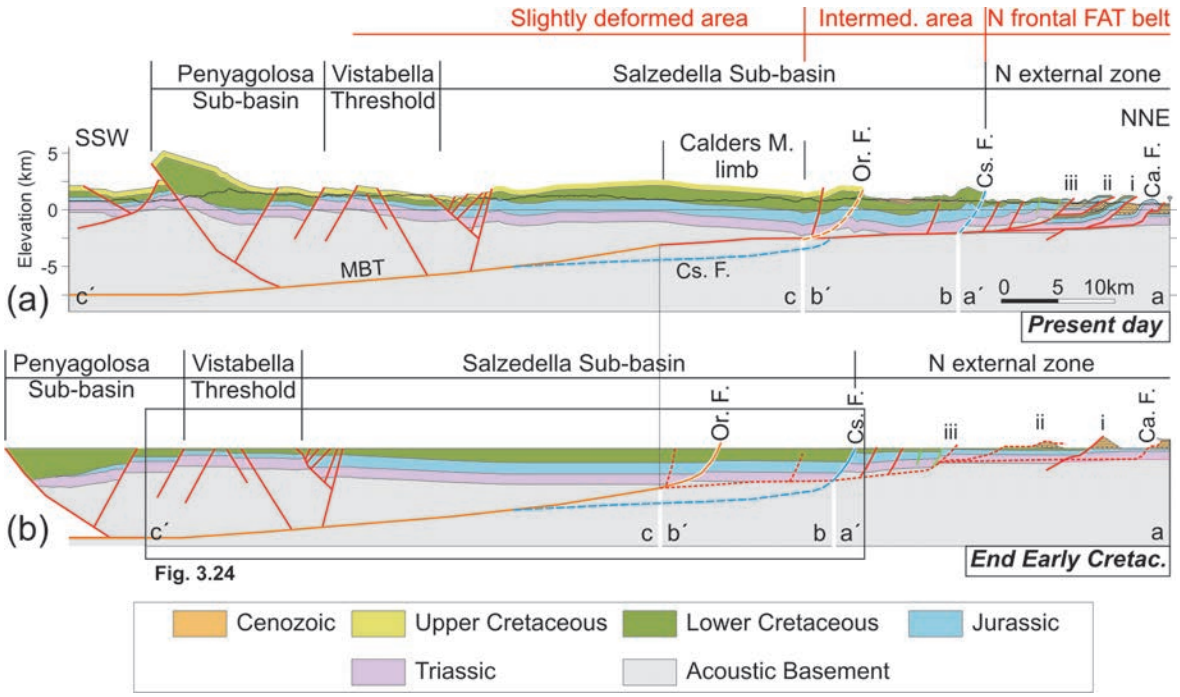

Figure 3.22. Idealized section of the study area and the Penyagolosa sub-basin, obtained by combining cross sections D–D', E–E' (Fig. 3.10) and an unpublished cross-section from GUIMERÀ. The interpreted evolution of the area studied is shown. See location in Fig. 3.15. Abbreviations: MBT-Maestrat Basement Thrust, Or.F.-Ortells Fault, Cs.F.-Castellote Fault, Ca.F.-Calanda Fault.

3.6.5 The Maestrat Basement Thrust geometry

The Calders monocline is interpreted as a fault-bend fold, which is the surface expression of a ramp to flat transition in a basement thrust, the Maestrat Basement Thrust (MBT, Figs. 3.22, 3.23). The low-dip of the Calders monocline frontal tilted limb, along with the wide extension of the uplifted area generated in the hinterland, suggest a low-angle dip for the Maestrat Basement Thrust ramp (Figs. 3.22a).

Taking into account the idealized section (Fig. 3.22), and the shortening values obtained for the frontal fold-and-thrust belt, a generalized interpretation of the geometry of the Maestrat basement thrust was modelled in 2D with the Move software (Fig. 3.23). This fault geometry was tested by displacing the restored horizons of the Salzedella sub-basin in the idealized cross-section, for 12km above the hanging wall of this fault, using the fault-bend-fold algorithm. The geometry of the fault was modified until obtaining a geometry in the supra-salt cover similar to that observed in the study area. The fault geometry obtained is shown in Fig. 3.23b, which was also included in the idealized section in Fig. 3.22. It has a low-dip ramp, with an approximately listric geometry, dipping about 9ºS in its shallowest part, and flattening downwards until reaching a depth of about 7.5km below the sea level. It extends southwards for more than 40km. Towards the north, the basement thrust ramp evolves into a very gentle south-dipping flat (Fig. 3.23).

In the model (Fig. 3.23b), the displacement of the basement in the hanging wall of the fault, above its low-dip ramp, generates an uplifted area of about 40km wide in the N-S-direction and a vertical tectonic step of about 1200m. A fault-bend-fold develops in the transition from ramp to flat, which has a frontal tilted limb about 12km wide and dips about 6ºN, which is very similar to the Calders monocline geometry.

The Calders monocline is wider in its central part and narrows laterally. For this reason it appears wider in the idealized section, which traverses it nearly through its widest central part, than in the cross-section E-E', which traverses it more to the west, in a narrower part.

The inversion of the NW-SE-trending, NE-dipping Penyagolosa normal fault, which generated the Penyagolosa sub-basin, also uplifted locally the Mesozoic cover and the basement (Fig. 3.23). These local structures also help to maintain elevated this wide area towards the S.

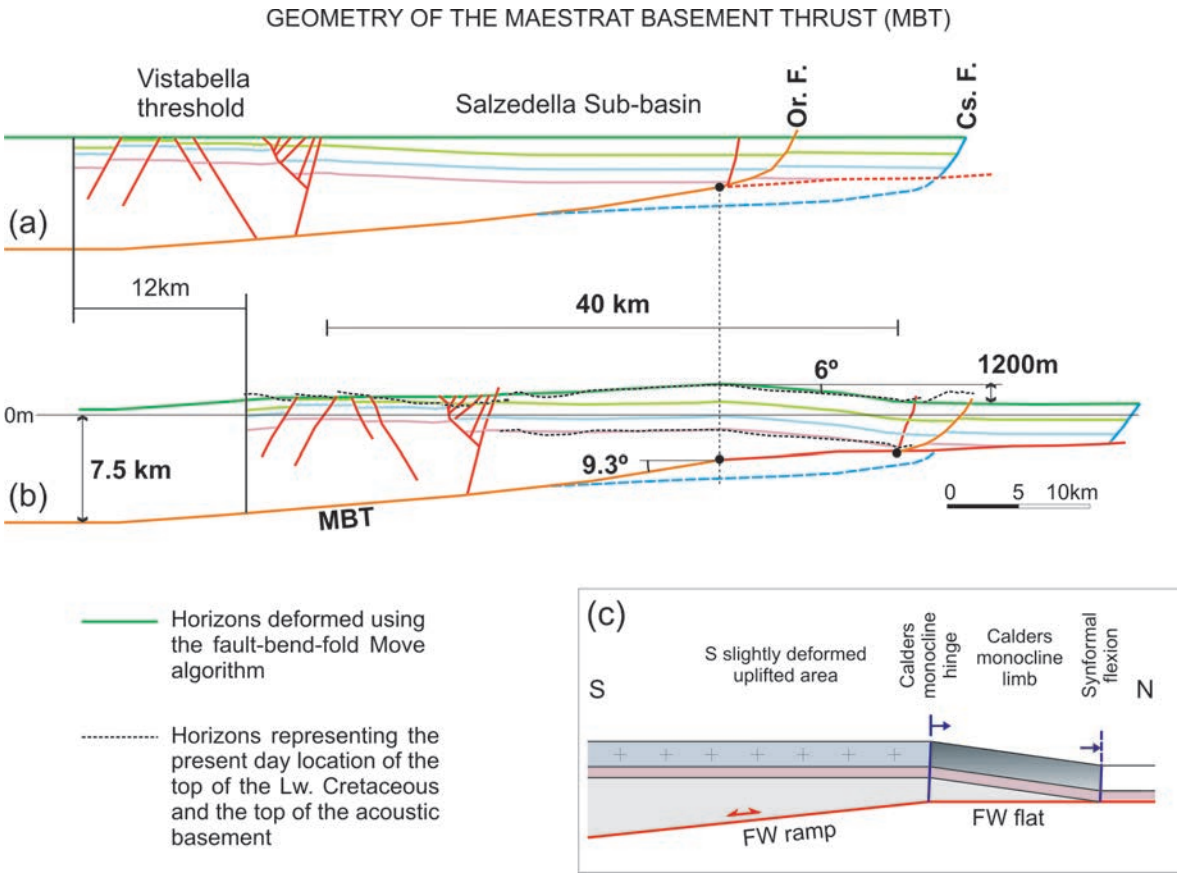

Figure 3.23. (a) Idealized section of the Salzedella sub-basin at the end of the Mesozoic extension (end of the Early Cretaceous). It is based on the generalized section in Fig. 3.22. (b) Forward modelling of section (a) using the fault-bend-fold deformation algorithm with Move®. The resulting horizons are compared to the corresponding horizons in the idealized section in Fig. 3.22 in order to test the geometry of the Maestrat Basement Thrust. The Castellote normal fault (Cs. F.) was not inverted in this model. Its upper segment across the supra-salt cover was only passively transported within the thrust system. (c) Conceptual model of the interpreted geometry of the Maestrat Basement Thrust. The transition from ramp to flat explains the formation of the Calders monocline fault-bend fold, and the low dip ramp explains the low dip of the monocline and the maintained uplifted area generated in the hinterland.

4. DISCUSSION

4.1 INTERPRETATION OF THE EXTENSIONAL STRUCTURE AND EVOLUTION OF THE MESOZOIC MAESTRAT BASIN IN THE STUDIED SECTOR

The interpretation of the Mesozoic extensional structure and evolution in the studied sector of the Maestrat basin is described below, which is based on the interpretation of the results described in Chapters 3.2 to 3.5.

4.1.1 Triassic

Although units in the acoustic basement are not recognized in the seismic profiles, previous studies (ÁLVARO et al., 1979; SALAS et al., 1997; BARTRINA and HERNÁNDEZ, 1990, SANCHEZ-MOYA, 1992) suggest that the high-angle normal faults affecting the acoustic basement would have been active during the deposition of the Buntsandstein facies (Late Permian-Anisian) until the deposition of the lower part of the Middle Muschelkalk facies (BARTRINA and HERNÁNDEZ, 1990; NEBOT and GUIMERÀ, 2016a), which displays great thickness variations (Fig. 4.1a). A period of lower extensional activity occurred during the deposition of the upper part of the Middle Muschelkalk facies and the Upper Muschelkalk carbonates (Ladinian), as they overlie the normal fault system, and the Upper Muschelkalk shows nearly constant thickness (Fig. 2.5, 4.1b).

East of the study area, near the Mediterranean coast, in the Salzedella-1 and the Maestrazgo-1 exploration-wells, no Muschelkalk sediments are found (Fig. 4.2), and the Buntsandstein facies is overlaid by the Keuper facies (Fig. 2.5, MARTÍNEZ-ABAD, 1991). More to the south, in the Desert de les Palmes area, N of Castelló (Fig. 4.2), there are only about 100m of Upper Muschelkalk carbonates, which directly overly the Buntsandstein facies (ESCUDERO-MOZO et al., 2015; LÓPEZ-GÓMEZ et al., 2005). A NE-SW-trending, NW-dipping, normal fault has been interpreted by MARTÍNEZ-ABAD (1991) and SALAS (pers. Com.) separating this sector with no or poor deposition of the Muschelkalk facies in the footwall of the fault, which can be associated to a basement high, from the area with a thick Middle Muschelkalk sequence in its hanging wall (Fig. 4.2). This interpretation is supported by a magnetotelluric survey (MARCUELLO et al., 2006), which detected quite different responses in the Triassic and Paleozoic rocks at both sides of the deduced fault.

The deposition of the upper part of the Middle Muschelkalk and the Upper Muschelkalk facies during a low extensional period (Ladinian), is in accordance with the observations in the Desert de les Palmes area, indicating that the Upper Muschelkalk carbonate platforms surpassed and covered the extensional structures which affected the acoustic basement and the lower part of the Middle Muschelkalk. In the northern part of the basement high, no Muschelkalk appears (Fig. 4.2), which could have been eroded or never been deposited.

The extensional activity resumed during the Late Triassic (Carnian-Norian). Some high angle normal faults in the acoustic basement were reactivated, but they did not propagate upwards across the Middle Muschelkalk, as it is deduced from the forced folds observed in the Upper Muschelkalk above some of these faults in the acoustic basement (Fig. 4.1c), and from the growth-strata in the Keuper seismic reflectors above the downthrown bloc of one of the forced folds.

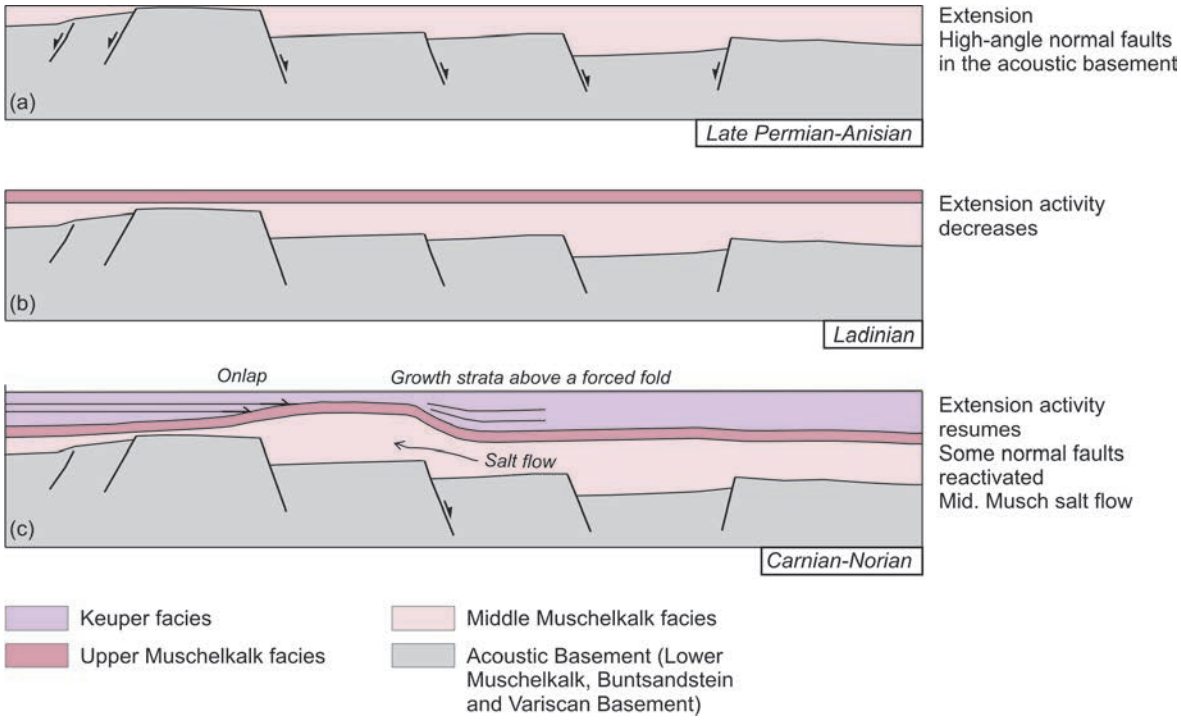

Figure 4.1. Sketches showing the interpreted evolution of the extensional structure during the Late Permian-Triassic, based on the seismic profiles interpreted and the exploration wells. (a) Deposition of the Buntsandstein, the Lower Muschelkalk and the lower part of the Middle Muschelkalk facies during extensional activity of high angle normal faults. (b) The extensional activity decreases and the upper part of the Middle Muschelkalk and the Upper Muschelkalk are deposited overlying the extensional structure. (c) The extensional activity resumes and some normal faults in the acoustic basement are reactivated, producing forced folds in the Upper Muschelkalk facies and Middle Muschelkalk salt flow. The Keuper facies is deposited during the extension, lapping on the folded Upper Muschelkalk and displaying growth strata above the forced folds.

In the study area, and in the southern Ebro Basin (BUTILLÉ, et al., 2012), some salt structures developed in the Middle Muschelkalk evaporitic facies. Conversely, in other areas of the Iberian Peninsula, the salt tectonics is associated to the Keuper facies (Prebetic (ORTÍ, 1973), Basque-Cantabrian Basin (SERRANO and MARTÍNEZ DEL OLMO, 2004), Parentis Basin (FERRER et al., 2012), Cotiella Basin-Pyrenees (LÓPEZ-MIR, 2015), etc.

In the seismic profiles some salt anticlines and welds are observed in the Middle Muschelkalk facies. The Upper Muschelkalk is folded above them, while the Keuper reflectors onlap the folded Upper Muschelkalk carbonates. Consequently, some Middle Muschelkalk salt flow occurred after the Upper Muschelkalk deposition, probably triggered by the reactivation of the extensional structures during the Keuper deposition. The differential load exerted by the Keuper, which was deposited adapting to the geometry of the folded Upper Muschelkalk, could have enhanced the salt flow.

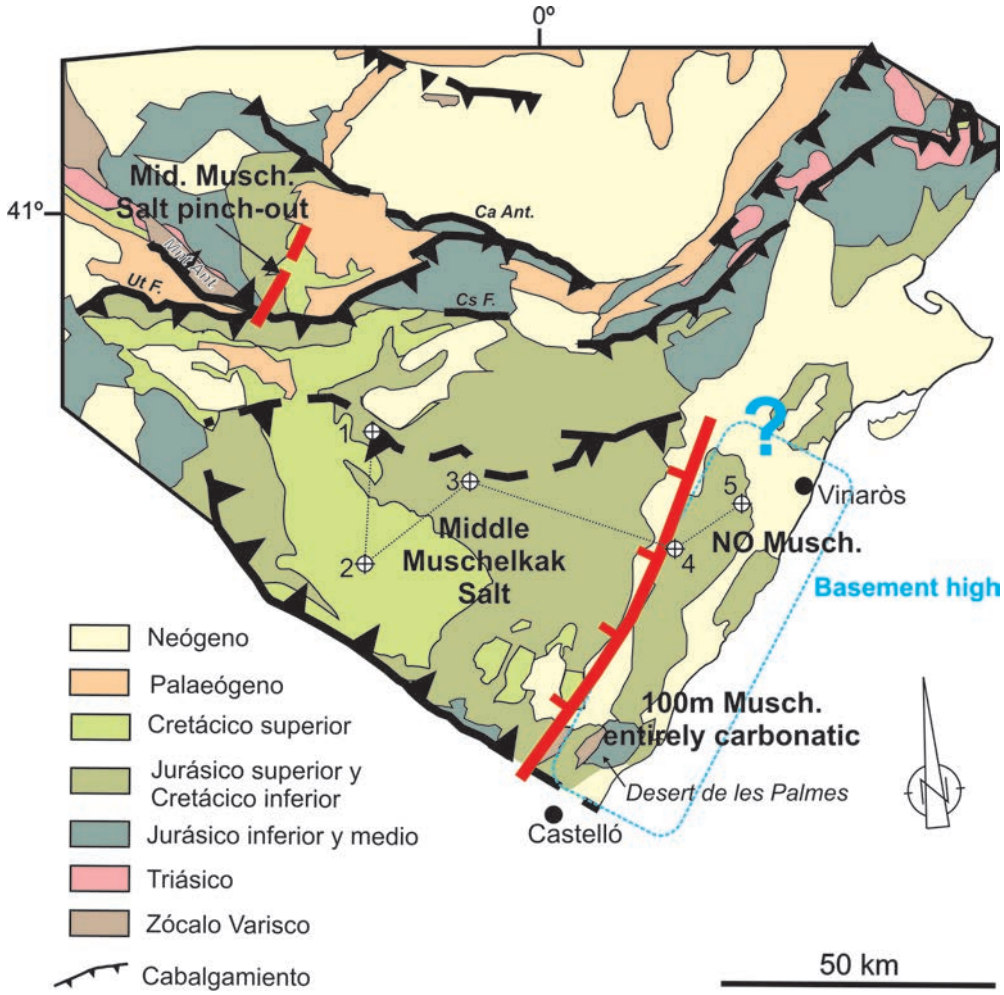

Figure 4.2. The NNE-SSW-trending WNW-dipping normal fault is based on MARTÍNEZ-ABAD (1991), SALAS (pers. Com.), MARCUELLO et al. (2006). The location of the exploration wells and the trace of their correlation in Fig. 2.5 is shown. Wells: 1= Mirambell-1, 2= Maestrazgo-2, 3= Bovalar-1, 4= Salzedella-1, 5= Maestrazgo-1. Ca Ant. = Calanda Anticline, Cs F., Castellote Fault, Mnt Ant.= Montalbán Anticline, Ut F.= Utrillas Fault. The western salt pinch-out is explained below, in Chapter 4.2.5. See Figs. 2.13, 4.7 for location reference.

4.1.2 Jurassic

In order to figure out the Jurassic structure it would be necessary to study a wider area than the present one, as the Jurassic sub-basins seem to be wider than the Lower Cretaceous ones.

The thickness variations observed in the Lower Lias units (Cortes de Tajuña and Cuevas Labradas Fms., Fig. 2.5), are in agreement with the hypothesis that some extensional tectonics occurred during this period (GINER, 1980; AURELL et al., 1992, SAN ROMAN and AURELL, 1992; ROCA et al., 1994; CAMPOS et al., 1996; BORDONABA and AURELL, 2001), commonly attributed to the post-rift of the Triassic rifting event (SALAS et al., 2001). AURELL et al (1992) described a rifting event during the Hettangian-Lower Pliensbachian, controlled by listric normal faults, which could have generated the thickness variations in the Lower Lias units. However, in other parts of the Iberian Chain the Cortes de Tajuña Fm. has also been related to evaporite solution, collapse and breccia formation (MORILLO-VELARDE and MELÉNDEZ, 1979; BORDONABA and AURELL, 2002; ORTÍ and SALVANY, 2004; GÓMEZ et al., 2007), which could also explain part of the thickness variations of this unit.

The rifting event during the Lower Lias (AURELL et al., 1992) was separated from the Malm rifting event by a lower extensional period occurred during the Upper Lias-Lower Malm, as units of this age (Ablanquejo Group, Chelva Fm. and Iàtova Fm.) show nearly constant thicknesses in the exploration-wells (Fig. 2.5). Furthermore, in the area studied, these units are thinner than in the surrounding areas, as in the Maestrazgo-1 exploration well (Fig. 2.5). In the northern external zone of the Maestrat basin, north of the Castellote normal fault, the units of these ages are missing, being the second syn-rift Polpis Fm. unconformably lying onto the Cuevas Labradas Fm.

Regarding the Malm units – except for the Iàtova Fm.– their thickness variations seem to be controlled by the same mechanisms that controlled the Lower Cretaceous deposition, as it also becomes thinner towards the north, towards the basin margin. Big thickness variations of these units can also be recognized by comparing the thicknesses in the area covered by the exploration-wells, 650-407m, in the central part of the Salzedella sub-basin, with the thicknesses in the adjacent area of Albarracín, about 250-270m (HERNÁNDEZ, 1985), in which the Lower Cretaceous is absent or very thin (locally reaches 110m). This suggests that the boundaries of the basin during the Jurassic extension probably do not coincide exactly with the Lower Cretaceous basin ones, and so a larger area should be considered in order to better characterize the thickness variations of the Malm.

However, some of these thickness variations can be associated to the same faults that controlled the Lower Cretaceous sedimentation. The Villarluengo normal fault, for example, separates 1122m of Jurassic rocks in the Mirambell-1 well, in its hanging wall, south of the fault, from about 610m measured in the Cabezo Gordo section, in its footwall, north of the fault (Fig. 3.5).

4.1.3 Cretaceous

The interpreted distribution of the Lower Cretaceous sub-basins developed within the Maestrat basin, and the distribution of the structures bounding them, slightly differ from the one described by SALAS and GUIMERÀ (1996). The present thesis proposes to differentiate the Ladruñán zone within the Salzedella sub-basin, whose northern boundary is displaced northwards, to the Castellote Fault (Fig. 3.6).

In the study area the distribution of the Lower Cretaceous rocks and the extensional structures, which display varying orientations, suggest a segmented system of normal faults, connected by relay ramps, bounding the different sub-basins.

The Maestrat basin filling, broadly becomes thinner towards the north, towards the northern boundary of the basin (Fig. 3.5b). However, as previously explained, the geometry of the Lower Cretaceous syn-rift filling of the Salzedella sub-basin resembles a wide wedge that thickens towards the North, to the hanging wall of the S-dipping main normal faults (Castellote and Bordón normal faults). The sedimentary filling (Barremian and Aptian units) is also controlled by the minor normal faults system that can be observed all around the basin (Fig. 3.6). This wedge geometry could be associated to a wide rollover, influenced by minor normal faults, some of them antithetic to the main S-dipping normal faults.

The Ladruñán zone thickens towards the NE, to the ESE-WNW-trending segment of the Castellote normal fault. The overall NE tilting can also be associated to a rollover fold developed in the hanging wall of the Castellote normal fault (Fig. 3.5c).

Although the Barremian and Aptian deposition was mostly controlled by the same extensional structures, the extension was more active during the Barremian than during the Aptian, as thickness variations of the Barremian units are bigger than the Aptian ones. Regarding the Escucha Formation, it was deposited during a period of extension, although the extensional structures that controlled it do not correspond to the ones that controlled the deposition during the Barremian and Aptian sedimentation. The Utrillas Fm. (Late Albian) and the Upper Cretaceous rocks covered the previous extensional structures, as they were deposited during the Late Cretaceous post-rift event.

If the contractional deformation is restored, a N-S-trending gentle anticline is found in the central part of the Ladruñán zone, modifying the rollover geometry (Fig. 3.5c, 3.9B-B'). The angular unconformity observed at both sides of this anticline, in which the post-rift units unconformably overlie different Lower Cretaceous units, indicates that this gentle anticline developed during the Early Cretaceous extension. It probably developed as a transverse fold above the relay zone between the Castellote and the Garrocha normal faults, in the hanging wall of the Ladruñán normal fault (breached relay ramp). This anticline was reactivated during the Cenozoic contraction, while the Castellote, the Ladruñán and the Garrocha normal faults were partially reactivated as reverse faults.

In map view, the Carrascosa and the Ladruñán breached relay ramps are aligned, coinciding with the NNE-SSW-trending segment of the Tarayuela normal fault, which can be interpreted as a relay fault zone (Fig. 3.5).

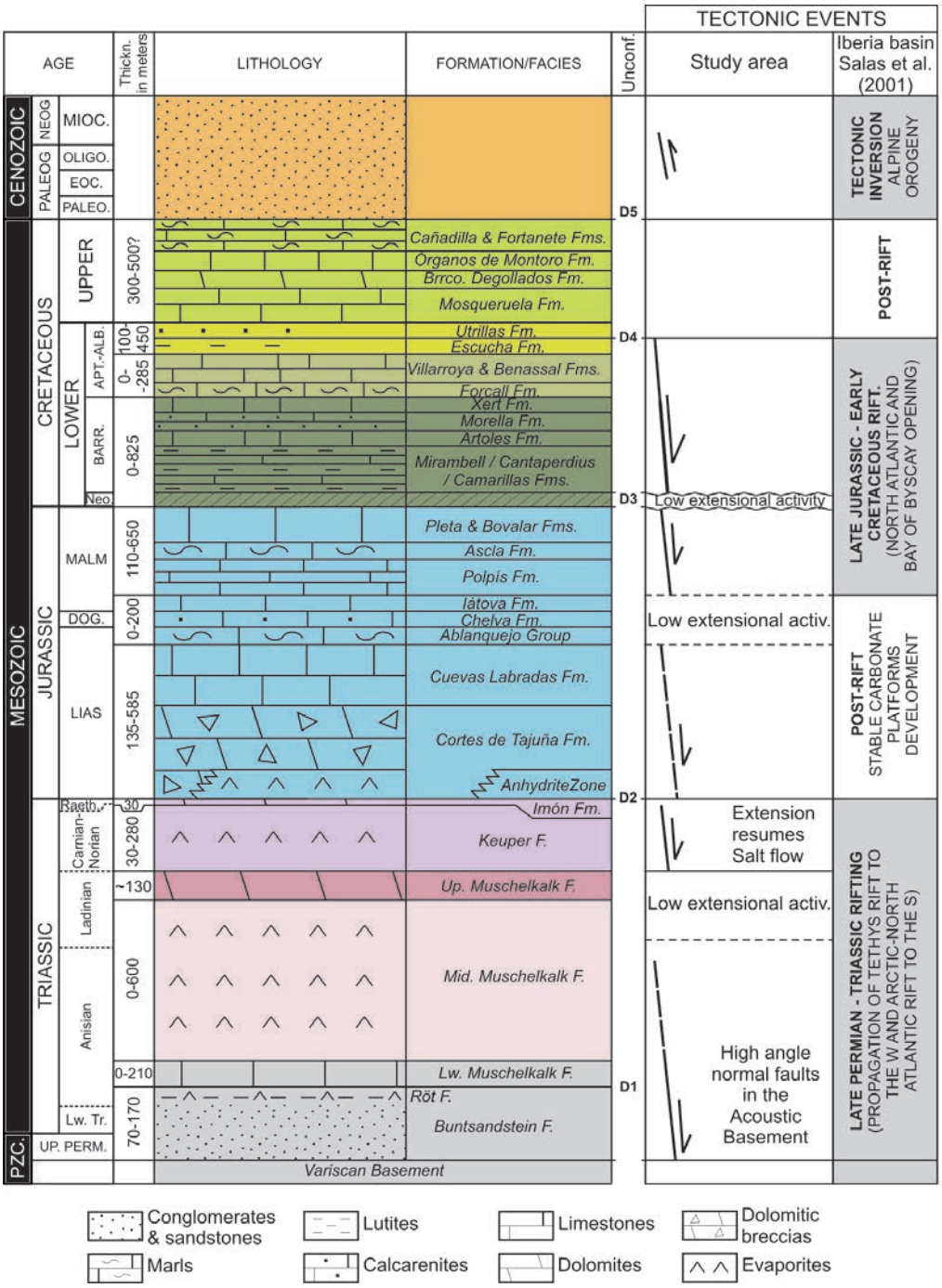

Figure 4.3.- Generalized stratigraphic sequence of the Eastern Salzedella sub-basin, and tectonic events in the study area. Modified from NEBOT and GUIMERÀ (2016), after SALAS (1987), SALAS et al. (2001), AURELL et al. (1992) for the Lias, and BOVER-ARNAL et al. (2015) for the Barremian–Aptian boundary. Thickness values are based on the exploration wells (Fig. 2.5, MARTÍNEZ-ABAD, 1991) and from the stratigraphic sections in Fig. 3.5.

4.2 INTERPRETATION OF THE CENOZOIC CONTRACTIONAL STRUCTURE AND EVOLUTION IN THE NORTHERN MARGIN OF THE MAESTRAT BASIN

4.2.1 Relationship between the Cenozoic contractional structures and the previous Mesozoic extensional ones

The Maestrat basin was controlled by a system of normal faults of multiple orientations. The normal faults were not continuous and the different faults segments were connected by relay ramps, which divided the basin into different sub-basins or zones, resulting in a heterogeneous sedimentary filling of varying thicknesses. Although the syn-rift units broadly become thinner towards the north, towards the basin margin, thicknesses of these units vary considerably, controlled by the normal fault system. As it was explained in chapter 3.6.1, during the Cenozoic inversion of the basin some contractional structures inherited the orientation of previous Mesozoic extensional structures, which resulted in the formation of folds and thrusts with different orientations.

Furthermore, structures with the lowest wavelengths (the northern fold-and thrust belt) developed in the northern external zone of the basin, as the syn-rift filling of the basin is the thinnest in this zone, and so it is the entire supra-salt cover, facilitating the formation of tighter structures. As the syn-rift filling becomes thicker towards the S, basinwards, the contractional structures developed become gentler, with open folds and more separated thrusts.

The orientation of previous extensional structures with regard to the transport direction could have influenced in their amount of inversion. Fault segments perpendicular to the transport direction show greater amount of inversion than segments oriented oblique to it. The Castellote fault is a good example as the amount of inversion varies along-strike, as well as its orientation. The inversion of this normal fault cut the post-rift rocks in its ESE-WNW-trending segment, normal to the transport direction, while in the NE-SW-trending segment the post-rift was only folded.

In the substratum of the Maestrat basin, the Middle Muschelkalk evaporitic facies also displayed significant thickness variations, resulting from the distribution of horsts and grabens in the acoustic basement, which also conditioned the development of some contractional structures, as the Bovalar anticline.

The Bovalar box-fold anticline is an example of the influence of previous extensional structures and of a thick evaporitic detachment level. This anticline coincides with a depressed basement block, above which, a thick Middle Muschelkalk was deposited (Fig. 3.3), which could have facilitated the development of a detachment anticline. However, the triggering factor could have been the Cenozoic inversion of a NNW-SSE-trending Triassic normal fault in the acoustic basement, like those interpreted in Figure 3.21b, as a tectonic vertical step can be deduced between both limbs of the Bovalar anticline in its northern segment, so a basement thrust was interpreted below it. Moreover, the Bovalar anticline becomes a N-verging monocline towards the NW. The thick Middle Muschelkalk evaporitic facies could have facilitated the propagation of the Bovalar anticline southwards as a detachment fold, beyond the

basement thrust termination.

As explained in chapter 3.2.3, in the study area other Cenozoic detachment folds are deduced, as there are the Tarayuela or the Cañada de Benatanduz anticlines, as the salt flew towards the lower-pressure cores of the rising anticlines, which generated elongated Middle Muschelkalk accumulations (Fig. 3.3e).

The Monchén salt anticline, located north of the Monchén basement high, could have conditioned the formation of the Mirambell anticline (Fig. 3.4, 3.20a). The Cenozoic NW-SE-trending Mirambell anticline involves the acoustic basement and includes in its core the Monchén salt anticline (Fig. 4.5a). If the Cenozoic anticline is unfolded, taking the base of the Jurassic as a datum (Fig. 4.4), the Upper Muschelkalk still remains folded above the Middle Muschelkalk salt accumulation, indicating two folding periods in the Mirambell anticline. The first one took place during the Late Triassic, as the Middle Muschelkalk evaporitic facies flew towards the Monchén salt anticline, folding the Upper Muschelkalk. The second one occurred during the Cenozoic, as the entire cover and the acoustic basement were folded coinciding with the salt anticline, which together with the structures in the acoustic basement, probably triggered and conditioned the location and the orientation of the Cenozoic fold (Fig. 4.5).

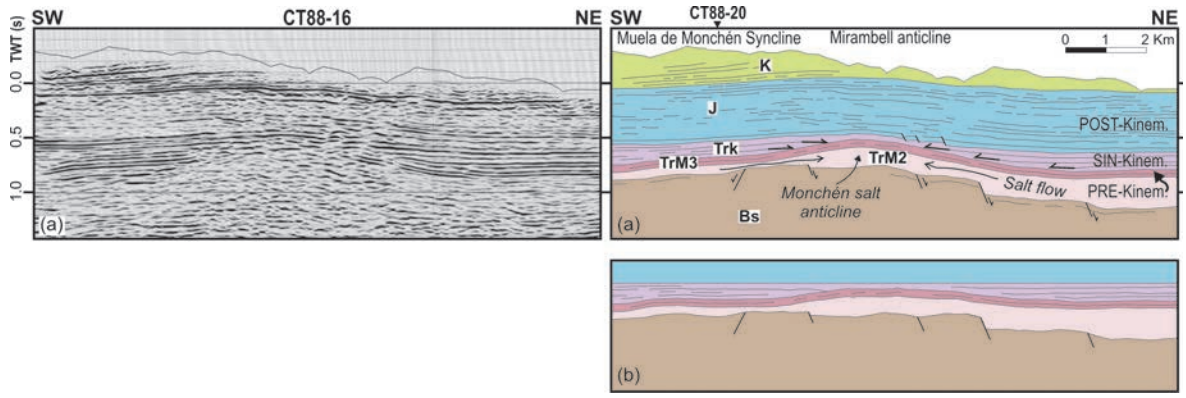

Figure 4.4. (a) Seismic profile CT88-16 and its interpretation. (b) The same seismic profile restored to the end of the Triassic. It has been unfolded using the base of the Jurassic as a datum. The geometry of the Monchén salt anticline at the end of the Triassic is shown. The Keuper seismic reflectors become horizontal and lap on the folded Upper Muschelkalk above the salt accumulation. During the Cenozoic contraction, the Mirambell anticline, which involves the acoustic basement, developed including the Mirambell salt anticline in its core, making the geometry of the salt anticline more pronounced.

4.2.2 Shortening in the northern margin of the Maestrat Basin

The shortening in the study area is mostly accumulated in the northern fold-and-thrust belt, which also coincides with the zone with most intense internal deformation of the supra-salt cover. Towards the hinterland, the internal deformation of thrust sheets decrease, and shortening is related to the northwards displacement of the thrust sheets above the sole thrust, rather than to their internal deformation (Fig. 3.22).

The total shortening measured in the supra-salt Mesozoic cover (about 12km) must be found somewhere in the acoustic basement. It could be distributed in several basement structures or concentrated in a unique one. The presence of the tectonic vertical step, the wide uplifted area, and especially, the 13km-wide Calders monocline fault-bend fold suggest a main basement thrust which displaced the basement in its hanging wall for about 11-13km. The difference in the shortening value obtained after the cross-sections (Fig. 3.12) and the one obtained from the geometry of the Calders monocline –which is 13km wide in its central widest part– is due to the position of the regional cross-section, which does not traverse the Calders monocline in its widest part; and to the fact that the regional cross-section was constructed in a conservative manner, and could accumulate additional shortening. The Calders monocline narrows laterally and eventually terminates, suggesting a differential displacement between the central part and the lateral parts.

4. 2.3 Kinematic evolution

The normal fault system that bound the Salzedella sub-basin, and are also located within it, were rooted in a sole listric normal fault in the acoustic basement (Fig. 3.22). During the Cenozoic contraction, this normal fault was inverted in its segment within the acoustic basement, generating the low-dip basement ramp of the Maestrat Basement thrust. The displacement of the basement above this ramp generated the tectonic uplifted area found in the hinterland of the Linking Zone. As the resulting thrust reached the Middle Muschelkalk evaporites, a short-cut developed along this level, generating a nearly horizontal continuation for the basement ramp, with a very gentle dip towards the S. Consequently, the normal fault segments within the supra-salt cover were not totally inverted, conversely they were displaced northwards above the sole thrust flat, together with the supra-salt cover. A fault-bend fold (Calders monocline) developed above the transition from the ramp to the flat of the Maestrat Basement Thrust (Figs. 3.22, 3.23).

North of the ramp-to-flat transition, the sole thrust propagated within the Middle Muschelkalk detachment, cutting the elevated parts of the acoustic basement in the footwalls of the main normal faults that it encountered in its way to the foreland. This acoustic basement fragments were incorporated to the thin-skinned thrust sheets and transported to the N within the thrust system (Fig. 3.17, 3.22). The entire western part of the Ladruñán zone incorporated a fragment of the acoustic basement, as the syn-rift filling is thinner, and consequently the entire Mesozoic supra-salt cover is thinner in this sector. Therefore, the sole thrust which in the eastern part of the basin propagated within the Middle Muschelkalk evaporites, in the thinner western part encountered, at the same depth, the acoustic basement in the footwall of the main normal faults (Carrascosa, Bordón or Ladruñán normal faults), which was cut and incorporated to the thrust sheet.

The sole thrust propagated towards the external zone of the Maestrat basin, within the Middle Muschelkalk facies, shallowing progressively as the Mesozoic cover became thinner towards the basin margin. Finally, the sole thrust emerged in the Calanda thrust sheet, which is the most external structure developed in the northern external margin of the Maestrat basin, thrusting the Cenozoic rocks of the Ebro foreland basin. However, more to the north, the isolated Variscan Basement outcrop of the Puig

Moreno (Carboniferous) is found among the Cenozoic rocks of the Ebro foreland Basin (Fig. 2.13). This outcrop was interpreted by SALAS et al. (2001) as the result of the uplifting of the basement in the hanging wall of a frontal basement thrust rooted in the basal thrust system of the Maestrat basin (Fig. 2.14), which in this thesis was interpreted as the Maestrat Basement Thrust. The Puig Moreno thrust sheet is interpreted to be the lateral continuation and eastwards termination of the Cameros thrust sheet (Fig. 2.13), the most frontal thrust of the western Iberian Chain (GUIMERÀ et al., 2004).

As explained in chapter 3.6.5, the low-dip of the Calders monocline fault-bend fold suggests a low-dip for the basement thrust ramp, which reaches a depth of 7.5km bsl, and extends for about 40km towards the south, in order to generate the wide uplifted area observed. The geometry obtained for the Maestrat Basement Thrust indicates that it was rooted in the upper crust, which is in agreement with the interpretations of other authors, who have attributed the thickening of the crust below the Iberian Chain to the upper crust (SEILLÉ et al., 2015), related to basement thrusts that only involve the upper crust, suggesting a detachment at a depth of 7-11km (GUIMERÀ and ÁLVARO, 1990).

The exact thickness of the Lower Muschelkalk and the Buntsandstein in not known, but after the oil-wells it is known that the total thickness of these units can vary between 70 and 380m (Fig. 2.5, MARTÍNEZ-ABAD, 1991). The Variscan Basement is clearly involved below the southern uplifted area and below the Calders monocline (Fig. 3.17), located in the hanging wall of the Maestrat Basement Thrust, as it nearly reaches 8km of depth (Fig. 3.22). However, the different fragments of the acoustic basement incorporated in the structures located above the flat of the Maestrat Basement Thrust (Fig. 3.17), could contain only the Lower Muschelkalk and the Buntsandstein facies, not necessarily including the Variscan Basement. These fragments of the acoustic basement could have been detached in the Buntsandstein evaporites (Röt facies), as it has been proposed in other structures of the Iberian Chain (ORTÍ, 1981; GUIMERÀ, 1988).

4. 2. 3. 1 Palinspastic restoration

If the supra-salt Mesozoic cover is restored to its position previous to the Cenozoic basin inversion, the traces at surface of the normal faults should be displaced southwards 12km (Fig. 4.5). After doing the restoration, it is observed that the Bordón and the Ortells normal faults broadly coincide with the deduced ramp (S) to flat (N) transition of the Maestrat Basement Thrust, as they become located about 7km north of the Calders monocline southern antiformal hinge (Fig. 4.5). If these traces at surface are linked to the ramp of the Maestrat Basement Thrust in the acoustic basement, the resulting normal fault surface within the supra-salt cover dips about 30ºS, which is similar to the dip obtained in the idealized cross-section for the Ortells fault (Fig. 3.22).

This suggests that in the studied area, the Maestrat Basement Thrust can be the result of the Cenozoic contractional inversion of the Bordón and the Ortells normal faults, at least in their segment within the acoustic basement, which inherited the geometry and orientation of these normal faults. The other normal faults of the Mesozoic normal fault system, were rooted in this basement fault (Fig. 3.22).

During the Cenozoic contraction, the normal faults located north of the Bordón and the Ortells faults,

were cut by the nearly horizontal short-cut thrust propagated within the Middle Muschelkalk evaporites, and their traces across the supra-salt cover were transported towards the basin margin within the thrust system. The lower segments, across the sub-salt basement, of these normal faults should be found in the footwall of the sole thrust and in a more internal position, as the Castellote fault in the idealized cross-section (Fig. 3.22).

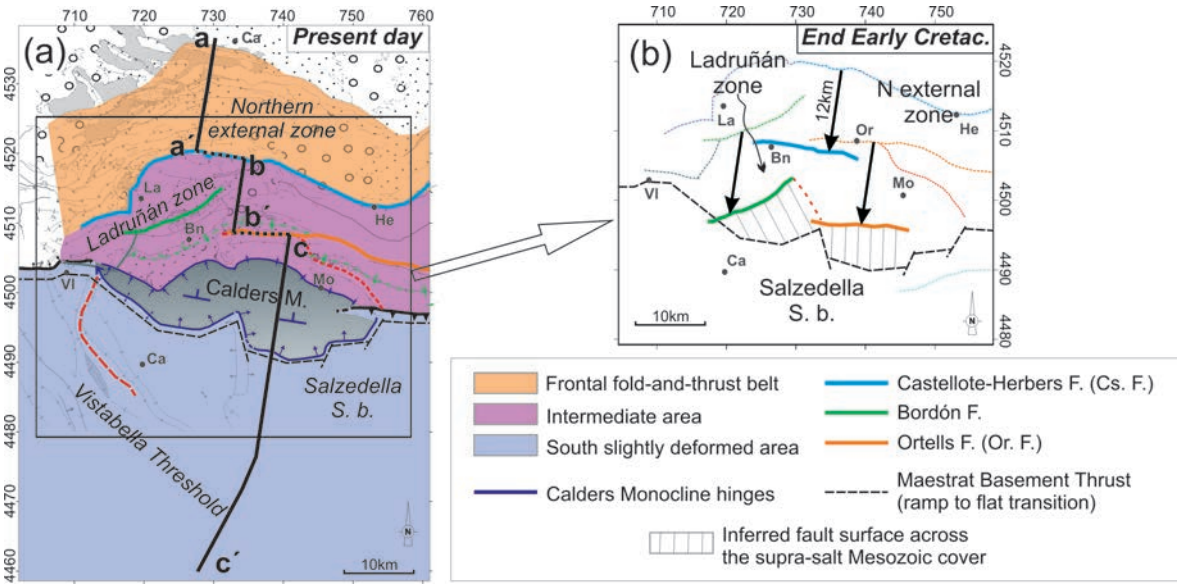

Figure 4.5. (a) Simplified structural map of the Cenozoic structures developed after the Maestrat basin inversion. Modified from NEBOt and GUIMERÀ (2016). (b)Palinspastic restoration of the normal faults within the Maestrat basin at the end of the Mesozoic extension (end of the Early Cretaceous).

4.2.4 Salient geometry

As previously explained, in the study area structures of the fold-and-thrust belt display a salient geometry –in the sense of Marshak (2004)– as their traces are convex to the N, to the sense of transport. After the palinspastic restoration of the Mesozoic normal faults, their location and orientation also display an arched geometry similar to the one observed in the Cenozoic fold-and-thrust belt, thus indicating that this was at least partially inherited. This normal fault system was transported to the north within the thrust system during the Cenozoic contractional inversion of the basin. Some differential displacements also occurred, as suggested by the Calders monocline geometry. Transport was bigger in the central part of the monocline, decreasing laterally, as the monocline narrows. Consequently, only gentle vertical axis rotation of structures at both sides of the salient is necessary to obtain its present-day arched geometry.

Besides the orientation of the Mesozoic structures, inherited by the Cenozoic inversion ones, the distribution of the Middle Muschelkalk evaporitic facies also influenced the salient geometry. The thick evaporitic layer deposited in the study area produced the décollement between the sub-salt Acoustic Basement and the supra-salt cover, and facilitated the displacement of the supra-salt cover towards the N. However, the Middle Muschelkalk evaporitic facies terminates laterally, towards the W. In the

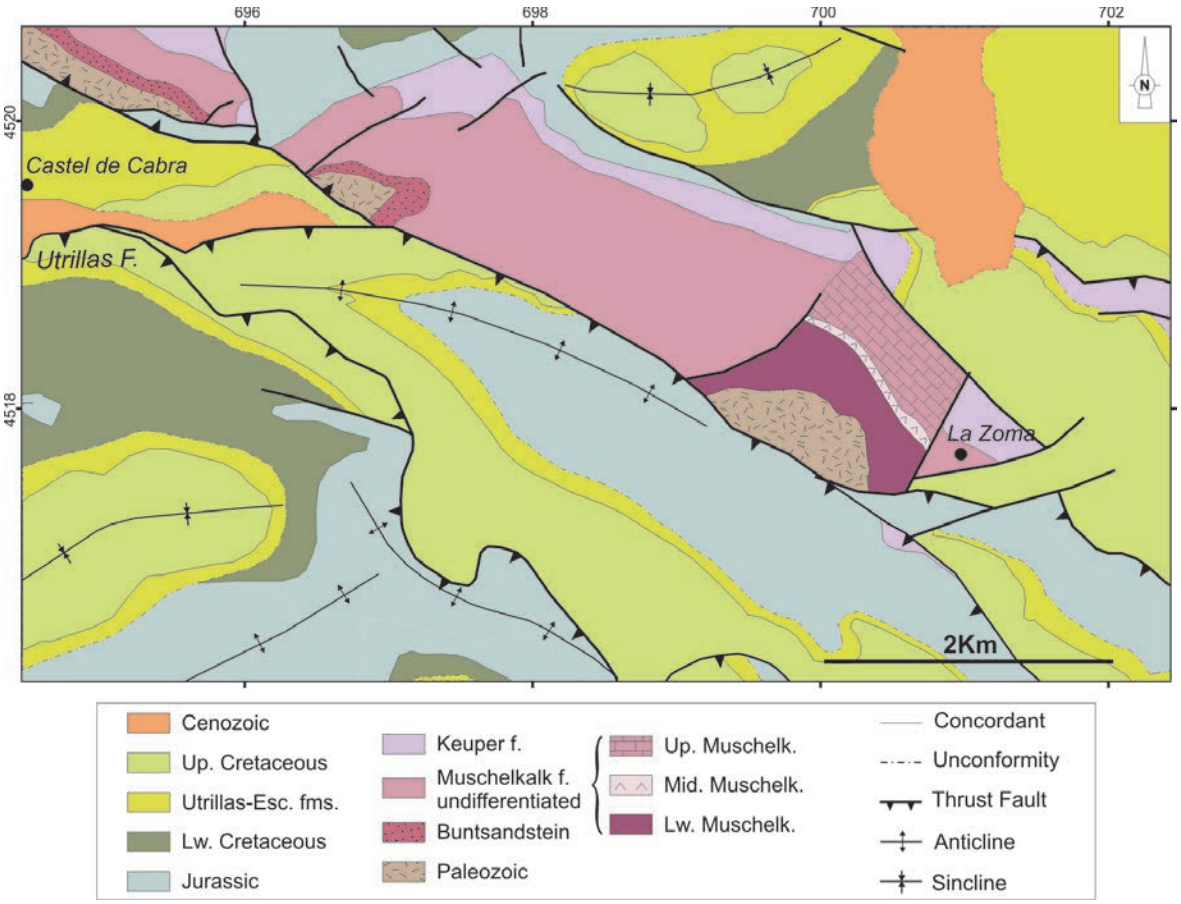

Figure 4.6. Geologic map of the southeastern termination of the Montalbán anticline. The Triassic and Paleozoic rocks in the NW-SE-trending Montalbán anticline are thrusted by the Cretaceous and Jurassic rocks of the E-W-trending thrust front of the Linking Zone. It is based on CANÉROT (1977), GUIMERÀ (1988) and the ortho-images interpretation. See location in Figure 3.9.

Triassic outcrop west of La Zoma (Fig. 4.6), only 15-20m of Middle Muschelkalk facies can be recognized, composed mostly of clays and marls. These rocks are located between at least 100m of Lower Muschelkalk dolostones and limestones, which are in contact with the Paleozoic rocks, and about 60-70m of dolomitic limestones of the Upper Muschelkalk facies (CRESPO ZAMORANO et al., 1977). More to the west, these three units cannot be differentiated, and a unique, mostly carbonatic, Muschelkalk package was mapped by CANÈROT (1977) overlying the Buntsandstein facies and covered by the Keuper facies (Fig. 4.6).

This lateral pinch-out of the Middle Muschelkalk evaporites (Fig. 4.2), the main detachment level in the study area, complicated the displacement towards the north of the supra-salt cover in the area where the Middle Muschelkalk salt terminates, favoring the differential displacement, as the sole thrust had to jump to another detachment level – the Keuper– or to transmit the displacement to other structures rooted in the Basement.

Furthermore, the NW-SE-trending Montalbán anticline, which involves the Variscan basement, started to develop before the emplacement of the E-W-trending fold-and-thrust belt in the Linking Zone,

as it is reflected in the Cenozoic rocks of the Montalbán basin, whose Cenozoic lower units are cut by the southern limb of the NW-SE-trending Montalbán anticline, which is unconformably overlaid by a younger Cenozoic unit which, in its turn its thrusted by the E-W-trending, N-verging Utrillas thrust (Guimerà, 1988; CASAS-SAINZ et al., 2000). In the eastern termination of the Montalbán anticline, this relationship is reflected in the Triassic and Paleozoic rocks of the anticline, which are thrusted by the Cretaceous and Jurassic rocks of the Linking Zone (Fig. 4.6), indicating that folding and erosion in the Montalbán anticline occurred previously to the displacement of the E-W-trending thrust front (Guimerà, 1988). The Montalbán anticline could have acted as a basement high (Fig. 4.7a) preventing the displacement of the Mesozoic cover, and favoring, together with the salt pinch-out (Fig. 4.7b), the appearance of the Aliaga recess (Fig. 4.7).

To the eastern part of the salient, east of Herbers, the Cenozoic contractional structures take a NE-SW trend (Fig. 3.9), the same orientation of structures in the Catalan Coastal Chain (Fig. 2.13). In this eastern part of the Portalrubio-Vandellòs fold-and-thrust belt, the Mesozoic structures already had NE-SW to N-S trends (Anadón et al., 1979; Salas and Guimerà, 1996) (Fig. 2.3). The Cenozoic contractional structures probably inherited the NE-SW orientation of the Mesozoic extensional ones, producing the Herbers recess (Fig. 4.7).

4.2.6 Role of the evaporites of the Middle Muschelkalk facies

During the Cenozoic contractional inversion of the basin, the décollement effect of the Middle Muschelkalk evaporitic facies differentiated the style of deformation between the sub-salt or acoustic basement, which was mainly faulted, and the supra-salt cover, which developed detachment folds, fault-bend folds and thrusts, and adapted to the geometry of the basement structures.

The propagation of the sole thrust though this level below the northern Portalrubio-Vandellòs fold-and-thrust belt, in the northern half of the study area, conditioned the inversion pattern of the Mesozoic extensional basins, which were mainly passively transported northwards and internally deformed, while the faults bounding them were only slightly inverted. The same basin configuration with no evaporitic detachment, and with the same amount of shortening, would have led to the total inversion of the basins which would have experienced more erosion, being the basement probably cropping out. Therefore, the thick evaporitic layer facilitated the generation of the northern fold-and-thrust belt. The lateral pinch-out of the salt, together with the other factors explained before, produced the salient geometry of the fold-and-thrust belt. The salt layer also controlled the formation of the Calders monocline, as it triggered the development of the nearly horizontal short-cut thrust which is the continuation towards the N of the Maestrat Basement Thrust ramp, generating its ramp- flat geometry.

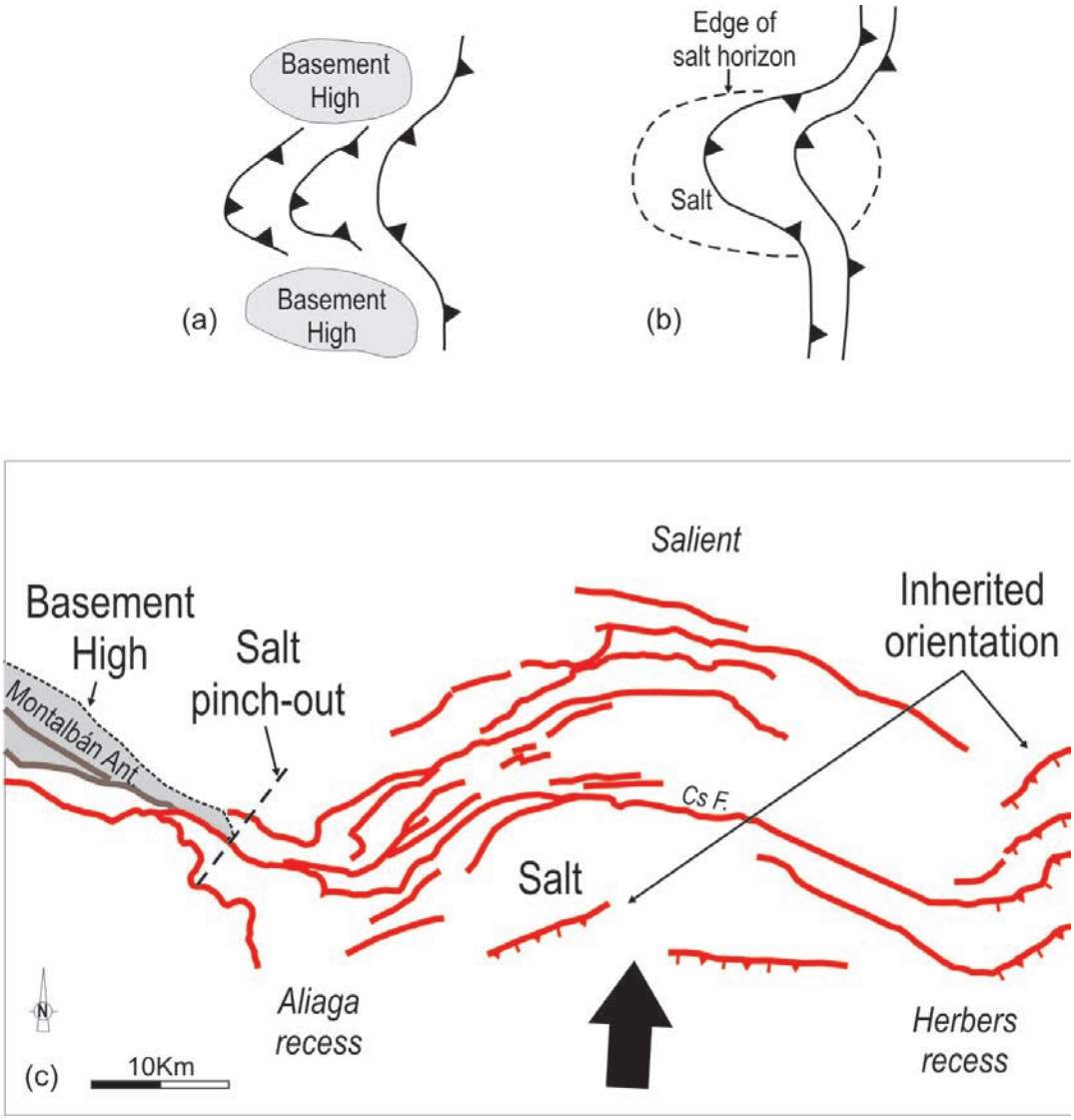

Figure 4.7. Map-view sketches illustrating possible processes leading to the formation of curved fold-thrusts belts. (a) Interaction with basement highs in the foreland. New thrusts forming between the two highs originate with curved traces. (b) Lateral pinch-out of a stratigraphic glide horizon. Thrusts propagate further to the foreland over the weak salt horizon and originate with curved traces. Modified from MARSHAK and SCOTT WILKERSON (2004). (c) Map-view showing the traces of principal structures (thrusts and folds) in the studied fold-and-thrust belt, and mechanisms that produced the salient geometry. Abbreviations: Ca F.= Calanda Fault, Cs F.= Castellote Fault, Ut F.= Utrillas Fault.

4.2.5 Orientation of structures

As previously explained, in the NW part of the studied area, the NW-SE-trending structures of the Iberian Chain converge with the broadly E-W-trending structures of the Linking Zone, more specifically with the NE-SW to ENE-WSW-trending structures in the western part of the salient (Fig. 3.16). In this sector, and in other parts of the western termination of the Linking Zone, some interference of structures occurs, as in the case of the NW-SE-tending Montalbán anticline and the E-W-tending Utrillas thrust sheet, which indicate that, predominantly, the NW-SE to N-S-trending structures of the Iberian Chain

developed previously to the broadly E-W-structures of the Linking Zone (SIMÓN, 1980, 2004; GUIMERÀ, 1988), which can be attributed to the superposition of structures developed in successive deformation events (SIMÓN, 2004). However, some examples also demonstrate the simultaneous formation of these two sets of structures (GUIMERÀ, 1988), as some of them change their trend abruptly along-strike, which can be explained as the inversion of a complex system of Mesozoic normal faults of different orientations linked by relay ramps (Fig. 3.5) and by the heterogeneous distribution of the Middle Muschelkalk facies evaporites, which, as previously explained, also conditioned the location and orientation of some Cenozoic structures.

In the slightly deformed area located in the hinterland of the Linking Zone, and therefore south of the broadly E-W-trending Portalrubio-Vandellòs fold-and-thrust belt, a system of NW-SE-trending folds developed, between Cantavieja and the Peñarroya Mountain, having the same orientation that the structures in the Iberian Chain (Fig. 3.9). One of these NW-SE-trending folds, the Camarillas syncline (Fig. 3.9), is cut by E-W-trending thrusts, being other example of superposition of structures (GUIMERÀ, 1988). Hence, the NW-SE-trending structures of the Iberian Chain extend through the western part of the Linking Zone, until Vistabella. The broadly E-W-trending fold-and-thrust belt developed afterwards, superposed to this system of NW-SE trending structures. However, within the fold-and-thrust belt and the Linking Zone, structures show very varying orientations as a result of the inheritance of orientations of previous structures, and also as a result of the synchronic activity of the NW-SE Iberian structures, the NE-SW structures of the Catalan Coastal Chain, and the E-W structures of the Linking Zone, during a lapse of time, at least during most part of the Oligocene (GUIMERÀ, 1988). CASAS-SAINZ et al. (2000) estimated that the NW-SE-trending Montalbán anticline, and the E-W-trending Utrillas thrust sheet were active during the same period, which dated mainly during the Late Eocene-Early Oligocene, although the Montalbán anticline started to develop earlier (CASAS-SAINZ et al., 2000; GONZÁLEZ, 1989).

4.3 THE STUDY AREA IN THE CONTEXT OF THE MAESTRAT BASIN

As previously explained, the Calders monocline narrows laterally and eventually terminates, suggesting a differential displacement between the central part and the lateral parts. However, the displacement of the basement thrust-sheet does not disappear at its lateral ends. It is transmitted to other structures, as the Turmell fault or the Villarluengo short-cut thrust (Fig. 3.18), and the structures located north of them.

The total shortening estimated for the Portalrubio-Vandellòs fold-and-thrust belt in the study area is of about 12km (NEBOT and GUIMERÀ, 2016b). In the Utrillas thrust sheet, west of the study area, GONZÁLEZ and GUIMERÀ (1993) and SIMÓN and LIESA (2011) estimated a maximum shortening of 6-5.9km and CASAS-SAINZ et al. (2000) of 8km, which was transported broadly towards the NNE, during the Late Eocene-Early Miocene (SIMÓN and LIESA, 2011). In the eastern NE-SW-trending part of the fold-and-thrust belt GUIMERÀ (2004) estimated a total shortening of 12km (Fig.3.8F-F').

The tectonic vertical step continues beyond the lateral termination of the Calders monocline , to the E

in the Turmell fault and to the W in the southern boundary of the Aliaga Cenozoic basin, suggesting that the Maestrat Basement Thrust can be continued towards the E and W. In the studied area, GONZÁLEZ et al. (1998) dated the formation of the tectonic relief associated to this basement thrust as Late Oligocene-Early Miocene, south of the Bordón Cenozoic basin (Fig. 3.9). In the Aliaga sector, SIMÓN and LIESA (2011) estimated the emplacement of the Cobatillas thrust, which produced the uplifting of the southern margin of the Aliaga Cenozoic basin (Fig. 3.9), starting by the Oligocene- Miocene boundary, until the Early Miocene. Therefore, the displacement of the Maestrat Basement Thrust occurred broadly at the same time both in the study area and in the western area of Aliaga.

However, the lateral termination of the Calders monocline suggests that the geometry of the Maestrat Basement Thrust changes laterally, and that the ramp to flat transition does not occur at both sides of the monocline. The total shortening accumulated in the supra-salt cover in the areas east and west of the Calders monocline cannot be explained by a unique basement structure, as it is done in the Calders monocline transect.

In the study area the displacement of the structures located north of the Calders monocline have been associated to the displacement of the Maestrat Basement Thrust, and therefore to the formation of the tectonic relief south of the Bordón Cenozoic basin. Consequently, it can be assumed that shortening in the study area started at least during the Late Oligocene. It could have started earlier, but the lack of datations of the piggy-back Cenozoic basins in the study area does not allow us to know when exactly contractional deformation started. In the area of Aliaga, the emplacement of the Utrillas thrust sheet or Muela de Montalbán thrust sheet (Figs. 2.15, 4.2) started earlier (GONZÁLEZ and GUIMERÀ, 1993; SIMÓN and LIESA, 2011) during the Late Eocene-Early Miocene (SIMÓN and LIESA, 2011), which is located in the footwall of the Maestrat Basement Thrust, North of it.

After the exposed data it can be assumed that shortening decreases towards the west from about 12km in the Calders monocline transect to about 6-8km in the Utrillas thrust transect. Although the NW-SE-trending structures starting to develop first, regarding the E-W-tending structures of the Portalrubio-Vandellòs fold-and-thrust belt, shortening started in the area of Aliaga, with the displacement of the Utrillas thrust during the Late Eocene, although it cannot be excluded that structures were also active in the study area during this period. During the Late Oligocene, the Maestrat Basement Thrust started its contractional displacement. In the study area it produced the tectonic relief to the hinterland, and the emplacement of the northern fold-and-thrust belt towards the foreland. In the Aliaga sector it produced the uplifting of the southern boundary of the Aliaga Cenozoic basin, owing to the inversion of the northern boundary of the Galve sub-basin (Cobatillas thrust). The emplacement of all these structures terminated during the Early Miocene (GONZÁLEZ et al.,1998; SIMÓN and LIESA, 2011).

4.4 THE STUDY AREA IN THE CONTEXT OF THE IBERIAN CHAIN AND THE IBERIAN PLATE

As previously explained, the Iberian Chain developed in an intraplate setting, in the eastern part of the Iberian plate, bounded by active plate boundaries, the Eurasian-Iberian to the north and the Iberian-Africa to the south, as a result of the convergence, generally in the N-S-direction, between the African, the Iberian and the European plates. The small dimensions of the Iberian plate facilitated that the tectonic activity in those boundaries was transmitted towards its interior, especially during the Cenozoic contraction (CAPOTE et al., 2002). Furthermore, the Mesozoic rifting had previously extended, and therefore weakened, the crust in the Iberian Rift system, which enhanced the capacity of this intraplate setting to absorb the alpine contractional stress transmitted from the plate boundaries (De VICENTE et al., 2004).

During the Late Cretaceous (Santonian, 83Ma)-Late Eocene a first stage of convergence occurred between the Eurasian and the Iberian plates, during which, Iberia moved as a part of the African plate, and the plate boundary was located in the Bay of Biscay, King's though and N Spanish trough (SRIVASTAVA et al., 1990; ROEST and SRIVASTAVA, 1991). Since the Late Eocene to the Early Miocene, Iberia moved as an independent plate (SRIVASTAVA et al., 1990; ROEST and SRIVASTAVA, 1991). A second stage of convergence occurred since the Late Oligocene to present, between the Iberian and the African plates. During this stage the plate boundary was found in the Azores-Gibraltar fracture zone, and Iberia moved as a part of the Eurasian plate (SRIVASTAVA et al., 1990; ROEST and SRIVASTAVa, 1991; ROCA et al., 2004). Simultaneously, sea-floor spreading occurred from the Late Oligocene to present, which produced the opening of the Gulf of Valencia-Gulf of Lyons and migration towards the E of the Balearic, Corsica and Sardinia blocks (GUEGUEN et al., 1998).

In this tectonic context, the Pyrenean (Late Cretaceous-Late Oligocene, MOUTHEREAU et al., 2014), the Iberian Chain (Late Eocene-early Miocene, SALAS et al., 2001; GONZÁLEZ et al., 1998) and the Betic (Burdigalian-Late Miocene, VERA, 2001) contractional orogens developed, being genetically related.

GUIMERÀ et al., (2004) estimated a total shortening for the Iberian Chain between 38.6km to 66.6 km (26%) in a NE-SW transect across the entire NW part of the Iberian Chain (Fig. 4.8A-A'), based on two possible interpretations of the Cameros thrust geometry at depth. Afterwards, GUIMERÀ (2013) estimated a shortening of 41 km (18,9%) for the western part of the Iberian Chain (Fig. 4.8B-B'), through the Cameros thrust sheet, and a shortening of 37 km (13,9%) for the eastern part of the Chain, based on two regional cross-sections that traverse the Iberian Chain from the Ebro to the Tajo foreland basins (Fig. 4.8C-C', D-D'). In the eastern sector, a shortening of 17 km (16,5%) have been estimated for the northern half of the Iberian Chain, which coincides with the sector of the fold-and-thrust belt in the Linking Zone studied in this thesis, although it covers a wider area, reaching the Teruel Cenozoic basin (Fig. 4.8D-D').

The shortening value obtained in this thesis is 12-13km, which was measured in the eastern part of the Iberian Chain, in the northern part of the Linking Zone, representing approximately one-third of the length of the eastern part of the Iberian Chain, in the N-S direction (Fig. 4.8E-E'). It has to be considered,

that the shortening in the Puig Moreno thrust-sheet was not estimated. However, this shortening value resembles more to the approximately 37-41km estimated by GUIMERÀ (2013) and the minimum shortening value of 39km obtained by GUIMERÀ et al. (2004), than to the maximum shortening value of nearly 67km also estimated by GUIMERÀ et al. (2004). MOUTHEREAU et al. (2014), in their estimation of the Iberian plate dynamics, also considered a shortening value of 40km for the Iberian Chain, rather than 67km, as they considered this value more consistent with a midcrustal detachment and thick-skin style of deformation characteristics described by DE VICENTE et al. (2007) for the Iberian Chain.

Shortening in the Pyrenees increases towards the E, from 75-114km (TEIXELL, 1998; TEIXELL et al., 2016) to 125km (VERGÉS et al., 1995); with a maximum value of 147-165km in the central Pyrenees, according to MUÑOZ (1992) and BEAUMONT et al., (2000) respectively. Although the shortening value in the Iberian Chain (37-41km) represents the 22-36% of the shortening in the Pyrenees (114-165 km, TEIXELL et al., 2016; BEAUMONT et al., 2000), as suggested by GUIMERÀ et al (2004) and as it has been done by MOUTHEREAU et al. (2014), the shortening in the Iberian Chain should be considered in any future reconstruction of the kinematic evolution of the African and Eurasian plates during the Cenozoic alpine contraction.

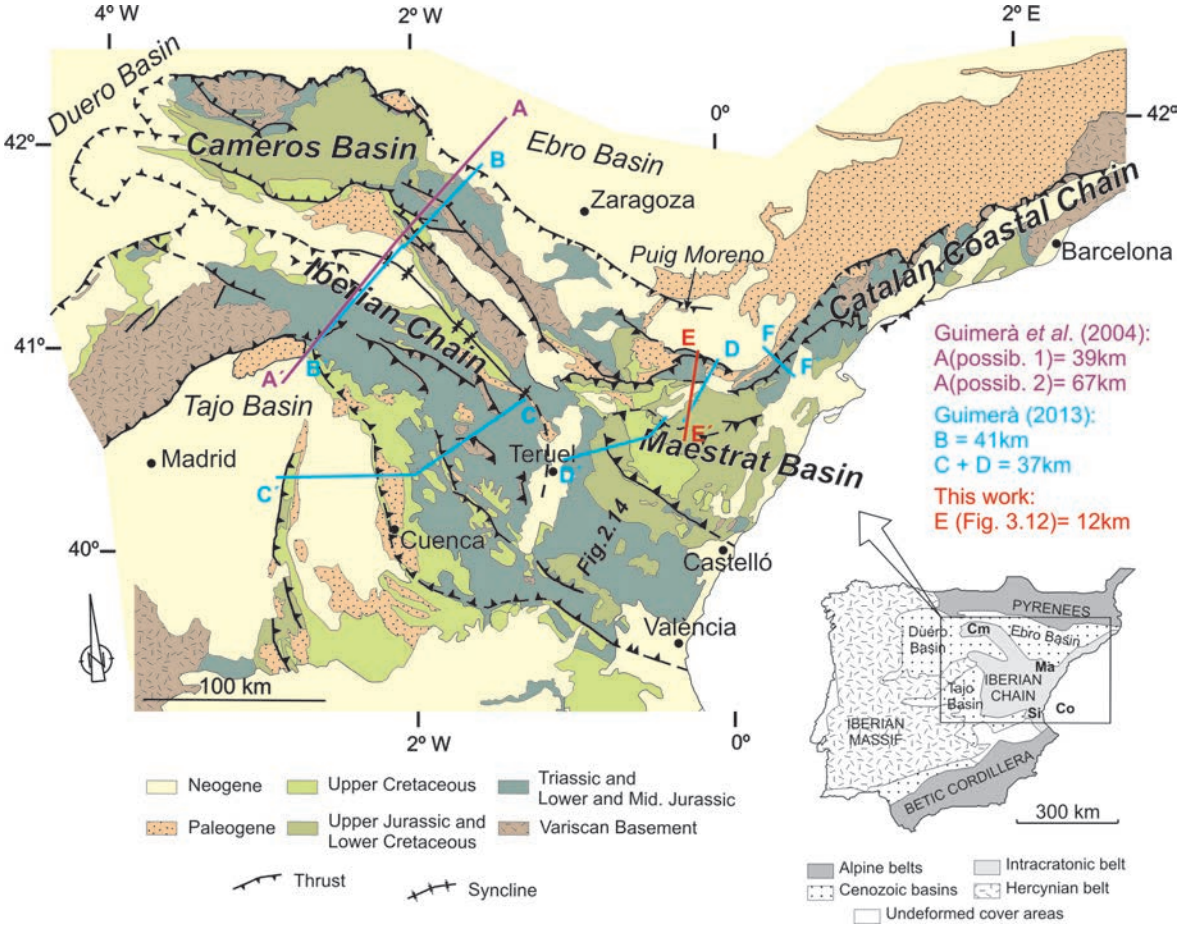

Figure 4.8. Location of cross-sections constructed by different authors in order to calculate the Cenozoic shortening in the intraplate Iberian Chain. The shortening values are shown.

5. CONCLUSIONS

5. CONCLUSIONS

During the Late Permian-Late Triassic rifting, a system of high-angle normal faults developed in the present-day acoustic basement of the Maestrat Basin. These faults define a system of horsts, grabens and half-grabens, which were active during the deposition of the Buntsandstein, the Lower Muschelkalk and the lower part of the Middle Muschelkalk facies (Late Permian-Anisian). As a result, depositional thickness variations within the Middle Muschelkalk facies appeared. The extensional activity decreased during the deposition of the upper part of the Middle Muschelkalk and the Upper Muschelkalk facies, which has a nearly constant thickness in the entire Maestrat basin.

The seismic profiles show that the Middle Muschelkalk evaporitic facies experienced some salt tectonics, as it performs salt anticlines and welds, which enhanced the depositional thickness variations of this unit. The Middle Muschelkalk salt flow occurred during the Late Triassic (Carnian-Norian) triggered by the resumed activity of some normal faults in the acoustic basement, while the Keuper facies was being deposited. This is deduced after the Keuper seismic reflectors, which overlie and lap on the folded Upper Muschelkalk facies above the salt accumulations. Some growth-strata can also be recognized in the Keuper seismic reflectors above some reactivated normal faults in the acoustic basement, which produced forced folds in the Upper Muschelkalk. The differential load exerted by the Keuper facies, which was deposited adapted to the folded Upper Muschelkalk, could have enhanced the Middle Muschelkalk salt flow. The last thickness variations within the Middle Muschelkalk were generated during the Cenozoic contraction, as the Mesozoic salt structures were amplified and new salt-cored detachment folds developed.

Although widely considered as the Triassic post-rift, some extension is needed during the Early Lias, as thickness variations within the units of this age are identified after comparing their thicknesses in the exploration wells, and in the field. During the Late Jurassic–Early Cretaceous rifting event, the Maestrat Basin developed, and within it, the Salzedella sub-basin, bounded to the N by S-dipping normal faults (Garrocha and Castellote normal faults). These faults separate Barremian and Aptian sequences of up to 1100m in their hanging walls from sequences of 0 to 300m, and locally 600m, in their footwalls, in the northern external zone of the basin. The Salzedella sub-basin contains in its northwestern end the Ladruñán zone, with intermediate thicknesses, separated from it by a system of normal faults (Bordón, Carrascosa and Villarluengo normal faults), which terminates towards the E while the Ladruñán zone merges with the Salzedella sub-basin. The interpreted normal faults, located in the margins of the basin and also within it, define a complex system of faults with different orientations and connected by relay ramps. Within the basin, minor normal faults of metric slips were also recognized, which probably contributed to the progressively northward thickening of the Salzedella sub-basin, from 350 to 1100m of Lower Cretaceous rocks.

During the Cenozoic contraction, the Maestrat basin was inverted by means of the inversion of the South-dipping normal fault system that formed the basin, at least in its lower segment within the acoustic basement, generating the Maestrat Basement Thrust. A 40km-wide uplifted area developed in its raised hanging wall, in the N-S direction. This uplifted area is bounded to the N by the E-W-trending, N-verging

Calders monocline, which is interpreted as a fault-bend fold, indicating a flat-ramp-flat geometry of the Maestrat basement thrust. The southern antiformal hinge of the Calders monocline is the superficial expression of the transition from ramp to flat in the basement thrust. The northern synformal hinge of the Calders monocline, located at the southern boundary of the Bordón Cenozoic Basin and in the Morella syncline indicates the transition from a thick-skinned (S) to a thin-skinned (N) styles of deformation.

The frontal tilted limb of the Calders monocline dips about 5º towards the N and has a maximum width of about 13km in its central part and narrows laterally, linking to the Turmell and the Villarluengo basement thrusts. The low dip of the Calders monocline, and the vast extension of the uplifted hanging wall of the Maestrat basement thrust suggest a very low-angle ramp for the basement thrust, rooted in the upper crust. Modelling the previous data with the Move® software, a 9° dip for the deep ramp was deduced, extending more than 40km southwards in the NNE–SSW orientation, and reaching a depth of 7.5km bsl. As the sole thrust reached the Mesozoic cover to the foreland, it propagated through the Middle Muschelkalk evaporitic unit, producing a nearly horizontal detachment, which spread to the N, generating the ramp to flat transition of the Maestrat Basement Thrust.

The Portalrubio–Vandellòs fold-and-thrust belt is the emergence of the Maestrat Basement Thrust, which is the sole thrust of the Cenozoic contractional system. The shortening is estimated to be *c.* 12km, mostly concentrated at the surface in the northern margin of the thrust belt, being the tectonic displacement towards the NNE. Most of the normal faults which bounded the Mesozoic basins were passively transported to the NNE inside the hanging-wall of the Maestrat Basement Thrust, experiencing low internal deformation. Some fragments of the acoustic basement (rocks below the Middle Muschelkalk) were also included in the thin-skinned thrust sheets. The displacement of the basement above the low-dip ramp of the Maestrat Basement Thrust generated the 40km-wide uplifted area in the hinterland of the Linking Zone.

The palinspastic restoration of the supra-salt cover supports the idea that, in the study area, the Maestrat Basement Thrust is the result of the inversion of the Mesozoic normal fault system in its segment across the basement, and also that the Portalrubio–Vandellòs frontal belt inherited the geometry and orientation of the Mesozoic normal faults.

The structures in the northern fold-and-thrust belt display a salient geometry, convex to the foreland, to the sense of transport (NNE). The salient geometry is interpreted to be originated by a combination of factors. On the one hand, the northern fold-and-thrust belt is detached in a thick Middle Muschelkalk evaporitic layer that terminates to the W, coinciding with the Aliaga recess. The Montalbán anticline could have acted as a basement high interacting with the displacement of the E-W-trending thrust front, as it started to develop earlier. Finally, the contractional structures inherited the orientation of the Mesozoic extensional faults, which in the NE-SW-trending eastern part of the fold-and-thrust belt could be the origin of the Herbers recess.

Therefore, the Mesozoic extensional structures with different orientations, together with a thick Middle Muschelkalk evaporitic unit, played an important role in the formation of the Cenozoic

contractional structures, affecting their location and orientation, and the different deformation styles between the acoustic basement and the supra-salt cover. The acoustic basement was mainly faulted while the supra-salt cover was mainly folded and thrusted, adapting to the basement structures.

The location of the Iberian Chain in an intraplate setting within the Iberian plate, between two active plate boundaries, and the shortening in the Iberian Chain, which represents about the 22-36% of the shortening in the central Pyrenees, should be considered in any future reconstruction of the kinematic evolution of the African and Eurasian plates during the Cenozoic Alpine contraction.

REFERENCES

AGUILAR, M.J., RAMÍREZ DEL POZO, J. and RIBA, O. 1971. Algunas precisiones sobre la sedimentación y paleontología del Cretácico inferior en la zona de Utrillas-Villarroya de los Pinares. *Estudios Geológicos*, 27 (6), 497-512.

ALMELA, A., MANSILLA, H., QUINTERO, I. and GÓMEZ, E. 1975. Oliete, sheet 493. Mapa Geológico de España 1:50.000. 2ª Serie. 1ª Edición. Madrid, Servicio de Publicaciones, Ministerio de Industria y Energía.

ALMERA, J., ANADÓN, P. and GODOY, A. 1982. Mora de Rubielos, sheet 591. Mapa Geológico de España 1:50.000. 2ª Serie. 1ª Edición. Madrid, Servicio de Publicaciones, Ministerio de Industria y Energía.

ÁLVARO, M. 1987. La subsidencia tectónica en la Cordillera Ibérica durante el Mesozoico. *Geogaceta*, 3, 34-37.

ÁLVARO, M., CAPOTE, R. and VEGAS, R. 1979. Un Modelo de evolución geotectónica para la cadena Celtibérica. *Acta Geológica Hispánica*, 14, 172-181.

ANADÓN, P. and ALBERT, J. F. 1973. Hallazgo de una fauna del Muschelkalk en el Trías del anticlinal de Calanda (Provincia de Teruel). *Acta Geológica Hispánica*, 8(5), 151-152.

ANADÓN, P., COLOMBO, F., ESTEBAN, M., MARZO, M., ROBLES, S., SANTANACH, P and SOLÉ I SUGRAÑES, L. 1979. Evolución tectonoestratigráfica de los Catalánides. *Acta Geológica Hispánica*, 14, 242-270.

AURELL, M., MELÉNDEZ, A., SAN ROMÁN, J., GUIMERÀ, J., ROCA, R., SALAS, R., ALONSO, A. and MAS, R. 1992. Tectónica sinsedimentaria distensiva en el límite Triásico-Jurásico en la cordillera ibérica. *Actas del III Congreso Geológico de España*, 1, 50-54.

BARTRINA, T. and HERNÁNDEZ, E. 1990. Las unidades evaportíticas del Triásico del subsuelo del Maestrazgo. In: Ortí, F., Salvany, J. M. (eds.). *Formaciones evaporíticas de la Cuenca del Ebro y cadenas periféricas, y de la zona de Levante. Nuevas aportaciones y guía de superficie*. Barcelona, ENRESA – Dep. Geoq. Prosp. Petrol. (UB), 34-38.

BEAUMONT, C., MUÑOZ, J. A., HAMILTON, J. and FULLSACK, P., 2000. Factors controlling the Alpine evolution of the central Pyrenees inferred from a comparison of observations and geodynamical models, *J. Geophys. Res.*, 105(B4), 8121–8145, doi:10.1029/1999JB900390.

BORDONABA, A. and AURELL, M., 2001. El Hettangiense–Sinemuriense (Jurásico inferior) en el sector de Montalbán–Oliete (Teruel): Análisis de facies y evolución tectosedimentaria. *Rev. Soc. Geol*. Esp. 14, 135–146.

BORDONABA, A. and AURELL, M., 2002. Variación lateral de facies en el Jurásico basal de la Cordillera Ibérica central: Origen diagenético temprano y tectónica sinsedimentaria. *Acta Geol. Hisp*. 37, 355–368.

BOURQUIN, S., DURAND, M., DIEZ, J.B., BROUTIN, J. and FLUTEAU, F. 2007. The Permian-Triassic boundary and Early Triassic sedimentation in Western European basins: an overview. *Journal of Iberian Geology*, 33 (2), 221-236.

BOVER-ARNAL, T., MARTÍN-MARTÍN, J.D., GOMEZ-RIVAS, E., TRAVÉ, A., SALAS, R., MORENO-BEDMAR, J.A., TOMÁS, S., 2009. Insights into the Upper Aptian carbonate succession of the South-Eastern Maestrat basin (E Iberia). In: Amorosi, A. (Ed.), *27th IAS Meeting of Sedimentologists*. Monduzzi Editore, International Proceedings, Pianoro (Bologna), pp. 123e128.

BOVER-ARNAL, T., MORENO-BEDMAR, J. A., FRIJIA, G., PASCUAL-CEBRIAN, E. and SALAS, R. 2016. Chronostratigraphy of the Barremian-Early Albian of the Maestrat Basin (E Iberian Peninsula): integrating strontium-isotope stratigraphy and ammonoid biostratigraphy. *Newsletters on Stratigraphy*, 49 (1), 41-68. Doi: 10.1127/nos/2016/0072.

BUTILLÉ, M., FERRER, O., GRANADO, P., ROCA, E., MUÑOZ, J.A., BALLESTEROS, J. C., GIMÉNEZ, A., VALLEJO, R. A. and GONZÁLEZ, P. 2012. Evidencias de deformaciones salinas en las sucesiones mesozoicas del sector sur de la Cuenca del Ebro. In: Fernández, L. P., Fernández, A., Cuesta, A., Bahamonde, J.R. (eds.). *Geo-Temas*, 13. Oviedo, VIII Congreso Geológico de España.

CAMPOS, S., AURELL, M., CASAS, A. 1996. Origen de las brechas de la base del Jurásico en Morata de Jalón (Zaragoza). *Geogaceta*, 20 (4), 887-889.

CANÉROT, J. 1974. Recherches géologiques aux confins des chaînes ibérique et catalane (Espagne). PhD Thesis. Université Paul Sabatier, 517pp.

CANÉROT, J. and LEYVA, F. 1972. Peñarroya de Tastavins, sheet 520. Mapa Geológico de España 1:50.000. 2ª Serie. 1ª Edición. Madrid, Servicio de Publicaciones, Ministerio de Industria y Energía.

CANEROT, J. and PIGNATELLI-GARCÍA, R. 1972. Aguaviva, sheet 519. Mapa Geológico de España 1:50.000. 2ª Serie. 1ª Edición. Madrid, Servicio de Publicaciones, Ministerio de Industria y Energía.

CANÉROT, J., CRESPO-ZAMORANO, A. and NAVARRO-VÁZQUEZ, D. 1977. Montalbán, sheet 518. Mapa Geológico de España 1:50.000. 2ª Serie. 1ª Edición. Madrid, Servicio de Publicaciones, Ministerio de Industria y Energía.

CANÉROT, J. and PIGNATELLI-GARCÍA, R. 1977. Mosqueruela, sheet 569. Mapa Geológico de España 1:50.000. 2ª Serie. 1ª Edición. Madrid, Servicio de Publicaciones, Ministerio de Industria y Energía.

CANÉROT, J., CUGNY, P., PARDO, G., SALAS, R. and VILLENA, J. 1982. Ibérica Central- Maestrazgo. In: Universidad Complutense de Madrid, Fac. Ciencias Geológicas-CSIC (eds.). *El Cretácico de España*, Madrid, 273-344.

CANÉROT, J., Faure, Ph., and Rahal, M. 1984. Donnée nouvelles sur le Jurassique du Maestrazgo méridional (prov. de Castellón, Espagne). *C. R. Acad Sc. Paris*, 298, série 11, núm. 15, 651-654.

CAPOTE, R., MUÑOZ, J. A., SIMÓN, J. L., LIESA, C. L. and ARLEGUI, L. E. 2002. Alpine tectonics I: the Alpine system north of the Betic Cordillera. In: GIBBONS, W. and MORENO, T. (eds.). *The Geology of Spain*. London, Geological Society, London, 367-400

CASAS-SAINZ, A.M. 1993. Oblique tectonic inversion and basement thrusting in the Cameros Massif (Northern Spain). *Geodinamica Acta*, 6, 3, 202-216.

CASAS-SAINZ, A.M., CASAS, A., PÉREZ, A., TENA, S., BARRIER, L., GAPAIS, D. and NALPAS, T. 2000. Syn-tectonic sedimentation and thrust-and-fold kinematics at the intra-mountain Montalbán Basin (northern Iberian Chain, Spain). *Geodinamica Acta*, 1, 1-17.

CASTILLO HERRADOR, F. 1974. Le Trias évaporitique des basins de la Vallée de l'Èbre et de Cuenca. *Bulletin de la Soc. Géologique de France*, 16(6), 666-675.

CERVERA, A., PARDO, G. and VILLENA, J. 1976. Algunas precisiones litoestratigráficas sobre la formación «Lignitos de Escucha». *Tecniterrae*, 14, 25-33.

CRESPO ZAMORANO, A., NAVARRO VÁZQUEZ, D. and CANÉROT, J., 1977. Montalbán, sheet 518. Memoria del Mapa Geológico de España 1:50.000. 2ª Serie. 1ª Edición. Madrid, Servicio de Publicaciones, Ministerio de Industria y Energía.

DE VICENTE, G., VEGAS, R. and CASAS, A. 2004. Estructura y evolución alpina de la Cadena Ibérica. In: Vera, J.A. (ed.). *Geología de España*. Madrid, SGE-IGME, 525-527.

DE VICENTE, G., VEGAS, R., MUÑOZ MARTÍN, A., SILVA, P.G., ANDRIESSEN, P., CLOETINGH, S., GONZÁLEZ CASADO, J.M., VAN WEES, J.D., ÁLVAREZ, J., CARBÓ, A. and OLAIZ, A. 2007. Cenozoic thick-skinned deformation and topography evolution of the Spanish Central System. *Global and Planetary Change*, 58(1–4), 335–381. Doi:10.1016/j.gloplacha.2006.11.042.

ESCUDERO-MOZO, M.J., MÁRQUEZ-ALIAGA, A., GOY, A., MARTÍN-CHIVELET, J., LÓPEZ-GÓMEZ, J., MÁRQUEZ, L., ARCHE, A., PLASENCIA, P., PLA, C., MARZO, M. and SÁNCHEZ-FERNÁNDEZ, D. 2015. Middle Triassic carbonate platforms in eastern Iberia: Evolution of their fauna and palaeogeographic significance in the western Tethys. *Palaeogeography, Palaeoclimatology, Palaeoecology*, 417, 236-260. Doi: http://dx.doi.org/10.1016/j.palaeo.2014.10.041

ESNAOLA, J. M. and CANÉROT, J. 1972. Albocácer, sheet 570. Mapa Geológico de España 1:50.000. 2ª Serie. 1ª Edición. Madrid, Servicio de Publicaciones, Ministerio de Industria y Energía.

FARRAN, M. 2008. IMAGE2SEGY: A software to convert seismic profiles images to SEG Y files. In: Pérez, F. J., Cabrera, M. C. (eds.). *Geo-Temas*, 10. Las Palmas de Gran Canaria, VII Congreso Geológico de España.

FERNÁNDEZ, O. 2004. Reconstruction of geological structures in 3D. An example from the Southern Pyrenees. PhD Thesis. University of Barcelona, 321 pp.

FERRER, O., JACKSON, M. P. A., ROCA, E. and RUBINAT, M. 2012. Evolution of salt structures during extension and inversion of the Offshore Parentis Basin (Eastern Bay of Biscay). In: Alsop, G. I., Archer, S. G., Hartley, A. J., Grant, N. T., Hodgkinson, R. (eds.). *Salt Tectonics, Sediments and Prospectivity*. London, Geological Society of London, Special Publications, 363, 361-379. Doi: 10.1144/SP363.16.

GARCÍA DE DOMINGO, A. and LÓPEZ OLMEDO, F. 1982. Horta de Sant Joan, sheet 496. Mapa Geológico de España 1:50.000. 2ª Serie. 1ª Edición. Madrid, Servicio de Publicaciones, Ministerio de Industria y Energía.

GAUTIER, F. 1978. Alcalà de la Selva, sheet 568. Mapa Geológico de España 1:50.000. 2ª Serie. 1ª Edición. Madrid, Servicio de Publicaciones, Ministerio de Industria y Energía.

GAUTIER, F. 1979. Villarluengo, sheet 543. Mapa Geológico de España 1:50.000. 2ª Serie. 1ª Edición. Madrid, Servicio de Publicaciones, Ministerio de Industria y Energía.

GAUTIER, F. and BARNOLAS, A. 1979. Villarluengo, sheet 543. Memoria del Mapa Geológico de España 1:50.000. 2ª Serie. 1ª Edición. Madrid, Servicio de Publicaciones, Ministerio de Industria y Energía.

GINER, J. 1980. Estudio sedimentológico y diagenético de las formaciones carbonatadas del Jurásico de los Catalánides, Maestrazgo y rama aragonesa de la Cordillera Ibérica (sector oriental). PhD Thesis. University of Barcelona, 316pp.

GÓMEZ, J.J. 1979. El Jurásico de facies carbonatadas del sector levantino de la Cordillera Ibérica. *Seminarios de Estratigrafia*. Serie Monografías, Universidad Complutense de Madrid, 4, 656 pp.

GÓMEZ, J.J. and GOY, A. 1979. Las unidades litoestratigráficas del Jurásico medio y superior en facies carbonatadas del Sector Levantino de la Cordillera Ibérica. *Estudios Geológicos*, 35, 17-57.

GÓMEZ, J. J. and GOY, A. 1998. Unidades litoestratigráficas del tránsito Triásico-Jurásico en la región de Lécera (Zaragoza). *Geogaceta*, 23, 63-66.

GÓMEZ, J. J. and GOY, A. 2004. Jurásico Inferior. In: Vera, J.A. (ed.). Geología de España. Madrid, SGE-IGME, 495-500.

GÓMEZ, J. J., COMAS-RENGIFO, M. J. and GOY, A. 2003. Las unidades litoestratigráficas del Jurásico inferior de las cordilleras Ibérica y Costeras Catalanas. *Revista de la Sociedad Geológica de España*, 16 (3-4), 227-237.

GÓMEZ, J.J., GOY, A. and BARRÓN, E. 2007. Events around the Triassic-Jurassic boundary in northern and Eastern Spain: A review. *Palaeogeography, Palaeoclimatology, Palaeoecology*, 244, 89-110. doi:10.1016/j.palaeo.2006.06.025

GONZÁLEZ, A. 1989. Análisis tectosedimentario del terciario del borde SE de la Depresión del Ebro (sector bajoaragonés) y de las cubetas ibéricas marginales. PhD Thesis. Universidad de Zaragoza, 507 pp.

GONZÁLEZ, A. and GUIMERÀ, J. 1993. Sedimentación sintectónica en una cuenca transportada sobre una lámina de cabalgamiento: la cubeta terciaria de Aliaga. *Revista de la Sociedad Geológica de España*, 6, 151-165.

GONZÁLEZ, A., GUIMERÀ, J. and LUZÓN, A. 1994. Relaciones tectónica-sedimentación en la Zona de Enlace y borde suroriental de la depresión del Ebro. In: González, A. (ed.). *Guía de Excursiones del II Congreso del Grupo Español del Terciario*, Jaca, 1-134.

GONZÁLEZ, A. and GUIMERÀ, J. 1997. Marco estructural de la sedimentación durante el Mioceno inferior en el extremo meridional de la Cuenca del Ebro. In: Calvo, J.P., Morales, J., (eds.). *Avances en el conocimiento del Terciario Ibérico*. III Congreso del Grupo Español del Terciario. Universidad Complutense de Madrid, Fac. Ciencias Geológicas-CSIC, 97-100.

GONZÁLEZ, A., GUIMERÀ, J. and LUZÓN, A. 1998. Edad Oligoceno superior-Mioceno inferior para las superficies de erosión conservadas en el flanco SW de la cubeta de Bordón (Província de Teruel, España). *Geogaceta*, 24, 155-158.

GOY, A., GÓMEZ, J.J., and YÉBENES, A. 1976. El Jurásico de la rama castellana de la Cordillera Ibérica (Mitad Norte). Unidades Litoestratigráficas. *Estudios Geológicos*, 32, 391-423.

GOY, A. and YÉBENES, A. 1977. Características, extensión y edad de la Formación Dolomías Tableadas de Imón. *Cuadernos de Geología Ibérica*, 4, 375–384.

GUEGUEN, E., DOGLIONI, C. and FERNÁNDEZ, M. 1998. On the post-25 Ma geodynamic evolution of the western Mediterranean. *Tectonophysics*, 298, 259-269.

GUIMERÀ, J. 1988. Estudi estructural de l'Enllaç entre la Serralada Ibérica i la Serralada costanera Catalana. PhD Thesis. Universitat de Barcelona, 600 pp.

GUIMERÀ, J. 2004. Cadenas con cobertera: Las Cadenas Ibérica i Costera Catalana. In: Vera, J. A. (ed.). *Geología de España*. Madrid, SGE-IGME, 602-607.

GUIMERÀ, J. 2013. Estructura y evolución tectónica de la Cadena Ibérica. In: Simón, J. L., Liesa, C. L. (eds.). *XLVII Curso de Geología Práctica. La Orogenia Alpina en la Cordillera Ibérica*. Universidad de Verano de Teruel, 1-9.

GUIMERÀ, J. and ÁLVARO, M. 1990. Structure et évolution de la compression alpine dans la Chaîne Ibérique et la Chaîne côtière catalane (Espagne). *Bulletin de la Société Géologique de France*, (8), VI (2), 339-340.

GUIMERÀ, J. and SALAS, R. 1996. Inversión terciaria de la falla normal mesozoica que limitaba la subcuenca de Galve (Cuenca del Maestrazgo). *Geogaceta,* 20(7), 1701-1703.

GUIMERÀ, J., MAS, R. and ALONSO, A. 2004. Intraplate deformation in the NW Iberian Chain: Mesozoic extenion and Tertiary contractional inversion. *Journal of the Geological Society*, London 161, 291-303.

GUIMERÀ, J., GONZÁLEZ, A., SALAS, R. and SANCHO, C. 2010. Origin and preservation of the late contractional relief of an intraplate thrust-belt: the NE Iberian Chain (Iberian Peninsula). *Geophysical Research Abstracts*, 12. EGU2010-5137, 2010.

GUIMERÀ, J., RIVERO, L., SALAS, R. and CASAS, A. 2016. Moho depth inferred from gravity and topography in an intraplate area (Iberian Chain). *Tectonophysics*, 666, 134-143. http://dx.doi.org/10.1016/j.tecto.2015.10.021

HAQ, B.U., HARDENBOL, J. and VAIL, P.R. 1988. Mesozoic and Cenozoic chronostratigraphy and cycles of sea-level change. *Society of Economic Paleontologists and Mineralogists*, v. 42, p. 71-108.

HARDENBOL, J., THIERRY, J., FARLEY, M.B., JACQUIN, T., DE GRACIANSKY, P.C., and VAIL, P., 1998. Mesozoic and Cenozoic sequence chronostratigraphic framework of European Basins, in P.C. GRACIANSKY, et al. (eds) *Mesozoic and Cenozoic sequence stratigraphy of European basins*: SEPM Special Publication 60, p. 3-13.

HERNÁNDEZ, A. 1985. Teruel, sheet 47. Memoria del Mapa Geológico de España 1:200.000. 1ª Edición. Madrid, Servicio de Publicaciones, Ministerio de Industria y Energía.

LANAJA, J. M. 1987. Contribución de la exploración petrolífera al conocimiento de la geología de España. Madrid, Instituto Tecnológico GeoMinero de España, 465 pp.

LIESA, C. L., SORIA, A. R., MELÉNDEZ, N. and MELÉNDEZ, A. 2006. Extensional fault control on the sedimentation patterns in a continental rift basin: El Castellar Formation, Galve sub-basin, Spain. *Journal of the Geological Society,* London, 163, 487-498.

LÓPEZ-GÓMEZ, J. and ARCHE, A. 1992. Las unidades litoestratigráficas del Pérmico y Triásico Inferior y Medio en el sector SE de la Rama Castellana de la Cordillera Ibérica. *Estudios Geológicos*, 48, 123-143.

LÓPEZ-GÓMEZ, J., ARCHE, A., CALVET, F. and GOY, A. 1998. Epicontinental marine carbonate sediments of the Middle and Upper Triassic in the westernmost part of the Tethys Sea, Iberian Peninsula. In: Bachmann, G.H., Lerche, I. (Eds.), *Epicontinental Triassic, Zentralb*. für Geol. und Paläontol., I, vol. 9–10, pp. 1033–1084.

LÓPEZ-GÓMEZ, J.,MÁS,R. and ARCHE, A. 1993. The evolution of theMiddle Triassic (Muschelkalk) carbonate ramp in the SE Iberian Ranges, eastern Spain: sequence stratigraphy, dolomitization processes and dynamic controls. *Sed. Geology*, 87, 165–193.

LÓPEZ-GÓMEZ, J., ARCHE, A., MÁRQUEZ-ALIAGA, A., SALAS, R., GOY, A., GUIMERÀ, J. and TOMÁS, S. 2005. El Pérmico y el Triásico del Desert de les Palmes, Cordillera Ibérica Oriental, Castellón. *Cidaris*, 27-28, 5-34.

LÓPEZ-MIR, B., MUÑOZ, J. A. and GARCÍA-SENZ, J. 2015. Extensional salt tectonics in the partially inverted Cotiella post-rift basin (south-central Pyrenees): structure and evolution. *International Journal of Earth Sciences,* 104(2), 419-434. Doi: 10.1007/s00531-014-1091-9.

MANCILLA, F. and DÍAZ, J. 2015. High resolution Moho topography map beneath Iberia and northern Morocco from receiver function analysis. *Tectonophysics*, 663, 205–213.

MARCUELLO, A., LEDO, J., ARANGO, C. and QUERALT, P. 2006. Campaña de AMT en EL Maestrazgo. Proyecto HIPROMA. IGME-Dept. Geodinàmica i Geofísica, Universitat de Barcelona, 38pp.

MARÍN, PH. and DUVAL, B. 1976. Castelseras, sheet 495. Mapa Geológico de España 1:50.000. 2ª Serie. 1ª Edición. Madrid, Servicio de Publicaciones, Ministerio de Industria y Energía.

MARÍN, PH., PALLARD, B., DUVAL, B. and DE MIROSCHEDJI, A. 1974. Calanda, sheet 494. Mapa Geológico de España 1:50.000. 2ª Serie. 1ª Edición. Madrid, Servicio de Publicaciones, Ministerio de Industria y Energía.

MARSHAK, S. 2004. Salients, recesses, arcs, oroclines, and syntaxes: A review of ideas concerning the formation of map-view curves in fold-and-thrust belts. In: K. R. McClay (ed.). *Thrust Tectonics and Hydrocarbon Systems.* AAPG, Memoir no. 82, 131-156.

MARSHAK, S. and SCOTT WILKERSON, M. 2004. Fold-Thrust belts. In: B. A.VAN DER PLUJIM and S. MARSHAK (eds.). *Earth Structure*. W. W. Norton & Company, Inc., 444-474.

MARTÍN, L., LEYVA, F. and CANÉROT, J. 1972. Morella, sheet 545. Mapa Geológico de España 1:50.000. 2ª Serie. 1ª Edición. Madrid, Servicio de Publicaciones, Ministerio de Industria y Energía.

MARTÍN-MARTÍN, J. D., GOMEZ-RIVAS, E., BOVER-ARNAL, T., TRAVÉ, A., SALAS, R., MORENO-BEDMAR, J.A., TOMÁS, S., CORBELLA, M., TEIXELL, A., VERGÉS, J. and STAFFORD, S.L. 2013. The Upper Aptian to Lower Albian syn-rift carbonate succession of the southern Maestrat Basin (Spain): Facies architecture and fault-controlled stratabound dolostones. *Cretaceous Research*, 41, 217-236. Doi: http://dx.doi.org/10.1016/j.cretres.2012.12.008

MARTÍNEZ-ABAD, J. L. 1991. Cuenca del Maestrazgo. Correlación de sondeos I-I'. In: López, F. (coord.) *Estudio geológico del Maestrazgo y de la mitad meridional de los Catalánides*. INYPSA- IGME, unpublished.

MENCOS, J. 2010. Metodologies de reconstrucció i modelització 3D d'estructures geològiques: anticlinal de Sant Corneli-Bóixols (Pirineus centrals). PhD Thesis. Universitat de Barcelona, 375 pp.

MORILLO-VELARDE, M.J. and MELÉNDEZ-HEVIA, F. 1979. El Jurásico de "La Alcarria"–"La Mancha". *Cuad. Geol. Univ. Granada*, 10, 149–166.

MOUTHEREAU, F., FILLEAUDEAU, P.-Y., VACHERAT, A., PIK, R., LACOMBE, O., FELLIN, M. G., CASTELLTORT, S., CHRISTOPHOUL, F., and MASINI, E., 2014. Placing limits to shortening evolution in the Pyrenees: Role ofmargin architecture and implications for the Iberia/Europe convergence, *Tectonics*, 33, 1-32, doi:10.1002/2014TC003663.

MUÑOZ, J. A. E. (1992), Evolution of a continental collision belt: ECORS-Pyrenees crustal balanced cross-section, in Thrust Tectonics, edited by K. McClay, pp. 235–246, Chapman and Hall, London.

Navarro-Vázquez, D., Crespo-Zamorano, A., Pérez-Castaño, A. and Canérot. J. 1972. Forcall, sheet 544. Mapa Geológico de España 1:50.000. 2ª Serie. 1ª Edición. Madrid, Servicio de Publicaciones, Ministerio de Industria y Energía.

NEBOT, M. and GUIMERÀ, J. 2016a. Structure of an inverted basin from subsurface and field data: the Late Jurassic-Early Cretaceous Maestrat basin (Iberian Chain). *Geologica Acta*, 14 (2), 155-177. Doi: 10.1344/GeologicaActa2016.14.2.5.

NEBOT, M. and GUIMERÀ, J. 2016b. Kinematic evolution of a fold-and-thrust belt developed during basin inversion: the Mesozoic Maestrat basin, E Iberian Chain. *Geological Magazine*, published online: october 2016. doi:10.1017/S001675681600090X

Olivet, J. L., 1996. La cinématique de la plaque Ibérique. *Bull. Cent. Rech. Explor. Prod. Elf Aquitaine*, 20, 131–195.

ORTÍ, F. 1973. El Keuper del Levante Español. Litoestratigrafía, petrología y paleogeografía de la cuenca. PhD Thesis. Universitat de Barcelona, 174 pp.

ORTÍ, F., 1974. El Keuper del Levante Español. *Estudios Geológicos*, 30, 7–46.

ORTÍ, F. 1981. Diapirismo de materiales triásicos y estructuras de zócalo, en el sector central valenciano (España). *Estudios geológicos*, 37 (3-4), 245-257.

ORTÍ, F. and SALVANY, J.M. (2004). Coastal salina evaporites of the Triassic-Liassic boundary in the Iberian Peninsula: the Alacón borehole. *Geologica Acta*, 2, 291-304.

PARDO, G. 1974. Nota previa sobre las características litoestratigráficas de las formaciones «Arenas de Utrillas» y «Lignitos de Escucha». *Acta Geológica Hispánica*, IX (2), 62-66.

QUEROL, X., SALAS, R., PARDO, G. and ARDEVOL, L. 1992. Albian coal-bearing deposits of the Iberian Range in northeastern Spain. *Geological Society of America, Special Papers*, 267, 193-208.

QUEROL, X. 1992. Distribución de materia mineral y azufre en los carbones de la formación escucha: relación con los factores geológicos, sedimentológicos y diagenéticos. PhD thesis, Universitat de Barcelona.

RAMOS, A., 1979. Estratigrafía y Paleogeografía del Pérmico y Triásico al oeste de Molina de Aragón (provincia de Guadalajara). *Seminarios de Estratigrafía*, 6, 1–313.

ROCA, E. and GUIMERÀ, J. 1992. The Neogene structure of the eastern Iberian margin: structural constraints on the crustal evolution of the Valencia through (western Mediterranean). *Tectonophysics*, 203, 203-218. Doi: 10.1016/0040-1951(92)90224-T.

ROCA, E., GUIMERÀ, R. and SALAS, R. 1994. Mesozoic extensional tectonics in the southeast Iberian Chain. *Geological Magazine*, 131(2), 155-168.

ROCA, E., FRIZON DE LAMOTTE, D., MAUFFRET, A., BRACÈNE, R., VERGÉS, J., BENAOUALI, N., FERNÀNDEZ, M., MUÑOZ and J.A., ZEYEN, H. 2004. TRANSMED Transect II. In: Cavazza, W., Roure, F., Spakman, W., Stampfli, G.M., Ziegler, P.A. (Eds.), *The TRANSMED Atlas – The Mediterranean Region from Crust to Mantle*. Springer, Heidelberg, Berlin.

ROSENBAUM, G., LISTER, G. S., and DUBOZ, C., 2002. Relative motions of Africa, Iberia and Europe during Alpine orogeny, *Tectonophysics*, 359(1–2), 117–129, doi:10.1016/S0040-1951(02)00442-0.

ROEST, W.R. and SRIVASTAVA, S.P. 1991. Kinematics of the plate boundaries between Eurasia, Iberia, and Africa in the North Atlantic from the Late Cretaceous to the present. *Geology*, 19, 613-616,

SALAS, R. 1987. El Malm i el Cretaci inferior entre el Massís de Garraf i la Serra d'Espadà. PhD Thesis. Universitat de Barcelona, 345 pp.

SALAS, R. 1989. Evolución estratigráfica secuencial y tipos de plataformas de carbonatos del intervalo Oxfordiense-Berriasiense en las cordilleras ibérica oriental y costero catalana meridional. C*uadernos de Geología Ibérica*, 13, 121-157.

SALAS, R. and CASAS, A. 1993. Mesozoic extensional tectonics, stratigraphy and crustal evolution during the Alpine cycle of the Eastern Iberian basin. *Tectonophysics*, 228, 33-35. Doi: 10.1016/0040-1951(93)90213-4.

SALAS, R., MARTÍN-CLOSAS, C., QUEROL, X., GUIMERÀ, J. and ROCA, E. 1995. Evolución tectonosedimentaria de las cuencas del Maestrazgo y Aliaga-Penyagolosa durante el Cretácico inferior. In: Salas, R., Martín-Closas, C. (eds.). *El Cretácico inferior del Nordeste de Iberia*. Barcelona, Universitat de Barcelona, 13-94.

SALAS, R. and GUIMERÀ, J. 1996. Rasgos estructurales principales de la cuenca cretácica inferior del Maestrazgo (Cordillera Ibérica oriental). *Geogaceta*, 20(7), 1704-1706.

SALAS, R., GUIMERÀ, J., GIMÈNEZ-MONTSANT, J., MARTÍN-CLOSAS, C. and ROCA, E. 1997. Mesozoic Rift structure, Stratigraphy and Palaeogene Inversion of the Maestrat basin. Iberian Range (NE Spain). *Field trip guide. IGCP Project-369. Comparative evolution of PeriTethyan Rift Basins*.

SALAS, R., GUIMERÀ, J., MAS, R., MARTÍN-CLOSAS, C., MELÉNDEZ, A. and ALONSO, A. 2001. Evolution of the Mesozoic Central Iberian Rift System and its Cainozoic inversion (Iberian chain). In: Ziegler, P.A., Cavazza, W., Robertson, A.H.F., Crasquin-Soleau, S. (eds.). *Peri-Tethys memoir, 6: Peri-Tethyan Rift/Wrench Basins and Passive Margins*. Paris, Mém Mus. natn. Hist. Nat., 186, 145-186.

SALAS, R., MARTÍN-CLOSAS, C., DELCLÒS, X., GUIMERÀ, J., CAJA, M. A. and MAS, R. 2005. Factores principales de control de la sedimentación y los cambios bióticos durante el tránsito Jurásico-Cretácico en la Cadena Ibérica. *Geogaceta*, 38, 15-18.

SALAS, R., GARCÍA-SENZ, J., GUIMERÀ, J. and BOVER-ARNAL, T. 2010. Opening of the Atlantic and development of the Iberian intraplate rift basins during the late Jurassic-early Cretaceous. *II Central and North Atlantic Conjugate Margins Conference*, 245-248.

SALAS, R., GUIMERÀ, J., BOVER-ARNAL, T. and NEBOT, M. 2016. Late Jurassic and Early Cretaceous intraplate rifting in the Eastern Mesozoic Iberian Rift System. Submitted .

SAN ROMÁN, J. and AURELL, M. 1992. Paleogeographical significance of the Triasssic-Jurassic unconformity in the north Iberian basin (Sierra del Moncayo, Spain). *Palaeogeography, Palaeoclimatology, Palaeoecology,* 99(1-2), 101-117. Doi: 10.1016/0031-0182(92)90009-T.

SÁNCHEZ-MOYA, Y., SOPEÑA, A., MUÑOZ, A. and RAMOS, A. 1992. Consideraciones teoricas sobre el análisis de la subsidencia: aplicación a un caso real en el borde de la cuenca triàsica ibérica. *Rev. Soc. Geol. España*, 5, 21-40.

SEILLÉ, H., SALAS, R., POUS, J., GUIMERÀ, J., GALLART, J., TORNE, M., ROMERO-RUIZ, I., DIAZ, J., CARBONELL, R. and MAS, R. 2015. Crustal structure of an intraplate thrust belt: The Iberian Chain revealed by wide-angle seismic, magnetotelluric soundings and gravity data. *Tectonophysics*, 663, 339-535. Doi: 10.1016/j.tecto.2015.08.027.

SERRANO, A. and MARTÍNEZ DEL OLMO, W. 2004. Estructuras diapíricas de la zona meridional de la Cuenca Vasco-Cantábrica. In: Vera, J. A. (ed.). *Geología de España*. Madrid, SGE-IGME, 334-338.

SIMÓN, J.L. 1980. Estructuras de superposición de plegamientos en el borde NE de la cadena Ibérica. *Acta Geológica Hispánica*, XV (5), 137-140.

SIMÓN, J. L. 1981. Reactivación alpina del desgarre del Segre en el borde NE de la Cadena Ibérica. *Revista del Instituto de Estudios Turolenses*, 65, 195-209.

SIMÓN, J.L. 1982. Compresión y distensión alpinas en la Cadena Ibérica Oriental. PhD Thesis. University of Zaragoza, 504 pp.

SIMÓN, J.L. 2004. Superposed buckle folding in the Eastern Iberian Chain, Spain. *Journal of Structural Geology*, 26, 1447-1464.

SIMÓN, J.L. and LIESA, C. L. 2011. Incremental slip history of a thrust: diverse transport directions and internal folding of the Utrillas thrust sheet (NE Iberian Chain, Spain). *London, Geological Society of London, Special Publications*, 349, 77-97. Doi: 10.1144/SP349.5

SRIVASTAVA, S. P., SCHOUTEN, H., ROEST, W. R., KLITGORD, K. D., KOVACS, L. C., VERHOEF, J., and MACNAB, R. 1990. Iberian Plate kinematics—A jumping plate boundary between Eurasia and Africa, *Nature*, 344(6268), 756–759, doi:10.1038/344756a0.

TEIXELL, A. 1998. Crustal structure and orogenic material budget in the west central Pyrenees, *Tectonics*, 17(3), 395–406, doi:10.1029/98TC00561.

TEIXELL A, LABAUME, P. and LAGABRIELLE, Y. 2016. The crustal evolution of the west-central Pyrenees revisited: Inferences from a new kinematic scenario. *C. R. Geoscience*, 348, 257-267, http://dx.doi.org/10.1016/j.crte.2015.10.010.

TRELL, A., CANÉROT, J. and MARTÍN, M. 1979. Villahermosa del Río, sheet 592. Mapa Geológico de España 1:50.000. 2ª Serie. 1ª Edición. Madrid, Servicio de Publicaciones, Ministerio de Industria y Energía.

VARGAS, H., GASPAR-ESCRIBANO, J.M., LÓPEZ-GÓMEZ, J., VANWEES, J.D., CLOETINGH, S., DE LA HORRA, R. and ARCHE, A. 2009. A comparison of the Iberian and Ebro Basins during the Permian and Triassic, eastern Spain: A quantitative subsidence modelling approach. *Tectonophysics*, 474, 160-183.

VEGAS, R., FONTBOTÉ, J.M., and BANDA, E. 1979. Widespread neogene rifting superimposed on alpine regions of the Iberian Peninsula. *Proc. Symp. Evol. Tectonic of the Western Mediterranean and surrounding areas*, EGS, Viena. Inst. Geog. Nac. Sp. Publ., 201, 109-128.

VERA, J.A. 2001. Evolution of the South Iberin Continental Margin. In: Ziegler, P.A., Cavazza, W., Robertson, A.H.F., Crasquin-Soleau, S. (eds.). Peri-Tethys memoir, 6: Peri-Tethyan Rift/Wrench Basins and Passive Margins. Paris, *Mém Mus. natn. Hist. Nat.*, 186, 109-143.

VERGÉS, J., MILLÁN, H., MUÑOZ, J. A., MARZO, M., CIRÈS, J., DEN BEZEMER, T., ZOETEMEIJER, R., and CLOETINGH, S. 1995. Eastern Pyrenees and related foreland basins: Pre-, syn- and post-collisional crustal-scale cross-sections, *Mar. Petrol. Geol*., 12(8), 893–915.

ZIEGLER, P.A. 1988. Evolution of the Arctic-North Atlantic and the Western Tethys. *Am. Assoc. Petrol. Geol., Mem*. 43: 198 p.

APPENDIX I. A

Structure of an inverted basin from subsurface and field data: the Late Jurassic-Early Cretaceous Maestrat basin (Iberian Chain)

Nebot, M. and Guimerà, J. 2016. *Geologica Acta*, 14 (2), 155-177
doi: 10.1344/GeologicaActa2016.14.2.5

Geologica Acta, Vol.14, Nº 2, June 2016, 155-177
DOI: 10.1344/GeologicaActa2016.14.2.5

geologica acta

Structure of an inverted basin from subsurface and field data: the Late Jurassic-Early Cretaceous Maestrat Basin (Iberian Chain)

M. NEBOT and J. GUIMERÀ

Geomodels Research Institute, Departament de Geodinàmica i Geofísica, Facultat de Geologia, Universitat de Barcelona (UB)
Martí i Franquès s/n, 08028 Barcelona, Spain. Nebot E-mail: marinanebotmiralles@gmail.com
Guimerà E-mail: joan.guimera@ub.edu

ABSTRACT

The Maestrat Basin experienced two main rifting events: Late Permian-Late Triassic and Late Jurassic-Early Cretaceous, and was inverted during the Cenozoic Alpine orogeny. During the inversion, an E-W-trending, N-verging fold-and-thrust belt developed along its northern margin, detached in the Triassic evaporites, while southwards it also involved the Variscan basement. A structural study of the transition between these two areas is presented, using 2D seismic profiles, exploration wells and field data, to characterize its evolution during the Mesozoic extension and the Cenozoic contraction.

The S-dipping Maestrat basement thrust traverses the Maestrat Basin from E to W; it is the result of the Cenozoic inversion of the lower segment–within the acoustic basement–of the Mesozoic extensional fault system that generated the Salzedella sub-basin. The syn-rift Lower Cretaceous rocks filling the Salzedella sub-basin thicken progressively northwards, from 350m to 1100m. During the inversion, a wide uplifted area –40km wide in the N-S direction– developed in the hanging wall of the Maestrat basement thrust. This uplifted area is limited to the North by the E-W-trending Calders monocline, whose limb is about 13km wide in its central part, dips about 5ºN, and generates a vertical tectonic step of 800-1200m. We interpreted the Calders monocline as a fault-bend fold; therefore, a flat-ramp-flat geometry is assumed in depth for the Maestrat basement thrust. The northern synformal hinge of the Calders monocline coincides with the transition from thick-skinned to thin-skinned areas. The vast uplifted area and the low-dip of the monocline suggest a very low-dip for the basement ramp, rooted in the upper crust. The Calders monocline narrows and disappears laterally, in coincidence with the outcrop of the Maestrat basement thrust.

The evaporitic Middle Muschelkalk detachment conditioned the structural style. Salt structures are also related to it; they developed during the Late Triassic extension, as deduced from the Keuper seismic reflectors that onlap the folded Upper Muschelkalk and form growth strata above some basement normal faults.

KEYWORDS | **Basin inversion. Fault-bend fold. Vertical tectonic step. Low-dip ramp. Salt flow.**

INTRODUCTION

The Iberian Chain, located in the eastern Iberian Peninsula (Fig. 1), is a fold-and-thrust belt that developed during the Cenozoic, due to the contractional inversion of the Mesozoic Iberian rift system (Álvaro *et al*., 1979; Guimerà and Álvaro, 1990; Salas *et al*., 2001). The Maestrat Basin, located in the eastern Iberian Chain, was one of the most subsident basins of the Mesozoic Iberian rift system during the Late Jurassic and Early Cretaceous. It contains up to 6.5km of Mesozoic sediments, among which up to 4km correspond to Upper Jurassic and Lower Cretaceous rocks (Fig. 2). It has been proposed that its formation was related to a system of listric extensional faults, some of them involving the Variscan basement. These faults bounded the basin, and also divided it into

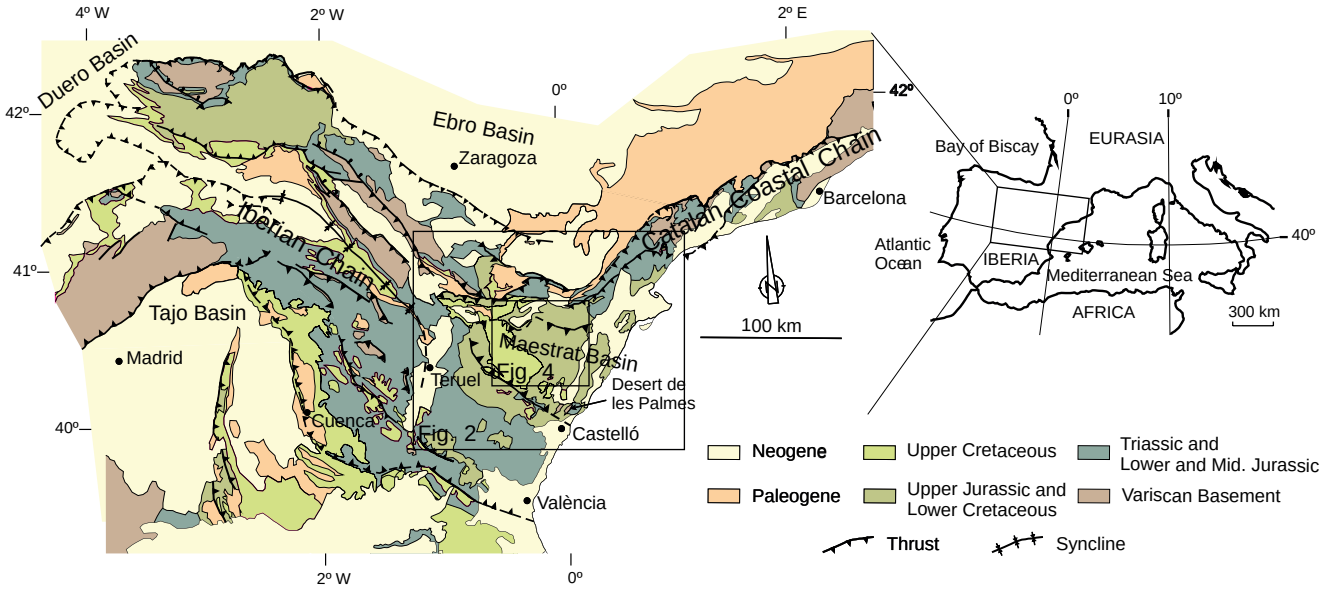

FIGURE 1. Structural map of the Iberian Chain and its location in the northeastern Iberian Peninsula (Modified from Guimerà, 2004, 2013).

sub-basins which contain different thicknesses of the Mesozoic sedimentary fill (Salas and Guimerà, 1996; Salas *et al*., 2001).

An E-W-trending, N-verging, fold-and-thrust belt developed along the northern boundary of the Maestrat Basin as a result of the Cenozoic contraction (Guimerà, 1988). This belt involved the Mesozoic cover in the northern–foreland–areas, with detachment levels located within the Triassic evaporitic units. Southwards, the thrust system also involved the Variscan basement. The aim of this paper is to characterize the structure of the transition between the thin-skinned and the thick-skinned areas, which coincides at the surface with an approximately E-W-trending vertical tectonic step. The formation of this tectonic relief has been associated with the Turmell fault zone (Salas and Guimerà, 1996; González and Guimerà, 1997), a WNW-trending, S-dipping fault zone resulting from the inversion of the Mesozoic extensional fault system (González *et al*., 1994; Guimerà and Salas, 1996). However, the Turmell fault zone does not match the structures that we recognize in the present study, so it is necessary to review this entire concept.

To this end, we studied the geometry and evolution of the Mesozoic and Cenozoic structures by integration of available subsurface data–2D seismic profiles and exploration wells–and new field data. Our results show that the wide uplifted area that developed during the Cenozoic inversion of the Maestrat Basin is bounded to the N by an E-W-trending monocline, the Calders monocline, which generates a tectonic relief. We interpret this monocline as a fault-bend fold developed in the hanging wall of a deep-basement thrust, the Maestrat basement thrust, as a result of its flat-ramp-flat geometry. It becomes narrower laterally and is linked to the direct outcrop of the Maestrat basement thrust. In order to characterize the structure of the study region, we present five cross-sections and a reconstruction of specific geological surfaces as well as interpreted seismic profiles. The role of the thick Middle Muschelkalk evaporitic unit during extension and contraction is also considered.

GEOLOGICAL SETTING

In the Iberian rift system, two major rifting cycles (Late Permian to Late Triassic, and Late Oxfordian to Late Albian) can be identified during the Mesozoic extension. Both were followed by episodes of lower rifting activity (Early and Middle Jurassic, and Late Albian to Maastrichtian) (Fig. 3, Salas *et al*., 2001); although a more complex evolution has been observed in the study area, which is described below.

Mesozoic rifting

The Late Permian to Late Triassic rifting was related to the westward propagation of the Tethys rift system and the southward propagation of the Arctic-North Atlantic rift system (Salas *et al*., 2001). An intraplate rift system developed within the central and eastern Iberian plate during this period, the Iberian rift system (Álvaro *et al*., 1979), bounded by high-angle normal faults. Sediments ranging from continental siliciclastics Upper Permian and Buntsandstein to marine carbonates (Muschelkalk) where

deposited (Salas *et al*., 2001) as well as different evaporite units (Middle Muschelkalk and Keuper).

During the Early and Middle Jurassic post-rift period, a system of shallow carbonate platforms developed, covering the previously formed extensional structures. Angular unconformities between the Jurassic and the tilted Triassic rocks appear in several locations within the Maestrat Basin (Guimerà, 1988; Aurell *et al*., 1992; Roca and Guimerà, 1992; San Román and Aurell, 1992; Roca *et al*., 1994; Campos *et al*., 1996).

The Late Oxfordian to Late Albian rifting is related to the opening of the North Atlantic Basin and the Bay of Biscay Basin, which separated Iberia from North America and Europe (Salas *et al*., 2001; Salas *et al*., 2010). During this rifting event, the carbonate platform system was broken and the Iberian Basin was divided into several separate basins. The Maestrat Basin (Fig. 2) is one of the most subsident basins that developed during this period (Salas and Guimerà, 1996; Salas *et al*., 2001). A system of listric extensional faults developed, detached in the Triassic evaporitic units or within the Variscan basement, that divided the Maestrat Basin into different subsident blocs (Fig. 2). During this rifting event, a period of more moderate extensional activity occurred from the Late Valanginian to Late Hauterivian (Neocomian) in which thermal subsidence predominated (Salas and Casas, 1993; Salas *et al*., 1995; Salas and Guimerà, 1996; Salas *et al*., 2001; Salas *et al*., 2010). Sediments of this age are lacking or partially eroded in some places of the Maestrat Basin.

During the Late Albian to Maastrichtian post-rift period, Iberia became separated from Europe and basin evolution was controlled by thermal subsidence and a rise in sea level (Salas *et al*., 2001). The fluvial sediments of the Utrillas Formation (Late Albian to Cenomanian) were deposited unconformably over the previously formed extensional basins. During the Cenomanian to Turonian marine transgression, carbonate platforms developed that connected the Atlantic and the Tethys oceans. By the end of the Cretaceous, the whole area of the Iberian rift system was emerged and lacustrine sediments were deposited (Salas *et al*., 2001) that may contain a few marine intercalations (Gautier and Barnolas, 1979).

Maestrat Basin

The Maestrat Basin (Fig. 2) is bounded by two systems of listric extensional faults. The northern system is formed by WNW-trending, S-dipping listric normal faults (including the Turmell fault zone), while the southwestern system is oriented NW-SE and is mostly NE-dipping. The double rollover geometry of the hanging walls of these listric faults generated the Salzedella sub-basin to the N and the Penyagolosa sub-basin to the S, separated by the Vistabella threshold (Fig. 2) (Salas and Guimerà, 1996; Salas *et al*., 2005). The E-W-trending Turmell fault zone is interpreted to be the main normal fault in the northern side of the Maestrat Basin (Fig. 2). It separates the more subsident inner part (Salzedella and Galve sub-basins) in its hanging wall (S) from its outer part (Morella and Aliaga sub-basins) in its footwall (N) (Salas and Guimerà, 1996).

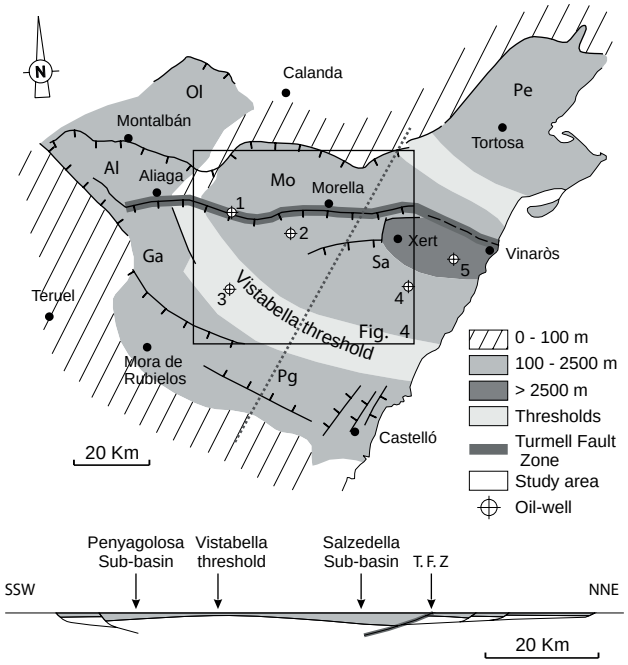

FIGURE 2. Simplified map of the Maestrat Basin during the Late Jurassic-Early Cretaceous rifting event. The basin was divided into several sub-basins: Ol= Oliete sub-basin, Al= Aliaga sub-basin, Mo= Morella sub-basin, Pe= Perelló sub-basin, Ga= Galve sub-basin, Sa= Salzedella sub-basin and Pg= Penyagolosa sub-basin. Wells: 1= Mirambell-1, 2= Bovalar-1 and Bovalar-2, 3= Maestrazgo-2, 4= Salzedella-1, 5= Maestrazgo-1. Modified from Salas and Guimerà (1996) and Salas ***et al.*** (2005).

The Maestrat Basin succession (Fig. 3) is mainly composed of shallow marine to lacustrine carbonates with intercalations of continental siliciclastic sediments (Early Aptian Morella Fm. and Early Albian to Cenomanian Escucha and Utrillas fms.) and a few intercalations of pelagic sediments. Valanginian-Hauterivian sediments are not represented in the western Salzedella sub-basin (Fig. 3).

Cenozoic Alpine contraction

The contractional deformation, related to the Alpine orogeny during which Iberia and Europe were again connected, occurred in the Maestrat Basin during the Late Eocene to Early Miocene (González, 1989). The inversion of the Maestrat Basin gave rise to the linking zone between the Iberian Chain and the Catalan Coastal Chain, with NW-SE and NE-SW structural trends, respectively

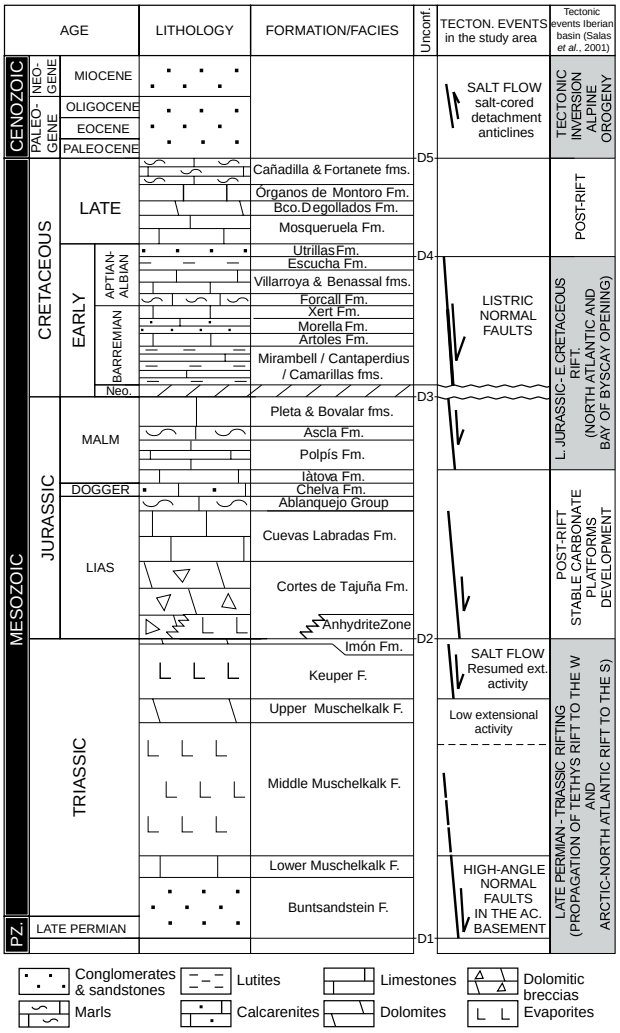

FIGURE 3. Tectonostratigraphic chart of the Maestrat Basin in the surroundings of the Mirambell-1 well (W Salzedella sub-basin). The different formations, their age and lithologies are shown. Abbreviations: Ac= Acoustic; Fm= Formation; F= facies; Neo= Neocomian (Berriasian, Valanginian and Hauterivian). The tectonic events described in the study area and those described by Salas *et al.* (2001) for the whole Iberian Basin, are indicated in the two right columns. Based on Canérot *et al.* (1982), Salas (1987) and Bover-Arnal *et al.* (2016) for the Barremian-Aptian boundary.

(Guimerà, 1988; Salas *et al.*, 2001). The Linking Zone is characterized by approximately E-W-trending, N-verging thrusts and folds, with a few areas where structures display virgation, and NE-SW and NW-SE structures appear (Guimerà, 1988). A detachment level is located within the Triassic evaporitic units in the North, and towards the S, the thrust system also involved the Variscan basement in the Turmell fault zone, (González and Guimerà, 1997). A roughly N-directed displacement direction was deduced for the linking zone thrust sheets (Guimerà and Álvaro, 1990). The Cenozoic inversion of the Turmell fault zone raised its hanging wall, generating a wide elevated area and a vertical tectonic step between the uplifted hanging wall and the footwall (González *et al.*, 1994; González and Guimerà, 1997). The internal deformation in the cover of this elevated area decreases towards the S (Guimerà, 1988), and resulted in a zone characterized by large folds (up to 25-30km along the trend) of long wavelengths (about 5km).

The uplifted area extends beyond the study area. It is nearly 40km wide in the NNE-SSW orientation, and more than 90km long in the E-W orientation, from the easternmost segment of the Turmell fault (Fig. 4) to the southern boundary of the Cenozoic Aliaga Basin (González and Guimerà, 1993; Guimerà and Salas, 1996). In it, a topographically elevated area (1300 to 2000m a.s.l.) containing Upper Cretaceous and Cenozoic rocks –the youngest pre-contractional rocks– is still preserved (Guimerà *et al.*, 2010).

The study area (Figs. 1; 2; 4) covers the western part of the Salzedella sub-basin, the Turmell fault zone (as defined by Salas and Guimerà, 1996) and the southern part of the fold-and-thrust belt North of the Turmell fault zone.

DATASET AND METHODOLOGY

Data

The seismic dataset (Fig. 5) comprises 29 2D seismic reflection profiles obtained in 1973 by Auxini, in 1979 by Campsa and in 1987-88 by Shell in the Maestrat Basin. Four oil exploration wells were used to constrain the seismic interpretation and the construction of the cross-sections: Mirambell-1, drilled by Auxini in 1974; Maestrazgo-2, by Campsa in 1981; and Bovalar-1 and Bovalar-2, drilled in 1963 by Coparex. Some of the subsurface data were collected from the Instituto Geológico y Minero de España (SIGECO) and from the Archivo Técnico de Hidrocarburos web databases. The other seismic profiles were scanned from printed copies.

More than 1000 strike-and-dip data were collected in the field; while another 750 strike-and-dip data were obtained after drawing the geological contacts on the ortho-images and the 3D topographic contour lines in a georeferenced environment (Microstation), using in-house macros developed by Fernández (2004). The 3D visualization, using Global Mapper, of the ortho-images draped on the DTM and their comparison with data collected in the field allowed us to monitor the quality of the in-room dip data.

Methods

Seismic profile images were converted to seg-y files using the IMAGE2SEGY Matlab application (Farran,

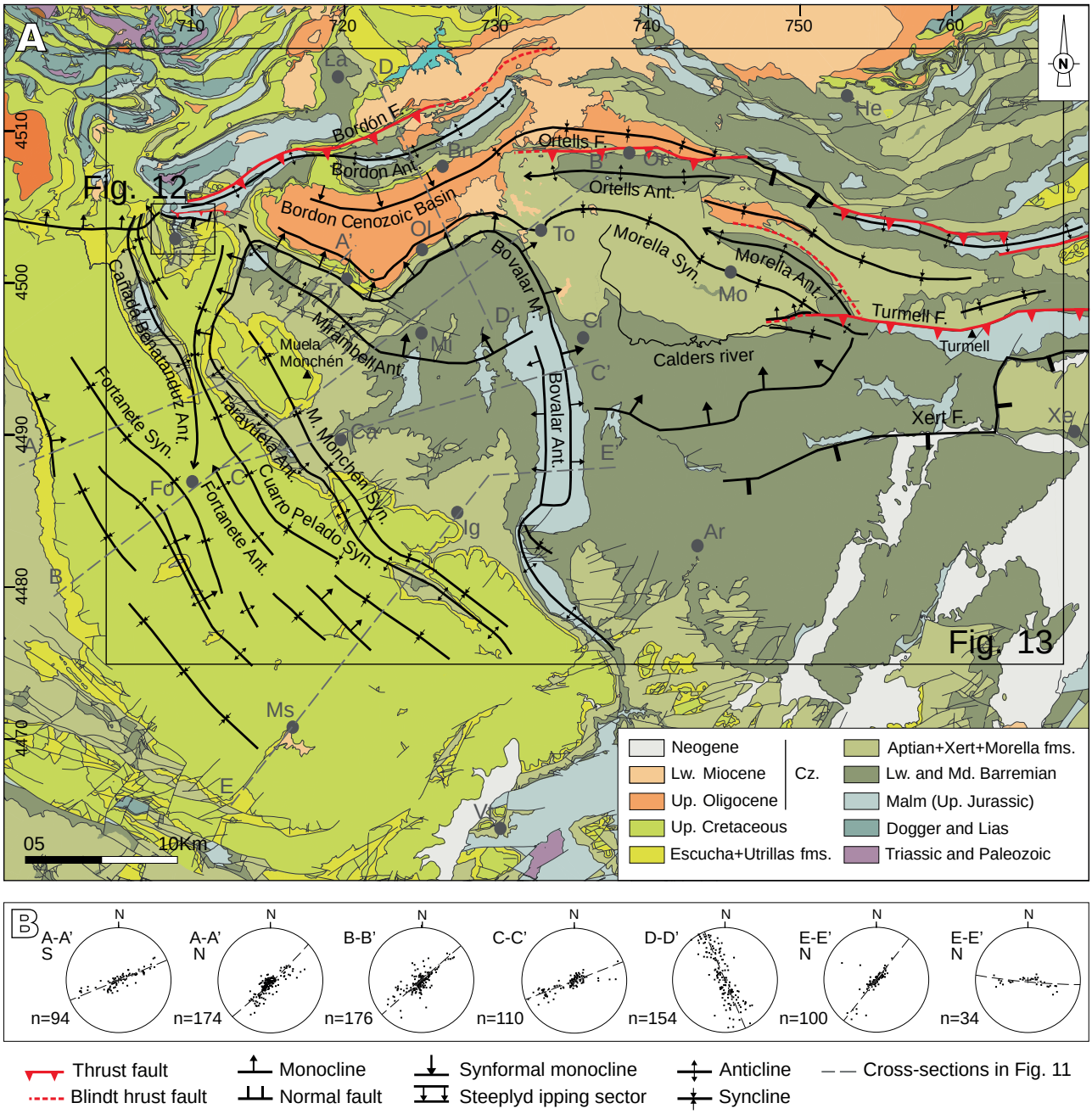

FIGURE 4. A) Simplified geologic map of the study area. Modified from the 1:50.000 IGME Magna geologic maps: Almera *et al.* (1982); Canérot and Leyva (1972); Canérot and Pignatelli-García (1972, 1977); Canérot *et al.* (1977); Esnaola and Canérot (1972); Gautier (1978, 1979); Martín *et al.* (1972); Navarro-Vázquez *et al.* (1972); Trell *et al.* (1979). Fold and fault trends are based on field observations and ortho-images interpretation. See location in Figure 1 and 2. Villages: Ar= Ares del Maestrat, Bn= Bordón, Ca= Cantavieja, Ci= Cinctorres, Fo= Fortanete, He= Herbés, Ig= La Iglesuela del Cid, La= Ladruñán, Mi= Mirambell, Mo= Morella, Ms= Mosqueruela, Ol= Olocau del Rei, Or= Ortells, To= La Todolella, Tr= Tronchón, Vl= Villarluengo, Vt= Vistabella del Maestrat, Xe= Xert. Abbreviations: Ant.= anticline, Syn.= syncline, M.= monocline, F.= fault. The location of cross-sections in Figure 11 is shown. UTM projection (zone 30, coordinates in km), ED50 datum. B) Lower hemisphere spheric equal-area projection of S0, showing the bedding orientation at different sectors of the study area, corresponding to the chosen cross-section traces. n= number of data.

2008) and interpreted using the Kingdom Suite software in a georeferenced environment. The seismic interpretation was constrained with the Mirambell-1 well tops, previously converted to two way time (TWT) with the velocities obtained from its sonic-log (Replacement velocity: 3250m/s, Cretaceous: 4985m/s, Jurassic and Imón Fm.: 5043m/s, Keuper and Upper Muschelkalk: 3491m/s, Middle Muschelkalk: 5441m/s). Seismic interpretation was converted to depth in meters using the same velocities obtained from the Mirambell-1 sonic-log.

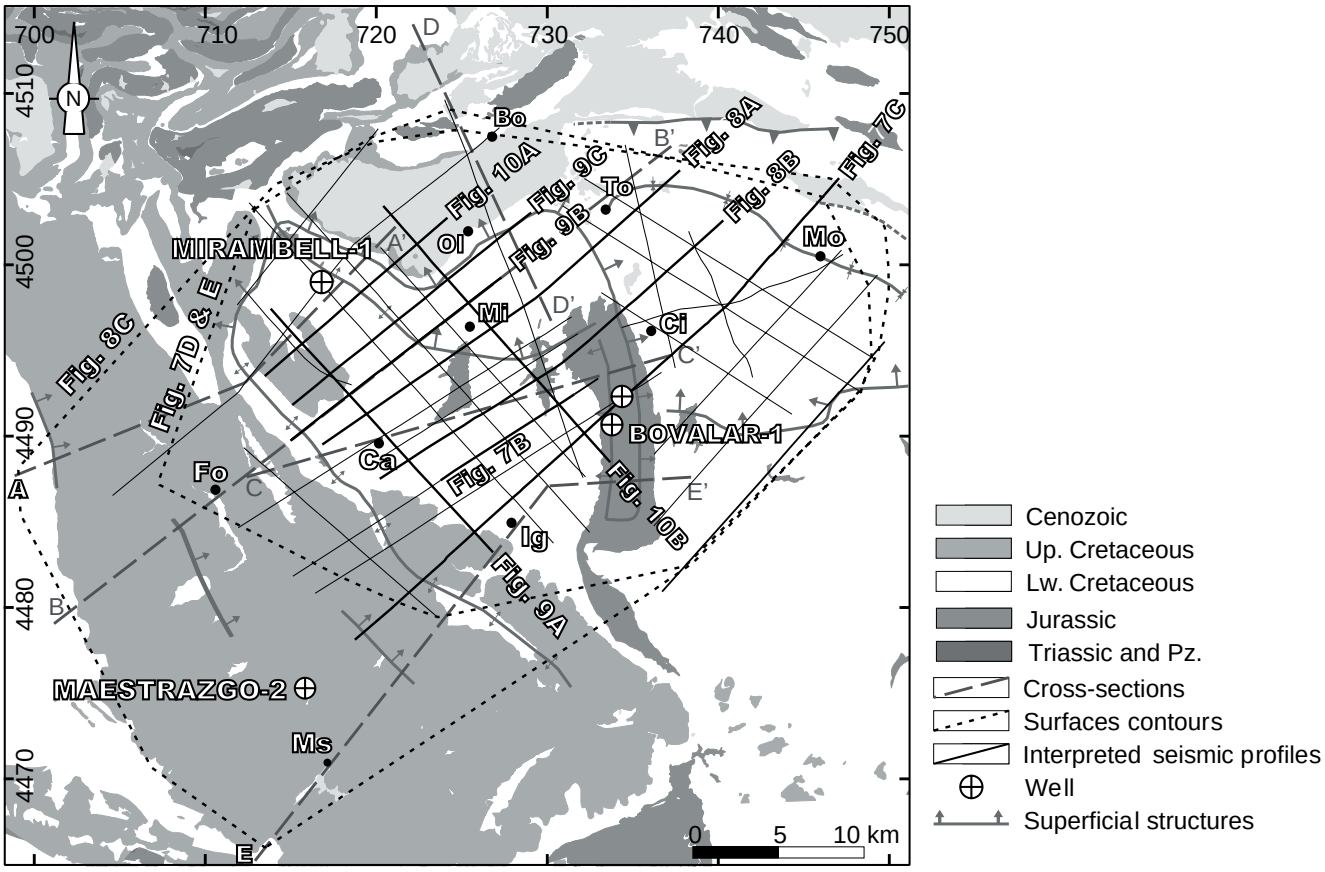

FIGURE 5. Location of the seismic profiles and exploration-wells used for the construction of cross-sections and geological surfaces, whose location is also shown. A simplified geological map and some main structures are shown for reference. UTM projection (zone 30, coordinates in km), ED50 datum.

Five cross-sections were constructed, normal to the different orientations of faults and axial fold planes observed in the study area (Fig. 4), in order to better characterize the geometry of the differently oriented structures.

Although the sections do not contain the roughly N-directed deduced displacement of the linking zone (Guimerà and Álvaro, 1990), and so are not restorable, they were unfolded using the flexural slip unfolding algorithm and the Upper Cretaceous base as a datum, in order to display the geometry of the syn-rift units. Cross-sections are based on field data, wells, and seismic interpretation converted to depth. Cross-section construction–using the Kink method–as well as unfolding were done both with Move and manually with Microstation software. Area conservation was assumed for the evaporitic units.

Two geological surfaces, the depth to the base of the Jurassic and the depth to the top of the acoustic basement, and the vertical thickness of the Middle Muschelkalk evaporitic unit were constructed with Gocad, based on seismic interpretation converted to depth, cross-sections and wells. The contours were later manually modified to better fit the structural trends and geometries.

INTERPRETATION OF THE SEISMIC PROFILES

Six stratigraphic units were differentiated in the seismic profiles (Fig. 6), attributed to the Cretaceous (K), Jurassic (J), Keuper (TrK), Upper Muschelkalk (TrM3), Middle Muschelkalk (TrM2), and the acoustic basement (Bs) (which includes the Lower Muschelkalk, Buntsandstein and the Variscan basement). Their correspondence with the seismic facies was established from the Mirambell-1 well tops in TWT (s).

The top of the acoustic basement–top of the Lower Muschelkalk carbonate unit and base of the Middle Muschelkalk salt unit–is characterized by a couple of seismic reflectors of near-constant thickness (Fig. 6). The Upper Muschelkalk is characterized by three parallel seismic reflectors that have an almost constant thickness throughout the seismic profiles. This unit is located between two transparent seismic facies that correspond to the Triassic evaporitic units: the Middle Muschelkalk unit below and the Keuper unit above. The latter unit has a variable seismic facies, showing parallel reflectors in some places. A couple of seismic reflectors of constant thickness are also

present at the base of the Jurassic unit, which are mainly parallel to the Upper Triassic Keuper reflectors, although, as previously explained, an angular unconformity has been recognized at the base of the Jurassic in other marginal places of the basin. The Imón Fm. (Fig. 3) is located below the Jurassic but it is too thin (about 30m) to be recognized in the seismic profiles. Above this couple of seismic reflectors, the Lower Jurassic is characterized by transparent seismic facies, with some discontinuous parallel seismic reflectors. That corresponds to the dolomitic breccias of the Cortes de Tajuña Fm. (Hettangian) (Fig. 3). In the Mirambell-1 well, about 100m of anhydrite intercalations were identified at the base of the Jurassic. That may be related to the "Anhydrite zone" or Lécera Fm. (Rhaetian-Hettangian age; Castillo Herrador, 1974; Gómez and Goy, 1998) equivalent in age to breccias of the Cortes de Tajuña Fm. (Fig. 3). This "Anhydrite zone" does not crop out in the study area. At the surface, the Cortes de Tajuña breccias overlie the Imón Fm., without the presence of evaporites. The Upper Lias and Dogger units have almost transparent facies with some quite continuous reflectors, and the Malm unit is characterized by continuous parallel seismic reflectors. The Cretaceous is characterized by continuous parallel seismic reflectors, but more separated than those of the Malm, indicating higher wavelength.

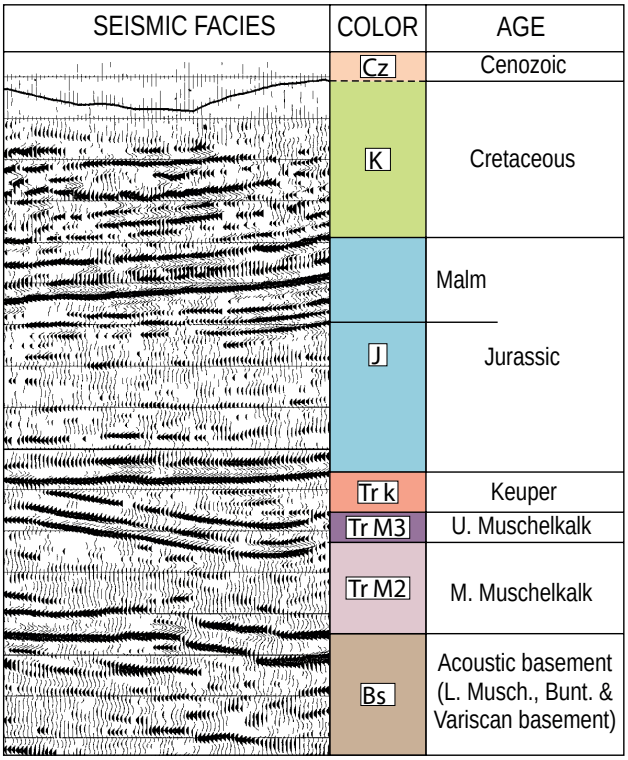

FIGURE 6. Seismic facies and horizons interpreted in the seismic profiles, and their correlation to the stratigraphy of the studied area. The Imón Fm. (Upper Triassic) is included in the impedance contrast at the base of the Jurassic, and is too thin (~30m) to be differentiated. The seismic-line shown is a segment of the northern part of the seismic profile CT88-15 (Fig. 8A).

MESOZOIC EXTENSIONAL STRUCTURE OF THE ACOUSTIC BASEMENT AND RELATIONSHIP WITH THE TRIASSIC DETACHMENT LEVEL

Different evaporitic units have been identified in the study area: the Middle Muschelkalk and Keuper units, and, locally, the Lower Jurassic Anhydrite zone or Lécera Fm. (Fig. 3).

The Middle Muschelkalk is composed of halite and anhydrite with lutite intercalations (Lanaja, 1987; Martínez-Abad, 1991). It constitutes the main detachment level, differentiating the structural deformation styles between the acoustic basement and the supra-salt Mesozoic cover. The interpretation of the seismic profiles allowed us to characterize the structural style of deformation in the basement, which is not always reflected in superficial structures, and also revealed some salt-related structures developed in the Middle Muschelkalk.

Structural style of the acoustic basement

Although the top of the acoustic basement–and base of the Middle Muschelkalk evaporitic unit–is not always easily recognized due to the quality of the seismic data, the network of seismic profiles allowed us to reconstruct this surface. We devised contour maps of the depth to the top of the acoustic basement (Fig. 7D) and of the present vertical thickness of the Middle Muschelkalk evaporitic unit (Fig. 7E). We took into account the fact that the surface representing the top of the acoustic basement was not restored to its Late Triassic stage. However, some non-inverted Triassic structures could be identified in the seismic profiles and permitted us to study the Triassic extensional event.

The acoustic basement is affected by a set of high-angle normal faults, developed during the Late Permian to Late Triassic rifting event, which are mainly oriented NW-SE to WNW-ESE, and some N-S (Fig. 7D, E). These faults have lengths between 2 and 7km, and dip-slips up to 500m, defining a system of horsts, grabens and half-grabens. Two NW-SE-trending basement highs were recognized. The western one (Monchén basement high, located under the Muela de Monchén) is a horst bounded by NW-SE normal faults (Fig. 7A, D). The eastern one (Iglesuela basement high, located North of Iglesuela del Cid village) is bounded to the S by a S-dipping normal fault; whereas on the northern side, the basement progressively deepens to the North and northeast (Fig. 7B, D). This could be a consequence of a SW-dipping

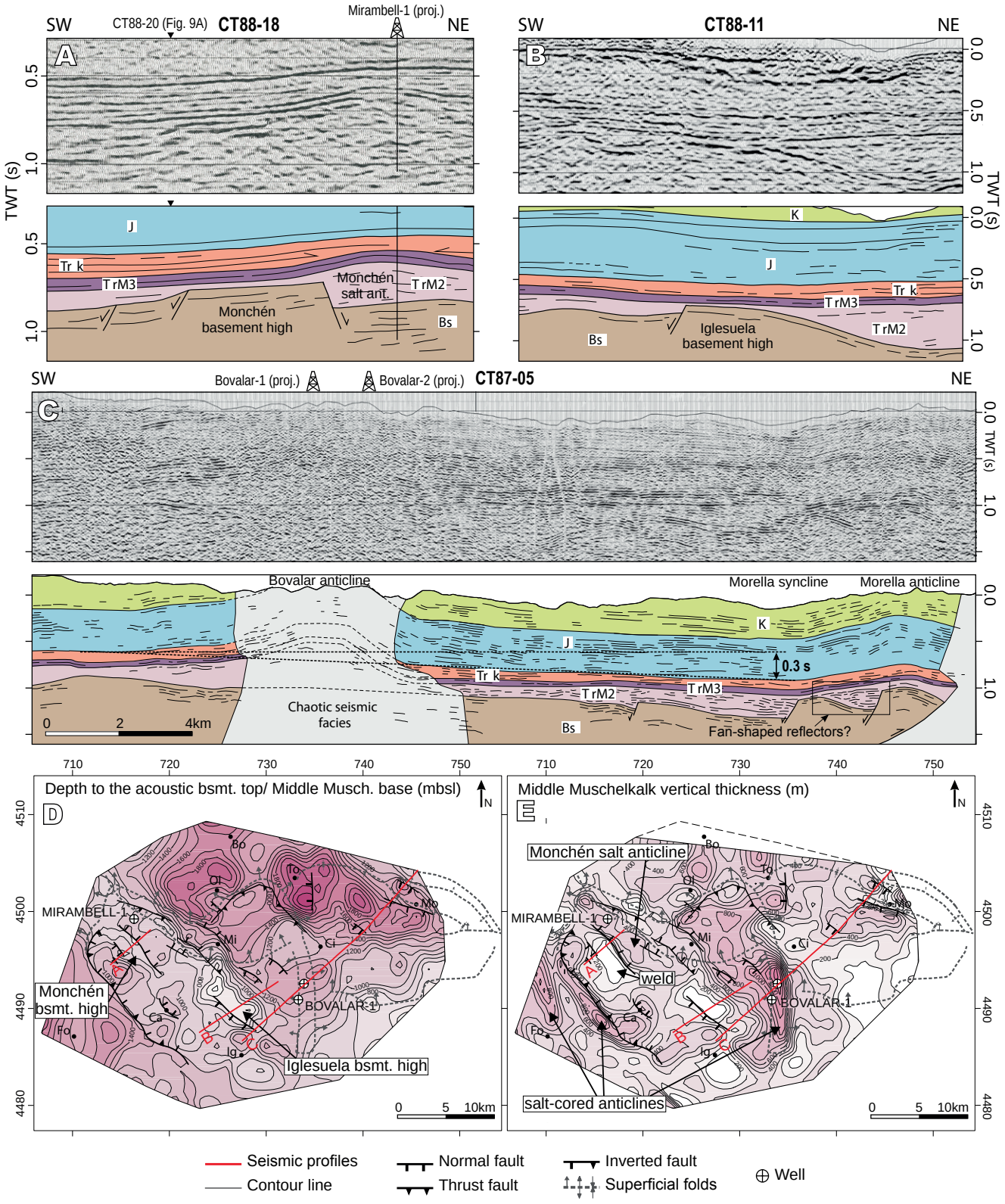

FIGURE 7. A, B) Details of seismic profiles CT88-18 (Fig. 10A) and CT88-11 and their interpretation, showing transversal sections of the Monchén and Iglesuela basement highs, respectively. C) Seismic profile CT87-05 and its interpretation. See Figure 6 for legend. D) Contour map of the depth to the top of the acoustic basement, *i.e.* base of the Middle Muschelkalk evaporitic unit (in m below the sea level). E) Contour map of the Middle Muschelkalk vertical thickness (in m). See Figure 5 for location. The location of A, B and C is shown in D and E. UTM projection (zone 30, coordinates in km), ED50 datum.

normal fault located N of the basement high, like those shown in Figure 8B.

Middle Muschelkalk thickness variations

North and east of the Iglesuela basement high, a NW-SE strip with a thick Middle Muschelkalk salt unit is identified, coinciding with the deeper basement. In the eastern part of this strip, the N-S-trending Bovalar detachment anticline developed, accumulating in its core more than 1200m of Middle Muschelkalk salt, as found in the Bovalar-2 well (Lanaja, 1987), located near the anticline hinge (Fig. 7D, E).

North of the Monchén basement high, another NW-SE strip of thickened Middle Muschelkalk evaporites is present: the Monchén salt anticline. It developed in the footwall of the normal fault that bounds the Monchén basement high to the N (Figs. 7; 9). This salt accumulation was pierced by the Mirambell-1 well, cutting through more than 625m of Middle Muschelkalk salt. 2km south of it, over the Monchén basement high, less than 100m of Middle Muschelkalk were identified in the seismic lines (Fig. 7A). It even disappears locally, as a salt weld is also observed above this basement high (Figs. 7E; 9A).

In the NE of the area studied, beneath the Morella syncline and anticline, some half-grabens can be observed (Fig. 7C), generated by S-dipping and probably WNW-ESE trending high-angle normal faults that displace the acoustic basement (Fig. 7D, E). The Middle Muschelkalk unit displays salt wedges thickening towards these faults and some fan-shaped reflectors can be identified against one of these faults (Fig. 7C highlighted in a box).

East of the area studied, near the Mediterranean coast, the exploration wells (Fig. 2) reveal that no Muschelkalk sediments are present. In the Salzadella-1 well, the Buntsandstein facies (70-150m) are overlaid by only 30m of Keuper clay and sandstone and in the Maestrazgo-1 well by about 250m of Keuper, composed mostly of halite and clay (Martínez-Abad, 1991). Southwards, in the Desert de les Palmes area, N of Castelló (Fig. 1), the Upper Muschelkalk overlies the Buntsandstein (Escudero-Mozo *et al*., 2015), and consists of about 100m of carbonate rocks, with no evaporites (López-Gómez *et al*., 2005).

Interpretation of the basin evolution during the Late Permian-Triassic rifting event

Timing of the Triassic extensional faults

Although the different units that form the acoustic basement cannot be distinguished in the seismic profiles, in accordance with Álvaro *et al*. (1979) and Salas *et al*. (1997) the Triassic extensional faults involve the Late Permian to Middle Muschelkalk evaporitic unit, at least its lower part (Bartrina and Hernández, 1990), which fills the relief generated by the system of horsts, grabens and half-grabens, while its upper part overlies all these structures.

Considering the flow capacity of the Middle Muschelkalk evaporitic unit, it cannot be completely ascertained whether normal faults were active or not during its deposition. However, in view of the salt distribution, at least the lower part of the Middle Muschelkalk was deposited during extension, because the maximum thicknesses of this unit coincide with the depressed blocks of the acoustic basement, and the minimum thicknesses with the acoustic basement highs. This structure is overlain by the subhoritzontal supra-salt cover, indicating that no changes occurred in the salt thickness after deposition (Fig. 7B). The fan-shaped reflectors towards one of the acoustic basement faults previously reported (Fig. 7C highlighted in a box) should also be taken into account; they indicate that no salt motion occurred there, with the original salt thickness being preserved. What seems clear is that the Upper Muschelkalk carbonate platform was deposited in a period of little extensional activity, as an almost constant thickness of this unit is observed in the seismic profiles. It is only affected by some faults that are not associated with thickness variations in this unit (Fig. 9A, C).

The extensional activity of some normal faults resumed during the Keuper deposition, as can be deduced from the extensional drape fold that affects the Upper Muschelkalk carbonate platform above the basement faults (Fig. 9C), which does not involve the younger Mesozoic cover. The Keuper seismic reflectors onlap these Upper Muschelkalk folds (Fig. 9B, C). In profile CT88-17 (Fig. 9C), some growth strata can be identified in the Keuper, over the downthrown block of the basement fault, indicating extensional activity of the basement faults while the Keuper facies was being deposited.

Salt-related structures that developed during Triassic extension

As mentioned above, Middle Muschelkalk thickness variations are mainly syn-depositional; although, we cannot definitively ascertain whether the entire evaporitic unit was deposited during extension. However, there is also evidence of salt flow that would have enhanced these thickness variations in some areas, as some salt-related structures can be observed in the seismic profiles.

As opposed to what happens in other Iberian locations, where salt tectonics is related to the Keuper

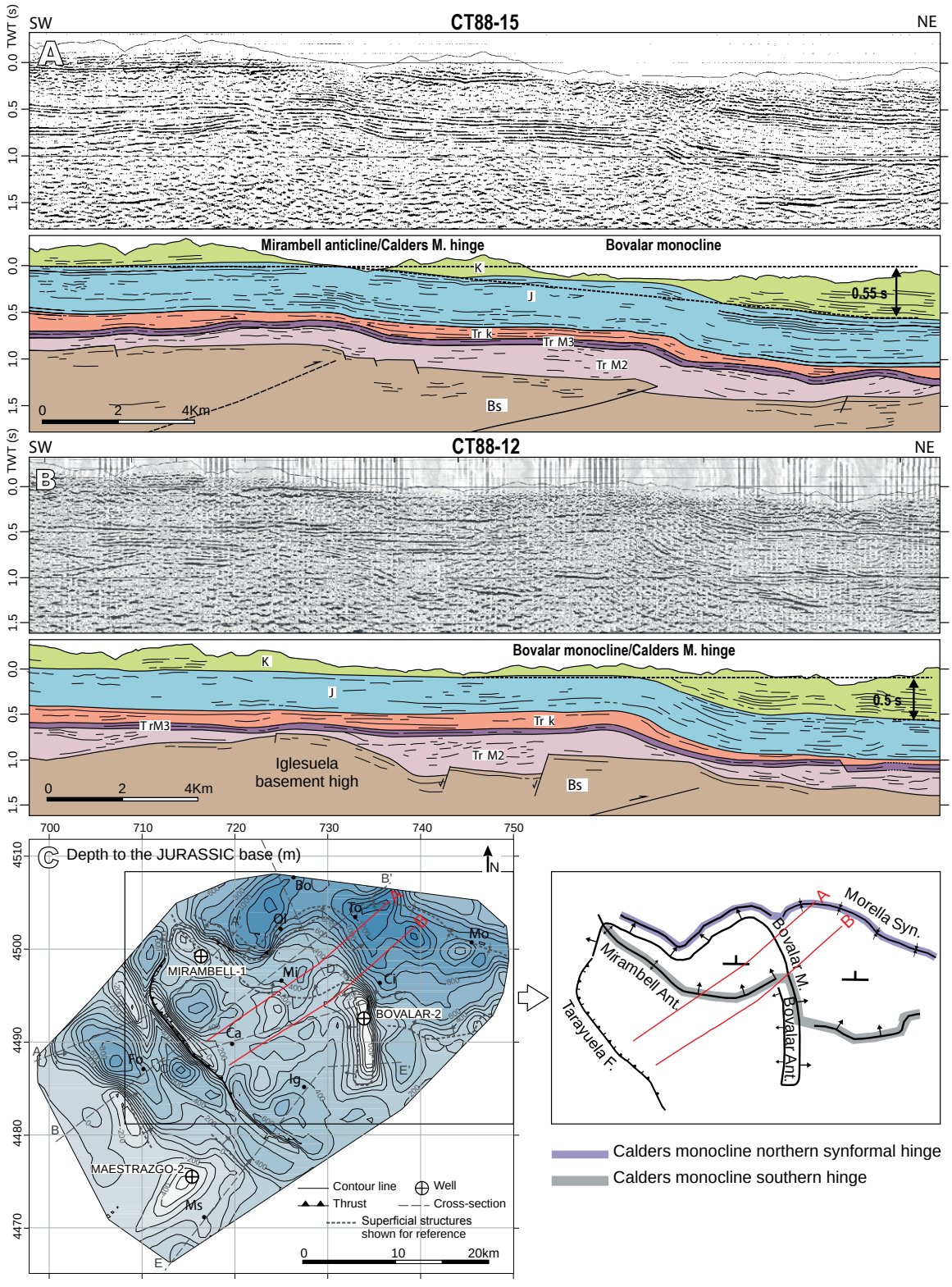

FIGURE 8. A) Seismic profile CT88-15 and its interpretation. The tilted limb of the Calders monocline and its southern hinge –which is the transition from the tilted limb to the flat uplifted area south of it– are displayed. Within the Calders monocline limb, the Bovalar monocline is superimposed. B) Seismic profile CT88-12 and its interpretation. The southern hinge of the Calders monocline is also observed, coinciding with the Bovalar monocline. A vertical tectonic step of at least 0.5s (about 1200m) can be measured between the flat uplifted area and the deepest parts of the tilted limb. C) Contour map of the depth to the base of the Jurassic (in m below the sea level). Some superficial folds are shown for reference, and the trend of the Calders monocline hinges has been traced in a sketch. See Figure 6 for legend and Figure 5 for location. UTM projection (zone 30, coordinates in km), ED50 datum.

evaporites –Prebetics (Ortí, 1973), Basque-Cantabrian Basin (Serrano and Martínez del Olmo, 2004), Parentis Basin (Ferrer *et al.*, 2012), Cotiella Basin-Pyrenees (López-Mir, 2015), etc.–in the current study area and in the southern Ebro Basin (Butillé *et al.*, 2012), the Middle Muschelkalk evaporitic unit is the only salt unit that experienced some salt flow, as previously indicated by Bartrina and Hernández (1990).

Keuper seismic reflectors onlapping the folded Upper Muschelkalk were identified in the two limbs of the Monchén salt anticline, located North of the Monchén basement high (Figs. 9B, C; 10A). This fold coincides with and is included in the Mirambell anticline core, and affects the whole Mesozoic cover and the basement. However, in the seismic profile CT88-16 (Fig. 9B), the anticline folding the supra-salt cover is tighter in the Upper Muschelkalk than in the Jurassic, so that by flattening the base of the Jurassic, the Keuper reflectors become subhorizontal, onlapping the Upper Muschelkalk that remains folded. Therefore, two folding phases occurred: the first during the sedimentation of the Keuper and the second during the Cenozoic contraction.

The interpreted Keuper growth strata over the Upper Muschelkalk drape fold in the seismic profile CT88-17 (Fig. 9C) and the parallel Keuper reflectors onlapping the salt-cored anticline (Monchén salt anticline) indicate that the Upper Muschelkalk anticline developed by migration of the Middle Muschelkalk salt towards its core. This took place before and during deposition of the Keuper, beneath an overburden of 130-160m of Upper Muschelkalk carbonate rocks. The salt weld over the Monchén basement high can be interpreted as the result of sideways salt migration from above the basement high, accumulating and generating the Monchén salt anticline (Fig. 9).

The salt flow could have been triggered by the resumed activity of the high-angle normal faults during the Late Triassic, while the Keuper facies was being deposited. This activity forced the development of drape folds in the Upper Muschelkalk, observed in CT88-15 and CT88-17 seismic profiles (Figs. 8A, 9C). The Keuper sediments were deposited filling the relief that was being generated by the folding of the Upper Muschelkalk. The differential load exerted by the Keuper sediments could also have enhanced the Middle Muschelkalk salt flow.

Conversely, in the southern Ebro Basin, while salt structures also mainly consist of the Middle Muschelkalk salt unit, they developed during the Early Cretaceous rifting event (Butillé *et al.*, 2012).

MESOZOIC EXTENSIONAL STRUCTURE DEVELOPED DURING THE JURASSIC TO EARLY CRETACEOUS RIFTING EVENT

The Maestrat Basin experienced a second rifting event during the Late Jurassic and Early Cretaceous. We analyzed this event to determine the configuration of the basin and the extensional structures bounding it.

Jurassic

Jurassic thickness variations

Jurassic thickness variations are difficult to establish in the seismic profiles, as the base of the syn-rift Malm unit cannot be clearly identified. Field measurements of the syn-rift Jurassic thicknesses are also scarce because its base hardly crops out in the area studied. The interpretation of the wells (located in Fig. 2) by Martínez-Abad (1991) shows that the greatest thickness variations within the Jurassic units are located in the Lower Lias units (Cortes de Tajuña and Cuevas Labradas Fms.). Although these units are commonly interpreted as the post-rift of the Triassic rifting, in the study area they vary from about 135m in the Bovalar-1 and Bovalar-2 wells, to 300m in the Maestrazgo-2 well (towards the SW) and 585m in the Mirambell-1 well (towards the NW, with the Anhydrite zone at its base). The Ablanquejo Group (Upper Lias) and the Chelva Fm. (Dogger) have gentle thickness variations. The first thickens towards ENE, from 54m in the Maestrazgo-2 well and 67m in the Mirambell-1 well, to 105m in the Bovalar-1 well. Conversely, the Chelva Fm. (Dogger) thickens gently towards SSE, from 63m in the Mirambell-1 well to 93m in the Bovalar-1 well and 116m in the Maestrazgo-2 well. The Iàtova Fm. (Lower Malm) presents a nearly constant thickness (about 25m), while the other Malm units (Polpís-Ascla and Bovalar-Pleta fms.) gently thicken towards ESE, from 407m (Mirambell-1) to 490m (Maestrazgo-2) and to more than 650m in the Bovalar anticline, (deduced from combining the wells (Bovalar-1 and 2) and field data).

Interpretation of the basin evolution during the Jurassic

In view of the thickness variations, some extension is needed during the Lias, which would be a consequence of the Hettangian-Lower Pliensbachian rifting event controlled by listric normal faults (Aurell *et al.*, 1992; Roca and Guimerà, 1992; San Roman and Aurell, 1992; Roca *et al.*, 1994); although in other parts of the Iberian rift system the Cortes de Tajuña Fm. has also been related to evaporite solution, collapse and breccia formation (Yébenes, 1973; Giner, 1980).

The Iàtova Fm. (Lower Malm) is considered the last pre-rift Malm (Salas *et al.*, 2001). Regarding the other Malm units, the major thickness variations are found when comparing the

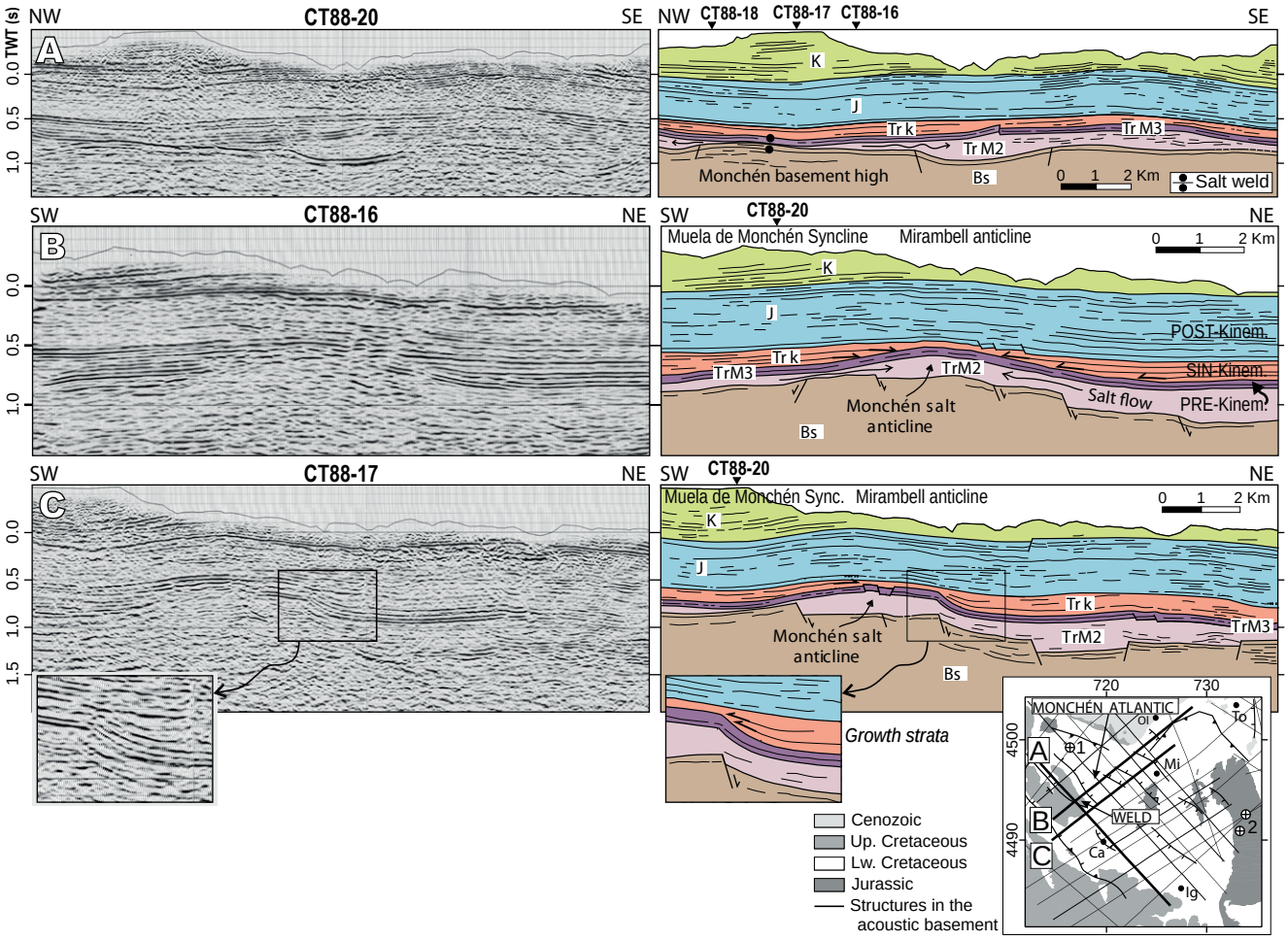

FIGURE 9. Seismic profiles A) CT88-20, B) CT88-16 and C) CT88-17 and their interpretation. A) A salt weld is observed over the Monchén basement high. The Middle Muschelkalk thickness variations are thus displayed. B) The Monchén salt anticline developed N of the Monchén basement high is shown, being the Keuper reflectors onlapping the folded Upper Muschelkalk. C) A drape fold of the Upper Muschelkalk forced by the resumed extensional activity of high-angle normal faults in the acoustic basement during the Late Triassic is shown. Some growth-strata in the Keuper reflectors are deduced, indicating that it was deposited during the extension. See location in Figure 5, and Figure 6 for legend.

thicknesses in the study area from 407m to more than 650m, with those in the adjacent area of Albarracín, about 250-270m (Hernández, 1985). Therefore, a larger area has to be considered to characterize the major thickness variations for the Malm, suggesting that the Jurassic boundaries of the basin probably do not coincide with the Lower Cretaceous ones.

Lower Cretaceous

Lower Cretaceous thickness variations and extensional structure

Lower Cretaceous thicknesses were obtained from field data, cross-sections, wells, and from Salas (1987). As previously explained, the Valanginian to Hauterivian rocks are only present in the eastern part of the study area: E of the Bovalar anticline and S of the Turmell fault, and mostly S of the Xert fault. The Barremian and Aptian thickness distributions show the presence of different scale normal faults. The major ones are the Villarluengo fault, Bordón fault, Ortells fault and Xert fault (Figs. 2; 11D-D').

The western normal fault is the Villarluengo fault (Fig. 12): an E-W-trending, S-dipping non-inverted Mesozoic normal fault, which brings Lower Cretaceous rocks in its hanging wall into contact with Jurassic rocks in its footwall. The Escucha Fm. (of Albian age) overlies the fault, indicating that it was active before its sedimentation.

The Bordón fault (Fig. 11D-D'), a NE-SW-trending, SE-dipping normal fault, separates 1100m of Barremian and Aptian rocks in its hanging wall (S) from about 365m in its footwall (N), in the surroundings of Ladruñán village (Canérot, 1974), about 6km to the North. Just North of the Bordón fault, about 150-200m of Barremian

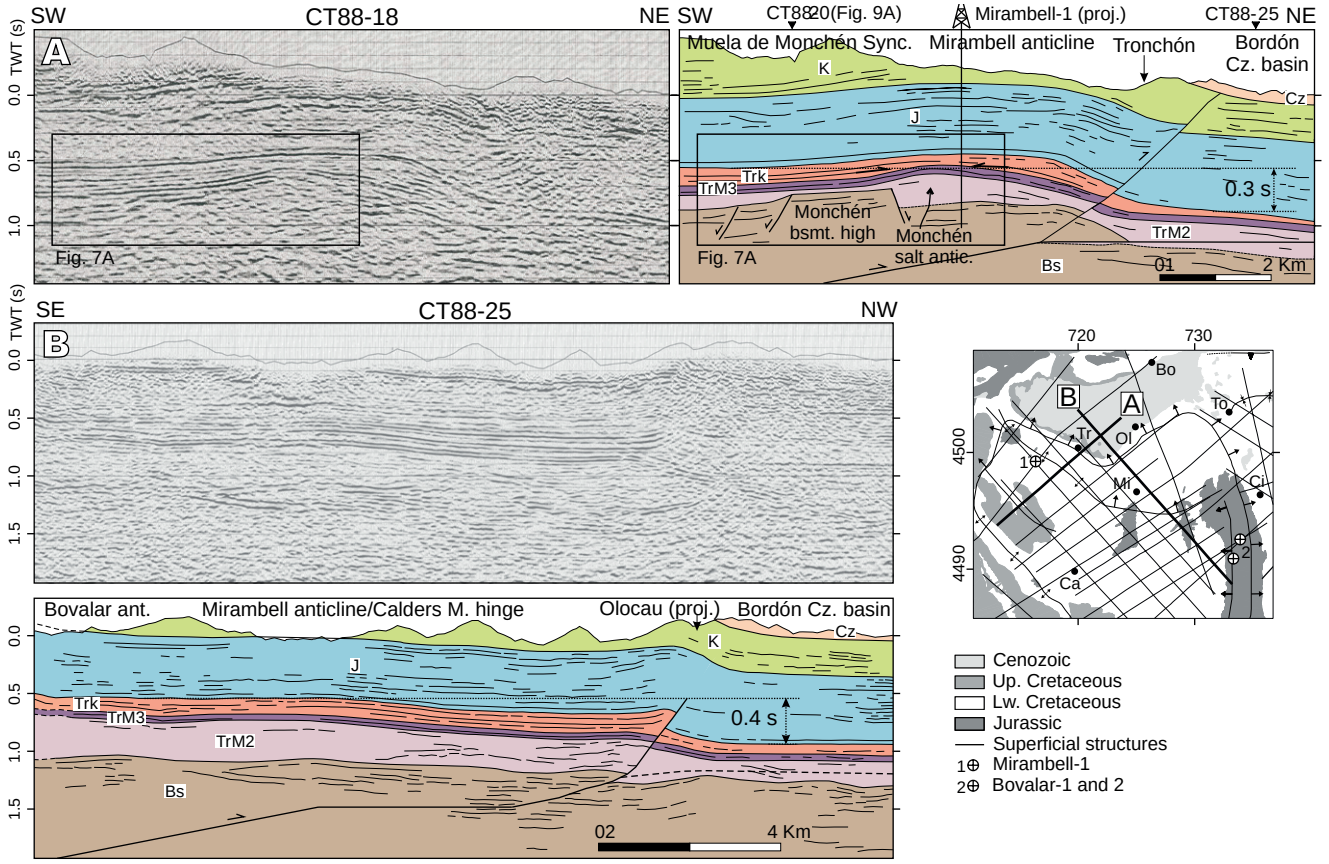

FIGURE 10. A) Seismic profile CT88-18 and its interpretation. A vertical tectonic step of 0.3s (about 800m) is deduced between the base of the Jurassic in the Muela Monchén syncline and below the Cenozoic Bordón Basin. See Figure 7A for a detail of the Keuper reflectors onlapping the folded Upper Muschelkalk. B) Seismic profile CT88-25 and its interpretation. The Calders monocline limb and its southern hinge are observed. A vertical tectonic step of 0.4s (about 1000m) is measured comparing the base of the Jurassic. See Figure 6 for legend.

rocks can be measured in a Cenozoic-cored syncline located in the footwall of the fault and attached to it. This Barremian thickness is similar to that measured in the Ladruñán sequence (about 190m of Barremian rocks), where the entire Aptian-Barremian succession is preserved. Comparing these Barremian thicknesses (150-200m) in the footwall of the fault with those measured in the Bordón anticline (more than 600m), located in the hanging wall of the fault, it can be ascertained that these thickness variations are related to the Bordón fault. Eastwards, the Paleogene alluvial rocks overlie the Bordón fault (Fig. 4). The lowest Cenozoic units are folded but not faulted. These folds are interpreted as being produced by the eastern continuation of the Bordón fault as a blind fault for about 7km. As no significant differences in the Barremian and Aptian sequences can be observed N and S of this blind fault segment, this is interpreted to be a newly formed thrust in this area, which grew during the Cenozoic contraction as a lateral continuation of the inverted normal fault. The Upper Cenozoic units unconformably overlie the folded Lower Cenozoic units (Fig. 4).

Towards the E, and located in a more internal position, the E-W-trending, S-dipping Ortells fault separates Barremian sequences of about 750m, in its hanging wall, from sequences of 570m in its footwall.

East of the area studied, more than 2.5km of Lower Cretaceous rocks are found in the downthrown hanging wall of the Xert fault, which is the depocenter of the Salzedella sub-basin, while in its footwall only about 1000m of Lower Cretaceous can be measured (Salas, 1987). The Xert fault (Fig. 4) is an E-W-trending, S-dipping normal fault of listric geometry, as deduced from the rollover geometry preserved in the Lower Aptian units in its hanging wall (Salas *et al.*, 1995). A listric normal fault has also been interpreted from seismic profiles (Antolín-Tomás *et al.*, 2007), which is probably the eastern continuation of the Xert fault.

In the southern limb of the Tarayuela anticline, a normal fault is deduced, the Tarayuela fault (Fig. 11), parallel to the fold trend (Fig. 4). It separates sequences of 380 and 350m of Barremian and Aptian rocks in its hanging wall (Tarayuela anticline–southwest of Cantavieja–and the

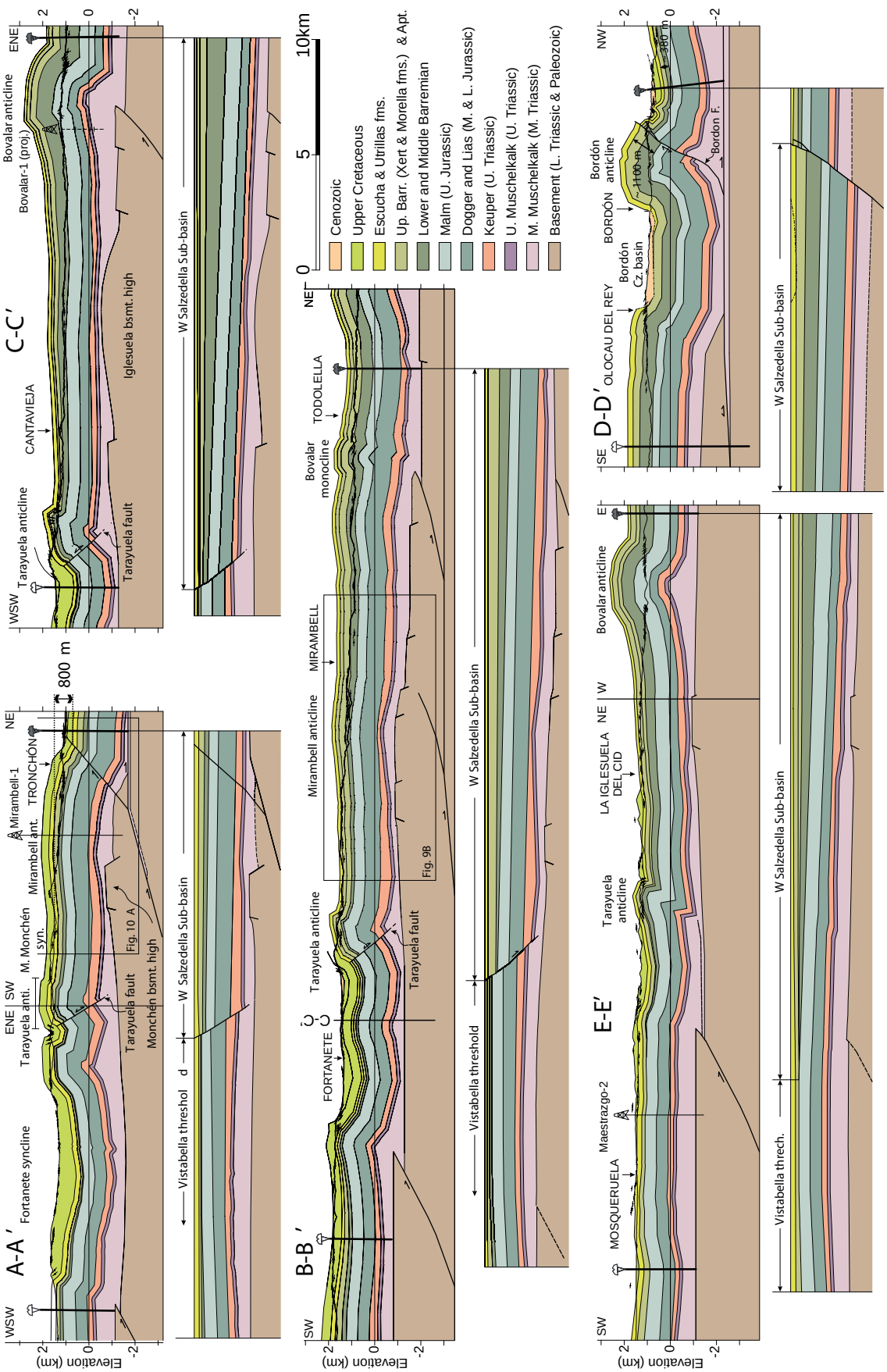

FIGURE 11. Balanced cross-sections of the studied area. The deformed and the unfolded sections at the end of the Late Jurassic-Early Cretaceous rifting are shown. Unfolded cross-sections are only drawn between the pin and the loose lines. See Figures 4 and 5 for location. A-A: a tectonic vertical step of 800m is measured comparing the elevation of the base of the Upper Cretaceous in the Muela de Monchén syncline (1500m a.s.l.) and the same level under the Cenozoic Bordón Basin (700m a.s.l.), the same vertical step that González ***et al.*** (1998) described comparing the base of the Utrillas Fm.

western part of the Mirambell anticline), from 150 and 180m in its footwall (Maestrazgo-2 well and eastern limb of the Cañada de Benatanduz anticline) (Fig. 4).

The Lower Cretaceous sequence in the Maestrazgo-2 well is 350m thick, including 200m of the Escucha and Utrillas fms. and 150m of the Upper Aptian formations (Villarroya de los Pinares and Benassal) which directly overlie the Bovalar Fm. (Malm) (Martínez-Abad, 1991). These Lower Cretaceous sequences decrease towards the SE and in the surroundings of Vistabella only 100m of Aptian rocks and a few meters of Escucha and Utrillas Fms. overlie the Polpís Fm. (Lower Kimmeridgian). In turn, the Polpís Fm. directly overlies the Triassic rocks (Canérot, 1974).

NW-SE-trending and mostly SW-dipping normal faults of metric slips are observed in the Mirambell and Tarayuela anticlines, affecting the Lower Cretaceous units. In the hanging wall of the Villarluengo normal fault, E-W-trending, S-dipping normal faults with metric slips are also observed (Fig. 12). These minor faults were also observed in other areas of the Maestrat Basin (in the Galve sub-basin; Liesa *et al.*, 2006) leading to the changes in thickness in the Lower Cretaceous units.

Main tectonostratigraphic domains and interpretation of basin evolution during the Lower Cretaceous rifting

Considering the thickness distribution of the Barremian and Aptian rocks, the study area partially comprises two of the principal paleogeographic units of the Maestrat Basin: the western part of the Salzedella sub-basin and the Vistabella threshold (Fig. 2).

i) Western Salzedella sub-basin. The Barremian and Aptian units progressively thicken towards the N, from the Tarayuela anticline (400m) to the Bordón anticline (about 1100m) (Fig. 11). The normal faults with metric slips probably lead to the northward thickening of the Lower Cretaceous units in the western Salzedella sub-basin. However, these faults were not considered during construction of the cross-sections, as they cannot be represented at that scale. Therefore, the Barremian and Aptian units display a major scale wedge geometry when the cross-sections are unfolded (Fig. 11). Sediments of Valanginian to Hauterivian age could have been eroded or never deposited W of the Bovalar anticline. The northern boundary of the Salzedella sub-basin is composed of different normal fault segments: the Villarluengo fault, Bordón fault, Ortells fault and, located in a more internal position, the Xert fault. In the southern margin of the Salzedella sub-basin the Vistabella threshold is found; which has been interpreted as the high block developed by the rollover folding in the hanging wall of the Mesozoic extensional fault system that formed the Salzedella sub-basin (Fig. 2) (Salas and Guimerà, 1996; Salas *et al.*, 2005). A NW-SE-trending, NE-dipping normal fault was deduced at this southern boundary (the Tarayuela fault), slightly modifying the geometry of the rollover. To the E, the Tarayuela fault ends and the geometry of the southern margin of the basin is only determined by the rollover geometry (Fig. 11E-E').

ii) Vistabella threshold. It is located S and W of the Salzedella sub-basin separating it from the Penyagolosa and the Galve sub-basins (Fig. 2). It was an elevated area containing only local remains of Lias and Dogger rocks, incomplete Upper Jurassic –overlying the Triassic rocks– and reduced Lower Cretaceous sequences. Therefore, deposition was poor at the Vistabella threshold, while some units were partially or totally eroded.

CENOZOIC CONTRACTIONAL STRUCTURE

As explained above, the inversion of the Maestrat Basin generated a wide uplifted area as a result of the uplifting of the hanging wall of the Maestrat basement thrust. In the area studied, this uplifted area includes the Calders monocline on its northern margin, which narrows laterally and is modified in its central part by the N-S-trending Bovalar anticline (Fig. 13).

Structure of the uplifted area south of the Calders monocline hinge

In its eastern part, the uplifted area (Fig. 13) includes a flat-lying region; while the western part is characterized by a system of large folds that involve the supra-salt cover–although some are rooted in the basement (Mirambell anticline). They are more than 10km long and have wavelengths of about 5km (Fig. 11). Their main orientation is NW-SE (Fig. 4) and to the North some folds progressively adopt a NNE-SSW trend (the Cuarto Pelado syncline and Tarayuela anticline). The Tarayuela anticline becomes a W-verging monocline in its NNE-SSW-trending segment, which generates a vertical tectonic step of 450m within the uplifted area, related to the inversion of the Tarayuela basement fault (Figs. 8C; 13). The formation of the S-verging Tarayuela anticline during the Cenozoic contraction could also have been triggered by the inversion of this normal fault, folding the Mesozoic cover without cutting the Upper Cretaceous rocks (Fig. 11A-A', B-B', C-C').

The Calders monocline

The Calders monocline hinge is located North of the Muixacre Mountain in the area E of the Bovalar anticline,

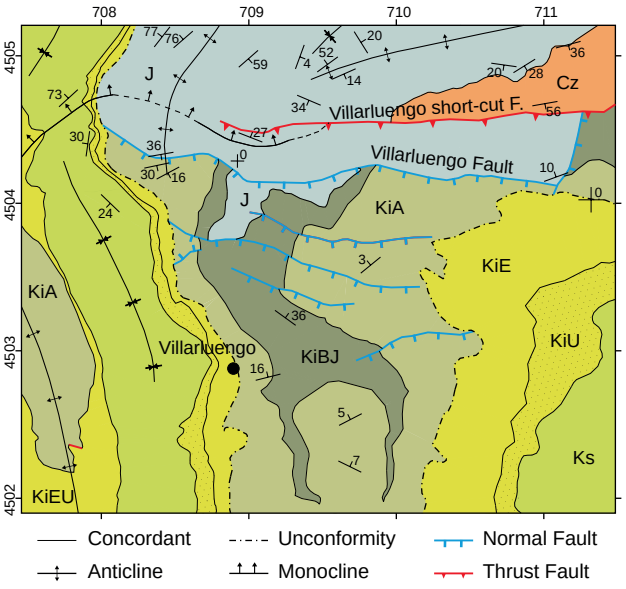

FIGURE 12. Detailed geological map of the Villarluengo normal fault and its short-cut thrust, located to the N. See location in Figure 4. Abreviations: Cz= Cenozoic, Ks= Upper Cretaceous, KiU= Utrillas Fm. (Late Albian), KiE= Escucha Fm. (Early and Middle Albian), KiA= Aptian, KiBJ= Barremian and Jurassic in Purbeck facies, J= Jurassic. The Villarluengo normal fault puts in contact the Lower Cretaceous units in the hanging wall with the Malm in the footwall, indicating that it was active during the Late Jurassic-Early Cretaceous rifting event. The Escucha Fm. covers the fault. Zone 30 UTM coordinates (km), datum ED50.

and south of Mirambell in the area W of the Bovalar anticline (Fig. 13).

W of the Bovalar anticline, the asymmetric NW-SE-trending Mirambell anticline is the continuation of the Calders Monocline (Fig. 4), which is above a vertical tectonic step of 800m – 0.3s (Figs. 10A; 11A-A'). Its northward tilted limb is divided into two dip domains: the southern, wider one (3-15N) and the steeply dipping northern one (25-70N) (Figs. 4; 11A-A'; 13). The Mirambell anticline frontal limb widens towards the E, and changes its trend to NE-SW (Fig. 13) SW of Olocau, where it is also divided into two dip domains. A vertical tectonic step of 0.4s (about 1000m) is measured in its limb (Fig. 10B).

Parallel to this frontal limb, there is the synformal flexion that constitutes the southern boundary of the Cenozoic Bordón Basin, trending NW-SE to NE-SW. This synformal flexion is the eastern continuation of the Morella syncline, mostly oriented WNW-ESE (Figs. 7; 8; 13). These synformal structures are the northern synformal hinge of the Calders monocline (Fig. 13), and also constitute the northern limit of the uplifted area.

N of the Calders monocline a synformal area appears (dashed synformal structures in Fig. 13), giving rise to the Cenozoic Bordón Basin. This is filled with flat-lying terrigenous sediments (González, 1989), which onlap the Upper Cretaceous rocks of its steeply dipping southern boundary and are accordingly gently deformed with it. This Cenozoic basin disappears towards the E, being thrust by the Ortells fault, which is the southern boundary of the Cenozoic basin in this eastern part. North of the Morella anticline, this synformal area reappears –partially filled with Cenozoic rocks– and continues towards the E in the footwall of the Turmell fault.

In the eastern part of the Calders monocline, the Ortells and Morella anticlines appear between the northern synformal hinge of the monocline, and the synformal area found N of it (dashed synformal structures in Fig. 13). The NW-SE-trending Morella anticline and E-W-trending Ortells anticline are located in the hanging wall of S-dipping thrusts, with the fault associated with the Ortells anticline cropping out in the inverted Ortells fault (Figs. 4; 7C; 13). These structures relay laterally, as they have in common the NE limb of the Morella syncline (Figs. 4; 13).

Structures within the Calders monocline frontal limb

The Calders monocline frontal limb is modified in its central part by the N-S-trending Bovalar anticline (Figs. 4; 8). Two segments can be differentiated: a northern NNW-SSE-trending, ENE-verging monoclinal segment –between La Todolella and Cinctorres– and a southern NNW-SSE to N-S-trending box-fold anticline (Figs. 4; 13).

Seismic profile CT88-15 (Fig. 8A) shows the Calders monocline hinge at the eastern continuation of the Mirambell anticline, with the Bovalar monocline located within the tilted limb of the Calders monocline. Conversely, in seismic profile CT88-12 (Fig. 8B) the Calders monocline hinge coincides with the Bovalar monocline. Towards the S, the Bovalar monocline evolves into a box-fold anticline, near Cinctorres, which also has its western limb more elevated than the eastern one (Figs. 7C; 11C-C'). South of the Bovalar-2 well, this vertical tectonic step disappears and both limbs of the anticline are at the same elevation (Fig. 11E-E'), located within the flat uplifted limb of the Calders monocline (Fig. 13).

The widest part of the Calders monocline limb is located in its central part, where a vertical tectonic step of 0.5s (about 1200m) was measured (Fig. 8). Towards the E, this tilted limb becomes narrower, as the Morella syncline and the monocline southern hinge converge; and the E-W-trending, N-verging Turmell fault (the direct outcrop of the Maestrat basement thrust) is found

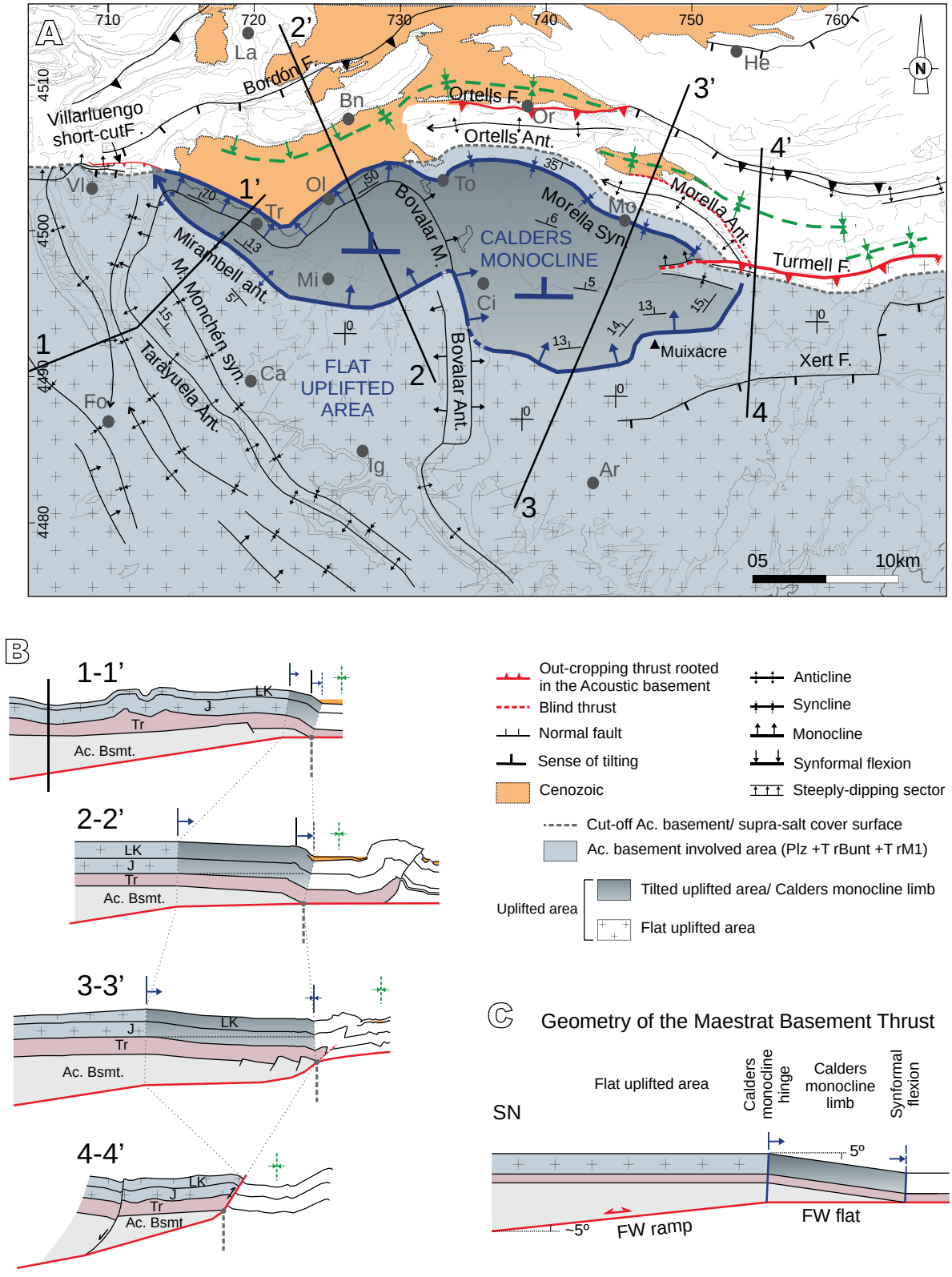

FIGURE 13. A) Structural map showing the major structures of the area studied and the location of schematic cross-sections (UTM projection (zone 30, coordinates in km), ED50 datum). B) Schematic cross-sections showing the lateral evolution of the Calders monocline. 1-1': based on cross-section A-A' (Fig. 11). 2-2': based on cross-section D-D' (Fig. 11) and seismic profile CT88-25 (Fig. 10B). 3-3': modified after an unpublished cross-section from Guimerà. 4-4': modified after cross-section XV in Guimerà (1988). C) Idealized cross-section showing the geometry of the Maestrat basement thrust deduced from the fold-bend fold (Calders monocline) observed at the surface.

to the E (Fig. 13). Its hanging wall is uplifted, resulting in a fault throw of about 800m. The Turmell fault cuts across the Calders monocline limb, continuing as a blind thrust for about 4km more, and at surface is an E-W-trending, N-verging monocline.

Towards the W, the Calders monocline also narrows, disappearing in the hanging wall of the E-W-trending, S-dipping Villarluengo short-cut thrust (Figs. 12; 13). This short-cut thrust continues towards the W as a blind thrust, which is expressed at surface as an E-W-trending, N-verging monocline (Fig. 13) that continues up to the southern and western margins of the Aliaga Cenozoic Basin (González and Guimerà, 1993; Guimerà and Salas, 1996). Therefore, the Calders monocline becomes narrower laterally while the associated vertical tectonic step also decreases from 0.5s (about 1200m) measured in its widest central part, towards the E and W (0.3s: 800m).

DISCUSSION

Summing up, the inversion of the Salzedella sub-basin generated a wide uplifted area (more than 3600km^2), bounded to the North by a vertical tectonic step of 800 to 1200m. This uplifted area is interpreted as the result of the inversion of the lower segment (within the acoustic basement) of the Mesozoic extensional fault system that generated the Salzedella sub-basin. This inverted fault is the Maestrat basement thrust, which extends from the southern boundary of the Aliaga Cenozoic Basin to the eastern limit of the Turmell fault. The surface expression of the Maestrat basement thrust is the Calders monocline in its central part. Towards the E and W of the Calders monocline, the Turmell and Villarluengo short-cut thrusts developed.

No Mesozoic thickness variations can be identified between the hanging wall and footwall of the Turmell fault, which is interpreted as a short-cut of the E-W-trending, S-dipping Xert listric normal fault located south of it (Fig. 13). The Xert fault, which has a rollover geometry preserved in its hanging wall (Salas and Guimerà, 1996), was only inverted in its lower segment within the acoustic basement; while in the upper segment, the short-cut–Turmell fault–developed (Fig. 13B, 4-4'). On the western side of the Calders monocline, the Villarluengo short-cut thrust is the result of the inversion of the Mesozoic Villarluengo normal fault (Fig. 12) which, similarly to the Xert fault, was also inverted in its lower segment. A short-cut containing in its hanging wall the non-inverted segment of the normal fault developed within its footwall (Fig. 12).

Interpretation of the Calders monocline

The Calders monocline is interpreted as a fault-bend fold that developed as the rising hanging wall adapted to the flat-ramp-flat geometry deduced for the Maestrat basement thrust (Fig. 13C). The wide extension of the uplifted area, which is maintained elevated for about 40km towards the S, and the low-angle dip (~5º) of the Calders monocline limb imply that the Maestrat basement thrust ramp has a very low-angle dip, and is rooted in the upper crust. This interpretation is in holding with Seillé *et al*. (2015) who suggested, after the interpretation of wide-angle seismic, magnetotelluric (MT) and gravity data, that the Cenozoic thickening in the Iberian Chain is concentrated in the upper crust, thereby coinciding with Guimerà and Álvaro (1990).

Assuming this low-dip geometry for the Maestrat basement thrust (Fig. 13C), the flat uplifted area is located above the footwall ramp of the Maestrat basement thrust, while the transition from ramp to flat is reflected at surface by the southern hinge of the Calders monocline. The monocline limb is above the hanging wall ramp and the footwall flat, and its width depends on the amount of displacement above the footwall flat. Therefore, the different orientations of the southern hinge of the Calders monocline show the orientation changes of the Maestrat basement thrust ramp, which is the result of the inversion of previous Mesozoic extensional fault segments with the same orientations.

Cut-off line of the acoustic basement in the hanging wall of the Maestrat basement thrust

In the area located west of the Bovalar anticline, the cut-off of the acoustic basement is located below the synformal flexion that constitutes the southern boundary of the Cenozoic Bordón Basin (Figs. 10; 11A-A'; 13). East of the Bovalar anticline, the cut-off of the acoustic basement coincides with the Morella syncline (Fig. 13). In this area, the Ortells and Morella thrusts–rooted in the Maestrat basement thrust–modified this synformal frontal flexion. Further E, this cut-off line is located in the hanging wall of the Turmell fault; while to the W, it is located in the hanging wall of the Villarluengo short-cut thrust.

Structures within the Calders monocline frontal limb: the Bovalar anticline

The NNW-SSE-trending Bovalar monocline is located within the Calders monocline limb, and modifies its geometry. The formation of the Bovalar

anticline and its northern monoclinal segment should be related to a NW-SE-trending basement thrust, at least in its northern part, where a vertical tectonic step is observed between the limbs of the anticline (Figs. 7C; 11C-C'). The origin of this thrust could be related to the inversion of previous Triassic normal faults. As shown in Figure 8B, some NW-SE-trending, SW-dipping Triassic normal faults where interpreted as bounding to the NE the Middle Muschelkalk accumulation located N of the Iglesuela basement high. Towards the S–below the N-S-trending, southern segment of the Bovalar anticline–this thrust probably terminates, as no vertical tectonic step can be identified (Fig. 11E-E'). Conversely, the superficial structure developed above it–the N-S-trending box-fold anticline–continues southwards for more than 8km as a salt-cored detachment fold. The thick Middle Muschelkalk originally deposited in that area (Fig. 7B, E) could have favored the development of this salt-cored fold as a continuation of the northern monocline, and its progression southwards beyond the termination of the acoustic basement thrust.

The Bovalar monocline and the basement thrust below it link to the NE-SW-trending steeply-dipping domain of the Calders monocline limb in the surroundings of Olocau. The seismic profiles also show that a thrust rooted in the Maestrat basement thrust cuts this steeply-dipping part of the monocline, both in the NE-SW Olocau sector and in the NW-SE Tronchón sector (Fig. 10), probably related to the inversion of Mesozoic normal faults with those orientations, making the steeply dipping domain more pronounced.

Middle Muschelkalk detachment level and salt-related structures developed during contraction

As mentioned above, the Middle Muschelkalk evaporitic unit played an important role during the Cenozoic contraction, by decoupling the acoustic basement and the supra-salt cover. During contraction, the basement was faulted while the supra-salt cover was folded and thrust, and adapted to the geometry of the basement structures. During the Cenozoic contraction, the last changes in the distribution of the Middle Muschelkalk salt resulted in its current distribution, due to the folding of the supra-salt cover. Previous salt structures were amplified (Monchén salt anticline) while new box-fold, salt-cored, anticlines developed (Bovalar, Tarayuela, and Cañada de Benatanduz anticlines; Figs. 4; 7E; 11). The Mesozoic cover was folded, detached in the Middle Muschelkalk evaporites, which flowed towards the lower-pressure cores of the rising anticlines, developing elongated salt accumulations (Fig. 7E).

Orientation of structures

As described, the main orientation of the Cenozoic contractional structures within the study area is mostly WNW-ESE; although they can vary to E-W and to N-S. Unlike other areas of the Maestrat Basin and the Iberian Chain, where superposition of structures generated in successive deformation events is clear –*i.e.*, within and North of the Aliaga Cenozoic Basin (Simón, 1980; Guimerà, 1988)– in the study area no superposition of this kind is observed. For this reason, the differently oriented structures are considered to be synchronous, resulting from the inversion of a complex system of previous Mesozoic extensional faults with different orientations, which resulted in the formation of thrusts and folds which change their orientation. The heterogeneous distribution of the detachment level (Middle Muschelkalk), which resulted from the distribution of horsts and grabens in the acoustic basement, and influenced the development of contractional structures, also has to be taken into account.

CONCLUSIONS

During the Late Permian-Late Triassic rifting, a system of high-angle normal faults developed in the present-day acoustic basement. These faults define a system of horsts, grabens and half-grabens, involving the Upper Permian to the Middle Muschelkalk units, which were filled and overlain by the Middle Muschelkalk evaporitic facies deposited during the extension. As a result, depositional thickness variations within the Middle Muschelkalk appeared, which were enhanced by salt flow during the Late Triassic due to the resumed activity of normal faults in the basement. This is deduced from the growth strata in the Keuper seismic reflectors, which onlap the Upper Muschelkalk folds. The last thickness variations within the Middle Muschelkalk were generated during the Cenozoic contraction, as the Mesozoic salt structures were amplified and new salt-cored detachment folds developed.

Although widely considered as the Triassic post-rift, some extension is needed during the Early Lias, as thickness variations of the units of this age are identified after comparison of thicknesses in exploration wells. During the Late Jurassic–Early Cretaceous rifting event, the Maestrat Basin developed, and within it, the Salzedella sub-basin, bounded to the N by the Villarluengo, Bordón, Ortells and Xert faults. These faults separate the Barremian and Aptian sequences of up to 1100-2500m in their hanging walls from sequences of about 400m in their footwalls. Within the basin, minor normal faults of metric slips probably resulted in the progressively northward thickening of the Salzedella sub-basin.

During the Cenozoic contraction, the Salzedella sub-basin was inverted. Its North-bounding normal fault system was inverted, at least in its lower segment within the acoustic basement (Maestrat basement thrust). A wide uplifted area developed in its raised hanging wall. This uplifted area is bounded to the N by the E-W-trending, N-verging Calders monocline, which is the surface expression of the Maestrat basement thrust. Laterally, the Calders monocline terminates and links to the outcropping Maestrat basement thrust in the Turmell and Villarluengo thrusts, which are short-cuts of the inverted Xert and Villarluengo Mesozoic normal faults.

The Calders monocline is interpreted as a fault-bend fold, indicating a flat-ramp-flat geometry of the Maestrat basement thrust, with the southern hinge of the Calders monocline being the superficial expression of the transition from ramp to flat in the basement thrust. The cut-off line of the acoustic basement in the hanging wall of the Maestrat basement thrust coincides with the northern synformal hinge of the Calders monocline, located at the southern boundary of the Bordón Cenozoic Basin and in the Morella syncline. The frontal tilted limb of the Calders monocline has a maximum width of about 13km and narrows laterally, linking to direct outcrops of the Maestrat basement thrust (Turmell and Villarluengo short-cut thrusts). In these two areas, the cut-off line of the acoustic basement is found in the hanging walls of the basement thrusts. This cut-off line makes the transition from thick-skin to thin-skin areas.

The monocline geometry is modified in its central part by the N-S trending Bovalar anticline, originated by the inversion of a previous Triassic normal fault and the presence of a thick Middle Muschelkalk evaporitic unit originally deposited in its hanging wall.

The uplifted hanging wall of the Maestrat basement thrust remains elevated for about 40km to the S, and the frontal limb of the Calders monocline dips about 5º towards the N. These observations indicate that a very low-angle ramp is needed for the Maestrat basement thrust ramp, rooted in the upper crust.

Mesozoic extensional structures with different orientations, together with a thick Middle Muschelkalk evaporitic unit, played an important role in the formation of the Cenozoic contractional structures, affecting their location and orientation, and the different deformation styles between the acoustic basement and the supra-salt cover. The acoustic basement was mainly faulted while the supra-salt cover was mainly folded and thrust, adapting to the basement structures.

ACKNOWLEDGMENTS

The authors wish to thank Antonio Casas-Sainz and Juan Luis Alonso for their helpful reviews. This work was supported by the projects INTECTOSAL (CGL2010-21968-C02-01/BTE) and CGL2008-04916/BTE. The Universitat de Barcelona is acknowledged for a PhD fellowship (APIF) to the first author. The authors also acknowledge Midland Valley, Paradigm, SMT and Bentley for providing the Move®, Gocad®, Kingdom Suite® and Microstation® software licenses, respectively. The authors also thank Christopher Evans (Serveis Lingüístics, UB) for the English revision of the manuscript.

REFERENCES

Almera, J., Anadón, P., Godoy, A., 1982. Mora de Rubielos, sheet 591. Mapa Geológico de España 1:50.000. Madrid, Servicio de Publicaciones, Ministerio de Industria y Energía, 2ª Serie, 1ª Edición.

Álvaro, M., Capote, R., Vegas, R., 1979. Un Modelo de evolución geotectónica para la cadena Celtibérica. Acta Geológica Hispánica, 14, 172-181.

Antolín-Tomás, B., Liesa, C.L., Casas, A.M., Gil-Peña, I., 2007. Geometry of fracturing linked to extension and basin formation in the Maestrazgo basin (Eastern Iberian Chain, Spain). Revista de la Sociedad Geológica de España, 20 (3-4), 351-365.

Archivo Técnico de Hidrocarburos. Ministerio de Industria, Energía y Turismo, Spain. Available at https://geoportal.minetur.gob.es/ATHv2/welcome.do (accessed 13 April 2016).

Aurell, M., Meléndez, A., San Román, J., Guimerà, J., Roca, E., Salas, R., Alonso, A., Mas, R., 1992. Tectónica sinsedimentaria distensiva en el límite Triásico-Jurásico en la cordillera ibérica. Actas del III Congreso Geológico de España, 1, 50-54.

Bartrina, T., Hernández, E., 1990. Las unidades evaportíticas del Triásico del subsuelo del Maestrazgo. In: Ortí, F., Salvany, J.M. (eds.). Formaciones evaporíticas de la Cuenca del Ebro y cadenas periféricas, y de la zona de Levante. Nuevas aportaciones y guía de superficie. Barcelona, Empresa Nacional de Residuos Radiactivos (ENRESA) i Universitat de Barcelona (UB, Departament de Geoquímica, Petrologia i Prospecció Geològica), 34-38.

Bover-Arnal, T., Moreno-Bedmar, J.A., Frijia, G., Pacual-Cebrian, E., Salas, R., 2016. Chronostratigraphy of the Barremian-Early Albian of the Maestrat Basin (E Iberian Peninsula): integrating strontium-isotope stratigraphy and ammonoid biostratigraphy. Newsletters on Stratigraphy, 49 (1), 41-68. DOI: 10.1127/nos/2016/0072

Butillé, M., Ferrer, O., Granado, P., Roca, E., Muñoz, J.A., Ballesteros, J.C., Giménez, A., Vallejo, R.A., González, P., 2012. Evidencias de deformaciones salinas en las sucesiones mesozoicas del sector sur de la Cuenca del Ebro. In: Fernández, L.P., Fernández, A., Cuesta, A., Bahamonde, J.R. (eds.). Oviedo, VIII Congreso Geológico de España. Geo-Temas, 13, 176.

Campos, S., Aurell, M., Casas, A., 1996. Origen de las brechas de la base del Jurásico en Morata de Jalón (Zaragoza). Geogaceta, 20 (4), 887-889.

Canérot, J., 1974. Recherches géologiques aux confins des chaînes ibérique et catalane (Espagne). PhD Thesis. Université Paul Sabatier, Toulouse, 517pp.

Canérot, J., Leyva, F., 1972. Peñarroya de Tastavins, sheet 520. Mapa Geológico de España 1:50.000. Madrid, Servicio de Publicaciones, Ministerio de Industria y Energía, 2ª Serie. 1ª Edición.

Canérot, J., Pignatelli-García, R., 1972. Aguaviva, sheet 519. Mapa Geológico de España 1:50.000. Madrid, Servicio de Publicaciones, Ministerio de Industria y Energía, 2ª Serie, 1ª Edición.

Canérot, J., Pignatelli-García, R., 1977. Mosqueruela, sheet 569. Mapa Geológico de España 1:50.000. Madrid, Servicio de Publicaciones, Ministerio de Industria y Energía, 2ª Serie, 1ª Edición.

Canérot, J., Crespo-Zamorano, A., Navarro-Vázquez, D., 1977. Montalbán, sheet 518. Mapa Geológico de España 1:50.000. Madrid, Servicio de Publicaciones, Ministerio de Industria y Energía, 2ª Serie, 1ª Edición.

Canérot, J., Cugny, P., Pardo, G., Salas, R., Villena, J., 1982. Ibérica Central- Maestrazgo. In: Dpto. de Estratigrafía de la Facultad de Ciencias Geológicas de la Universidad Complutense de Madrid, y Alonso, A, Arias, C., García, A., Mas, R., Rincón, R, Vilas, L. del CSIC (eds.). El Cretácico de España. Madrid, 273-344.

Castillo Herrador, F., 1974. Le Trias évaporitique des basins de la Vallée de l'Èbre et de Cuenca. Bulletin de la Société Géologique de France, 16 (6), 666-675.

Escudero-Mozo, M. J., Márquez-Aliaga, A., Goy, A., Martín-Chivelet, J., López-Gómez, J., Márquez, L., Arche, A., Plasencia, P., Pla, C., Marzo, M., Sánchez-Fernández, D., 2015. Middle Triassic carbonate platforms in eastern Iberia: Evolution of their fauna and palaeogeographic significance in the western Tethys. Palaeogeography, Palaeoclimatology, Palaeoecology, 417, 236-260. DOI: 10.1016/j.palaeo.2014.10.041

Esnaola, J.M., Canérot, J., 1972. Albocácer, sheet 570. Mapa Geológico de España 1:50.000. Madrid, Servicio de Publicaciones, Ministerio de Industria y Energía, 2ª Serie, 1ª Edición.

Farran, M., 2008. IMAGE2SEGY: Una aplicación informática para la conversión de imágenes de perfiles sísmicos a ficheros en formato SEG Y. In: Pérez, F.J., Cabrera, M.C. (eds.). Las Palmas de Gran Canaria, VII Congreso Geológico de España. Geo-Temas, 10, 1215-1218.

Fernández, O., 2004. Reconstruction of geological structures in 3D. An example from the Southern Pyrenees. PhD Thesis. University of Barcelona, Barcelona, 321pp.

Ferrer, O., Jackson, M.P.A., Roca, E., Rubinat, M., 2012. Evolution of salt structures during extension and inversion of the Offshore Parentis Basin (Eastern Bay of Biscay). In: Alsop, G.I., Archer, S.G., Hartley, A.J., Grant, N.T., Hodgkinson, R. (eds.). Salt Tectonics, Sediments and Prospectivity. London, Geological Society of London, 363 (Special Publications), 361-379. DOI: 10.1144/SP363.16

Gautier, F., 1978. Alcalà de la Selva, sheet 568. Mapa Geológico de España 1:50.000. Madrid, Servicio de Publicaciones, Ministerio de Industria y Energía, 2ª Serie, 1ª Edición.

Gautier, F., 1979. Villarluengo, sheet 543. Mapa Geológico de España 1:50.000. Madrid, Servicio de Publicaciones, Ministerio de Industria y Energía, 2ª Serie, 1ª Edición.

Gautier, F., Barnolas, A., 1979. Villarluengo, sheet 543. Memoria del Mapa Geológico de España 1:50.000. Madrid, Servicio de Publicaciones, Ministerio de Industria y Energía, 2ª Serie, 1ª Edición, 45pp.

Giner, J., 1980. Estudio sedimentológico y diagenético de las formaciones carbonatadas del Jurásico de los Catalánides, Maestrazgo y rama aragonesa de la Cordillera Ibérica (sector oriental). PhD Thesis. Barcelona, University of Barcelona, Barcelona, 316pp.

Gómez, J.J., Goy, A., 1998. Unidades litoestratigráficas del tránsito Triásico-Jurásico en la región de Lécera (Zaragoza). Geogaceta, 23, 63-66.

González, A., 1989. Análisis tectosedimentario del terciario del borde SE de la Depresión del Ebro (sector bajoaragonés) y de las cubetas ibéricas marginales. PhD Thesis. Universidad de Zaragoza, Zaragoza, 507pp.

González, A., Guimerà, J., 1993. Sedimentación sintectónica en una cuenca transportada sobre una lámina de cabalgamiento: la cubeta terciaria de Aliaga. Revista de la Sociedad Geológica de España, 6, 151-165.

González, A., Guimerà, J., 1997. Marco estructural de la sedimentación durante el Mioceno inferior en el extremo meridional de la Cuenca del Ebro. In: Calvo, J.P., Morales, J., (eds.). Avances en el conocimiento del Terciario Ibérico. III Congreso del Grupo Español del Terciario. Universidad Complutense de Madrid, Facultad de Ciencias Geológicas y Consejo Superior de Investigaciones Científicas (CSIC), 97-100.

González, A., Guimerà, J., Luzón, A., 1994. Relaciones tectónica-sedimentación en la Zona de Enlace y borde suroriental de la depresión del Ebro. In: González, A. (ed.). Jaca, Guía de Excursiones del II Congreso del Grupo Español del Terciario, 1-134.

González, A., Guimerà, J., Luzón, A., 1998. Edad Oligoceno superior-Mioceno inferior para las superficies de erosión conservadas en el flanco SW de la cubeta de Bordón (Provincia de Teruel, España). Geogaceta, 24, 155-158.

Guimerà, J., 1988. Estudi estructural de l'Enllaç entre la Serralada Ibérica i la Serralada costanera Catalana. PhD Thesis. Barcelona, University of Barcelona, Barcelona, 600pp.

Guimerà, J., 2004. Cadenas con cobertera: Las Cadenas Ibérica y Costera Catalana. In: Vera, J.A. (ed.). Geología de España. Madrid, Sociedad Geológica de España (SGE) y Instituto Geológico y Minero de España (IGME), 602-607.

Guimerà, J., 2013. Estructura y evolución tectónica de la Cadena Ibérica. In: Simón, J.L., Liesa, C.L. (eds.). XLVII Curso

de Geología Práctica. La Orogenia Alpina en la Cordillera Ibérica. Universidad de Verano de Teruel, 1-9.

Guimerà, J., Álvaro, M., 1990. Structure et évolution de la compression alpine dans la Chaîne Ibérique et la Chaîne Côtière Catalane (Espagne). Bulletin de la Société Géologique de France (8), VI (2), 339-340.

Guimerà, J., Salas, R., 1996. Inversión terciaria de la falla normal mesozoica que limitaba la subcuenca de Galve (Cuenca del Maestrazgo). Geogaceta, 20 (7), 1701-1703.

Guimerà, J., González, A., Salas, R., Sancho, C., 2010. Origin and preservation of the late contractional relief of an intraplate thrust-belt: the NE Iberian Chain (Iberian Peninsula). EGU2010-5137, EGU General Assembly Geophysical Research Abstracts, 12.

Hernández, A., 1985. Teruel, sheet 47. Memoria del Mapa Geológico de España 1:200.000. Madrid, Servicio de Publicaciones, Ministerio de Industria y Energía, 1ª Edición, 192pp.

Lanaja, J.M., 1987. Contribución de la exploración petrolífera al conocimiento de la geología de España. Madrid, Instituto Tecnológico GeoMinero de España, 465pp.

Liesa, C.L., Soria, A.R., Meléndez, N., Meléndez, A., 2006. Extensional fault control on the sedimentation patterns in a continental rift basin: El Castellar Formation, Galve sub-basin, Spain. London, Journal of the Geological Society, 163, 487-498.

López-Gómez, J., Arche, A., Márquez-Aliaga, A., Salas, R., Goy, A., Guimerà, J., Tomás, S., 2005. El Pérmico y el Triásico del Desert de les Palmes, Cordillera Ibérica Oriental, Castellón. Cidaris, 27-28, 5-34.

López-Mir, B., Muñoz, J.A., García-Senz, J., 2015. Extensional salt tectonics in the partially inverted Cotiella post-rift basin (south-central Pyrenees): structure and evolution. International Journal of Earth Sciences, 104 (2), 419-434. DOI: 10.1007/s00531-014-1091-9

Martín, L., Leyva, F., Canérot, J., 1972. Morella, sheet 545. Mapa Geológico de España 1:50.000. Madrid, Servicio de Publicaciones, Ministerio de Industria y Energía, 2ª Serie, 1ª Edición.

Martínez-Abad, J.L., 1991. Cuenca del Maestrazgo. Correlación de sondeos I-I'. In: López, F. (coord.). Estudio geológico del Maestrazgo y de la mitad meridional de los Catalánides. INYPSA y Instituto Geológico y Minero de España (IGME), unpublished.

Navarro-Vázquez, D., Crespo-Zamorano, A., Pérez-Castaño, A., Canérot, J., 1972. Forcall, sheet 544. Mapa Geológico de España 1:50.000. Madrid, Servicio de Publicaciones, Ministerio de Industria y Energía, 2ª Serie, 1ª Edición.

Ortí, F., 1973. El Keuper del Levante Español. Litoestratigrafía, petrología y paleogeografía de la cuenca. PhD Thesis. Barcelona, Universitat de Barcelona, 174pp.

Roca, E., Guimerà, J., 1992. The Neogene structure of the eastern Iberian margin: structural constraints on the crustal evolution of the Valencia through (western Mediterranean). Tectonophysics, 203, 203-218. DOI: 10.1016/0040-1951(92)90224-T

Roca, E., Guimerà, R., Salas, R., 1994. Mesozoic extensional tectonics in the southeast Iberian Chain. Geological Magazine, 131 (2), 155-168.

Salas, R., 1987. El Malm i el Cretaci inferior entre el Massís de Garraf i la Serra d'Espadà. PhD Thesis. Barcelona, Universitat de Barcelona, 345pp.

Salas, R., Casas, A., 1993. Mesozoic extensional tectonics, stratigraphy and crustal evolution during the Alpine cycle of the Eastern Iberian basin. Tectonophysics, 228, 33-35. DOI: 10.1016/0040-1951(93)90213-4

Salas, R., Guimerà, J., 1996. Rasgos estructurales principales de la cuenca cretácica inferior del Maestrazgo (Cordillera Ibérica oriental). Geogaceta, 20 (7), 1704-1706.

Salas, R., Martín-Closas, C., Querol, X., Guimerà, J., Roca, E., 1995. Evolución tectonosedimentaria de las cuencas del Maestrazgo y Aliaga-Penyagolosa durante el Cretácico inferior. In: Salas, R., Martín-Closas, C. (eds.). El Cretácico inferior del Nordeste de Iberia. Barcelona, Universitat de Barcelona, 13-94.

Salas, R., Guimerà, J., Giménez-Montsant, J., Martín-Closas, C., Roca, E., 1997. Mesozoic Rift structure, Stratigraphy and Palaeogene Inversion of the Maestrat basin. Iberian Range (NE Spain). Field trip guide. IGCP Project-369. Comparative evolution of PeriTethyan Rift Basins, Barcelona, Universitat de Barcelona, 70pp.

Salas, R., Guimerà, J., Mas, R., Martín-Closas, C., Meléndez, A., Alonso, A., 2001. Evolution of the Mesozoic Central Iberian Rift System and its Cainozoic inversion (Iberian chain). In: Ziegler, P.A., Cavazza, W., Robertson, A.H.F., Crasquin-Soleau, S. (eds.). Peri-Tethys memoir, 6: Peri-Tethyan Rift/Wrench Basins and Passive Margins. Paris, Mémoires du Muséum National d'Histoire Naturelle, 186, 145-186.

Salas, R., Martín-Closas, C., Delclòs, X., Guimerà, J., Caja, M.A., Mas, R., 2005. Factores principales de control de la sedimentación y los cambios bióticos durante el tránsito Jurásico-Cretácico en la Cadena Ibérica. Geogaceta, 38, 15-18.

Salas, R., García-Senz, J., Guimerà, J., Bover-Arnal, T., 2010. Opening of the Atlantic and development of the Iberian intraplate rift basins during the late Jurassic-early Cretaceous. II Central and North Atlantic Conjugate Margins Conference, 245-248.

San Román, J., Aurell, M., 1992. Paleogeographical significance of the Triasssic-Jurassic unconformity in the north Iberian basin (Sierra del Moncayo, Spain). Palaeogeography, Palaeoclimatology, Palaeoecology, 99 (1-2), 101-117. DOI: 10.1016/0031-0182(92)90009-T

Seillé, H., Salas, R., Pous, J., Guimerà, J., Gallart, J., Torne, M., Romero-Ruiz, I., Diaz, J., Ruiz, M., Carbonell, R., Mas, R., 2015. Crustal structure of an intraplate thrust belt: The Iberian Chain revealed by wide-angle seismic, magnetotelluric soundings and gravity data. Tectonophysics, 663, 339-353. DOI: 10.1016/j.tecto.2015.08.027

Serrano, A., Martínez del Olmo, W., 2004. Estructuras diapíricas de la zona meridional de la Cuenca Vasco-Cantábrica. In: Vera, J.A. (ed.). Geología de España. Madrid, Sociedad

Geológica de España (SGE) y Instituto Geológico y Minero de España (IGME), 334-338.

SIGECO. Sistema de consulta y difusión web de cartografía geológica. Instituto Geológico y Minero de España. Ministerio de Economía y Competitividad, Spain. Available at http://cuarzo.igme.es/sigeco/default.htm (accessed 13 April 2016).

Simón, J.L., 1980. Estructuras de superposición de plegamientos en el borde NE de la cadena Ibérica. Acta Geológica Hispánica, 15 (5), 137-140.

Trell, A., Canérot, J., Martín, M., 1979. Villahermosa del Río, sheet 592. Mapa Geológico de España 1:50.000. Madrid, Servicio de Publicaciones, Ministerio de Industria y Energía, 2ª Serie, 1ª Edición.

Yébenes, A., 1973. Estudio petrogenético de las carniolas de la Cordillera Ibérica. Licentiate Thesis. Madrid, Universidad Complutense de Madrid, 118pp.

Manuscript received July 2015;
revision accepted February 2016;
published Online April 2016.

APPENDIX I. B

Kinematic evolution of a fold-and-thrust belt developed during basin inversion: the Mesozoic Maestrat basin, E Iberian Chain.

Nebot, M. and Guimerà, J. 2016. *Geological Magazine*, published obline: october 2016
doi:10.1017/S001675681600090X

Geol. Mag.: page 1 of 11 © Cambridge University Press 2016
doi:10.1017/S001675681600090X

Kinematic evolution of a fold-and-thrust belt developed during basin inversion: the Mesozoic Maestrat basin, E Iberian Chain

MARINA NEBOT* & JOAN GUIMERÀ

Geomodels Research Institute, Departament de Dinàmica de la Terra i de l'Oceà, Facultat de Geologia, Universitat de Barcelona (UB), Martí i Franquès s/n, 08028 Barcelona, Spain

(*Received* 25 April 2016; *accepted* 29 August 2016)

Abstract – The Maestrat basin was one of the most subsident basins of the Mesozoic Iberian Rift system, developed by a normal fault system which divided it into sub-basins. Its Cenozoic inversion generated the N-verging Portalrubio–Vandellòs fold-and-thrust belt in its northern margin, detached in the Triassic evaporites. In the hinterland, a 40 km wide uplifted area, in the N–S direction, developed, bounded to the N by the E–W-trending, N-verging Calders monocline. This monocline is interpreted as a fault-bend fold over the ramp to flat transition of the E–W-trending, N-verging Maestrat Basement Thrust, and also indicates the transition from a thick-skinned (S) to a thin-skinned (N) style of deformation. This paper presents a kinematic evolutionary model for the northern margin of the basin and a reconstruction of the Maestrat Basement Thrust geometry, generated by the inversion of the Mesozoic normal fault system. It contains a low-dip ramp (9°) extended southwards more than 40 km, attaining a depth of 7.5 km. As this thrust reached the Mesozoic cover to the foreland, it propagated across the Middle Muschelkalk evaporitic detachment, generating a nearly horizontal thrust which transported northwards the supra-salt cover, and the normal fault segments within it, for *c.* 11–13 km. The displacement of the basement in the hanging-wall of the low-dip basement ramp generated the 40 km wide uplifted area, while the superficial shortening was accumulated in the northern margin of the basin – which contains the thinnest Mesozoic cover – developing the Portalrubio–Vandellòs fold-and-thrust belt.

Keywords: basin inversion, low-dip ramp, tectonic relief, salient, fold-and-thrust belt.

1. Introduction

The Linking Zone resulted from the Cenozoic inversion of the Mesozoic Maestrat basin, located between the NW–SE-trending Iberian Chain and the NE–SW-trending Catalan Coastal Chain (Guimerà, 1984, 1988; Fig. 1). Its northern part contains the Portalrubio–Vandellòs fold-and-thrust belt, broadly E–W-trending and N-verging, while a wide tectonically elevated area developed in its southern part (Guimerà, 1988; Guimerà *et al.* 2010). Nebot & Guimerà (2016) recognized a new structure separating these two areas, the decakilometric-scale Calders monocline (Figs 2, 3), interpreting it as a fault-bend fold over ramp to flat geometries of a deep-seated thrust (the Maestrat Basement Thrust; Nebot & Guimerà, 2016). The aim of this paper is to provide new data to support the interpretations of Nebot & Guimerà (2016) and to establish the kinematic evolution of the fold-and-thrust belt. More specifically, the objectives of this paper are (i) to estimate the shortening of the fold-and-thrust belt, located N of the Maestrat Basement Thrust ramp, and (ii) to characterize the Mesozoic extensional structure whose Cenozoic contractional inversion developed the belt.

With this purpose, two new cross-sections have been constructed, containing the deduced transport orientation. Determining the shortening in this area is complex as, on the one hand, main structures show varying orientations and, on the other hand, late to post-tectonic Cenozoic outcrops cover some areas which otherwise would be the most suitable for the regional cross-section construction. Moreover, the thickness of the Mesozoic cover is difficult to establish, as its base hardly ever crops out and no subsurface data are available. Nevertheless, new Lower Cretaceous stratigraphic sections were also obtained from new field data which, combined with previous stratigraphic data, permitted the characterization of the syn-sedimentary extensional structure during this period.

After these data, a palinspastic restoration of the main structures during the Early Cretaceous is proposed, as well as a reconstruction of the geometry of the Maestrat Basement Thrust, more accurate than that proposed by Nebot & Guimerà (2016). Finally, this paper presents a kinematic evolutionary model for the N margin of the inverted Maestrat basin, which constitutes a good example of a fold-and-thrust belt developed during basin inversion, presenting in its foreland a thin-skinned fold-and-thrust belt conditioned by an evaporitic detachment level, while in its thick-skinned hinterland generated the uplift of a wide area.

2. Geological setting

The Iberian Chain developed during the Cenozoic Alpine orogeny, as a result of the contractional

*Authors for correspondence: marinanebotmiralles@gmail.com

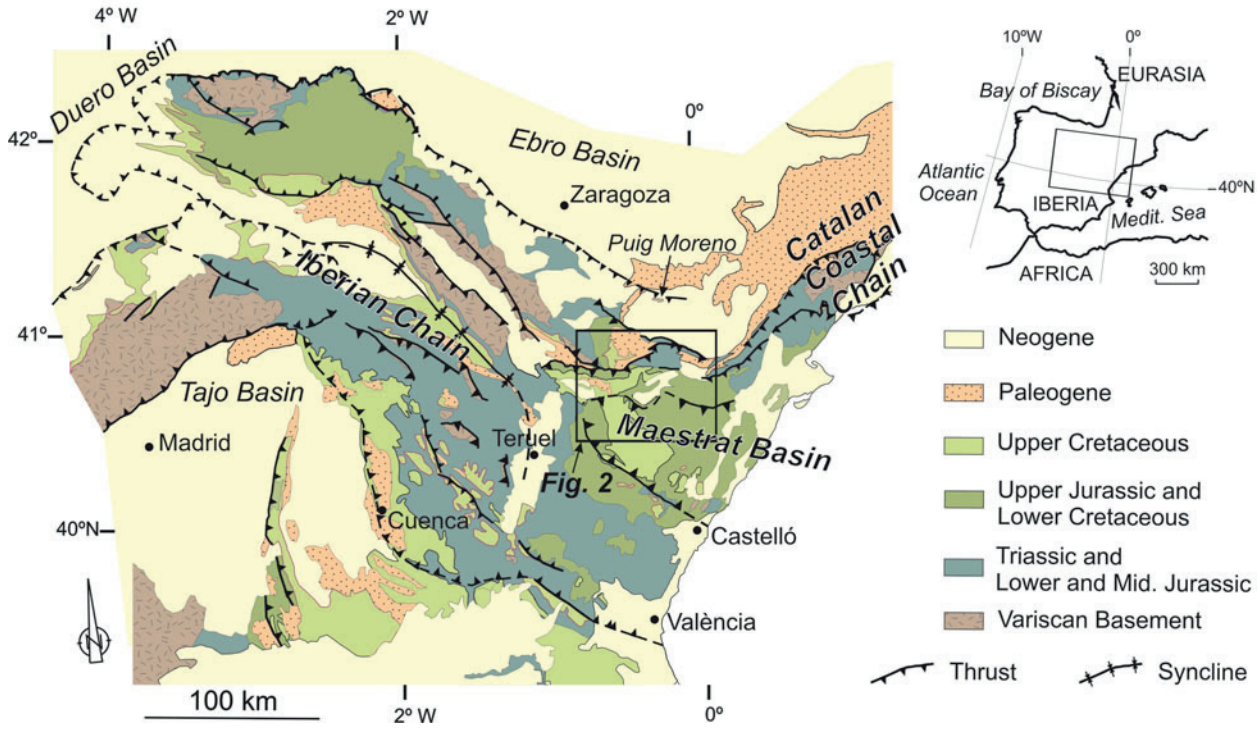

Figure 1. (Colour online) Simplified geological map of the Iberian Chain, and its location in the eastern Iberian Peninsula. Location of the area studied (Fig. 2) is also shown. Modified from Nebot & Guimerà (2016) after Guimerà (2004).

inversion of the Iberian Rift System (Álvaro, Capote & Vegas, 1979; Salas *et al.* 2001; Guimerà, Mas & Alonso, 2004), which was active during the Mesozoic, and experienced two main rifting events, during the Late Permian – Late Triassic and during the Late Oxfordian – Late Albian (Fig. 4; Salas *et al.* 2001), followed by events of lower rifting activity (Early and Middle Jurassic, and Late Albian to Maastrichtian).

The Maestrat basin was one of the most subsident basins within the Iberian Rift System, developed during the Jurassic to Early Cretaceous rifting event. Its sedimentary filling was dominated by shallow marine to lacustrine carbonates, with intercalations of continental siliciclastic sediments, and a few intercalations of pelagic sediments (R. Salas, unpub. Ph.D. thesis, Univ. Barcelona, 1987). Some evaporitic layers are recognized in the Triassic: the Keuper and the Middle Muschelkalk. The latter was the regional detachment during the Cenozoic contraction, differentiating two structural packages (Fig. 3): the supra-salt cover (units above the Middle Muschelkalk) and the sub-salt or acoustic basement (units below the Middle Muschelkalk) (Nebot & Guimerà, 2016).

The Cenozoic inversion of the northern margin of the Maestrat basin generated the Portalrubio–Vandellòs fold-and-thrust belt (Guimerà, 1988), in the northern part of the Linking Zone (Fig. 3). In the study area, this fold-and-thrust belt displays a salient (in the sense of Marshak, 2004), as traces of thrusts and folds take curved shapes convex to the N, in the sense of transport (Fig. 3). Therefore the adjacent areas of Ejulve–Aliaga and Herbers (Fig. 3) could be associated with recesses containing superposition of structures with different orientations (Simón, 1980; Guimerà, 1988).

South of this fold-and-thrust belt, the E–W-trending Calders monocline bounds to the north the tectonically elevated area (Nebot & Guimerà, 2016; Figs 2, 3). This monocline has been interpreted as a fault-bend fold that is the surface expression of the ramp–flat geometry of the Maestrat Basement Thrust in the study area, resulting from the Cenozoic inversion of the Mesozoic extensional fault system of the Maestrat basin across the basement (Nebot & Guimerà, 2016). A vertical tectonic step of 800–1200 m can be measured above the Calders monocline (Fig. 3; González, Guimerà & Luzón, 1998; Nebot & Guimerà, 2016) whose tilted limb dips *c.* 5° N and is 13 km wide in its central part, narrowing laterally (Fig. 2).

3. Methodology

About 1200 new strike-and-dip data were obtained both in the field and from 3D geological contacts drawn on ortho-images and 3D topographic contour lines in a georeferenced environment (Microstation®), using in-house macros developed by O. Fernández (unpub. Ph.D. thesis, Univ. Barcelona, 2004). Based on these new strike-and-dip data, new mapping after field work and ortho-image interpretation, and also the previous geological maps (Canérot & Leyva, 1972; Canérot & Pignatelli, 1972, 1977; Esnaola & Canérot, 1972; Martín, Leyva & Canérot, 1972; Navarro-Vázquez *et al.* 1972; Marín *et al.* 1974; Almela *et al.* 1975; Marín & Duval, 1976; Canérot, Crespo-Zamorano & Navarro-Vázquez,

http://dx.doi.org/10.1017/S001675681600090X

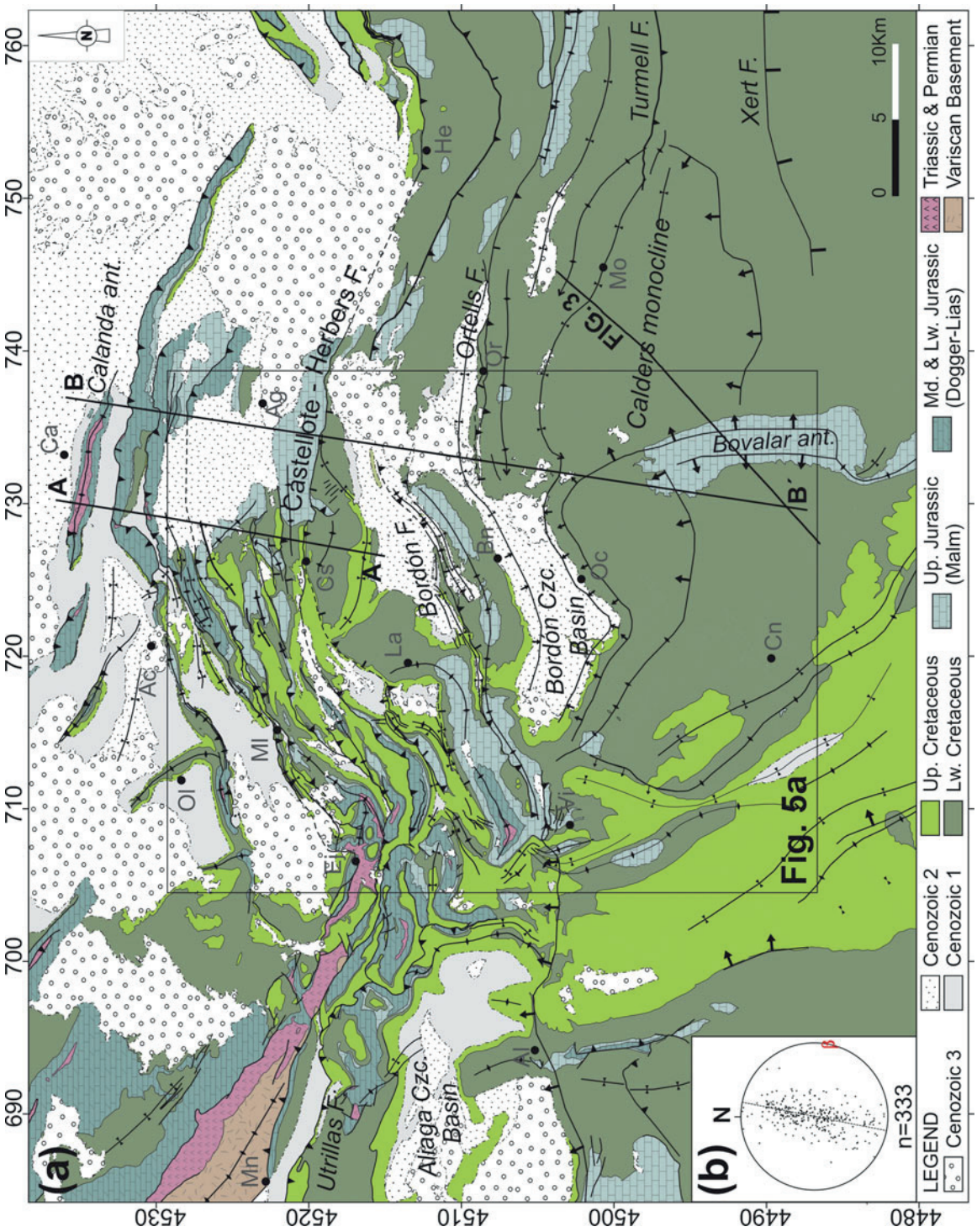

Figure 2. (Colour online) (a) Geological map of the Linking Zone between the Iberian Chain and the Catalan Coastal Chain. The Portalrubio–Vandellòs fold-and-thrust belt is located in its northern part. Cenozoic 1, 2 and 3 are the pre-orogenic, syn-orogenic and late to post-orogenic units, respectively (based on González, 1989). See location in Figure 1. Villages: Ac – Alcorisa; Ag – Aiguaviva; Al – Aliaga; Bn – Bordón; Ca – Calanda; Cn – Cantavieja; Cs – Castellote; Ej – Ejulve; He – Herbers; La – Ladruñán; Mo – Morella; Mn – Montalbán; Ml – Molinos; Oc – Olocau del Rei; Ol – Oliete; Or – Ortells, Vi – Villarluengo. Abbreviations: Czc.-Cenozoic; F.-fault; ant.- anticline. The location of the map in Figure 5a, the seismic profile in Figure 3, and the cross-sections in Figure 6 are shown. UTM projection (Zone 30 N, coordinates in km), ED50 datum. (b) Lower hemisphere spherical equal-area projection of bedding, corresponding to the cross-section traces. n = number of data, dashed line = cyclograph of the best-fit plane of the strike-and-dip data, β = pole of the cyclograph, used as projection vector of data to the cross-section plane.

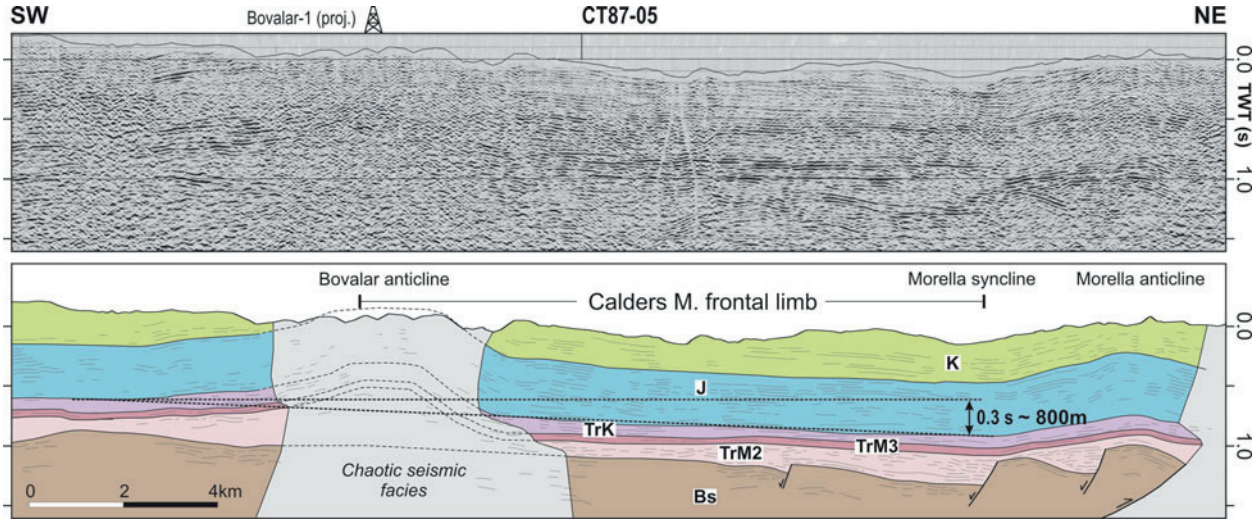

Figure 3. (Colour online) Seismic profile CT87-05 and its interpretation. It shows a wide area of gentle dip towards the N, the frontal tilted limb of the Calders monocline (Nebot & Guimerà, 2016). Abbreviations: K– Cretaceous; J – Jurassic; TrK – Keuper; TrM3 – Upper Muschelkalk; TrM2 – Middle Muschelkalk; Bs – acoustic basement. See Figure 2 for location. Modified from Nebot & Guimerà (2016).

1977; Gautier, 1978, 1979; González, 1989), two cross-sections were constructed and restored, and a complete geological map of the study area was made.

Cross-section constructions – based on the Kink method – and their restoration using the flexural-slip unfolding algorithm were performed with the Move® software. An idealized cross-section of the entire N margin of the basin was also elaborated by combining different cross-section segments, which allowed us to reconstruct, with the Move® software, the geometry of the basement fault that fits the generation of the elevated area during the Cenozoic inversion. The seismic profiles and the exploration wells available S of the study area (Lanaja, 1987; Nebot & Guimerà, 2016) were also considered, in order to estimate the structure and the thicknesses of stratigraphic units which do not crop out in the study area (Fig. 4).

4. Mesozoic extensional structure

Thicknesses of the syn-rift Lower Cretaceous filling of the Maestrat basin (Fig. 5) were established from field data, exploration wells and after R. Salas (unpub. Ph.D. thesis, Univ. Barcelona, 1987). Significant thickness variations were found in the Barremian units, while the Aptian units have a more constant thickness (Fig. 5). After these variations, the Maestrat basin is divided into two zones: (1) the northern external zone (Salas & Guimerà, 1996), containing a very thin or no Lower Cretaceous rocks, and (2) the Salzedella sub-basin (Salas & Guimerà, 1996; Nebot & Guimerà, 2016), which contains the Ladruñán zone with intermediate characteristics (Fig. 5).

The Salzedella sub-basin is located in the hanging-wall of the Castellote–Herbers and the Garrocha normal faults, while other Mesozoic faults are found within it (Fig. 5a). The Ladruñán zone is located at the NW end of the Salzedella sub-basin, separated by the Bordón and the Villarluengo normal faults, and merges towards the E with the Salzedella sub-basin (Fig. 5a). In the northern external zone, the Barremian and Aptian units are concentrated in the outcrops located N of Castellote (Figs 5a, 6A–A′) and N of Aiguaviva (Figs 5a, 6B–B′). The distribution of the Lower Cretaceous rocks and the varying orientation of structures suggest a segmented system of normal faults connected by relay ramps bounding the different zones (Fig. 5a).

The Jurassic broadly becomes thinner towards the N (Nebot & Guimerà, 2016), with major thickness variations in the syn-rift Malm and in the Lower Lias units (Figs 4, 5a). Regarding the Triassic, the lower Triassic units are only known by sub-surface data in the S part of the study area. To construct the cross-sections in Figure 6, an average value of 500–400 m was considered for the Middle Muschelkalk, estimated after the analysis of the isopach map obtained by Nebot & Guimerà (2016). Towards the N the Middle Muschelkalk becomes thinner, as wells in the Ebro basin reveal an average thickness of 200 m (Lanaja, 1987).

5. Cenozoic contractional structure

5.a. Structural style variations

Three main structural domains were differentiated in the study area (Fig. 7), based on the new field work here presented and also the previous work of Guimerà (1988) and Nebot & Guimerà (2016).

5.a.1. Southern slightly deformed area

This area contains the 40 km wide – in the N–S direction – tectonically elevated area (Fig. 7), developed in the hanging-wall of the Maestrat Basement Thrust, and the Calders monocline, which bounds it to the N,

http://dx.doi.org/10.1017/S001675681600090X

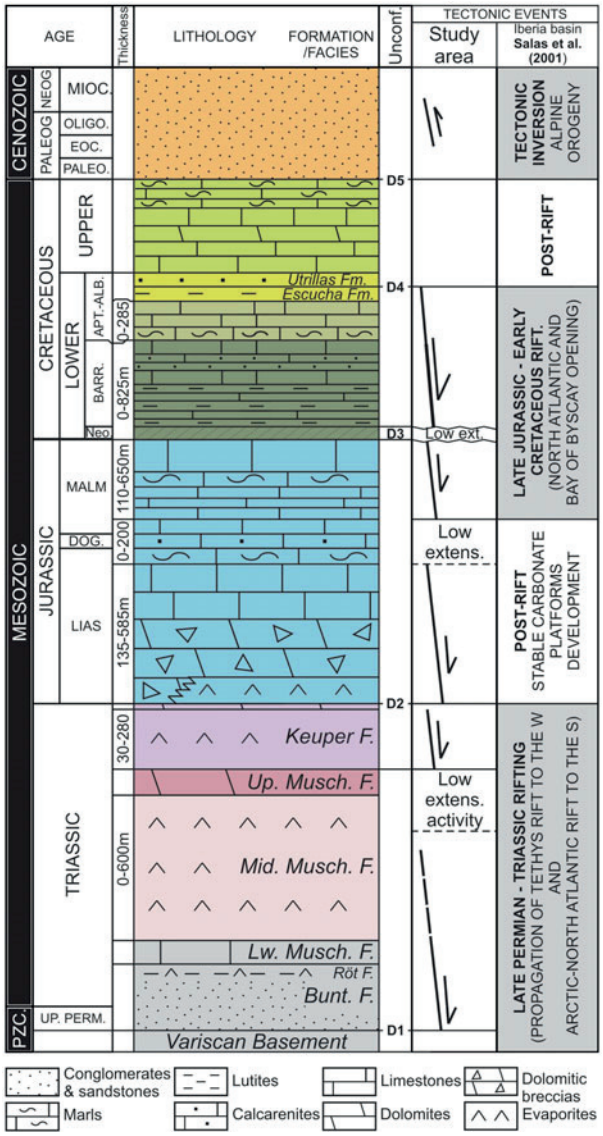

Figure 4. (Colour online) Generalized stratigraphic sequence of the Eastern Salzedella sub-basin. Modified from Nebot & Guimerà (2016), after R. Salas (unpub. Ph.D. thesis, Univ. Barcelona, 1987), Salas *et al.* (2001), Aurell *et al.* (1992) for the Lias, and Bover-Arnal *et al.* (2015) for the Barremian–Aptian boundary.

therefore it is located over the transition from ramp to flat of the Maestrat Basement Thrust (Nebot & Guimerà, 2016). Structures at the surface have kilometric wavelengths and are rooted mostly in the acoustic basement, although detachment folds developed, rooted in the Middle Muschelkalk evaporites (Guimerà, 1988; Nebot & Guimerà, 2016).

5.a.2. Intermediate area

This area is characterized by folds of kilometric wavelengths detached in the Middle Muschelkalk, although some fragments of the acoustic basement are also incorporated in the thrust sheets. It is bounded to the N by the Castellote–Herbers Fault and to the S by the Calders monocline synformal frontal hinge (Fig. 7).

5.a.3. Northern frontal fold-and-thrust belt (N FAT belt)

The northern part of the study area is characterized by tight structures, with wavelengths of hundreds of metres to a few kilometres. They are detached in the Triassic units (Middle Muschelkalk and locally in the Keuper), and in some cases also incorporate fragments of the acoustic basement in the hanging-wall of the thrust sheets (Figs 6, 7). This area coincides with the northern external zone of the Maestrat basin, containing the thinnest supra-salt cover (Fig. 7). The Calanda anticline, the northernmost structure of this fold-and-thrust belt, is detached in the Middle Muschelkalk (Fig. 6) as Upper Muschelkalk rocks crop out in its core (Anadón & Albert, 1973).

In the most frontal part of the fold-and-thrust belt, the major thrust-sheet displacement is transferred towards the foreland from the W, where it is concentrated in the Molinos thrust sheet (Fig. 2), to the E, accumulated mostly in the Calanda thrust sheet (Fig. 6).

SW of the Calanda anticline, structures change their trend from ESE–WNW and E–W to NE–SW, as they display the salient geometry, convex to the N, previously described. In this area, the *N FAT belt* structures and the NW–SE-trending structures of the Iberian Chain converge, producing fold interferences (Simón, 1980, 2004; Guimerà, 1988) and a NE–SW-trending back-thrust in the convergence area (Fig. 2).

5.b. Inversion structures

Some normal faults were partially inverted as thrusts, which inherited their orientations, folding the Upper Cretaceous post-rift in the Garrocha fault or the Ortells fault in its eastern part (Figs 2, 6B–B′). In other cases, the Upper Cretaceous post-rift was thrusted by the inverted fault, their slips being of only a few metres, and the extensional slip being not recovered, as in the Bordón fault (Fig. 2). These two cases are observed in the Castellote fault, which changes the amount of inversion along-strike, being minimum in its western NE–SW-trending segment, where the Upper Cretaceous post-rift is only folded (Fig. 2), and increasing to the E, where the Upper Cretaceous is thrusted in its E–W-trending segment (Fig. 6). Newly formed thrusts also appeared, most of them in the N external zone.

5.c. Transport direction and estimated shortening

Most structures in the Linking Zone are ESE–WNW-trending, parallel to the Calders monocline trace (Fig. 7b), such as the Calanda anticline and the two thrust sheets south of it, the Castellote fault in its northernmost segment, the Ortells fault, or the overall strike of the Utrillas fault (Fig. 2). Therefore, the transport direction is assumed to be parallel to the vector normal to these ESE–WNW-trending structures, and the sense of transport to the foreland, hence to the NNE, which coincides with the one proposed by Guimerà & Álvaro (1990) for the Iberian Chain.

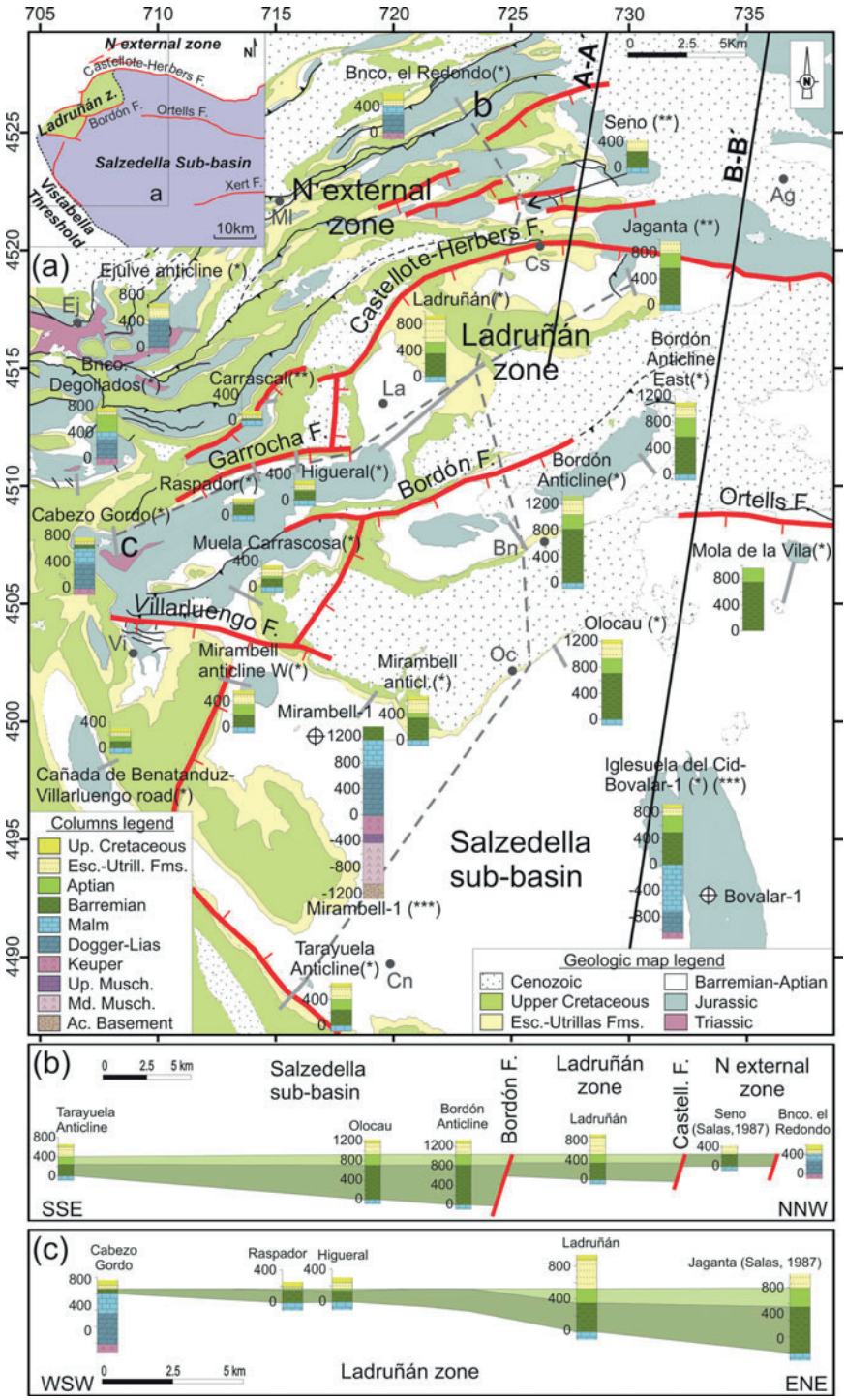

Figure 5. (Colour online) (a) Stratigraphic sections of the studied area, and the main tectonostratigraphic domains recognized and the structures bounding them. The normal faults interpreted for the Barremian and Aptian period are shown. The stratigraphic sections were obtained from new field data (*) and were combined with sections obtained by R. Salas (unpub. Ph.D. thesis, Univ. Barcelona, 1987) (**), and with sub-surface data (***) (exploration wells after Lanaja, 1987, and seismic data converted to depth by Nebot & Guimerà, 2016). (b, c) Simplified correlation of the Barremian and Aptian units in some stratigraphic sections in directions roughly perpendicular (b) and parallel (c) to the geological structures. Different tectonostratigraphic domains and the structures bounding them are depicted. The datum is the base of the Escucha Fm. (top of the Aptian), as this formation developed small sub-basins different from the Barremian–Aptian ones.

Two cross-sections were constructed containing the NNE–SSW transport direction: a regional cross-section that intersects the Calders monocline near its central part (Fig. 6B–B′) and a more local one placed *c.* 7 km W of this regional cross-section (Fig. 6A–A′). The shortening estimated by restoring the regional cross-section (Fig. 6B–B′) is of *c.* 10.5 km, which can be considered a minimum value for the N margin of the Maestrat basin, as cross-sections were constructed in a conservative manner, not including the deformation

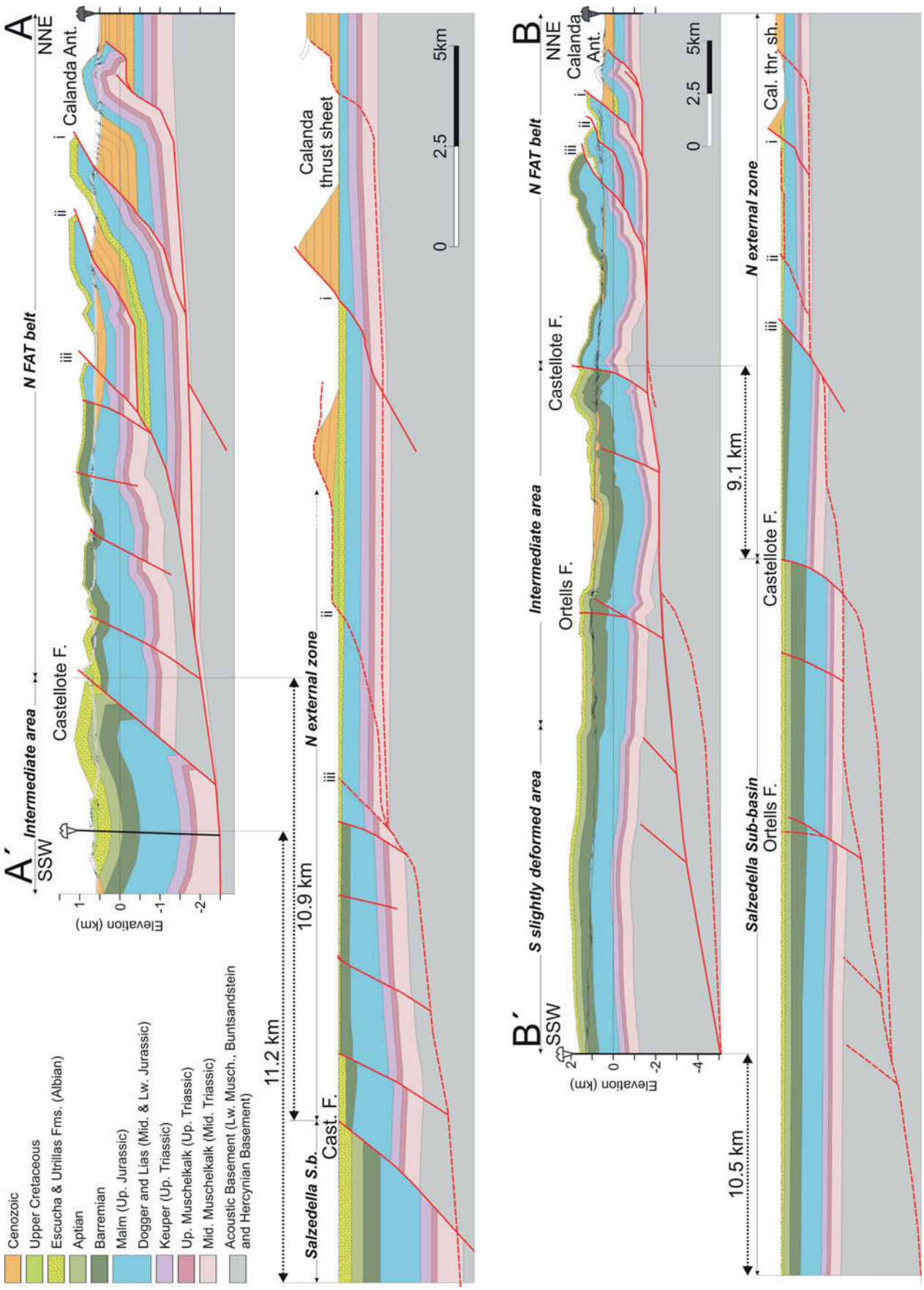

Figure 6. (Colour online) Cross-sections A–A′ and B–B′. See location in Figure 2. They contain the NNE–SSW transport direction.

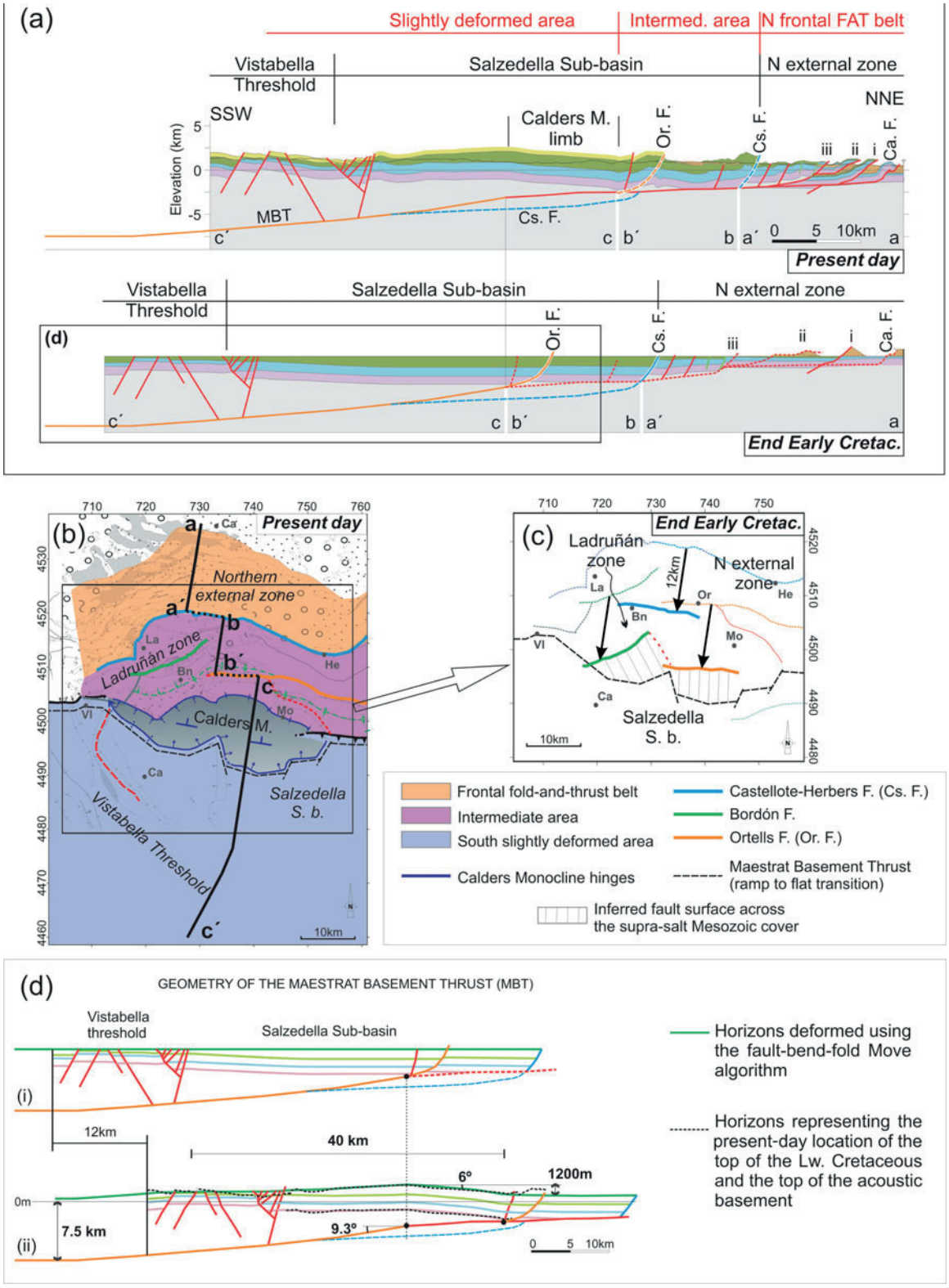

Figure 7. (Colour online) (a) Idealized section of the study area, obtained by combining cross sections A–A′, B–B′ (Fig. 6) and an unpublished cross-section from Guimerà. The interpreted evolution of the area studied is shown. (b) Simplified structural map of the Cenozoic structures developed after the Maestrat basin inversion. Modified from Nebot & Guimerà (2016). (c) Palinspastic restoration of the normal faults within the Maestrat basin at the end of the Mesozoic extension (end of the Early Cretaceous). (d. i) Idealized section of the Salzedella sub-basin at the end of the Mesozoic extension (end of the Early Cretaceous). It is based on the generalized section in (a). (d. ii) Forward modelling of section (d. i) using the fault-bend-fold deformation algorithm with Move®. The resulting horizons are compared to the corresponding horizons in the idealized section in (a) in order to test the geometry of the Maestrat Basement Thrust. The Castellote normal fault was not inverted in this model. Its upper segment across the supra-salt cover was only passively transported within the thrust system.

http://dx.doi.org/10.1017/S001675681600090X

associated with mesostructures, and also, the structures below the wide Cenozoic outcrops intersected by this cross-section were simplified and could accumulate additional shortening. The shortening obtained for the cross-section A–A′, which intersects mainly the frontal fold-and-thrust belt, is 11.2 km. The shortening measured in the *N FAT belt* – placing the pin line in the Cenozoic rocks in the footwall of the Calanda thrust sheet, and the loose line in the Castellote fault – is of 10.9 km (40 %) in the cross-section A–A′ and of 9.1 km (35 %) in the cross-section B–B′. Assuming that shortening does not vary laterally in this ESE–WNW-trending part of the *N FAT belt*, cross-section B–B′ could accumulate *c.* 1.8 km of additional shortening in the *N FAT belt*, which was not recorded in cross-section B–B′ due to the Cenozoic rocks covering some of the Mesozoic outcrops. Consequently, it could reach a total shortening of 12.3 km (Fig. 6B–B′).

5.d. Geometry of the Maestrat Basement Thrust

To explain the wide uplifted area in the hinterland, Nebot & Guimerà (2016) proposed a very low-dip ramp for the Maestrat Basement Thrust, deduced after the geometry of the Calders monocline. The present work presents a more accurate reconstruction that takes into account the estimated shortening in the northern margin of the Maestrat basin just presented. This reconstruction was modelled with the Move® software, and was tested by displacing the restored horizons of the Salzedella sub-basin in the idealized cross-section (Fig. 7a), above the hanging wall of this fault, using the fault-bend-fold algorithm, until obtaining a geometry similar to that observed in the study area and until the upper segments of the normal faults across the supra-salt cover are placed in their present-day location. To achieve this, a displacement of 12 km was needed, giving additional support to the shortening value estimated after restoring the cross-sections.

The resulting fault (Fig. 7d) has a low-dip ramp, with an approximately listric geometry, which dips *c.* 9° in its shallowest part, flattening downwards, until reaching a depth of 7.5 km below sea level, extending southwards for more than 40 km. When the restored horizons of the Salzedella sub-basin (Fig. 7d.i) are transported above this fault for 12 km, a wide flat area is uplifted in its hanging-wall, while a fault-bend fold, similar to the Calders monocline, is generated above the transition from ramp (S) to flat (N) of the fault, whose frontal tilted limb is *c.* 12 km wide and dips *c.* 6° towards the N. A vertical step of 1200 m is obtained between horizons in the uplifted area and in the downthrown area (Fig. 7d.ii).

6. Discussion

6.a. Shortening in the Maestrat basin northern margin

Shortening in the Mesozoic supra-salt cover concentrates mostly in the frontal fold-and-thrust belt, while southwards, in the intermediate and southern areas, the thrust sheets experienced low internal deformation by folding and partial inversion of the Mesozoic normal faults. In the sub-salt basement, shortening accumulated in a more internal and lower position, where the thrust sheet involves the basement (Fig. 7a).

The shortening obtained by restoring the regional cross-section (*c.* 12 km; Fig. 7B–B′) is less than the maximum 13 km estimated after analysing the geometry of the Calders monocline (Nebot & Guimerà, 2016). This difference may result from the fact that the regional cross-section does not cross the widest part of the Calders monocline, and also that the cross-sections were constructed in a conservative manner, and could accumulate more shortening.

Although the Calders monocline geometry suggests a differential shortening, as it narrows laterally (Nebot & Guimerà, 2016), the thrust-sheet displacement does not disappear at the lateral ends of the monocline, as it is transmitted to other structures, indicating that the geometry of the Maestrat Basement Thrust changes laterally, out of the area studied.

6.b. Kinematic evolution

The Mesozoic extensional fault system was inverted in its lower segment across the acoustic basement, generating the Maestrat Basement Thrust. As this thrust reached the Mesozoic cover, rather than inverting the normal fault segments across the supra-salt cover, a nearly horizontal short-cut developed, propagating to the N within the Middle Muschelkalk evaporites, producing the deduced ramp–flat geometry (Fig. 7a).

It continued to the N, shallowing progressively as the Mesozoic cover became thinner towards the N, cutting across a fragment of the acoustic basement in the footwall of the Castellote fault (Fig. 6), and in the footwall of the main normal faults, incorporating the acoustic basement into the thrust sheets and transporting it to the N within the thin-skinned fold-and-thrust belt (Figs 6, 7). The sole thrust ends up in the Calanda thrust sheet, expressed at the surface as the Calanda anticline (Figs 6, 7a). As previously explained, wavelengths of the contractional structures decrease to the N, as a result of the thinning of the Mesozoic cover (Fig. 7a).

About 22 km N of the Calanda anticline, an isolated outcrop of Paleozoic rocks is found among the Cenozoic rocks of the Ebro foreland basin, the Puig Moreno outcrop (Fig. 1). In order to explain it, Salas *et al.* (2001) interpreted a more frontal basement thrust which towards the S branches to the Maestrat Basement Thrust.

The 12–13 km displacement of the basement above the ramp of the Maestrat Basement Thrust uplifted the 40 km wide area, in the N–S direction, bounded to the N by the Calders monocline, developed above the transition from ramp to flat (Nebot & Guimerà, 2016), during the Late Oligocene – Early Miocene (González, Guimerà & Luzón, 1998).The upper segments of the Mesozoic normal faults across the supra-salt cover were

http://dx.doi.org/10.1017/S001675681600090X

passively transported to the N above the sole thrust flat, experiencing low internal deformation, as this accumulated in the northern external zone, which developed the *N FAT belt* (Fig. 7).

The low angle of the Calders monocline fault-bend fold, and the width of the uplifted area, implies a low dip for the Maestrat Basement Thrust ramp (Nebot & Guimerà, 2016), which was estimated at *c.* 9°, extending southwards for more than 40 km (Fig. 7). The Variscan basement must be involved above this ramp (Nebot & Guimerà, 2016), as it reaches a depth of *c.* 8 km in the upper crust (Fig. 7d). North of it, the acoustic basement fragments incorporated in the thin-skinned thrust system could contain only the Lower Muschelkalk and the Buntsandstein, which vary between 70 and 380 m thick in the exploration wells (Lanaja, 1987), probably having their detachment level at the Buntsandstein top evaporites (Röt facies), as has been deduced in other structures of the Iberian Chain (Ortí, 1981; Guimerà, 1988).

Restoring the Mesozoic supra-salt cover to the end of the Early Cretaceous, the traces at the surface of the normal faults should be displaced southwards a minimum of 12 km (Fig. 7c). The Bordón and Ortells faults become located *c.* 6 km north of the southern antiformal hinge of the Calders monocline, i.e. the Maestrat Basement Thrust transition from ramp to flat (Fig. 7c). In order to link these traces at the surface with the Maestrat Basement Thrust in the acoustic basement, the dip of the normal fault surface across the supra-salt cover should be of *c.* 30°, similar to that obtained in the idealized cross-section for the Ortells fault (Fig. 7a). This indicates that in the area studied, the Maestrat Basement Thrust can be the result of the Cenozoic inversion of the Bordón and the Ortells normal faults (at least its western part), giving additional support to the interpretation of Nebot & Guimerà (2016) that the Maestrat Basement Thrust was the result of the inversion of the Mesozoic normal fault system. The Mesozoic normal faults located N of the Bordón and Ortells faults were cut, during the Cenozoic contraction, by the nearly horizontal short-cut developed within the Middle Muschelkalk detachment, and were transported northwards together with the supra-salt Mesozoic cover. The lower segments of these faults across the acoustic basement should be found in the footwall of the sole thrust, in a more internal position, similarly to the Castellote fault (Fig. 7a).

The orientation and position of the restored normal faults (Fig. 7c) suggest that the present-day arched geometry (salient) of the fold-and-thrust belt (Fig. 2) was partially inherited, as the normal faults during the Mesozoic broadly display an arched geometry (Fig. 7c). During the Cenozoic contraction, this normal fault system was transported northwards within the thrust system, with differential transport, major in the central part, decreasing laterally. In this case, only gentle vertical axis rotation of structures was needed to develop the salient geometry displayed by the fold-and-thrust belt.

7. Conclusions

The Portalrubio–Vandellòs fold-and-thrust belt is the emergence of the Maestrat Basement Thrust, which is the sole thrust of the Cenozoic contractional system. The deep geometry of the latter was deduced after the Calders Monocline, interpreted as a fault-bend fold above a ramp to flat transition. The up-ramp displacement of this basement thrust sheet generated a 40 km wide uplifted area, bounded to the N by the Calders Monocline. Modelling the previous data with the Move® software, a 9° dip for the deep ramp was deduced, extending more than 40 km southwards in the NNE–SSW orientation, and reaching a depth of 7.5 km.

The shortening is estimated to be *c.* 12 km, mostly concentrated at the surface in the northern margin of the thrust belt, being the tectonic displacement towards the NNE. As the sole thrust reached the Mesozoic cover, it propagated through the Middle Muschelkalk evaporitic unit, producing a nearly horizontal detachment, which spread to the N.

Most of the normal faults which bounded the Mesozoic basins were passively transported to the NNE inside the hanging-wall of the Maestrat Basement Thrust, experiencing low internal deformation. Some fragments of the acoustic basement (rocks below the Middle Muschelkalk) were also included.

The palinspastic restoration of the supra-salt cover supports the idea that, in the study area, the Maestrat Basement Thrust is the result of the inversion of the Mesozoic normal fault system in its segment across the basement, and also that the Portalrubio–Vandellòs frontal belt inherited the geometry and orientation of the Mesozoic normal faults.

Acknowledgements. This work was supported by the projects INTECTOSAL (CGL2010-21968-C02-01/BTE) and CGL2008-04916/BTE. The University of Barcelona is acknowledged for a Ph.D. fellowship (APIF) to the first author. The authors also acknowledge Midland Valley and Bentley for providing the Move® and Microstation® software licences. An anonymous reviewer is acknowledged for helpful comments.

References

ALMELA, A., MANSILLA, H., QUINTERO, I. & GÓMEZ, E. 1975. *Oliete, sheet 493. Mapa Geológico de España 1:50.000. 2ª Serie. 1ª Edición*. Madrid: Servicio de Publicaciones, Ministerio de Industria y Energía.

ÁLVARO, M., CAPOTE, R. & VEGAS, R. 1979. Un modelo de evolución geotectónica para la cadena Celtibérica. *Acta Geológica Hispánica* **14**, 172–81.

ANADÓN, P. & ALBERT, J. F. 1973. Hallazgo de una fauna del Muschelkalk en el Trías del anticlinal de Calanda (Provincia de Teruel). *Acta Geológica Hispánica* **8**(5), 151–2.

AURELL, M., MELÉNDEZ, A., SAN ROMÁN, J., GUIMERÀ, J., ROCA, R., SALAS, R., ALONSO, A. & MAS, R. 1992. Tectónica sinsedimentaria distensiva en el límite Triásico-Jurásico en la cordillera ibérica. *Actas del III Congreso Geológico de España* **1**, 50–4.

BOVER-ARNAL, T., MORENO-BEDMAR, J. A., FRIJIA, G., PACUAL-CEBRIAN, E. & SALAS, R. 2015. Chronostratigraphy of the Barremian–Early Albian of the Maestrat Basin (E Iberian Peninsula): integrating strontium-isotope stratigraphy and ammonoid biostratigraphy. *Newsletters on Stratigraphy*, **49**(1), 41–68.

CANÉROT, J., CRESPO-ZAMORANO, A. & NAVARRO-VÁZQUEZ, D. 1977. *Montalbán, sheet 518. Mapa Geológico de España 1:50.000. 2ª Serie. 1ª Edición*. Madrid: Servicio de Publicaciones, Ministerio de Industria y Energía.

CANÉROT, J. & LEYVA, F. 1972. *Peñarroya de Tastavins, sheet 520. Mapa Geológico de España 1:50.000. 2ª Serie. 1ª Edición*. Madrid: Servicio de Publicaciones, Ministerio de Industria y Energía.

CANÉROT, J. & PIGNATELLI, R. 1972. *Aguaviva, sheet 519. Mapa Geológico de España 1:50.000. 2ª Serie. 1ª Edición*. Madrid: Servicio de Publicaciones, Ministerio de Industria y Energía.

CANÉROT, J. & PIGNATELLI, R. 1977. *Mosqueruela, sheet 569. Mapa Geológico de España 1:50.000. 2ª Serie. 1ª Edición*. Madrid: Servicio de Publicaciones, Ministerio de Industria y Energía.

ESNAOLA, J. M. & CANÉROT, J. 1972. *Albocácer, sheet 570. Mapa Geológico de España 1:50.000. 2ª Serie. 1ª Edición*. Madrid: Servicio de Publicaciones, Ministerio de Industria y Energía.

GAUTIER, F. 1978. *Alcalà de la Selva, sheet 568. Mapa Geológico de España 1:50.000. 2ª Serie. 1ª Edición*. Madrid: Servicio de Publicaciones, Ministerio de Industria y Energía.

GAUTIER, F. 1979. *Villarluengo, sheet 543. Mapa Geológico de España 1:50.000. 2ª Serie. 1ª Edición*. Madrid: Servicio de Publicaciones, Ministerio de Industria y Energía.

GONZÁLEZ, A. 1989. Análisis tectosedimentario del terciario del borde SE de la Depresión del Ebro (sector bajoaragonés) y de las cubetas ibéricas marginales. Ph.D. thesis, Universidad de Zaragoza, Zaragoza, Spain, 507 pp. Published thesis.

GONZÁLEZ, A., GUIMERÀ, J. & LUZÓN, A. 1998. Edad Oligoceno superior-Mioceno inferior para las superficies de erosión conservadas en el flanco SW de la cubeta de Bordón (Província de Teruel, España). *Geogaceta* **24**, 155–8.

GUIMERÀ, J. 1984. Palaeogene evolution of deformation in the northeastern Iberian Peninsula. *Geological Magazine* **121**(5), 413–20.

GUIMERÀ, J. 1988. Estudi estructural de l'Enllaç entre la Serralada Ibérica i la Serralada Costanera Catalana. Ph.D. thesis, Universitat de Barcelona, Barcelona, Spain. Published thesis. Available at: http://www.tesisenred.net/handle/10803/1936

GUIMERÀ, J. 2004. Cadenas con cobertera: Las Cadenas Ibérica i Costera Catalana. In *Geología de España* (ed. J. A. Vera), pp. 602–7. Madrid: Sociedad Geológica de España & Instituto Geológico y Minero de España.

GUIMERÀ, J. & ÁLVARO, M. 1990. Structure et évolution de la compression alpine dans la Chaîne Ibérique et la Chaîne côtière catalane (Espagne). *Bulletin de la Société Géologique de France* **8**, VI(2), 339–48.

GUIMERÀ, J., GONZÁLEZ, A., SALAS, R. & SANCHO, C. 2010. Origin and preservation of the late contractional relief of an intraplate thrust-belt: the NE Iberian Chain (Iberian Peninsula). *Geophysical Research Abstracts* **12**, EGU2010–5137.

GUIMERÀ, J., MAS, R. & ALONSO, A. 2004. Intraplate deformation in the NW Iberian Chain: Mesozoic extension and Tertiary contractional inversion. *Journal of the Geological Society, London* **161**, 291–303.

LANAJA, J. M. 1987. *Contribución de la exploración petrolífera al conocimiento de la geología de España*. Instituto Tecnológico GeoMinero de España, 465 pp.

MARÍN, PH. & DUVAL, B. 1976. *Castelseras, sheet 495. Mapa Geológico de España 1:50.000. 2ª Serie. 1ª Edición*. Madrid: Servicio de Publicaciones, Ministerio de Industria y Energía.

MARÍN, PH., PALLARD, B., DUVAL, B. & DE MIROSCHEDJI, A. 1974. *Calanda, sheet 494. Mapa Geológico de España 1:50.000. 2ª Serie. 1ª Edición*. Madrid: Servicio de Publicaciones, Ministerio de Industria y Energía.

MARSHAK, S. 2004. Salients, recesses, arcs, oroclines, and syntaxes: a review of ideas concerning the formation of map-view curves in fold-and-thrust belts. In *Thrust Tectonics and Hydrocarbon Systems* (ed. K. R. McClay), pp. 131–56. American Association of Petroleum Geologists, Memoir no. 82.

MARTÍN, L., LEYVA, F. & CANÉROT, J. 1972. *Morella, sheet 545. Mapa Geológico de España 1:50.000. 2ª Serie. 1ª Edición*. Madrid: Servicio de Publicaciones, Ministerio de Industria y Energía.

NAVARRO-VÁZQUEZ, D., CRESPO-ZAMORANO, A., PÉREZ-CASTAÑO, A. & CANÉROT, J. 1972. *Forcall, sheet 544. Mapa Geológico de España 1:50.000. 2ª Serie. 1ª Edición*. Madrid: Servicio de Publicaciones, Ministerio de Industria y Energía.

NEBOT, M. & GUIMERÀ, J. 2016. Structure of an inverted basin from subsurface and field data: the Late Jurassic–Early Cretaceous Maestrat basin (Iberian Chain). *Geologica Acta*, **14**(2), 155–77.

ORTÍ, F. 1981. Diapirismo de materiales triásicos y estructuras de zócalo, en el sector central valenciano (España). *Estudios Geológicos* **37**(3–4), 245–57.

SALAS, R. & GUIMERÀ, J. 1996. Rasgos estructurales principales de la cuenca cretácica inferior del Maestrazgo (Cordillera Ibérica oriental). *Geogaceta* **20**(7), 1704–6.

SALAS, R., GUIMERÀ, J., MAS, R., MARTÍN-CLOSAS, C., MELÉNDEZ, A. & ALONSO, A. 2001. Evolution of the Mesozoic Central Iberian Rift System and its Cainozoic inversion (Iberian chain). In *Peri-Tethys memoir, 6: Peri-Tethyan Rift/Wrench Basins and Passive Margins* (eds P. A. Ziegler, W. Cavazza, A. H. F. Robertson & S. Crasquin-Soleau), pp. 145–86. Mémoires de Muséum National d'Histoire Naturelle, no. 186.

SIMÓN, J. L. 1980. Estructuras de superposición de plegamientos en el borde NE de la cadena Ibérica. *Acta Geológica Hispánica* **15**(5), 137–40.

SIMÓN, J. L. 2004. Superposed buckle folding in the Eastern Iberian Chain, Spain. *Journal of Structural Geology* **26**, 1447–64.

APPENDIX II. A

La extensión Triásica en el substrato de la Cuenca del Maestrat, y evidencias de tectónica salina en las evaporitas en facies Muschelkalk medio (Cadena Ibérica Oriental).

IX Congreso Geológico de España. Huelva, 12-14 de septiembre 2016
Póster. Sesión T2- Geología Sedimentaria

La extensión Triásica en el substrato de la Cuenca del Maestrat, y evidencias de tectónica salina en las evaporitas en facies Muschelkalk medio (Cadena Ibérica Oriental)

Triassic extension in the Maestrat basin substratum, and evidences of Middle Muschelkalk facies salt tectonics (Eastern Iberian Chain)

M. Nebot[1], J. Guimerà[1]

1 GEOMODELS Research Institute, Departament de Geodinàmica i Geofísica, Facultat de Geologia, Universitat de Barcelona (UB), Martí i Franquès s/n, 08028 Barcelona, Spain. marinanebotmiralles@gmail.com, joan.guimera@ub.edu

Resumen: La Cuenca del Maestrat fue una de las más subsidentes del sistema de rift Ibérico, desarrollado durante el Mesozoico. Durante la primera etapa de extensión (Pérmico Superior-Triásico Superior) se desarrolló un sistema de fallas extensivas de alto ángulo que compartimentaron el zócalo varisco en un sistema de *horsts*, *grabens* y *semigrabens*. Estas fallas habrían sido activas durante el depósito de la facies Buntsandstein, hasta depositarse los sedimentos en facies Muschelkalk medio, al menos su parte inferior, que rellena el sistema de *horsts* y *grabens* originando importantes diferencias de espesor en esta facies. La parte alta de ésta, en cambio, rebasa y recubre los *horsts*, indicando una disminución de la actividad extensiva que duró hasta depositarse los carbonatos en facies Muschelkalk superior, de potencia casi constante. Durante el depósito de la facies Keuper se reactivaron algunas fallas de zócalo, desencadenando migraciones de sal del Muschelkalk medio, que formó anticlinales de sal y *welds*, aumentando las diferencias de potencia deposicionales de esta facies. La edad del flujo de sal se deduce a partir de los reflectores del Keuper, que se disponen en *onlap* sobre el Muschelkalk superior plegado sobre las acumulaciones de sal. Además, estos reflectores de la facies Keuper también forman abanicos de capas sobre pliegues forzados del Muschelkalk superior sobre algunas fallas de zócalo reactivadas.

Palabras clave: rifting, Triásico, evaporitas, tectónica salina

Abstract: *The Maestrat Basin was one of the most subsident basins of the Mesozoic Iberian Rift System. During the first stage of extensional activity (Late Permian-Late Triassic) a high angle normal fault system developed, which fragmented the Variscan basement into a system of horsts, grabens and half-grabens. Those faults were active during the deposition of the Buntsandstein facies and lasted until the lower part of the Middle Muschelkalk facies was deposited, filling the system of horsts and grabens and generating depositional thickness variations. The fault system was overstepped by the upper part of the Middle Muschelkalk, indicating a decrease in the extensional activity that lasted until the carbonates of the Upper Muschelkalk facies were deposited, as they present nearly constant thickness. During the Keuper facies deposition, the extensional activity of some normal faults in the acoustic basement resumed, triggering the Middle Muschelkalk salt flow, which developed salt anticlines and welds, increasing the depositional thickness variations of this facies. The age of the salt flow is deduced from the Keuper facies reflectors lapping on the folded Upper Muschelkalk above the salt accumulations. Growth-strata above some Upper Muschelkalk forced folds are also recognized, developed above some reactivated normal faults in the basement.*

Key words: *rifting, Triassic, evaporites, salt tectonics*

INTRODUCCIÓN

La zona de estudio se sitúa en la parte central de la Cuenca mesozoica del Maestrat, localizada en el extremo oriental de la Cadena Ibérica (Fig. 1). La Cadena Ibérica es el resultado de la inversión del sistema de rift Ibérico, que experimentó dos máximos de actividad extensiva: Pérmico Superior-Triásico y Oxfordiense Superior-Albiense Superior (Salas et al., 2010). La Cuenca del Maestrat, desarrollada durante el segundo episodio extensivo, fue una de las más subsidentes de este sistema de rift. El hecho de que algunos de los materiales depositados durante el primer episodio extensivo no afloren en gran parte de la Cuenca del Maestrat ha hecho que la afectación de este episodio en el substrato de la cuenca no sea tan conocida como la del segundo. El análisis de los perfiles sísmicos obtenidos en los años 70 y 80 del

Siglo XX, así como de los sondeos disponibles (Fig. 1), han permitido analizar con mayor precisión esta primera etapa extensiva.

El objetivo de este trabajo es caracterizar más detalladamente la estratigrafía y la estructura de la parte central de la Cuenca del Maestrat durante el episodio de rifting del Pérmico Superior-Triásico, así como estudiar las variaciones de espesor y las acumulaciones de evaporitas en facies Muschelkalk medio previamente descritas por Bartrina y Hernández (1990) en la Cuenca del Maestrat. En esta zona, igual que en la Cuenca del Ebro (Butillé et al., 2012) la tectónica salina está localizada en los materiales en facies Muschelkalk medio, a diferencia de lo que ocurre en la mayor parte de la Península Ibérica, donde las estructuras salinas se desarrollaron en las evaporitas en facies Keuper.

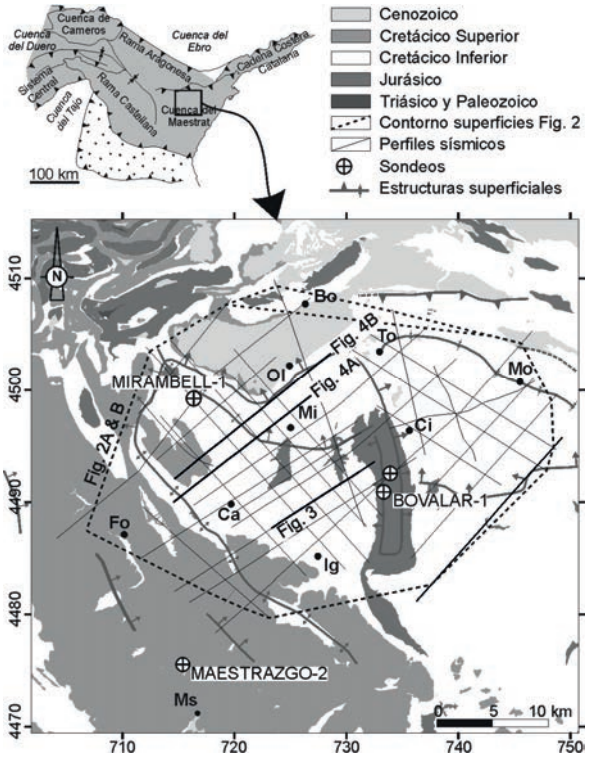

FIGURA 1. *A: Mapa de situación de la zona de estudio, en la parte central de la Cuenca del Maestrat. En gris, áreas con zócalo involucrado; en punteado, áreas con sólo la cobertera involucrada. B: Mapa geológico simplificado de la zona de estudio y localización de los perfiles sísmicos y los sondeos analizados. Abreviaciones de localidades: Bo-Bordón, Ca-Cantavieja, Ci-Cinctorres, Fo-Fortanete, Ig-Iglesuela del Cid, Mi-Mirambell, Mo-Morella, Ms-Mosqueruela, Ol-Olocau del Rey.*

CONTEXTO GEOLÓGICO

La extensión triásica estuvo relacionada con la propagación hacia el oeste del sistema de rift del Tethys y hacia el sur del sistema de rift Ártico-Atlántico norte. Más tarde, durante el Oxfordiense superior-Albiense superior, la apertura del Atlántico norte y el Golfo de Vizcaya ocasionó un segundo período de rift. Ambos episodios extensivos fueron seguidos de episodios de menor actividad extensiva durante el Hettangiense superior-Oxfordiense y el Cretácico superior-Paleoceno (Salas et al., 2010). Durante el Paleógeno, este sistema extensivo se invirtió, relacionado con la orogenia Alpina.

El Triásico depositado en el substrato de la Cuenca del Maestrat está representado en facies germánica, conteniendo varias intercalaciones de evaporitas, las principales en las facies Muschelkalk medio y Keuper. La facies Muschelkalk medio está formada por halita, anhidrita e intercalaciones de lutita (Lanaja, 1987; Martínez-Abad, 1991), y actuó como despegue principal durante la contracción cenozoica (Nebot y Guimerà, 2016), diferenciando dos paquetes estructurales: la cobertera supra-salina, y el zócalo infra-salino o acústico, que incluye el Muschelkalk inferior, el Buntsandstein y el zócalo varisco.

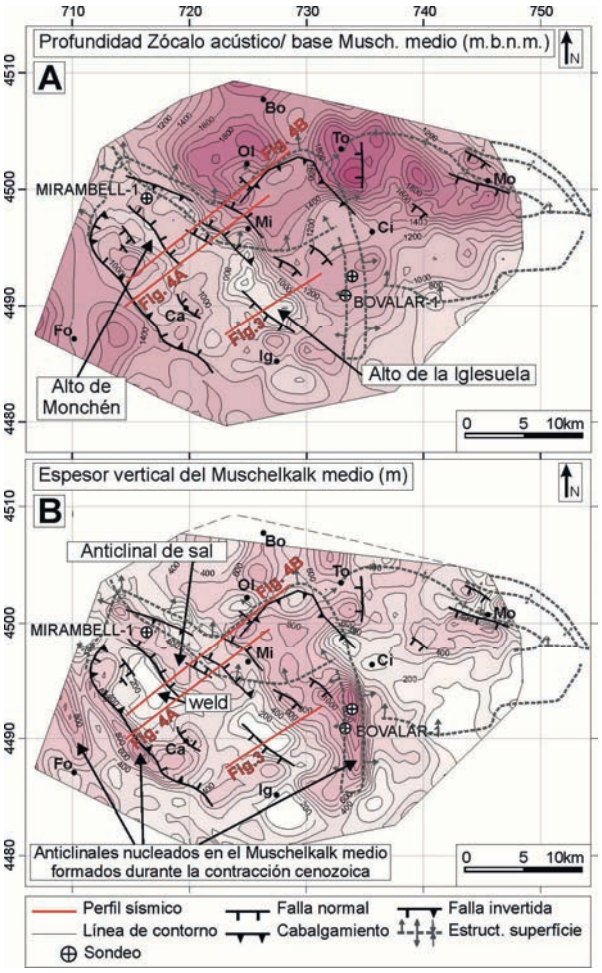

FIGURA 2. *A: Mapa de contornos de la profundidad del zócalo acústico o base del Muschelkalk medio, en metros bajo el nivel del mar (m.b.n.m.). B: Mapa de isopacas del Muschelkalk medio.*

METODOLOGÍA

Se han analizado 29 perfiles sísmicos de reflexión obtenidos entre 1973 y 1988 por *Auxini*, *Campsa* y *Shell*, y 4 sondeos. Las imágenes de los perfiles sísmicos fueron convertidas a formato seg-y mediante

la aplicación de Matlab IMAGE2SEGY (Farran, 2008) y posteriormente interpretadas en un contexto georreferenciado. La malla de perfiles sísmicos disponibles (Fig. 1) nos permitió reconstruir un mapa de contornos de la profundidad del zócalo acústico (Fig. 2A) así como el espesor vertical de la facies Muschelkalk medio (Fig. 2B).

ESTRUCTURA EXTENSIVA

Tal y como se muestra en la Fig. 2A, el zócalo acústico está fragmentado por fallas de alto ángulo, que forman un sistema de *horsts*, *grabens* y *semigrabens*. En la zona se pueden identificar dos *horsts* con orientación NW-SE (Fig. 2A): el alto de basamento de Monchén, y el alto de basamento de la Iglesuela (Fig. 3), ambos limitados por fallas normales con la misma orientación (Nebot y Guimerà, 2016). Al analizar los perfiles sísmicos se observan grandes cambios de espesor de la facies Muschelkalk medio, tal y como se muestra en el mapa de espesores de esta unidad. Si se analizan junto con el mapa de contornos de la base de esta unidad (Fig. 2A) se puede observar que los espesores máximos de la facies Muschelkalk medio coinciden con bloques hundidos del zócalo acústico, mientras que los espesores mínimos coinciden con altos de basamento.

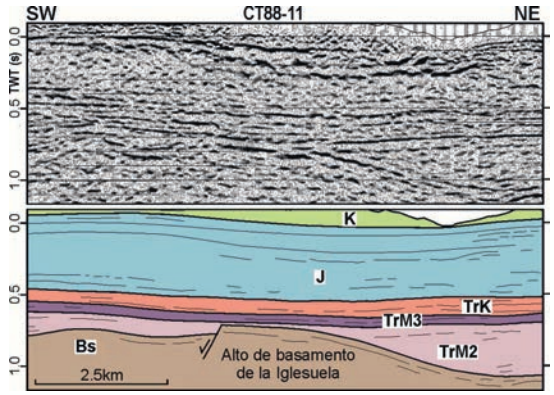

FIGURA 3. *Perfil sísmico CT88-11 y su interpretación. Se muestran los cambios de espesor deposicionales de la facies Muschelkalk medio. Ver localización en la Fig. 1. Abreviaciones: K-Cretácico, J-Jurásico, TrK-Keuper, TrM3-Muschelkalk superior, TrM2-Muschelkalk medio, Bs-Zócalo acústico.*

Considerando la capacidad para fluir de las evaporitas de la facies Muschelkalk medio, no se puede asegurar por completo que las fallas de basamento fueran activas durante el depósito de esta, pero la distribución de espesores observada hace pensar que al menos su parte inferior se depositó durante la extensión. Por el contrario, la parte alta de la facies Muschelkalk medio rebasa y recubre las estructuras de zócalo, indicando una disminución de la extensión durante su depósito (Fig. 3). Pese a que las unidades que forman el zócalo acústico no se pueden distinguir en los perfiles sísmicos, los estudios previos (Álvaro et al., 1979; Salas et al., 1997; Bartrina y Hernández, 1990) sugieren que las fallas que afectan el zócalo habrían sido activas durante el depósito de la facies Buntsandstein (Pérmico Superior-Triásico Inferior), hasta el depósito de la parte baja de la facies Muschelkalk medio (Triásico Medio). Esta estructura está cubierta por una cobertera supra-salina indeformada (Fig. 3), que indica que los principales cambios de espesor de la facies Muschelkalk medio son deposicionales, y que no variaron después de su depósito, a excepción del episodio de tectónica salina ocurrido con posterioridad. La potencia de los carbonatos en facies Muschelkalk superior es prácticamente constante, lo que implica la finalización de la actividad de las fallas activas durante la sedimentación de las unidades anteriores.

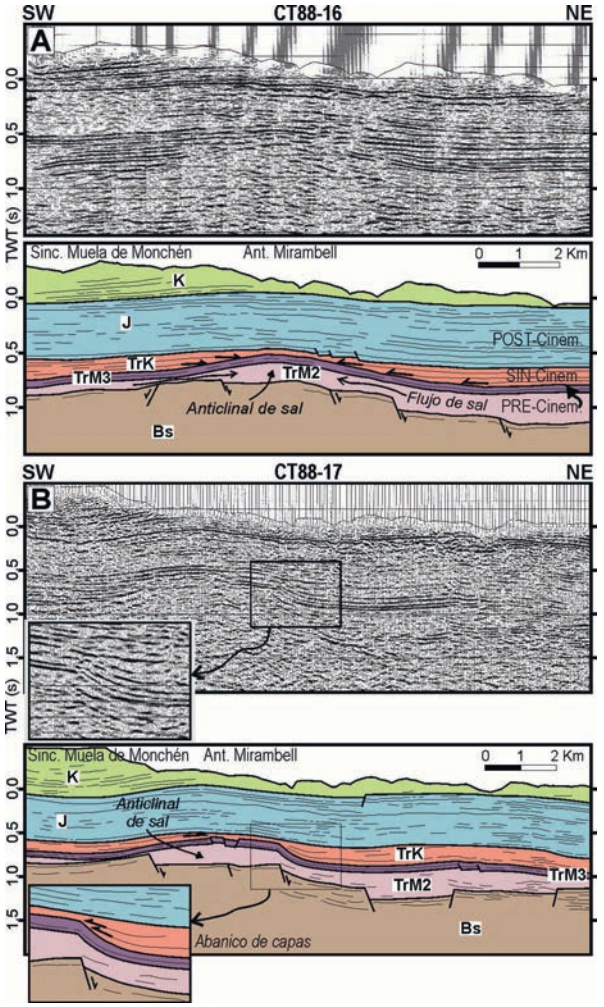

FIGURA 4. *A: Perfil sísmico CT88-16 y su interpretación. Se muestra un anticlinal de sal de la facies Muschelkalk medio y los reflectores del Keuper en onlap sobre el Muschelkalk superior plegado por la acumulación de sal. Pre-, sin-, y post-cinemático se refieren al flujo de sal. B: Perfil sísmico CT88-17 y su interpretación. Se muestra un pliegue forzado del Muschelkalk superior sobre una falla de zócalo reactivada durante el depósito de la facies Keuper, que forma un abanico de capas sobre el pliegue. Ver localización en la Fig. 1.*

DEFORMACIÓN SALINA

Los perfiles sísmicos sugieren que hubo migración de sal de la facies Muschelkalk medio ya que se

observan estructuras salinas relacionadas con esta facies, como anticlinales de sal y *welds* (Fig. 4). Los carbonatos en facies Muschelkalk superior se encuentran plegados por las acumulaciones de sal, mientras que los reflectores de la facies Keuper se disponen en *onlap* sobre el Muschelkalk superior plegado (Fig. 4A). También se pueden observar abanicos de capas (Fig. 4B) en los reflectores de la facies Keuper sobre pliegues forzados del Muschelkalk superior, que sugieren la reactivación de fallas extensivas de zócalo durante el depósito de la facies Keuper. Esta reactivación de la extensión durante el depósito de la facies Keuper (Triásico Superior) podría ser la responsable de la migración de sal del Muschelkalk medio, que se habría potenciado por las diferencias de carga ejercidas por las variaciones laterales de espesor de la facies Keuper, que se depositó adaptándose al Muschelkalk superior plegado.

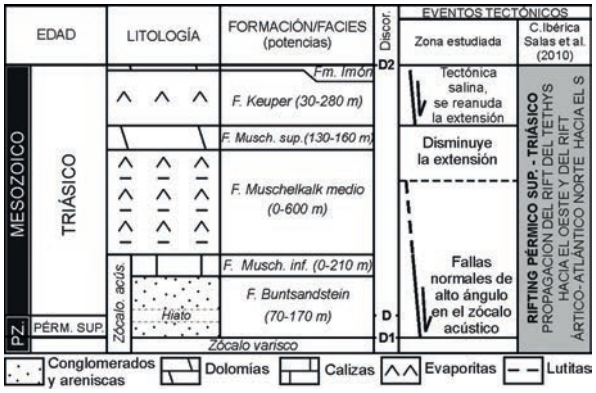

FIGURA 5. *Esquema tectonoestratigráfico del Triásico en la parte central de la Cuenca del Maestrat.*

CONCLUSIONES

Durante el episodio de rifting del Pérmico Superior-Triásico se fragmentó el basamento acústico en un sistema de *horsts*, *grabens* y *semi-grabens* limitados por fallas normales de alto ángulo que fueron activas durante el depósito de la facies Buntsandstein, hasta el depósito de la parte inferior de la facies Muschelkalk medio (Fig. 5). Esta última presenta importantes cambios de espesor deposicionales. La actividad extensiva disminuyó durante el depósito de la parte superior de la facies Muschelkalk medio y la facies Muschelkalk superior, que presenta una potencia casi constante en toda la cuenca del Maestrat. Los perfiles sísmicos muestran indicios de tectónica salina afectando a la facies Muschelkalk medio, que forma anticlinales de sal y *welds*, aumentando las diferencias de potencia deposicional de ésta. Los reflectores de la facies Keuper recubren y se disponen en *onlap* sobre el Muschelkalk superior plegado sobre las acumulaciones de sal, pudiéndose diferenciar en algún caso abanicos de capas en los reflectores del Keuper sobre fallas normales en el zócalo acústico. Esto indica que, tras depositarse la facies Muschelkalk superior y durante el depósito de la facies Keuper, se reactivaron algunas fallas normales en el basamento acústico, provocando los desplazamientos de la sal del Muschelkalk medio y pliegues forzados en el Muschelkalk superior sobre algunas fallas reactivadas.

AGRADECIMIENTOS

Este trabajo ha sido financiado por los proyectos INTECTOSAL (CGL2010-21968-C02-01/BTE) y CGL2008-04916/BTE. El primer autor agradece a la Universitat de Barcelona la financiación recibida mediante una beca de doctorado APIF.

REFERENCIAS

Álvaro, M., Capote, R. y Vegas, R. (1979): Un Modelo de evolución geotectónica para la cadena Celtibérica. *Acta Geológica Hispánica*, 14: 172-181.

Bartrina, T. y Hernández, E. (1990): Las unidades evaporíticas del Triásico del subsuelo del Maestrazgo. En: *Formaciones evaporíticas de la Cuenca del Ebro y cadenas periféricas, y de la zona de Levante. Nuevas aportaciones y guía de superficie*. (F. Ortí y J.M. Salvany, eds.). ENRESA –Dep. Geoq. Prosp. Petrol. (UB), Barcelona, 34-38.

Butillé, M., Ferrer, O., Granado, P., Roca, E., Muñoz, J.A., Ballesteros, J.C., Giménez, A., Vallejo, R.A. y González, P. (2012): Evidencias de deformaciones salinas en las sucesiones mesozoicas del sector sur de la Cuenca del Ebro. En: *VIII Congreso Geológico de España*, Geo-Temas, 13: 176.

Farran, M. (2008): IMAGE2SEGY: A software to convert seismic profiles images to SEG Y files. En: *VII Congreso Geológico de España*. Geo-Temas, 10: 1215-1218.

Lanaja, J.M. (1987): *Contribución de la exploración petrolífera al conocimiento de la geología de España*. Instituto Tecnológico GeoMinero de España, Madrid, 465 p.

Martínez-Abad, J.L. (1991): Cuenca del Maestrazgo. Correlación de sondeos I-I'. En: *Estudio geológico del Maestrazgo y de la mitad meridional de los Catalánides* (F. López, coord.). INYPSA-IGME, inédito.

Nebot, M. y Guimerà, J. (2016): Structure of an inverted basin from subsurface and field data: the Late Jurassic-Early Cretaceous Maestrat basin (Iberian Chain). *Geologica Acta*. En prensa.

Salas, R., Guimerà, J., Gimènez-Montsant, J., Martín-Closas, C. y Roca, E. (1997): *Mesozoic Rift structure, Stratigraphy and Palaeogene Inversion of the Maestrat basin. Iberian Range (NE Spain). Field trip guide*. IGCP Project-369. Comparative evolution of PeriTethyan Rift Basins, 70 p.

Salas, R., García-Senz, J., Guimerà, J. y Bover-Arnal, T. (2010): Opening of the Atlantic and development of the Iberian intraplate rift basins during the late Jurassic-early Cretaceous. En: *II Central and North Atlantic Conjugate Margins Conference*, 245-248.

APPENDIX II. B

Inversión cenozoica de la Cuenca mesozoica del Maestrat: evolución cinemática del cinturón de pliegues y cabalgamientos desarrollado en su margen norte (Cadena Ibérica oriental).

IX Congreso Geológico de España. Huelva, 12-14 de septiembre 2016
Comunicación oral. Simposio S10-del Cinturón Varisco al Sistema Alpino: tectónica y neotectónica de Iberia. Simposio en homenaje a Ramón Capote.

Inversión cenozoica de la Cuenca mesozoica del Maestrat: evolución cinemática del cinturón de pliegues y cabalgamientos desarrollado en su margen norte (Cadena Ibérica oriental).

Cenozoic inversion of the Mesozoic Maestrat Basin: kinematic evolution of the fold-and-thrust belt developed in its northern margin (Eastern Iberian Chain).

M. Nebot[1], J. Guimerà[1]

1 GEOMODELS Research Institute, Departament de Geodinàmica i Geofísica, Facultat de Geologia, Universitat de Barcelona (UB), Martí i Franquès s/n, 08028 Barcelona, Spain. marinanebotmiralles@gmail.com, joan.guimera@ub.edu.

Resumen: La Cuenca del Maestrat fue una de las más subsidentes del Sistema de Rift Ibérico durante el Jurásico superior-Cretácico inferior. Se generó mediante un sistema de fallas extensivas que la dividían en sub-cuencas. Este sistema se invirtió durante el Cenozoico, desarrollándose el Cabalgamiento de Zócalo del Maestrat, que atraviesa la cuenca de E a W, con vergencia N, como resultado de la inversión de la falla basal mesozoica en el zócalo. Al alcanzar la cobertera mesozoica, este cabalgamiento se propagó por el nivel de despegue del Muschelkalk medio, transportando la cobertera supra-salina, y los segmentos de fallas normales a través de ésta, hacia el NNE, unos 11-13 km. El cabalgamiento resultante se deduce que tiene una geometría de rampa-rellano, con una rampa de bajo ángulo que alcanza una profundidad de unos 8 km, enraizada en la corteza superior. El desplazamiento del zócalo en el bloque superior de esta rampa generó una zona elevada de 40 km de ancho en dirección N-S, limitada al norte por el monoclinal de Calders, que se interpreta como un pliegue de adaptación al paso de rampa a rellano de la falla en el zócalo, y que marca también el tránsito de un estilo estructural de piel gruesa al S, a piel fina al N. El acortamiento en superficie se acumuló en el margen norte de la cuenca, donde la cobertera es más delgada, formando el cinturón de pliegues y cabalgamientos de Portalrubio-Vandellòs.

Palabras clave: Inversión tectónica, cinturón de pliegues y cabalgamientos, relieve tectónico, rampa de bajo ángulo, Cadena Ibérica.

Abstract: *The Maestrat basin was one of the most subsident basins of the Iberian Rift system during the Late Jurassic-Early Cretaceous, generated by a normal fault system which divided it into sub-basins. The E-W-trending, N-verging Maestrat Basement Thrust developed during its Cenozoic inversion, traversing the entire basin, as a result of the inversion of the Mesozoic fault system within the basement. As this thrust reached the Mesozoic cover, it propagated across the Middle Muschelkalk detachment level, transporting the supra-salt cover, and the normal fault segments within it, about 11-13 km towards the North. The basement thrust is deduced to have a ramp-flat geometry, with a low dip ramp which reaches 8 km depth, rooted in the upper crust. The displacement of the basement in the hanging wall of this ramp generated a 40 km-wide uplifted area, in the N-S direction, bounded to the N by the Calders monocline, interpreted as a fault-bend-fold adapted to the ramp to flat transition in the basement thrust. It also indicates the transition from a thick-skinned style of deformation in the S, to a thin-skinned style to the N. The superficial shortening accumulated in the northern margin of the basin, containing the thinnest Mesozoic cover, developing the Portalrubio-Vandellòs fold-and-thrust belt.*

Key words: *Basin inversion, fold-and-thrust belt, tectonic relief, low-dip ramp, Iberian Chain.*

INTRODUCCIÓN

La zona de estudio se sitúa en la Zona de Enlace (Guimerà, 1988) entre la Cadena Ibérica, de orientación NW-SE, y la Cadena Costera Catalana, de orientación NE-SW (Fig. 1). Dichas cadenas son el resultado de la inversión cenozoica del Sistema de Rift Ibérico desarrollado durante el Mesozoico. La Cuenca del Maestrat es una de las más subsidentes del sistema de Rift Ibérico durante el Jurásico superior-Cretácico inferior, con espesores de hasta 6.5 km de la serie mesozoica (Salas y Guimerà, 1996). La inversión contractiva cenozoica de la cuenca originó en su margen norte el cinturón de pliegues y cabalgamientos de Portalrubio-Vandellòs (Guimerà, 1988) de orientación aproximadamente E-W y vergencia N, despegado a favor de las evaporitas del Triásico,

mientras que hacia el sur también involucra el zócalo varisco.

El objetivo de este trabajo es estudiar el paso de un estilo estructural de piel gruesa a piel fina, así como caracterizar las estructuras desarrolladas durante cada episodio de deformación, para finalmente establecer la evolución cinemática de la zona. Con este propósito, se han tenido en cuenta datos nuevos de superficie y los datos de subsuelo disponibles, que constan de sondeos y perfiles sísmicos. El análisis de estos datos ha permitido proponer un modelo de evolución cinemática para el margen norte de la Cuenca del Maestrat. También se ha podido hacer una reconstrucción de las principales sub-cuencas en que se encontraba dividida durante el Mesozoico y de las estructuras que las limitaban, así como de las estructuras contractivas desarrolladas durante el Cenozoico, pudiéndose establecer la relación entre ambas.

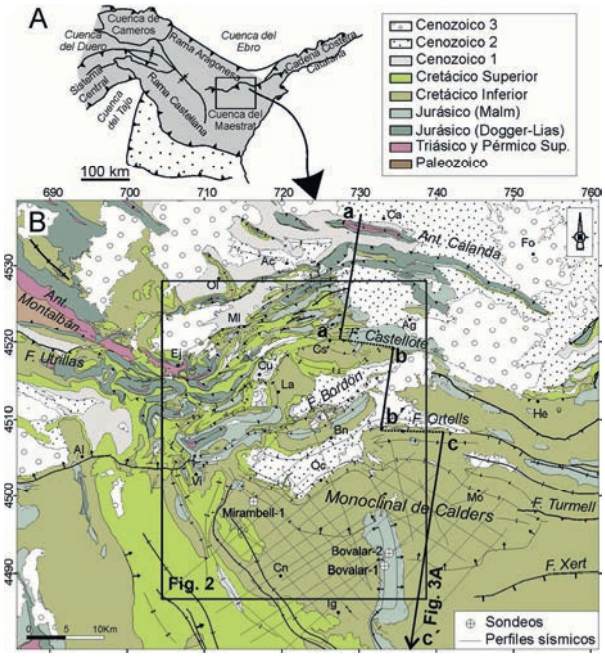

FIGURA 1. A: *Mapa estructural esquemático de la Cadena Ibérica. En gris, áreas con zócalo involucrado; en punteado, áreas con sólo la cobertera involucrada. B: Mapa geológico de la zona de estudio, situada en la Zona de Enlace entre la Cadena Costera Catalana y la Cadena Ibérica.*

CONTEXTO GEOLÓGICO

El Sistema de Rift Ibérico se desarrolló durante el Mesozoico y experimentó dos máximos de actividad extensiva: durante el Pérmico superior-Triásico, relacionado con la propagación hacia el oeste del sistema de rift del Tethys y hacia el S del sistema de rift Ártico-Atlántico norte, y durante el Oxfordiense superior-Albiense superior, relacionado con la apertura del Atlántico norte y el Golfo de Vizcaya. Ambos episodios extensivos fueron seguidos de episodios de menor actividad extensiva durante el Hettangiense superior-Oxfordiense y el Cretácico superior-Paleoceno (Salas *et al.*, 2001, 2010). Durante el Paleógeno, este sistema extensivo se invirtió, relacionado con la Orogenia Alpina. La inversión de la Cuenca del Maestrat dio lugar a la Zona de Enlace, de orientación mayoritariamente E-W, y al cinturón de pliegues y cabalgamientos de Portalrubio-Vandellòs en su parte frontal que, en la zona estudiada, presenta una geometría en arco convexo hacia el antepaís. Este cinturón de pliegues y cabalgamientos está despegado a favor de las evaporitas triásicas (Muschelkalk medio, mayoritariamente, y Keuper), aunque hacia el sur, el cabalgamiento basal pasa a involucrar el zócalo en una franja E-W (Zona de Falla del Turmell, Salas y Guimerà, 1996) en la que se produce un escalón tectónico de entre 800 y 1200m (González *et al.*, 1998; Nebot y Guimerà, 2016a).

EXTENSIÓN MESOZOICA

Durante el Malm y el Cretácico inferior, la Cuenca del Maestrat quedó dividida en diversas sub-cuencas limitadas por fallas fundamentalmente normales. En la zona estudiada, se pueden distinguir las sub-cuencas de la Salzedella y de Ladruñán, limitadas por fallas normales de diversas orientaciones conectadas por rampas de relevo (Fig. 2A). El espesor de los materiales sin-extensivos, en el conjunto del margen norte de la cuenca disminuye hacia el N, aunque en cada sub-cuenca aumenta de espesor hacia el N, hacia las fallas normales inclinadas hacia el S que las limitan (Fig. 2B). En la zona más externa de la cuenca, situada al norte de la falla de Castellote, el Cretácico inferior varía entre 0 y 300 m, donde se han interpretado fallas normales que se relevan y que generan pequeñas cuencas de Cretácico inferior sinformes y transversales a las fallas.

ESTRUCTURA CONTRACTIVA CENOZOICA

La Zona de Enlace se puede dividir en tres grandes sectores, atendiendo al estilo estructural observado (Fig. 3B). El más meridional está poco deformado, y contiene una extensa zona elevada de unos 40 km de anchura en dirección N-S, donde predominan los pliegues laxos de longitudes de onda kilométricas, despegados mayoritariamente a favor del Muschelkalk medio y algunos en el zócalo infra-salino. La zona levantada está limitada al norte por el Monoclinal de Calders, de orientación E-W, cuyo flanco frontal buza unos 6º hacia el norte y tiene una anchura de unos 13 km en su parte central, estrechándose lateralmente hasta conectar con dos fallas de zócalo. Este monoclinal se ha explicado como un pliegue de flexión de falla que se adapta a una geometría de rampa-rellano de la falla de zócalo principal. En la parte central o intermedia, situada al norte del monoclinal de Calders, las estructuras también tienen longitudes de onda kilométricas, estando despegadas a favor del Muschelkalk medio, aunque incorporan fragmentos del zócalo infra-salino en las láminas de cabalgamiento. En

la parte frontal se desarrolló el cinturón de pliegues y cabalgamientos de Portalrubio-Vandellòs (Guimerà, 1988), en que las estructuras son más apretadas, con longitudes de onda de centenares de metros a pocos kilómetros, estando despegado mayoritariamente en las evaporitas triásicas (Fig. 3A).

La dirección de transporte (NNE-SSW) se ha interpretado como perpendicular a la traza del monoclinal de Calders (Fig. 3B) y el sentido hacia el antepaís (hacia el NNE) coincidiendo con Guimerà y Álvaro (1990), y siendo perpendicular a la mayoría de las estructuras en la franja central de la zona (Fig. 1). Se ha construido un corte geológico del margen norte de la Zona de Enlace paralelo a la dirección de transporte tectónico (Fig. 3A). Este corte revela un acortamiento mínimo de unos 11 km, aunque teniendo en cuenta la anchura del flanco frontal del Monoclinal de Calders en su parte central más extensa, el acortamiento podría llegar a los 13 km. Los extensos afloramientos cenozoicos tardi a postectónicos no permitieron realizar un corte regional continuo, coincidiendo con la parte más ancha del monoclinal.

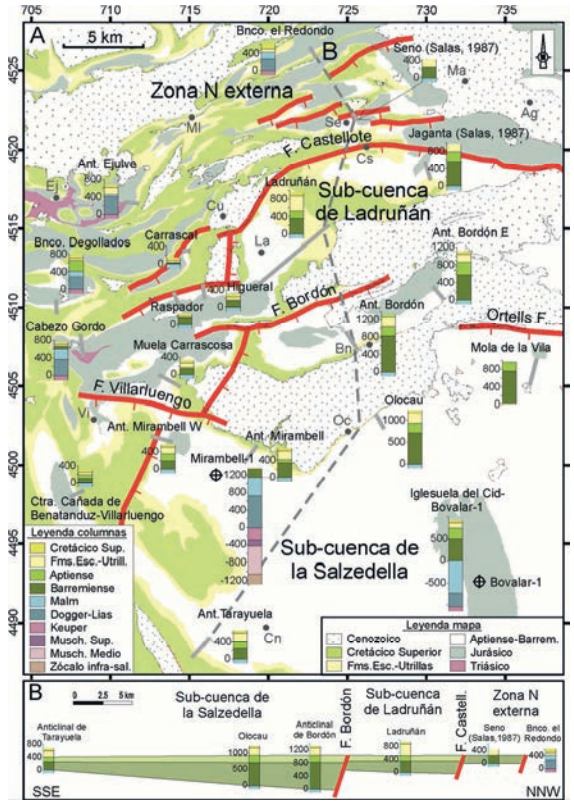

FIGURA 2. A: *Columnas estratigráficas simplificadas de la zona de estudio. B: Correlación N-S de las columnas más significativas. Se muestra como a grandes rasgos el relleno sin-extensivo del Cretácico inferior se adelgaza hacia el N, donde se sitúa el margen de la cuenca, controlado por fallas normales que buzan hacia el S y que dividieron la cuenca del Maestrat en diferentes sub-cuencas.*

EVOLUCIÓN CINEMÁTICA

Durante la contracción cenozoica se invirtió el sistema de fallas normales mesozoicas que formó la sub-cuenca de la Salzedella en su tramo a través del zócalo, lo que generó el Cabalgamiento de Zócalo del Maestrat (CZM), que atraviesa la Cuenca del Maestrat en dirección E-W. Se trata de un cabalgamiento de bajo ángulo, que buza unos 9º hacia el S, alcanzando una profundidad de unos 8 km, y que estaría enraizado en la corteza superior, coincidiendo con Seillé *et al.* (2015). Este cabalgamiento no se propagó a la cobertera supra-salina, sino que desarrolló un *short-cut* sub-horizontal que se propagó hacia el N a través del nivel de despegue del Muschelkalk medio, transportando hacia el N la cobertera supra-salina unos 11-13 km. De este modo, los segmentos de las fallas normales a través de la cobertera supra-salina no se invirtieron por completo, sino que fueron transportados hacia el norte en el bloque superior de esta falla basal. El desplazamiento del zócalo sobre la rampa de bajo ángulo del CZM, levantó un área de unos 40 km de anchura en la dirección N-S, limitada al norte por el Monoclinal de Calders, que es la manifestación en superficie del CZM, ya que su charnela S antiforme (Fig. 3B) la interpretamos como la adaptación de la lámina al paso de rampa a rellano del CZM (Fig. 3A). La charnela N sinforme, a grandes rasgos, marca el paso de un estilo estructural de piel gruesa, al S, a un estilo estructural de piel final al N. La longitud de onda de las estructuras contractivas disminuye hacia el norte, hacia el margen de la cuenca, coincidiendo con un adelgazamiento de la cobertera supra-salina. Ésta fue desplazada hacia el norte despegada en las evaporitas del Muschelkalk medio, incorporando al bloque superior de la falla basal algunos segmentos del zócalo infra-salino, sobre todo en el bloque inferior de las fallas normales principales (Fig. 3A), debido a los cambios bruscos de espesor de la cobertera que éstas generan (Nebot y Guimerà, 2016b).

CONCLUSIONES

La inversión cenozoica de la cuenca extensiva mesozoica del Maestrat generó el Cabalgamiento de Zócalo del Maestrat, resultado de la inversión de la falla basal que enraizaba el sistema de fallas normales mesozoicas. El sector de la falla en el zócalo infra-salino se invirtió, mientras que al alcanzar ésta el nivel de despegue del Muschelkalk medio se propagó a través de éste, transportando la cobertera supra-salina unos 11 a 13 km hacia el norte. El acortamiento se acumuló en superficie mayormente en la parte frontal más externa de la cuenca, coincidiendo con una cobertera más delgada, donde se generó el cinturón de pliegues y cabalgamientos de Portalrubio-Vandellòs. El desplazamiento del zócalo sobre la rampa del CZM generó una amplia zona levantada de unos 40 km de ancho, limitada al norte por el Monoclinal de Calders, que es un pliegue de adaptación al paso de rampa a rellano del CZM. El paso de un estilo estructural de piel gruesa al S a piel fina al N coincide con la charnela sinforme frontal del Monoclinal de Calders.

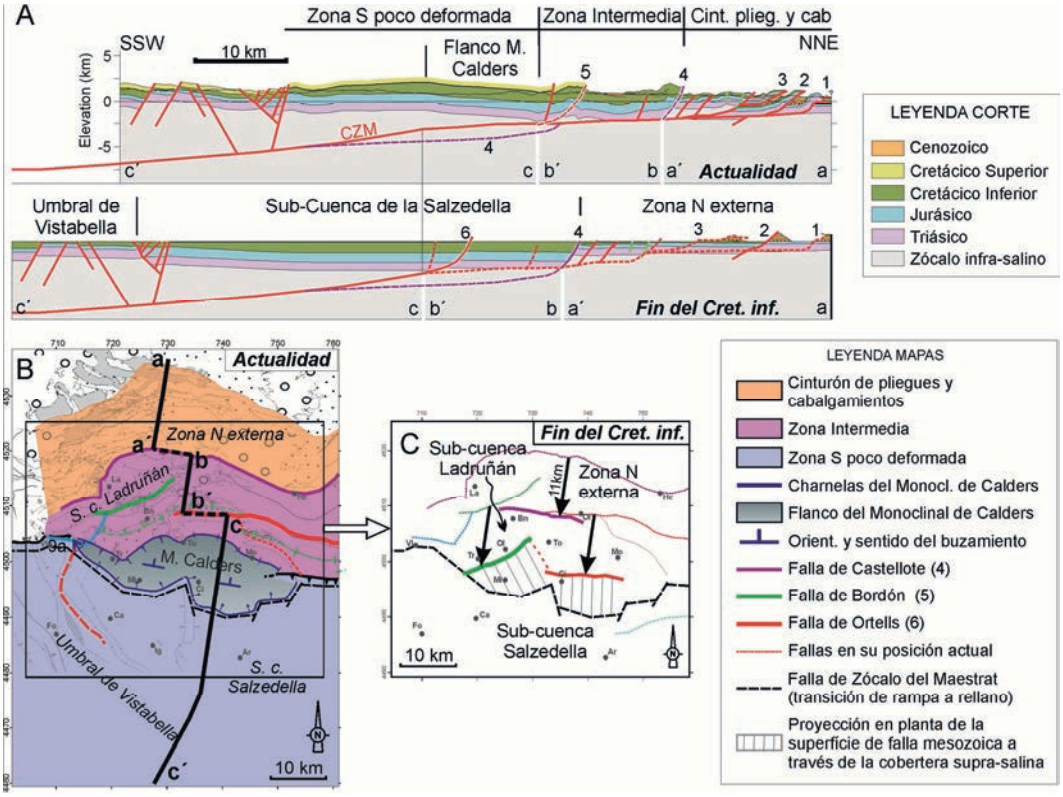

FIGURA 3. *A: Corte regional de la parte central del margen norte de la Cuenca del Maestrat. B: Principales estructuras contractivas desarrolladas durante la inversión cenozoica de la cuenca. Diferenciación en zonas según el estilo estructural. El segmento NNE-SSW de la traza del corte contiene la dirección de transporte, deducida como perpendicular a la traza del Monoclinal de Calders. C: Restitución palinspástica, antes de la contracción cenozoica, de las cuencas mesozoicas y las estructuras extensivas que las limitaban durante el Cretácico inferior.*

AGRADECIMIENTOS

Este trabajo ha sido financiado por los proyectos INTECTOSAL (CGL2010-21968-C02-01/BTE) y CGL2008-04916/BTE. El primer autor agradece a la Universitat de Barcelona la financiación recibida mediante una beca de doctorado APIF.

REFERENCIAS

González, A., Guimerà, J. y Luzón, A. (1998): Edad Oligoceno superior-Mioceno inferior para las superficies de erosión conservadas en el flanco SW de la cubeta de Bordón (Província de Teruel, España). *Geogaceta*, 24: 155-158.

Guimerà, J. (1988): *Estudi estructural de l'Enllaç entre la Serralada Ibérica i la Serralada costanera Catalana*. Tesis Doctoral, Univ. de Barcelona, 600 p.

Guimerà, J. y Álvaro, M. (1990): Structure et évolution de la compression alpine dans la Chaîne Ibérique et la Chaîne côtière catalane (Espagne). *Bulletin de la Société Géologique de France*, (8), VI (2): 339-340.

Nebot, M. y Guimerà, J. (2016a): Structure of an inverted basin from subsurface and field data: the Late Jurassic-Early Cretaceous Maestrat basin (Iberian Chain). *Geologica Acta*. En prensa.

Nebot, M. y Guimerà, J. (2016b): Kinematic evolution of a fold-and-thrust belt developed during basin inversion: the Mesozoic Maestrat basin, E Iberian Chain. Manuscrito presentado en *Geological Magazine*.

Salas, R. (1987): *El Malm i el Cretaci inferior entre el Massís de Garraf i la Serra d'Espadà*. Tesis Doctoral, Univ. de Barcelona, 345 p.

Salas, R. y Guimerà, J. (1996): Rasgos estructurales principales de la cuenca cretácica inferior del Maestrazgo (Cordillera Ibérica oriental). *Geogaceta*, 20(7): 1704-1706.

Salas, R., Guimerà, J., Mas, R., Martín-Closas, C., Meléndez, A. y Alonso, A. (2001): Evolution of the Mesozoic Central Iberian Rift System and its Cainozoic inversion (Iberian chain). En: *Peri-Tethys memoir, 6: Peri-Tethyan Rift/Wrench Basins and Passive Margins* (P.A. Ziegler, W. Cavazza, A.H.F. Robertson y S. Crasquin-Soleau, eds.). Mém Mus. nat. Hist. Nat., Paris, 186, 145-186.

Salas, R., García-Senz, J., Guimerà, J. y Bover-Arnal, T. (2010): Opening of the Atlantic and development of the Iberian intraplate rift basins during the late Jurassic-early Cretaceous. En: *II Central and North Atlantic Conjugate Margins Conference*, 245-248.

Seillé, H., Salas, R., Pous, J., Guimerà, J., Gallart, J., Torne, M., Romero-Ruiz, I., Diaz, J., Ruiz, M., Carbonell, R. y Mas, R. (2015): Crustal structure of an intraplate thrust belt: The Iberian Chain revealed by wide-angle seismic, magnetotelluric soundings and gravity data. *Tectonophysics*, 663: 339-353. Doi: 10.1016/j.tecto.2015